ЖУРНАЛ
ПРИКЛАДНОЙ ХИМИИ

Vol. 31 No. 2

February 1958

JOURNAL OF
APPLIED CHEMISTRY
OF THE USSR

(ZHURNAL PRIKLADNOI KHIMII)

IN ENGLISH TRANSLATION

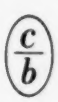

CONSULTANTS BUREAU, INC.

Vol. 31 No. 2

February 1958

JOURNAL OF
APPLIED CHEMISTRY
OF THE USSR

(ZHURNAL PRIKLADNOI KHIMII)

A publication of the Academy of Sciences of the USSR

IN ENGLISH TRANSLATION

Year and issue of first translation:
vol. 23, no. 1 January 1950

	U. S. and Canada	*Foreign*
Annual subscription	*$60.00*	*$65.00*
Annual subscription for libraries of non-profit academic institutions	*20.00*	*25.00*
Single issue	*7.50*	*7.50*

CONSULTANTS BUREAU INC.
227 W. 17th ST., NEW YORK 11, N. Y.

Printed in the United States

JOURNAL OF APPLIED CHEMISTRY OF THE USSR

Volume 31, Number 2 February 1958

CONTENTS

CONTENTS (continued)

PREPARATION OF CERIUM MONOSULFIDE

G. V. Samsonov, N. M. Popova, and L. I. Tikhomirova

Cerium sulfides are refractory compounds, with typical metallic properties; this makes them promising for use in metallurgy and chemistry, for example, as refractory and chemically resistant materials [1].

Further investigation and utilization of these compounds is hindered because methods for their preparation are complex and have been studied little.

The phase diagram of the system Ce—S has been studied [2]; it was found that the region between CeS and Ce_2S_3 contains two maxima, corresponding to the compounds CeS and Ce_3S_4, which melt congruently. The compounds CeS and Ce_3S_4 form a eutectic which melts at about 2000° (the position of the eutectic point depends on the S/Ce ratio, about 1.14). Ce_3S_4 and Ce_2S_3 probably form a continuous series of solid solutions. In addition, there are indications of the existence of the compound CeS_2.

Cerium monosulfide, CeS, is a copper-yellow compound with high electrical conductivity and melting point, and low thermal dissociation pressure; it has good resistance to fused metals and salts [1]. An important property of CeS is its low coefficient of thermal expansion, so that articles made from CeS can be heated at rates up to 1000°/min without destruction. CeS is fairly resistant to water, and dissolves rapidly in cold dilute acids with liberation of H_2S and H_2. Cerium monosulfide is less resistant to the action of water vapor. The oxidation of CeS begins at 200-300°. Finely-divided cerium sulfides, including CeS, are pyrophoric.

Black cerium sulfide, Ce_3S_4, has a lower melting point and a higher vapor pressure. Appreciable oxidation of Ce_3S_4 by oxygen begins at 700°, chlorine attacks it vigorously from 200°, steam decomposes Ce_3S_4 at temperatures above 300°. Solid solutions of Ce_3S_4—Ce_2S_3 are resistant to many fused metals [3].

Red cerium sulfide, Ce_2S_3, has the lowest melting point (1840°) and very high electrical resistance, similar to that of the oxides Al_2O_3 and ThO_2. Under the action of a current of H_2S for 20 hrs at 580-600°, Ce_2S_3 passes into a sulfide of the composition CeS_2. The reaction $2Ce_2S_3 + 2S = 4CeS_2$ is accompanied by absorption of 18.6 kcal/mole. Ce_2S_3 is a brittle compound similar in mechanical properties to porcelain. Its coefficient of thermal expansion is fairly low, so that articles made from Ce_2S_3 can be heated at rates up to 100°/min.

The sulfide CeS_2 is a yellow-brown compound, rather unstable in air and water. It is made by the action of H_2S on anhydrous cerium sulfate [4-5] at 720-750°.

It dissolves in HCl with precipitation of sulfur, so that it must be regarded as a polysulfide, and not as the chemical compound CeS_2.

The principal properties of cerium sulfides are given in Table 1.

The methods given in the literature for the preparation of cerium sulfides can be summarized as follows.

Preparation of Ce_2S_3 from Ce and S is effected by the action of heat on cerium in sulfur vapor [7]. A method for the synthesis of Ce_2S_3 has been described in detail [9].

The action of heat on CeO_2 with carbon black in a current of H_2S. The preparation of Ce_2S_3 by this method [6] is effected in somewhat complicated apparatus in accordance with the equations

$$6CeO_2 + 4H_2S = 3Ce_2O_2S + 4H_2O + SO_2,$$
$$Ce_2O_2S + 2H_2S + 2C = Ce_2S_3 + 2CO + 2H_2$$

TABLE 1

Properties of Cerium Sulfides

Properties	Sulfides			
	CeS	CeS_2	Ce_3S_4	Ce_2S_3
Color	Brassy-yellow [6]	Yellow-brown [7]	Black [6]	Red [6]
Structure	Cubic [6]	–	Cubic [6]	Cubic [6]
Lattice constants (in A):				
a	5.766 ± 0.02 [2]	–	8.6173 [2]	8.6076 [2]
c	–	–	–	–
Density (in g/cm^3)	5.93 [2]	4.90 [7]	5.70 (calculated)	5.25 (calculated)
Melting point (in °C)	~2450± 100 [6]	Decomposes at > 720° [7]	2050 ± 75 [6]	~ 1890 [2], 1840 [6]
Heat of formation at 298°K (in kcal)	± 117.9 [8]	–	± 421.5 [8]	+300.5 [8]
Specific resistance (in $\mu\Omega \cdot cm$)	90 [6]	–	400 [6]	> 109 [6]
Temperature at which P = $= 10^{-3}$ mm (in °C)	1900 [4]	–	1840 [6]	Liberates S on heating
Magnetic susceptibility (in electromagnetic units · $\cdot 10^6$)	2140 [6]	–	2200 [6]	2520 [6]
Ce–S spacing (in A)	2.88 [2]	–	2.97 [2]	2.28 [2]
at 1200-1400° during 2-3 hrs.				

For preparation of CeS, cerium hydride CeH_3 is first prepared; this is then reacted with the sulfide Ce_2S_3:

$$2Ce + 3H_2 = 2CeH_3,$$
$$2Ce_2S_3 + 2CeH_3 = 6CeS + 3H_2.$$

Finally, the compound Ce_3S_4 is made by the reaction

$$Ce_2S_3 + CeS = Ce_3S_4.$$

The action of heat on CeO_2 in a current of H_2S. When CeO_2 is heated in a graphite boat in a current of dry H_2S at 1600-1800°, Ce_2S_3 is formed [10]. On further increase of the temperature Ce_2S_3 decomposes with formation of Ce_3S_4 or products of intermediate composition. If the reaction is interrupted at 1000-1300°, the oxysulfide Ce_2O_2S is formed.

Exchange reactions of cerium halides with hydrogen sulfide. The sesquisulfide Ce_2S_3 can be prepared by exchange reactions of cerium chloride, bromide, or iodide with H_2S at 600-1000° [10, 11]. The reaction takes tens of hours.

Thus, the methods for the preparation of cerium sulfides, especially CeS, are complex and require rather complicated apparatus.

The purpose of the present work was to find a simple method for the preparation of one of the sulfides of cerium – the monosulfide, CeS.

The materials used were cerium oxide CeO_2 (98% CeO_2, < 0.01% Fe, 1.4% ignition loss), and carbon black containing 99.4% C and 0.4% ash, which were heated at 900° and 400°, respectively, and purified flowers of sulfur containing 99.9% S.

The method first chosen was that of Eastman and Brewer [6], but instead of a three-stage process (preparation of CeH_3, Ce_2S_3, and CeS), an attempt was made to obtain the sulfide CeS in a single stage by the reaction

$$CeO_2 + 2C + H_2S = CeS + H_2 + CO$$

with reduction of CeO_2 by carbon and conversion of the cerium so formed to the sulfide by the action of hydrogen sulfide. The composition of the reaction mixtures was calculated for the theoretical amount of carbon necessary for its removal in the form of CO, and also to correspond to the following carbon contents (in %): 50, 25 and 15, and 0 (CeO_2; $CeO_2 + 0.25C$; $CeO_2 + 0.5C$; $CeO_2 + C$; $CeO_2 + 1.5C$; $CeO_2 + 2C$). The experiments on sulfide formation were performed in a tube furnace (into which the mixture was placed in porcelain boats) in a current of nitrogen at 1050° for 4-8 hrs. The reaction products were analyzed for Ce, S_{total} and S_{bound}. The results are given in Table 2. It follows from these results that S_{total} increases somewhat with increasing content of carbon black in the mixture, the cerium content decreases somewhat, while the sum of Ce + S_{total} in the reaction products remains almost constant, and does not exceed 90-92%. The remaining 8-10% is apparently oxygen not removed in the course of reduction, and the corresponding residual carbon. Determination of carbon in sulfides is difficult because the same absorbents are used for SO_2 and CO_2; therefore, as a rough approximation, the amounts of cerium combined with sulfur and oxygen respectively may be calculated on the following considerations. Since the reaction was carried out at 1050°, the amount of oxygen removed must be proportional to the amount of carbon removed (in the form of CO); from this it is possible to calculate the amounts of carbon and oxygen remaining in the charge after the reaction, provided that only the carbon of the mixture reduces the CeO_2. These conditions lead to the formulas given in Table 2 for the cerium sulfides. However, it also follows from this table that when pure CeO_2 (without carbon) is converted to sulfide a product of analogous composition is formed; in other words, dissociated hydrogen sulfide can also reduce CeO_2.

For comparison of the relative participation of sulfur, hydrogen sulfide, and carbon black in the reduction of CeO_2, the variations in the decrease of free energy with the temperature were calculated for the reactions:

$$CeO_2 + C + H_2S = CeS + CO + H_2O \quad (1)$$
$$CeO_2 + 2S = CeS + SO_2, \quad (2)$$

the respective values being:

$$\Delta F_1 = -271\,500 - 39.98\,T \text{ and}$$
$$\Delta F_2 = -279980 - 73.52\,T.$$

It follows from these results that sulfur is a more active reducing agent for CeO_2 than carbon. Therefore, in the conversion of a mixture of CeO_2 + C to sulfide by means of hydrogen sulfide, both the carbon and the sulfur formed by decomposition of hydrogen sulfide, and in part also the hydrogen of the H_2S, act as the reducing agents.

With increasing content of carbon black in the charge, the carbon removes increasing relative amounts of oxygen from CeO_2, in the form of CO, and therefore more sulfur is utilized in the reaction with cerium and less is involved in the reduction of CeO_2 (Table 2). Since it is not possible to determine exactly the carbon contents of the reaction products, or the relative participation of the sulfur and carbon in the reduction, the formulas in Table 2 are nominal.

It was found by x-ray analysis of the product of Experiment No. 6 (Table 2), containing 76.1% Ce and 13.66% S_{bound}, performed with an exposure of 10 hrs with copper radiation with an Al filter, that the lines correspond satisfactorily to a simple cubic lattice with $\underline{a} = 5.74 \pm 0.15$ A. According to literature data (Table 1), CeS has $\underline{a} = 5.766 \pm 0.002$ A, so that the product formed in Experiment No. 6 is satisfactorily identified as CeS, despite the fact that the nominal formula of the sulfide, based on the foregoing formal consideration, is $CeS_{1.17}$. Thus, the reaction products are mixtures of CeS, CeO_2 (or lower oxides of cerium), and carbon black.

In subsequent experiments the sulfidation of cerium in mixtures of $CeO_2 + xS$ by means of hydrogen sulfide (at 1050° for 4 hrs) was studied. The mixture compositions were calculated for the following molar ratios of CeO_2 to S, with participation of hydrogen sulfide in the reduction of CeO_2 and sulfidation taken into account: 1) $CeO_2 + 0.5S$, 2) $CeO_2 + S$, 3) $CeO_2 + 1.5S$, 4) $CeO_2 + 2S$, 5) $CeO_2 + 2.2S$, 6) $CeO_2 + 2.5S$.

TABLE 2

Results of Chemical Analyses of the Products Formed in the Reaction of Hydrogen Sulfide with Mixtures of CeO_2 + xC (at 1250°)

Expt. no.	Composition of mixture	Reaction time (hours)	Chemical composition (%)			Total of $Ce + S_{total}$ (in %)	S^{*}_{bound} (in %)	C (in %)	O (in %)	Ce_{bound} with O (in %)	Ce_{bound} with S (in %)	$\frac{Ce_{bound}}{S_{bound}}$ **	Nominal formula
			Ce	S_{total}	S_{free}								
1	CeO_2	4	77.7	12.1	0.16	89.8	11.9	—	10.2	44.6	33.1	2.79	$CeS_{1.56}$
1	$CeO_2 + 0.25$ C . . .	4	78.31	10.54	0.10	88.85	10.44	4.8	6.35	27.8	46.1	4.39	$CeS_{0.996}$
3	$CeO_2 + 0.5$ C	4	77.5	12.9	0.17	90.4	12.79	4.13	5.47	23.9	53.5	4.2	$CeS_{1.04}$
4	$CeO_2 + C$	4	76.9	13.6	0.11	90.5	13.5	4.08	5.42	23.7	53.2	3.94	$CeS_{1.12}$
5	$CeO_2 + 1.5$ C	4	76.2	13.8	0.1	90.0	13.7	4.9	5.7	25.0	51.2	3.73	$CeS_{1.17}$
6	$CeO_2 + 2$ C	4	76.1	13.85	0.20	89.95	13.65	4.31	5.74	25.1	51.0	3.72	$CeS_{1.17}$
7	$CeO_2 + 2$ C	4 + 4	78.0	14.65	0.23	92.65	14.42	2.70	3.65	16.0	62.0	3.55	$CeS_{1.23}$
8	$CeO_2 + 2$ C	8	73.0	16.4	0.27	89.4	16.13	4.50	6.10	26.7	46.3	2.89	$CeS_{1.54}$

* Calculated as the sulfide phase.

** The Ce_{bound}/S_{bound} ratios are: for CeS = 4.38, Ce_2S_3 = 2.93, Ce_3S_4 = 3.29, CeS_2 = 2.19.

TABLE 3

Results of Chemical Analyses of the Products Formed in the Sulfidation of Cerium in Mixtures of CeO_2 + xS (at 1050°, during 4 hrs)

Expt. no.	Composition of mixture	Chemical composition of sulfidation product (in %)			Total of $Ce + S_{total}$ (in %)	S^{*}_{bound}	O (in %)	Ce combined with O (in %)	Ce combined with S (in %)	$\frac{Ce_{bound}}{S_{bound}}$	Composition of sulfides
		Ce	S_{total}	S_{free}							
1	$CeO_2 + 0.5$ S	80.0	13.9	0.01	93.9	13.89	6.1	26.7	53.3	3.86	$CeS_{1.15}$
2	$CeO_2 + S$	80.1	14.1	0.02	94.2	14.08	5.82	25.4	54.7	3.86	$CeS_{1.15}$
3	$CeO_2 + 1.5$ S	81.4	14.1	0.01	95.5	14.09	4.51	19.7	61.7	4.39	$CeS_{0.995}$
4	$CeO_2 + 2$ S	81.5	16.3	0.01	97.8	16.29	2.21	9.70	71.8	4.42	$CeS_{0.995}$
5	$CeO_2 + 2.25$ S	81.4	18.5	0.02	99.9	18.48	0.1	0.5	80.9	4.40	CeS
6	$CeO_2 + 2.5$ S	81.1	14.7	0.04	95.8	14.66	4.2	18.2	62.9	4.19	$CeS_{0.997}$

* Calculated as the sulfide phase.

The analytical data for the reaction products formed in these experiments are given in Table 3. It is seen that the content of Ce and S_{bound} both increase with increasing atomic content of sulfur in the charge, as the total of Ce + S_{total} reaches 99.9% at $S/CeO_2 = 2.25$. The sulfidation product then has the exact composition CeS. The composition of the sulfidation product deteriorates with further increase of the sulfur content, probably owing to volatilization of the excess sulfur, which entrains sulfur intended for the reduction and sulfidation reaction. A similar effect was observed in other cases with the use of volatile reducing agents, for example, in the thermal reduction of a number of oxides by magnesium, when the excess magnesium volatilizes and takes with it the greater part of the magnesium intended for the reaction MeO + Mg = Me + MgO, so that part of the oxide remains unreduced.

X-ray analysis of the reaction product of Experiment No. 5 (Table 3) revealed a cubic lattice with $\underline{a} = 5.76$ A.

The above method for the preparation of CeS is much simpler and more convenient than the method proposed by Brewer et al. [6].

LITERATURE CITED

[1] G. Jaeger, Metall. 9, 358-366 (1955).

[2] W. Zachariasen, Argonic National Laboratory, Chicago, Ill., private communication cited through [5].

[3] E. Eastman, L. Brewer, A. Bromley, R. Gilles, and N. Longfreen, J. Am. Ceramic Soc. 34, 128-134 (1951).

[4] J. Sterba, Ann. Chim. Phys. B 2, 193-232 (1904).

[5] W. Muthmann and T. Stützel, Ber. 32, 3413-3419 (1899).

[6] E. Eastman , L. Brewer, A. Bromley, R. Gilles, and N. Longfreen, J. Am. Chem. Soc. 72, 2248-2250 (1950).

[7] M. P. Slavinskii, Physicochemical Properties of the Elements (Metallurgy Press, 1952).*

[8] L. Brewer et al., Thermodynamic and Physical Properties of Miscellaneous Materials IV, 19 B, 40-59 (1950).

[9] E. Strotzer, W. Bietz, and K. Meisel, Z. anorg. u. allg. Chem. 238, 76 (1938).

[10] M. Picon, Compt. rend. 192, 684 (1931).

[11] E. Eastman, L. Brewer, et al., Abstracts of Papers, 115th Meeting of the American Chemical Society, 3 (1949).

Received July 2, 1956

* In Russian.

INVESTIGATION OF THE CALCINATION OF TECHNICAL SODIUM BICARBONATE

E. M. Mitkevich

All-Union Institute of the Soda Industry

Despite the great industrial importance of the drying and calcination of technical sodium bicarbonate formed in the production of sodium carbonate by carbonation of ammoniacal salt solutions, not enough information on these processes is available in the literature.

Of the available publications, the papers by Caven and Sand [1], Avdeeva [2], and others should be mentioned.

Caven and Sand determined the equilibrium total pressures of CO_2 and H_2O over sodium bicarbonate at various temperatures. They gave the following approximate equation for the reaction isochore:

$$\log P = 11.8185 - \frac{3340}{T},$$

where P is the total equilibrium pressure of CO_2 and H_2O (in mm Hg), T is the temperature (in °K).

Their analysis of the equilibrium gaseous phase showed that the molecular ratio of H_2O to CO_2 is 1.

They therefore concluded that the dissociation of sodium bicarbonate proceeds according to the equation $2NaHCO_3 = Na_2CO_3 + H_2O + CO_2$.

Avdeeva investigated the variations of the equilibrium pressure of H_2O and CO_2 over sodium bicarbonate and its decomposition products with decrease of the amount of carbon dioxide present in the solid phase, in the temperature range 100-120°, and at 145° at the end of the decomposition. The total pressures of CO_2 and H_2O were measured by a static method. It was found that the total equilibrium pressure of the gases at the given temperature remains constant until $^1/_3$ of the amount of CO_2 which should be liberated in the complete decomposition of the sample of sodium bicarbonate to sodium carbonate has been given off. When more than $^1/_3$ CO_2 has been removed, the equilibrium pressure drops to about $^1/_4$ of its initial value, and then remains constant until the sodium bicarbonate has been completely decomposed. The equilibrium pressure before $^1/_3$ CO_2 has been given off are in good agreement with the data of Caven and Sand.

From these results, Avdeeva concluded that in the dissociation of sodium bicarbonate an intermediate solid phase is formed with the composition $4NaHCO_3 \cdot Na_2CO_3$, which has a lower dissociation pressure. Therefore, Avdeeva represented the calcination process by the following two consecutive stages:

$$6NaHCO_3 = Na_2CO_3 \cdot 4NaHCO_3 + H_2O + CO_2, \quad (1)$$

$$Na_2CO_3 \cdot 4NaHCO_3 = 2Na_2CO_3 + 2H_2O + 2CO_2. \quad (2)$$

The formation of the double salt was confirmed by its synthesis from Na_2CO_3, H_2O and CO_2 in accordance with Eq. (2), and by determination of its dissociation pressure.

The paper cited also described a study of the rate of decomposition of sodium bicarbonate at various temperatures, with different compositions of the gas phase in the reaction space (thermostat).

It was found that the rate of decomposition is almost independent of the composition of the gas phase, but depends very much on the temperature.

In an analysis of the performance of the calciner in the light of the results obtained, the following conclusion is drawn in the paper: "In order that the calcination should proceed at a rate adequate for industrial purposes, the mass in the calciner must be kept at a temperature above 140°."

Similar data on the decomposition rate of sodium bicarbonate are quoted in the monographs on soda production by Gol'dshtein [3] and Te Pan Go [4].

Apart from some practical details, the foregoing represents all the available literature data on the calcination process.

A critical consideration of these data in relation to the actual industrial calcination process raises the following points.

1. The crude bicarbonate subjected to calcination contains, in addition to $NaHCO_3$, from 4 to 6% of sodium carbamate ($NaCO_2NH_2$) [5-8]. The considerations of the liberation of NH_3 from technical bicarbonate, as published in the literature, are based on the assumption that the bicarbonate contains ammonium carbonates, and are therefore erroneous.

2. In both the return and nonreturn feeding processes the moist bicarbonate is prepared for calcination by a process which involves mixing of the bicarbonate with soda ash or with pulp containing soda ash.

The literature contains no information concerning the physicochemical processes which take place during the mixing, and consequently on the processes which actually take place in the calciner.

3. There is no information on the temperatures of the mass in the calciner at which the individual stages of the calcination process occur.

These processes were studied both in the laboratory and in production conditions in calciners.*

Microscopic and thermographic methods were used in investigation of the chemistry of the processes which occur when moist technical bicarbonate is mixed with soda ash and when the resultant mass is calcined.

EXPERIMENTAL

The following experimental procedure was used. Technical bicarbonate, previously moistened to contain 18% H_2O, was mixed with soda ash. The weight ratio of soda ash to moist bicarbonate was varied in the range 0.5-1.

The mixing was performed in a vessel kept at 60°, over a period of 3-4 min. The soda ash was charged into the vessel at 130°, and the moist technical bicarbonate at 25°.

Under these conditions, after half a minute of stirring the temperature of the mixture became 95-100°, which is the temperature at the exit of the mass from the mixer of the calciner. The mixed mass became dry and friable. The mixture and the starting materials were investigated under the microscope and subjected to thermographic analysis.

For determination of the heating curves, the materials were kept in an air thermostat with automatic temperature control, under the following standard conditions.

A 45 g sample was placed in a glass cylinder, the capacity of which was such that the sample filled it almost completely. The cylinder was closed by means of a cork with a narrow groove down one side, to allow free escape of the reaction gases without their dilution with air; a thermometer with 0.1° scale divisions was inserted into the mass through the center of the cork. The cylinder was placed in the thermostat and the heater was then turned on. The heating rate was 2°/min. The temperature in the thermostat was taken to 145°, and then kept constant to within ± 0.5°.

* These results were partly obtained in a study published in E. M. Mitkevich's dissertation: "Investigation of processes which take place in the calcination of technical sodium bicarbonate" (Odessa Polytechnic Institute, 1953), and partly as part of the research program of the All-Union Institute of the Soda Industry (VISP) with participation of members of the Institute and of the soda works.

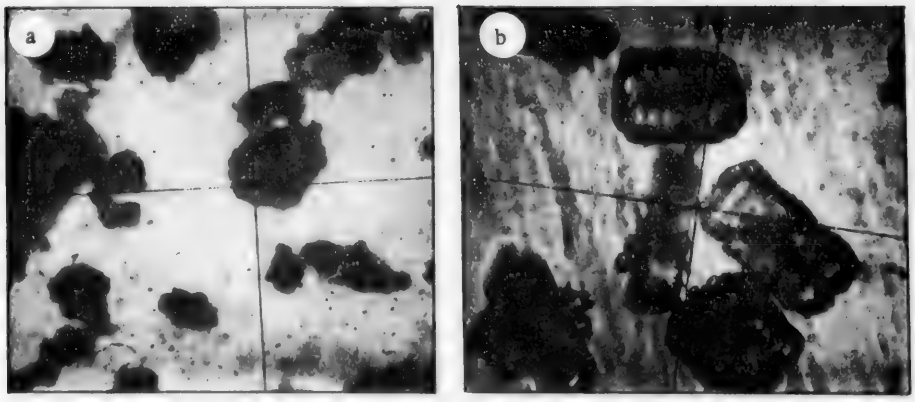

Fig. 1. Microphotographs. a) Works soda ash containing 99.5% Na_2CO_3; b) air-dry technical sodium bicarbonate containing (in %): $NaHCO_3$, 94.8; Na_2CO_3, 2.4; $NaCO_2NH_2$, 1.8.

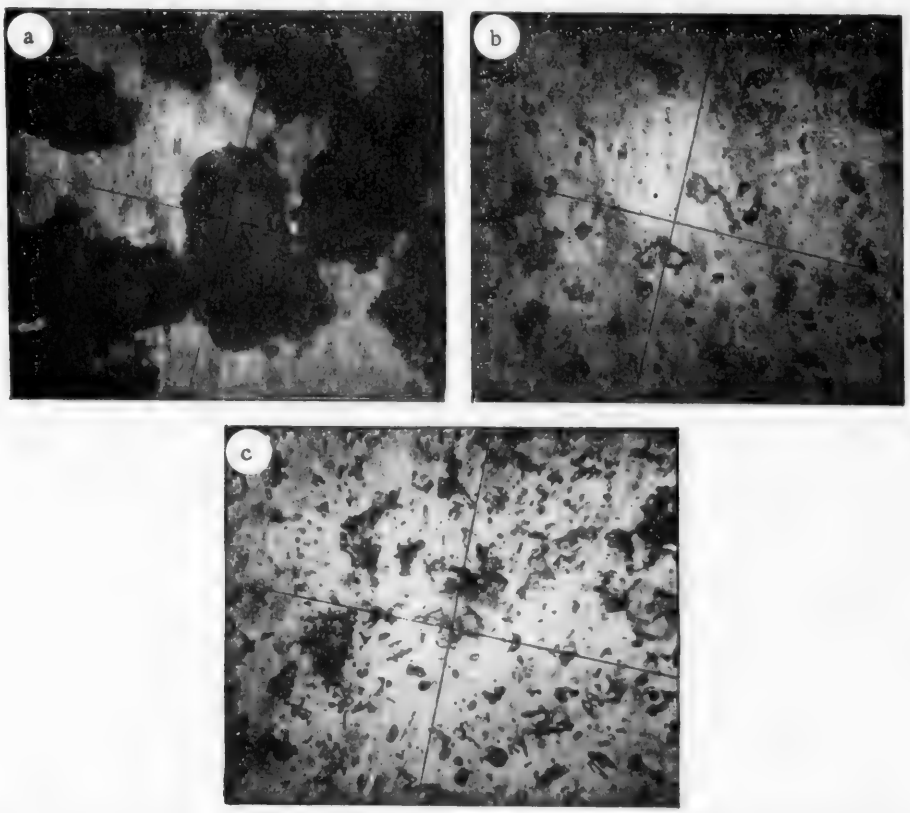

Fig. 2. Microphotographs. a) Mixture of soda ash with moist technical sodium bicarbonate of the following composition (in %): $NaHCO_3$, 53.8; Na_2CO_3, 36.7; H_2O, 9.1; b) crushed crystals of technical sodium bicarbonate; c) crushed aggregates of the mixture.

The temperature recordings were started at 96° (the tenth-degree thermometer was graduated between 96° and 150°). It was first confirmed that no phase changes took place while the substance was heated up to 96°.

The simple method of temperature recording by means of a tenth-degree thermometer was satisfactory in view of the large heat effects expected.

Results in close agreement were obtained in parallel experiments. The results of the microscopic and thermographic analyses are given in Figs. 1-3.

Figure 4 shows the heating curve of analytical-grade sodium bicarbonate, determined at a heating rate of ~ 15°/min, the final thermostat temperature being 250°.

It is clear from the microphotographs that crystals of technical sodium bicarbonate have a characteristic barrel shape, and are transparent to light.

The crystalline aggregates formed as the result of mixing resemble the original crystals of technical bicarbonate in shape, but are not transparent.

The structure of these aggregates was elucidated by comparison of microphotographs of mechanically destroyed crystals of technical bicarbonate and of aggregates of the mixture. It is seen that the microphotographs of the crushed aggregares contain numerous small crystals of a regular needle shape, which indicate that a new solid phase is formed during the mixing process.

It follows that the crystalline aggregates in the mixture are concretions, the centers of which are residues of sodium bicarbonate crystals, surrounded by fine crystals of the new solid phase.

The heating curve of the mixture (Fig. 3) shows a halt at 110.2° and two distinct changes of slope, at 122 and 127°. A comparison of the positions of the heat effects on the heating curve of the mixture with the positions of the heat effects on the heating curves of standard substances (sodium bicarbonate and trona) shows that the mixture consists of trona and sodium bicarbonate.

Therefore, trona is formed when moist technical bicarbonate is mixed with soda ash, and therefore an essential stage of the calcination process in the calciner is formation of sodium carbonate from trona and sodium bicarbonate (the formation of sodium carbonate from sodium carbamate is considered separately). In the return process, the ratio of the amounts of trona to sodium bicarbonate in the mixture entering the calciner is determined by the moisture content of the technical sodium bicarbonate.

We now consider the chemistry and the temperature ranges of the individual stages of the calcination process, in the light of the thermographic data.

Sodium bicarbonate (analytical grade). The heating curve of analytical-grade sodium bicarbonate has one distinct horizontal plateau at 119.8° (Fig. 3). This is preceded by a temperature rise to 122.4°. Analysis of the mass after the temperature had reached 123° showed that the bicarbonate was almost completely (98.3%) converted into carbonate.

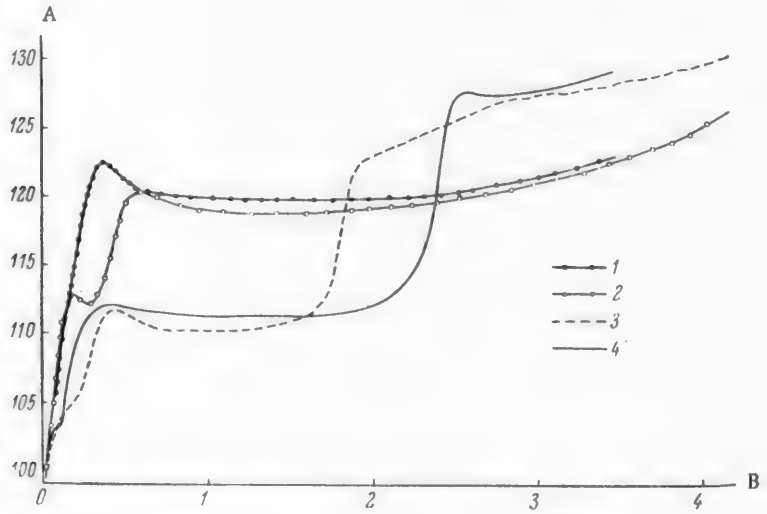

Fig. 3. Thermograms. 1) $NaHCO_3$, 2) technical bicarbonate, 3) mixture, 4) trona, $Na_2CO_3 \cdot NaHCO_3 \cdot 2H_2O$. A) Temperature (in °C), B) time (hrs).

The absence of a second heat effect above 125° on the heating curve (the equilibrium vapor pressure of the compound discovered by Avdeeva [2] reaches 1 atmos at 125°) shows that sodium bicarbonate is converted directly into the carbonate without formation of intermediate compounds.

The formation of the double salt $Na_2CO_3 \cdot 3NaHCO_3$ (Avdeeva gives the formula $Na_2CO_3 \cdot 4NaHCO_3$, owing to the inaccuracy of her experiments; in reality she obtained the compound $Na_2CO_3 \cdot 3NaHCO_3$, known in the literature [9, 10] as Wegscheider's salt) in Avdeeva's experiments was the result of a secondary process – the interaction of gaseous CO_2 and H_2O, liberated in the decomposition of $NaHCO_3$, with sodium carbonate. Wegscheider's salt must have been formed in Avdeeva's experiments because the gas phase was removed after equilibrium was established in the reaction vessel.

The horizontal plateau is formed on the heating curve because the rates of heat transfer and of the chemical process are equal. Therefore, in cases in which the rate of heat transfer and the rate of the chemical dissociation of the substance change comparably with the temperature, the heat effect on the heating curve is displaced with changes of the heating rate.

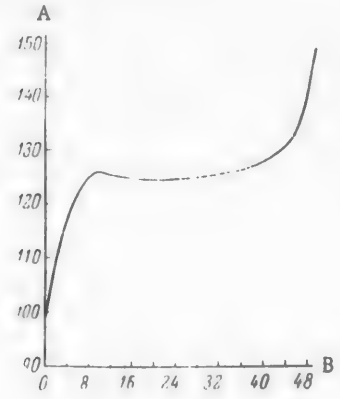

Fig. 4. Thermogram of $NaHCO_3$. A) Temperature of $NaHCO_3$ (in °C), B) time (min).

The heating curve in Fig. 4 corresponds to the heating of sodium bicarbonate when the difference between the thermostat temperature and the temperature of the bicarbonate (during the decomposition stage) is 125°, i. e., when Δt is five times that of the experiment plotted in Fig. 3. It is seen that the heat effect is displaced by only 4.7°.

This indicates that the decomposition of sodium bicarbonate in the calciner occurs when the temperature of the mass is in the 120-130° range.

Technical sodium bicarbonate. The heating curve of technical sodium bicarbonate (air-dry) has two distinct heat effects. The first halt is very brief, and occurs at 112°. The short duration of the first halt indicates that relatively little heat is expended in the process which occurs there. 112° is very close to the first phase transition of trona (111.3°). This leads to the suggestion that the small amount of Na_2CO_3 present in technical bicarbonate is combined in the form of trona.

A second and long halt is found at 118.8°; this corresponds to dissociation of sodium bicarbonate.

Trona ($Na_2CO_3 \cdot NaHCO_3 \cdot 2H_2O$). The heating curve of trona has two halts (the very short third halt at 103.4° is caused by dissociation of 2% monohydrate present in the trona). The first halt occurs at 111.3°, and the second at 127.4°.

The dissociation of trona at 100° was studied by Lescoeur [11]. He found that during dissociation trona first loses its water of crystallization and is converted into the double salt, and the double salt then decomposes. He did not establish the composition of the double salt. According to his results, the first halt on the heating curve of trona is due to the loss of water of crystallization, and the second, to decomposition of the double salt to give sodium carbonate.

The total equilibrium pressure $P_{CO_2} + P_{H_2O}$ found by Lescoeur for the double salt was 183 mm Hg.

The total equilibrium pressure $P_{CO_2} + P_{H_2O}$ found by Avdeeva for Wegscheider's salt at 100° was 182 mm Hg.

The fact that the same dissociation pressures were found in the same system $Na_2CO_3 - NaHCO_3 - CO_2 - H_2O$ leads to the conclusions that the double salt formed by the dissociation of trona is Wegscheider's salt ($NaCO_3 \cdot 3NaHCO_3$).

It follows from these results that the calcination of technical sodium bicarbonate consists of three consecutive stages which take place in the 110-130° range:

1) dehydration of trona $3(Na_2CO_3 \cdot NaHCO_3 \cdot 2H_2O) = Na_2CO_3 \cdot 3NaHCO_3 + 2Na_2CO_3 + 6H_2O$;

2) decomposition of sodium bicarbonate $2NaHCO_3 = Na_2CO_3 + H_2O + CO_2$;

3) decomposition of Wegscheider's salt $2(Na_2CO_3 \cdot 3NaHCO_3) = 5Na_2CO_3 + 3H_2O + 3CO_2$.

These conclusions were tested by direct trials in working calciners.

Examination of the heating curves, for example of $NaHCO_3$, shows that the dissociation process occurs mainly at constant temperature, and the temperature of the mass increases a little only at the end of the decomposition.

Figure 5 shows variations of the titer of the product with the temperature of the calcined mass for (a) return and (b) nonreturn calciners, characteristic of the end of the decomposition process. These results were obtained by analysis of samples taken from the discharge conveyor, the temperature being recorded simultaneously.

It follows from Fig. 5 that in the return calciner the calcination process is virtually complete when the mass has reached 130°; this is in good agreement with the foregoing thermographic data. This temperature is somewhat displaced in the nonreturn calciner; the calcination process is complete when the mass is at 142°. The reason for this difference is that granules are present in the soda in nonreturn calciners. These granules are formed by rolling of the mass in the feeding zone of the technical sodium bicarbonate. Therefore, at 130° (a temperature at which a titer of 98% is obtained in return calciners) the temperature within the granules is lower, and they contain undecomposed bicarbonate, which lowers the total titer of the product.

The general course of the calcination process along the furnace, for the case when the process terminates when the mass reaches the discharge conveyor, is shown in Fig. 6.

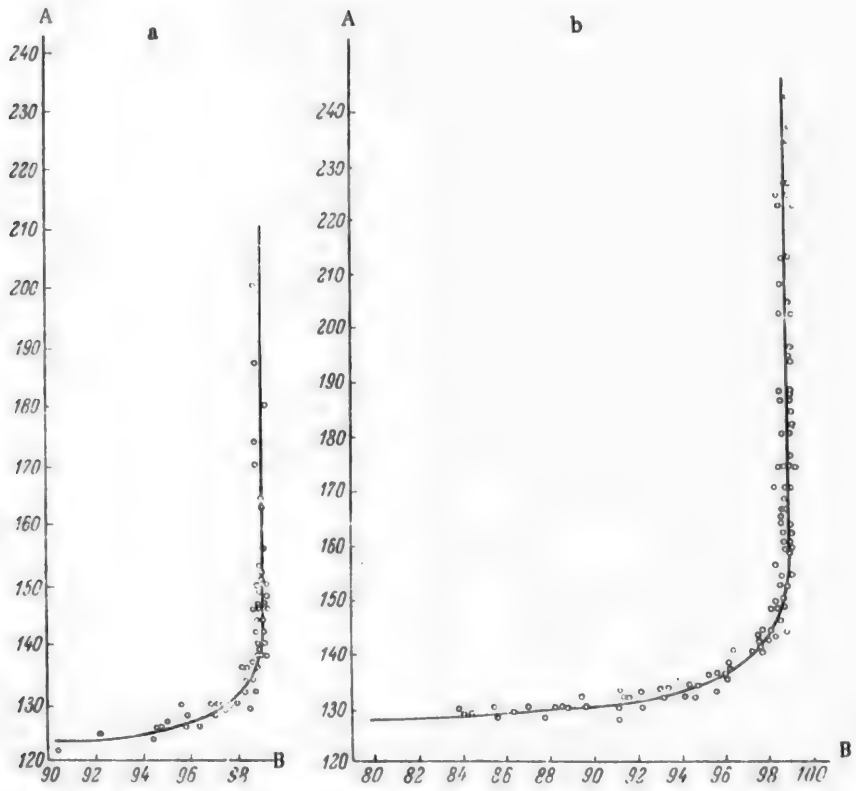

Fig. 5. Variation of titer with the temperature of the calcination mass in return (a) and nonreturn (b) calciners. A) Temperature (°C), B) titer (in%).

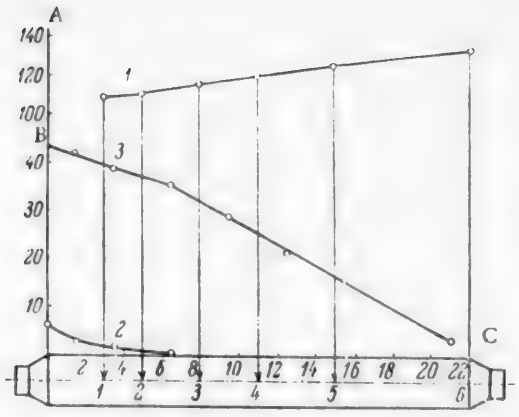

Fig. 6. Variation of the composition of the mass along the calciner under normal operating conditions. A) Temperature (in °C) (1), B) contents of H_2O (2) and $NaHCO_3$ (3) in the mass (in %), C) distance (in m).

These results were obtained by analysis of samples and temperature determinations along the length of a working calciners in No. 2 unit of the Slaviansk soda combine.

The temperature of the mass along the calciner was measured by means of KhA thermocouples and a six-point electronic potentiometer type EPP-09 with a 0-200° scale, class 0.5.

The thermocouples, in sheaths of special design, were suspended from a steel cable at the points indicated in Fig. 6 by numbered arrows. The point marked 6 indicates the temperature of the soda at discharge. This temperature was determined by means of an ordinary 300° thermometer.

The cable was stretched along the center of the calciner between the shell of the discharge screw and the wall of the feed compartment.

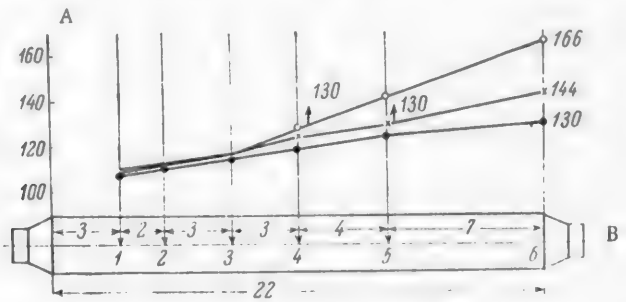

Fig. 7. Variation of the composition of the mass along the calciner at different states of the calcination process. A) Temperature of mass (in °C), B) distance (in m).

The feed rate of the calciner during the sampling was 170 tons per day.

It follows from Fig. 6 that dehydration of the mass occurs mainly along the first portion of the drum, and is completed over a length of 6-6.5 m. The temperature of the mass varies from 108 to 114°. Decomposition of sodium bicarbonate and of Wegscheider's salt proceeds along the whole length of the calciner, and terminates when the mass is at ~ 130°. Vigorous decomposition of these salts begins at the instant the mass becomes dehydrated.

It is seen that this picture of the course of the calcination process in the calciner is in good agreement with the thermographic data. It is, however, necessary to note the superposition of the processes in the dehydration zone, i. e., simultaneous processes involving decomposition of the HCO_3^- ion. This is caused by the heat transfer conditions between the metallic wall of the calciner and the calcination mass. The average temperature of the calciner wall is about 300°. Therefore, all the processes take place simultaneously in the layer in immediate contact with its surface. The carbon dioxide which is liberated, with an equivalent amount of water, by decomposition of HCO_3^- ions at the wall does not combine completely with formation of Wegscheider's salt as it passes through the mass. This is what leads to the partial superposition of the processes in the dehydration zone.

The picture presented in Fig. 6 must be regarded as reflecting the normal course (regime) of the calcination process along the calciner, as in this case the whole heating surface of the drum is involved in useful processes, associated with the formation of soda ash.

Figure 7 shows the curves for the course of the calcination process along the calciner, with elevated temperatures of the exit soda.

It is seen that very slight increases of the temperature of the soda at the exit result in shifts of the point at which the calcination process terminates (see thepoints marked 130°)into the drum of the calciner, to very considerable distances from the discharge point. The point of the end of calcination inside the calciner is shifted to 7 and 11 meters at 144 and 166°, respectively.

Under normal operating conditions, about 15 and 25% of the total heat is transferred in these regions of the drum. These results show that maintenance of the temperature of the exit soda within narrow limits, representing the end of the calcination process, is a necessary condition for maximum productivity and high technical and economic efficiency at any heat-transfer rates in the calciner.

SUMMARY

1. When moist crude sodium bicarbonate is mixed with hot soda ash in the mixer of the calciner (with return feeding) or at the point of the bicarbonate feed (with nonreturn feeding) trona is formed according to the equation

$$Na_2CO_3 + NaHCO_3 + 2H_2O = Na_2CO_3 \cdot NaHCO_3 \cdot 2H_2O.$$

2. It is shown that the calcination of crude sodium bicarbonate includes two essential consecutive stages which occur in the 110-130° temperature range: a) dehydration of trona, b) decomposition of bicarbonate and of Wegscheider's salt.

3. It is shown that for the highest technical and economic efficiency in the calcination process the soda must be discharged from the calciners at a temperature corresponding to the end of the calcination process (130° for return and 142° for nonreturn calciners).

LITERATURE CITED

[1] R. Caven and H. Sand, J. Chem. Soc. 99, 1359 (1911); 105, 2752 (1914).

[2] A. V. Avdeeva, J. Appl. Chem. (USSR) 8, 17, 4 (1931).

[3] Ia. R. Gol'dshtein, Production of Soda Ash [in Russian] (Moscow, Goskhimizdat, 1934).

[4] T'ieh P'ang Kuo, Soda Production [in Russian] (Goskhimizdat, 1948).

[5] E. I. Orlov, Ukrain. Chem. J. 1, 12 (1928); 4, 132 (1928).

[6] Z. V. Dolganova, Dissertation (Kharkov Polytechnic Institute, 1950).*

[7] T. Kuki, S. Niwo, and R. Hara, J. Soc. Chem. Ind. Japan 43, 3, 76 (1940).

[8] T. Kuki and R. Hara, J. Soc. Chem. Ind. Japan 43, 4, 118 (1940).

[9] M. Wegscheider, Monatsh. 49, 283 (1928).

[10] Waldeck, Lunn, and Hill, J. Am. Chem. Soc. 56, 43 (1934).

[11] Gmelin's Handbuch der anorg. Chem. 7, 21 (1927).

Received June 16, 1956

* In Russian.

PARTIAL VAPOR PRESSURE OF SULFURIC ACID AND WATER OVER SULFURIC ACID SOLUTIONS

A. I. Baranova

Contact-Acid Laboratory, Scientific Research Institute of Fertilizers and Insectofungicides

The vapor pressures of sulfuric acid and water have been determined for acids containing 75-90% H_2SO_4 in the 100-180° range.

The total vapor pressure of sulfuric acid of various concentrations has been studied by many workers – Burt [1], Briggs [2], Sorel [3], Regnault [4], Daudt [4], McHaffie [6], and others.

There have been few investigations of the partial pressure of sulfuric acid vapor (Thomas and Ramsay [7], Thomas and Barker [8]), and no data are available at all for acids containing less then 89% sulfuric acid.

The vapor pressure results are usually represented by the Avgusta*(Clausius-Clapeyron) equation [9]:

$$\log P = A - \frac{B}{T}. \qquad (1)$$

In 1925 Greenwalt [10] published a critical review of work on determination of total vapor pressure over sulfuric acid–water mixtures; he used what he regarded as the most reliable data to determine the coefficients A and B in the above equation for acid concentrations from 10 to 100%. The most recent determinations of the total vapor pressure over sulfuric acid–water mixtures deal mainly with more accurate data at 25° [11-15]. This was associated with the need to determine standard values for thermodynamic calculations.

Variations of the concentration during the course of the experiments were not taken into account in any of these numerous determinations of vapor pressure either by the dynamic or by the static method; this undoubtedly resulted in low total vapor pressure values. Burt's data are generally accepted for a wide range of concentrations and temperatures, and yet his values must be regarded as low owing to evaporation of the acid in the course of boiling for 1 to 2 hrs during the experiment.

In 1955 Tarasenkov [16] published data on the total vapor pressure over aqueous solutions of sulfuric acid with concentrations from 10 to 83.28%, at temperatures between 0 and 100°, determined by a static method. He points out that the acid concentrations were determined after each experiment, since the concentration varied during evacuation of air from the vessel. Preference should therefore be given to Tarasenkov's recent data, since none of the earlier workers took into account changes in the acid concentration at the end of the experiment.

The work of Thomas and Ramsay on determination of the partial vapor pressure over sulfuric acid solutions has lost its significance because of the very low results owing to adsorption of sulfuric acid on glass wool. Glass wool was used for removal of sulfuric acid mist.

Thomas and Barker determined the partial vapor pressures of sulfuric acid and water over solutions containing from 89 to 99% H_2SO_4, in the 180-290° range. They used the transpiration method, with air bubbled through the acid. According to the authors themselves, the error of the results was of the order of 5-15%.

The dissociation of sulfuric acid in the vapor phase is not taken into account in Thomas and Barker's data. The vapor pressure of sulfuric acid vapor over 95% acid also seems doubtful; in the 180-225° range this is higher

* Transliteration of Russian – Publisher's note.

than $P_{H_2SO_4}$ for 98% acid. The total vapor pressures found by Thomas and Barker are lower than Greenwalt's data. It seems likely that the partial vapor pressures of sulfuric acid are not very accurate either, especially as the possibility of mist formation was not taken into account in the absorption of sulfuric acid vapor.

Amelin [17] analyzed Thomas and Barker's results and determined the coefficients A and B in Eq. (1) for calculation of the partial vapor pressures of sulfuric acid in the 85-95% H_2SO_4 region. Dissociation of sulfuric acid vapor was not considered in calculation of the coefficients and therefore, as the author points out, these values may be used in calculations for temperature below 250°. Abel [18] used the activities and dissociation constants of sulfuric acid vapor and certain other thermodynamic data to calculate $P_{H_2SO_4}$, P_{SO_3}, and P_{H_2O} over sulfuric acid solutions in the concentration range 20-100%, for the 25 to 300° temperature range. These calculations are rather complicated, and some of the physicochemical data used are extremely unreliable.

EXPERIMENTAL

The transpiration method was used in this investigation, as determinations of low vapor pressures of H_2SO_4 (below 1 mm) by the static method involve great experimental difficulties.

In our method air, previously saturated with water vapor to an extent approximately corresponding to the expected water vapor pressure, was passed into a reaction vessel containing the acid. In this way the acid concentration remained unchanged during prolonged experiments.

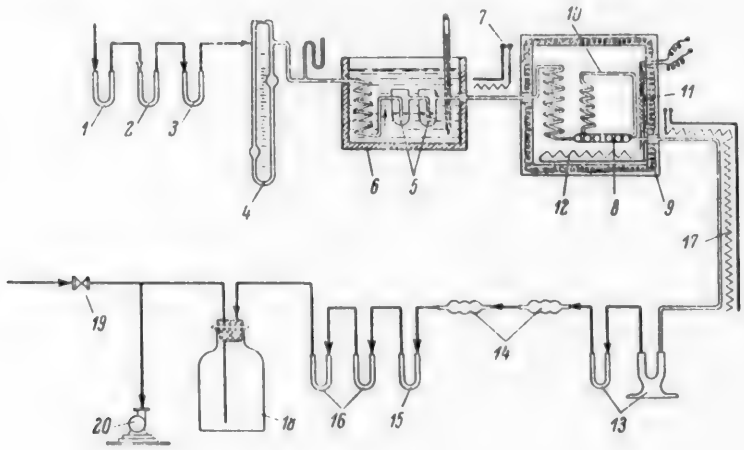

Fig. 1. Apparatus for determination of H_2SO_4 vapor pressure. 1) Tube with soda lime; 2, 15) tubes with $CaCl_2$; 3, 16) tubes with P_2O_5; 4) flow meter; 5) vessel for saturation with water; 6) water thermostat; 7) Nichrome spiral; 8) reaction vessel; 9) air thermostat; 10) siphon over reaction vessel; 11) heater for siphon bend; 12) open heater for air thermostat; 13) condensation vessels; 14) tubes with cotton wool plugs; 17) exit-tube heater; 18) air cushion; 19) by-pass valve; 20) vacuum pump.

The air rate was 250 cm^3/min ($v_0 \simeq 13$ liters/hr), so that most of the experiments could be performed within 3-6 hrs.

Storonkin and Susarev [19] and Bates and Kirschman [20] report the results of investigations at which air rates up to 10 liters/hr were used, and the results of preliminary experiments at rates up to 20 liters/hr agreed with data obtained at normal rates.

The apparatus used in the present investigation is shown in Fig. 1. Water vapor and CO_2 were removed from the air in U tubes filled with soda lime 1, calcium chloride 2, and P_2O_5 3; the air then passed through the flow meter 4 and entered a coil and two absorption bulbs 5 for preliminary saturation with water vapor. The absorption bulbs were contained in an air thermostat 6 equipped with a stirrer, thermometer, and thermoregulator. The air containing water vapor then passed along a short connecting tube, heated externally by means of a

Nichrome spiral 7, into the reaction vessel 8 contained in the air thermostat 9. The reaction vessel consisted of a glass tube 20 mm in diameter, with several U bends, of total length ~ 170 cm. This apparatus was filled with acid (~ 220 cm^3) which underwent mixing during the experiment, while circulating along a closed cycle consisting of the reaction vessel and the siphon 10. The mixing of the acid was effected by gentle heating of one of the ends of the siphon (a section about 5 cm long, and 1 cm^3 in volume) by means of a few turns of the Nichrome coil 11. The heated acid ascended up the siphon and returned to the thermostat temperature after passing through the siphon and coil.

The air thermostat was provided with two electric heaters. One passed within the thermostat walls, and maintained a temperature somewhat below the experimental, with the aid of an ammeter and rheostats. The second heater 12 was exposed on the thermostat floor, and was connected in circuit with a cathode relay and magnetic thermometer. The temperature fluctuations in the air thermostat did not exceed ± 0.15° owing to the operation of a fan, the adequate sensitivity of the magnetic thermometer, and the small thermal inertia of the open electric heater.

The absorption system consisted of two condensation vessels 13, two tubes 14 containing cotton wool plugs for absorption of H_2SO_4 mist, and U tubes 15 and 16, containing calcium chloride and P_2O_5, respectively.

The water -vapor pressure was calculated from the weight increase of the absorption system after subtraction of the weight of H_2SO_4 vapor, by means of the equation

$$P_{H_2O} = \frac{(P - p_1) \cdot v_{H_2O}}{(v_a + v_{H_2O} + v_{H_2SO_4})} .$$

where P is atmospheric pressure (in mm Hg), p_1 is the pressure reduction in the reaction vessel (in mm Hg), and v_{H_2O}, $v_{H_2SO_4}$, and v_a are the volumes of water, sulfuric acid, and air (in liters) reduced to standard conditions.

The amount of condensed sulfuric acid was determined volumetrically by means of 0.1 N and 0.01 N alkali solutions. The alkali was standardized against standard sulfuric acid and thrice-recrystallized oxalic acid. The standard sulfuric acid was checked gravimetrically. The partial vapor pressure of sulfuric acid was calculated by means of the equation

$$P_{H_2SO_4} = \frac{(P - p_1) \cdot v_{H_2SO_4}}{(v_a + v_{H_2O} + v_{H_2SO_4})} .$$

The concentration of the acid put into the reaction vessel was determined both gravimetrically and volumetrically. The agreement between the results of the two methods was quite satisfactory, and it was therefore only necessary to use the volumetric method for checking the acid concentrations during the experiments.

Acid samples for the concentration checks were taken into slightly warmed glass bulbs through a capillary sealed centrally in the upper portion of the loop-shaped reaction vessel. The acid concentrations both before and after each experiment were determined in triplicate. The change of acid concentration (ΔC) in the course of an experiment was 0.05-0.15%.

The amount of air passed through the reaction vessel was calculated from its flow rate through the flow meter and from the duration of the experiment. This calculation method was permissible because large amounts of air (from 40 to 290 liters) were passed through in the course of an experiment, and the flow meter was accurately calibrated. The accuracy of the meter readings was checked at intervals. Tests were first performed with air rates pf 20, 250, and 500 cm^3/min. These tests showed that equilibrium saturation of the vapor phase is obtained quite satisfactorily in our apparatus even at an air rate of 500 cm^3/min (Table 1).

To check the accuracy of the results given by this apparatus, the vapor pressures of pure water were determined at three different temperatures, and the results were compared with well-known literature data [21]. In the determinations of the vapor pressure of pure water the mean absolute error was 0.70 mm Hg, and the mean relative error was 0.85%.

The acid solutions used for determinations of the vapor pressures of sulfuric acid and water contained 91.15, 88.15, 84.5, 79.65, and 75.20% H_2SO_4, for experiments in the 100-182° range, and one experiment was performed with 91% acid at 191°.

TABLE 1

Results of Experiments with Different Air Rates

Air rate (cm^3/min)	Acid concentration (in %)	Experimental temp. (°C)	P (mm Hg)		Amount of air passed (liters)
			H_2SO_4	H_2O	
50	90.40	182	0.85	79.34	17.489
500	90.40	18	0.86	79.26	41.914
20 •	88.13	161	0.208	56.95	5.865
250	88.10	161	0.212	56.70	52.316

• The total volume of the air passed was measured in an aspirator in experiments at 20 cm^3/min.

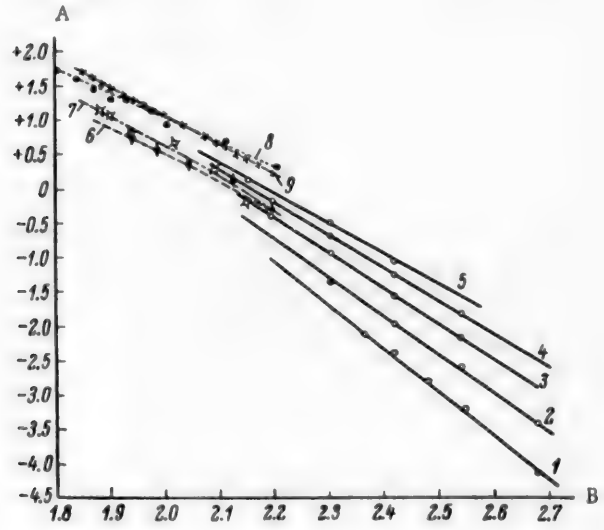

Fig. 2. Variation of log $P_{H_2SO_4}$ with 1/T for sulfuric acid solutions. A) Values of log $P_{H_2SO_4}$, B) values of $1/T \cdot 10^3$. Concentrations of H_2SO_4 (in %): 1) 75.20, 2) 79.65, 3) 84.50, 4) 88.15, 5) 91.15, 6) 89.25, 7) 91.26, 8) 95.26, 9) 98.06. Curves 1-5) results of the present investigation; 6-9) Thomas and Barker's data.

The equilibrium constant for the dissociation of H_2SO_4 vapor at 191°, calculated from the Bodenstein and Katayama equation [22], is

$$\log K = 3.0 - \frac{5000}{464} + 1.75 \cdot 2.6665 - 5.7 \cdot 10^{-4} \cdot 464 = -3.3741,$$

$$K = 0.00042.$$

The vapor pressure of sulfur trioxide, P_{SO_3}, in the vapor phase over 91% acid at 191°, according to this equation, is 0.0046 mm at $P_{H_2SO_4}$ = 1.373 mm (if the vapor phase is assumed to be a mixture of ideal gases). Thus, the degree of dissociation of sulfuric acid vapor at the maximum experimental temperature, over the strongest acid, is only 0.338%. It is therefore permissible to represent all the results in the form of partial pressures, $P_{H_2SO_4}$ and P_{H_2O}. These results are given in Tables 2-6. It is seen that the partial pressures of sulfuric acid are very low; most of the values are tenths, hundredths, or thousandths of a millimeter. The relative error for $P_{H_2SO_4} \approx 2.0\%$, and for $P_{H_2O} \approx 1.0\%$. Only in the case of the 75.20% acid, when $P_{H_2SO_4}$ is exceptionally

TABLE 2

Results of Experiments with Acid Containing 91.15% H_2SO_4

Experimental temperature (in °C)	Acid concentration (in %)	P (mm Hg)		Mean P	
		H_2SO_4	H_2O	H_2SO_4	H_2O
140	91.07	0.087	12.25	0.089	12.03
	91.15	0.091	11.81		
161	91.11	0.329	32.81	0.327	33.00
	91.20	0.324	33.19		
191	91.12	1.342	93.12	1.336	92.50
	91.21	1.331	91.88		

TABLE 3

Results of Experiments with Acid Containing 88.15% H_2SO_4

Experimental temperature (in °C)	Acid concentration (in %)	P (mm Hg)		Mean P	
		H_2SO_4	H_2O	H_2SO_4	H_2O
120	88.12	0.0165	9.23	0.0164	9.25
	88.09	0.0163	9.28		
140	88.09	0.057	22.66	0.059	23.04
	88.14	0.061	23.24		
	88.13	0.060	23.22		
161	88.08	0.212	56.70	0.210	56.83
	88.16	0.208	56.95 *		
182	88.32	0.689	122.15	0.678	122.73
	88.23	0.666	123.30		

* Air rate 20 cm^3/min.

TABLE 4

Results of Experiments with Acid Containing 84.5% H_2SO_4

Experimental temperature (°C)	Acid concentration (in %)	P (mm Hg)		Mean P	
		H_2SO_4	H_2O	H_2SO_4	H_2O
120	84.29	0.0075	21.96	0.0071	22.47
	84.27	0.0070	22.41		
	84.22	0.0068	23.04		
140	84.37	0.0288	48.05	0.0287	48.77
	84.47	0.0289	49.55		
	84.46	0.0283	48.70		
161	84.46	0.117	118.3	0.117	122.8
	84.57	0.114	112.4		
	84.51	0.119	112.6		
182	84.59	0.409	241.6	0.407	240.1
	84.57	0.406	238.6		

TABLE 5

Results of Experiments with Acid Containing 79.65% H_2SO_4

Experimental temperature, °C	Acid concentration (%)	P (mm Hg)		Mean P	
		H_2SO_4	H_2O	H_2SO_4	H_2O
100	80.07	0.00037	18.17	0.00039 •	18.37 •
	80.07	0.00038	18.32		
	79.78	0.00041	18.62		
120	79.69	0.00274	51.17	0.00273	50.67
	79.60	0.00268	50.52		
	79.69	0.00277	50.33		
140	79.62	0.0114	111.6	0.0113	109.7
	79.70	0.0111	110.0		
	79.61	0.0114	107.5		
161	79.50	0.0502	249.9	0.0484	246.9
	79.80	0.0467	243.8		

• This point was interpolated for 79.65% concentration, and the interpolated value is shown in Fig. 4.

TABLE 6

Results of Experiments with Acid Containing 75.20% H_2SO_4

Experimental temperature, °C	Acid concentration (%)	P (mm Hg)		Mean P	
		H_2SO_4	H_2O	H_2SO_4	H_2O
100	75.22	0.000076	39.01	0.000076	39.01
120	75.00	0.00075			
120	75.12	0.00073	99.01	0.00063	101.30
	75.20	0.00056	103.00		
	75.24	0.00051	102.00		
130	75.20	0.0023	149.10	0.0016	149.15
	75.20	0.0023	149.20		
	75.65	0.0012	—		
140	75.22	0.0047	208.5	0.0042	206.0
	75.20	0.0045	203.9		
	75.39	0.0035	205.4		
150	75.04	0.0084	315.1	0.0081	309.7
	75.00	0.0077	304.3		

TABLE 7

Coefficients A and B for Determination of $P_{H_2SO_4}$

Acid concentration (%)	Coefficients		Acid concentration (%)	Coefficients	
	A	B		A	B
75.20	12.592	6206	75.0	12.640	6237
79.65	11.415	5528	80.0	11.375	5500
84.50	10.914	5143	85.0	10.840	5095
88.15	10.403	4806	90.0	9.850	4525
91.15	9.456	4330			

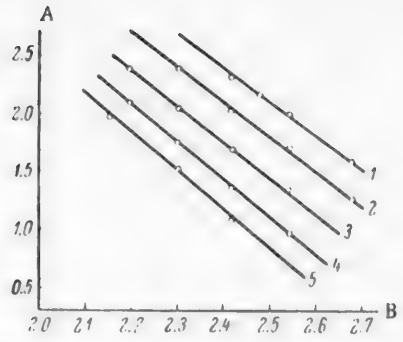

Fig. 3. Variation of log P_{H_2O} with 1/T for sulfuric acid solutions. A) Values of log P_{H_2O}, B) values of $1/T \cdot 10^3$. Concentrations of H_2SO_4 (in %): 1) 75.20, 2) 79.65, 3) 84.50, 4) 88.15, 5) 91.15.

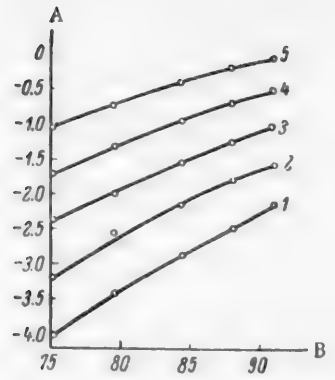

Fig. 4. Variations of log $P_{H_2SO_4}$ with the concentration of sulfuric acid. A) Values of log $P_{H_2SO_4}$, B) acid concentration (in %). Temperature (in °C): 1) 100, 2) 120, 3) 140, 4) 161, 5) 182.

TABLE 8

Partial Pressures of H_2SO_4 Vapor Over 91.2% Acid

Temperature (in °C)	Values of $P_{H_2SO_4}$ (mm Hg)		
	from this investigation	experimental, from Amelin's coefficients	rounded-off data of Thomas and Barker
140	0.094	0.128	—
161	0.302	0.344	—
191	1.333	1.213	0.832 •

• Experimental value 0.60.

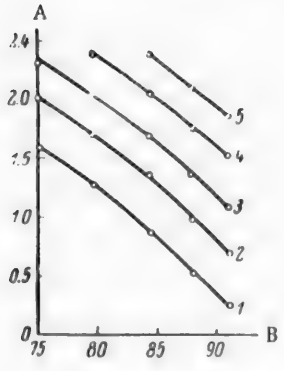

Fig. 5. Variation of log P_{H_2O} with the sulfuric acid concentration. A) Values of log P_{H_2O}, B) acid concentration (in %). Temperature (in °C): 1) 100, 2) 120, 3) 140, 4) 161, 5) 182.

small (from 0.000076 to 0.0081 mm) is the relative error ≃ 17%. In Figs. 2 and 3 the results are presented in the form of log P against 1/T. The values fit well on straight lines. Variations of log P_{H_2O} and log $P_{H_2SO_4}$ with the sulfuric acid concentration are plotted in Figs. 4 and 5. The slopes of the plots of the water vapor pressure increase with concentration and are not quite linear, being slightly concave toward the lower end.

The slopes of the plots of H_2SO_4 vapor pressure are similar, but diminish with increase of temperature. The results were used to calculate the coefficients A and B in the Clausius-Clapeyron equation for all the acid concentrations studied, and also for rounded values of the concentration — 75, 80, 85, and 90% H_2SO_4. The method of least squares was used for the calculations. The results are given in Table 7.

The vapor pressures of acids containing less than 91.2% H_2SO_4 were determined in this investigation.

Thomas and Barker gave the vapor pressures of stronger acids. Both sets of data are given in Figs. 2 and 6 in the form of plots of log P against 1/T.

TABLE 9

Partial Pressures of H_2O Vapor over Sulfuric Acid Solutions – Experimental and Calculated Results of Different Workers

Acid concentration (in %)	Temperature (°C)	P_{H_2O} (in mm Hg) found		
		in this study	by Tarasenkov	by Greenwalt
75	120	100.2	93.33	76.56
	140	225.4	218.8	169.8
80	140	102.8	90.16	85.51
	160	222.3	199.5	187.1
	180	447.7	416.9	382.0
85	140	44.36	38.91	35.56
	160	99.5	85.12	80.72
	180	207.5	177.8	169.9
90	140	16.29	—	11.12
	160	38.11	—	26.61
	180	82.60	—	59.0

TABLE 10

Coefficients A and B for Determination of P_{H_2O}

Acid concentration (in %)	Coefficients		Acid concentration (in %)	Coefficients	
	A	B		A	B
75.20	9.264	2862	75.0	9.266	2855
75.65	9.240	2975	80.0	9.240	2985
84.50	9.235	3119	85.0	9.231	3132
88.15	9.207	3239	90.0	9.195	3297
91.15	9.186	3337			

Our values are higher than the experimental data of Thomas and Barker (Table 8). The probable reason why their values are low is that they did not trap the sulfuric acid mist, as it was not detected visually. However, it is quite possible not to notice low concentrations of mist in observations of a small layer of air in a glass tube.

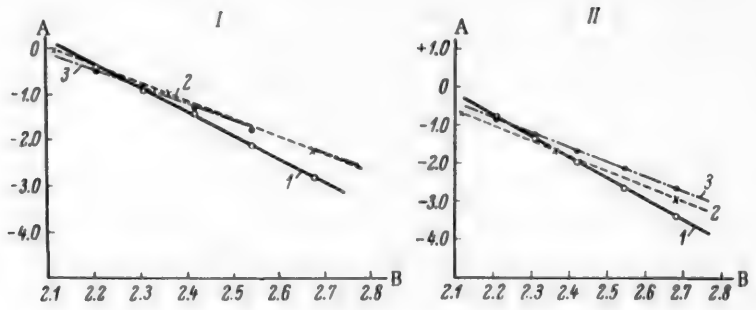

Fig. 6. Variation of log $P_{H_2SO_4}$ with 1/T for 85% (I) and 80% (II) acids. A) Values of log $P_{H_2SO_4}$, B) values of $1/T \cdot 10^{-3}$. 1) Our data, 2) Abel's calculated values, 3) extrapolated data of Thomas and Barker in Amelin's analysis.

TABLE 11

Test of the Results Obtained by Means of the Duhem-Gibbs Equation

Acid concentration (/)	Temperature (°C)	M	$-\frac{dP_1}{dP_2}$	$\frac{P_1 \cdot (1-M)}{P_2 \cdot M}$
75.5	120	0.361	0.0000129	0.0000128
	140	0.361	0.000030	0.000032
80.5	120	0.431	0.000091	0.000089
	140	0.431	0.000172	0.000177
	180	0.431	0.00054	0.00060
85.5	120	0.520	0.00051	0.00047
	140	0.520	0.00079	0.00081
	180	0 520	0.0019	0.0020
90.5	120	0.636	0.0019	0.0023
	140	0.636	0.0036	0.0032
	180	0.636	0.0035	0.0055

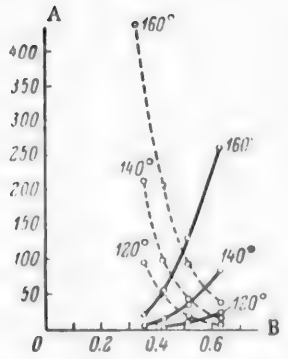

Fig. 7. Partial pressure of H_2SO_4 and H_2O over solutions of sulfuric acid as functions of their mole fractions. A) Partial pressure (mm Hg), B) mole fraction of H_2SO_4. Continuous line) $P_{H_2SO_4}$, broken line) P_{H_2O}.

The results of the present investigation were compared with Abel's calculated data and the experimental values as given by Amelin's analysis, over the entire range studied (Table 9). If these results are represented in the form of plots of log P against 1/T, it is seen that the slope of the line representing our data is somewhat different from the others (Fig. 6).

The coefficients A and B for determination of the pressure of H_2O vapor are given in Table 10. These coefficients were calculated by the method of least squares from the experimental results. The values found for the pressure of water vapor are compared in Table 9 with the values obtained by Tarasenkov and Greenwalt. Tarasenkov's values only go up to 100°. However, the results give satisfactory log P−1/T linear plots, so that the total vapor pressures over the temperature range in question, 100-180°, can be determined with reasonable reliability.

The accuracy of the results obtained in the present investigation was tested by means of the Duhem-Gibbs equation [23].

Since the increase of the mole fraction of the 1st component $dM(H_2SO_4)$ is equal to the increase of the mole fraction of the 2nd component $d(1-M)$, we may write:

$$\frac{dP_1}{dP_2} = \frac{P_1(1-M)}{P_2 \cdot M}. \qquad (2)$$

The results of the calculations are given in Table 11. The good agreement between the left-hand and the right-hand sides of the equation shows that the results obtained are fairly accurate; despite the exceptionally low values of $P_{H_2SO_4}$, they demonstrate a consecutive regularity in the variations of the partial pressures $P_{H_2SO_4}$ and P_{H_2O} with the composition of the liquid phase (Fig. 7).

The heats of evaporation of water and sulfuric acid from sulfuric acid solutions, calculated from the slope of the log P−1/T plots, are given in Table 12 and Fig. 8. The heats of evaporation of water found from the data of this investigation are fairly close to the values found both by Abel and by Porter [24]. Abel found the heats of evaporation of water by thermodynamic calculations based on experimental determinations of the heat capacity

TABLE 12

Heats of Evaporation of Water and Sulfuric Acid from Sulfuric Acid Solutions in the 100-180° Range

Acid concentration (in %)	Heat of evaporation of water (in kcal/mole) from data of			Heat of evaporation of H_2SO_4 (in kcal/mole)
	this study	Abel	Porter	
90.0	15.10	15.58	15.54	20.701
85.0	14.33	14.67	14.16	23.310
80.0	13.66	14.20	12.86	25.162
75.0	13.06	13.53	12.00	28.535

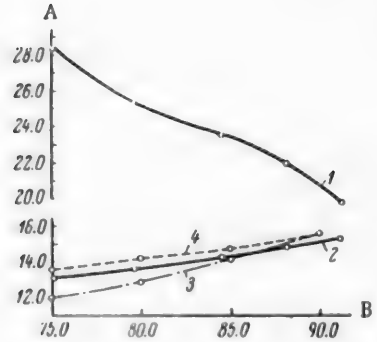

Fig. 8. Heats of evaporation of water and sulfuric acid from sulfuric acid solutions. A) Heat of evaporation (in kcal/mole), B) acid concentration (in %). Heats of evaporation from the data of: 1, 2) present investigation, for H_2SO_4 and H_2O, respectively; 3) Porter, for H_2O; 4) Abel for H_2O.

of the acid, carried out by Biron [25] and by Sokolik and Zavaritskii [26]. Porter's values for the heat of evaporation of water were calculated from the differential heat of dilution and the heat of evaporation of pure water. For determination of the differential heat of dilution, Porter used Pfaundler's [27] and Brösted's [28] experimental data on the heat of solution of SO_3.

There is little information [29-32] in the literature on the heats of evaporation of sulfuric acid and its solutions, and no data at all are available on acids containing from 57 to 98% H_2SO_4.

In contrast to the heat of evaporation of water, the heat of evaporation of sulfuric acid increases with decrease of the acid concentration (Table 12 and Fig. 8).

SUMMARY

1. In determinations of the vapor pressures of H_2SO_4 and H_2O over sulfuric acid solutions, the acid concentration can be maintained constant during the experiment if the transpiration method is used.

2. The pressures of water vapor found in this investigation are higher than the accepted values, and are in good agreement with Tarasenkov's data, obtained by a static method in 1955.

3. The heats of evaporation of sulfuric acid from 75-91% solutions, not reported in the literature, have been determined; values of the heat of evaporation of water from sulfuric acid have also been determined, the results being in good agreement with literature data.

In conclusion, I offer my deep gratitude to Professor A. G. Amelin for valuable advice in the course of this work, and to V. V. Illarionov and A. S. Lenskii for critical examination of the material.

LITERATURE CITED

[1] B. C. Burt, J. Chem. Soc. (London) 85, 1339 (1904).

[2] B. Briggs, J. Soc. Chem. Ind. 22, 1275 (1903).

[3] E. Sorel, Bull. Soc. Ind. Mulhouse 59, 240 (1889); Z. angew. Chem. 2, 272 (1889).

[4] H. V. Regnault, Ann. chem. phys. 3, 15, 129 (1845).

[5] W. Daudt, Z. Phys. Chem. 106, 255 (1923).

[6] I. R. McHaffie, J. Chem. Soc. 112 (1927).

[7] J. S. Thomas and A. G. Ramsay, J. Chem. Soc. 123, 3256 (1923).

[8] J. S. Thomas and W. F. Barker, J. Chem. Soc. 127, 2820 (1925).

[9] M. Kh. Karapet'iants, Chemical Thermodynamics [in Russian] (Goskhimizdat, 1949), p. 174.

[10] G. H. Greenwalt, Ind. Eng. Chem. 17, 522 (1925).

[11] J. R. I. Hupburn, Proc. Phys. Soc. 40, 249 (1928).

[12] A. Grollman and J. Frazer, J. Amer. Chem. Soc. 47, 712 (1925).

[13] S. Schankman and A. Gordon, J. Amer. Chem. Soc. 61, 2370 (1939).

[14] E. W. Hornung and W. J. Giauque, J. Amer. Chem. Soc. 77, 10, 2744 (1955).

[15] E. M. Collins, J. Phys. Chem. 37, 9, 1191 (1933).

[16] D. N. Tarasenkov, J. Appl. Chem. (USSR) 28, 10, 1098 (1955).*

[17] A. G. Amelin, Theoretical Principles of Mist Formation in Chemical Industries [in Russian] (Goskhimizdat, 1951), p. 136.

[18] E. Abel, Z. Phys. Chem. 3, 50, 260, 83 (1946).

[19] A. V. Storonkin and M. P. Susarev, J. Leningrad Univ. 6 (1952).

[20] S. J. Bates and H. D. Kirschman, J. Amer. Chem. Soc. 12, 12, 1991 (1919).

[21] Technical Encyclopedia, Physicochemical Data 5, 362.

[22] M. Bodenstein and M. Katayama, Z. phys. Chem. 69, 26 (1909).

[23] B. F. Dodge, Chemical Engineering Thermodynamics [Russian translation] (IL, Moscow, 1950), p. 626.

[24] A. W. Porter, Trans. Faraday Soc. 13, 373 (1918).

[25] E. Biron, J. Russ. Phys.-Chem. Soc. 31, 171 (1899).

[26] A. S. Sokolik, J. Gen. Chem. (USSR) 2, 311 (1932).

[27] L. Pfaundler, Ber. 4, 75 (1871); Wien, Ber. 64, 240 (1871).

[28] J. N. Brönsted, Z. phys. Chem. 56, 664 (1906); 75, 325 (1911).

[29] E. Beckman, Z. phys. Chem. 53, 129 (1905).

[30] C. C. Person, Compt. rend. 23, 336, 926 (1847).

[31] M. S. Vrevskii, J. Russ. Phys.-Chem. Soc. 59, 69 (1927).

[32] M. S. Vrevskii and B. N. Nikol'skii, J. Russ. Phys.-Chem. Soc. 59, 77 (1927).

Received February 25, 1957

* Original Russian pagination. See C. B. translation.

PURIFICATION OF EXHAUST GASES OF THE TOWER SULFURIC ACID SYSTEM IN EQUIPMENT OF THE VENTURI-TUBE TYPE

M. L. Varlamov, G. A. Manakin, and Ia. I. Starosel'skii

The Odessa Polytechnic Institute

The aim of this work was to test equipment of the Venturi-tube type for removal of spray, sulfuric acid mist, and nitrogen oxides from exhaust gases of the tower sulfuric acid system. An experimental model of the tower system used in one of the sulfuric acid plants was used for the experiments. Apart from prevention of air pollution, it should be possible to decrease nitric acid consumption and sulfuric acid losses by this method.

The acidity of exhaust gases in tower systems is due mainly to the presence of nitrogen oxides (~ 0.2-0.35% of NO and NO_2, or 6-10 g of HNO_3/m^3 gas), usually with NO at a low degree of oxidation, which makes the purification considerably more complicated.

In addition, the gases contain spray, sulfuric acid mist (1.5-3 g of H_2SO_4/m^3 gas), and sulfur dioxide [1, 2].

The acidity of the exhaust gas depends on the operating rate of the system, its design characteristics, technological process parameters, the technical state of the equipment, the acid-distributing devices, etc.

Separation of H_2SO_4 spray and mist may be effected by means of wet electrical precipitators installed at the end of the system; however, these do not trap the gaseous components, nitrogen oxides and SO_2. Electrical precipitators do not always give a sufficiently high degree of gas purification [3].

The contents of H_2SO_4 in the exhaust gas can be roughly halved by the use of concentrated sulfuric acid for spraying the last absorption tower of the system [4], while losses of nitrogen oxides are reduced by 30-35% [5]. The use of imported acid is hardly suitable, because of the high consumption.

Tall stacks do not solve the problem of purification of the exhaust gases and removal of valuable constituents from them, but merely diminish the harmful effects of the gases on the surroundings.

Devices of the Venturi-tube type are successfully used for purification of exhaust gases in a number of industries [6-8]. To the best of our knowledge, such equipment has not been used in tower sulfuric acid plants.

The experimental plant used for the experiments consisted of two units – a small unit operating at up to 50 m^3/hr, and a large unit operating at up to 500 m^3/hr. The small unit was used for tests on: Tube No. 1 (Fig. 1), with oblique liquid feed, and Tube No. 2 (Fig. 2), with liquid fed tangentially into a mixing chamber, from which the liquid was distributed uniformly around the divergent perimeter of the tube. In this design of the tube the gap between the convergent and divergent tubes can be varied by rotation of the apparatus head.

In Apparatus No. 3 (Fig. 3) the liquid was fed radially. The separator in the small unit had concentric walls, so that the passing gas impinged twice on the liquid surface.

The large unit was used for tests on Tube No. 4 (Fig. 4) with radial feed of liquid in mutually perpendicular directions, with a short-cyclone separator of the TsKTI (Central Scientific Research Institute for Boilers and Turbines) type. Central feeding of the liquid was not used in the experiments described.

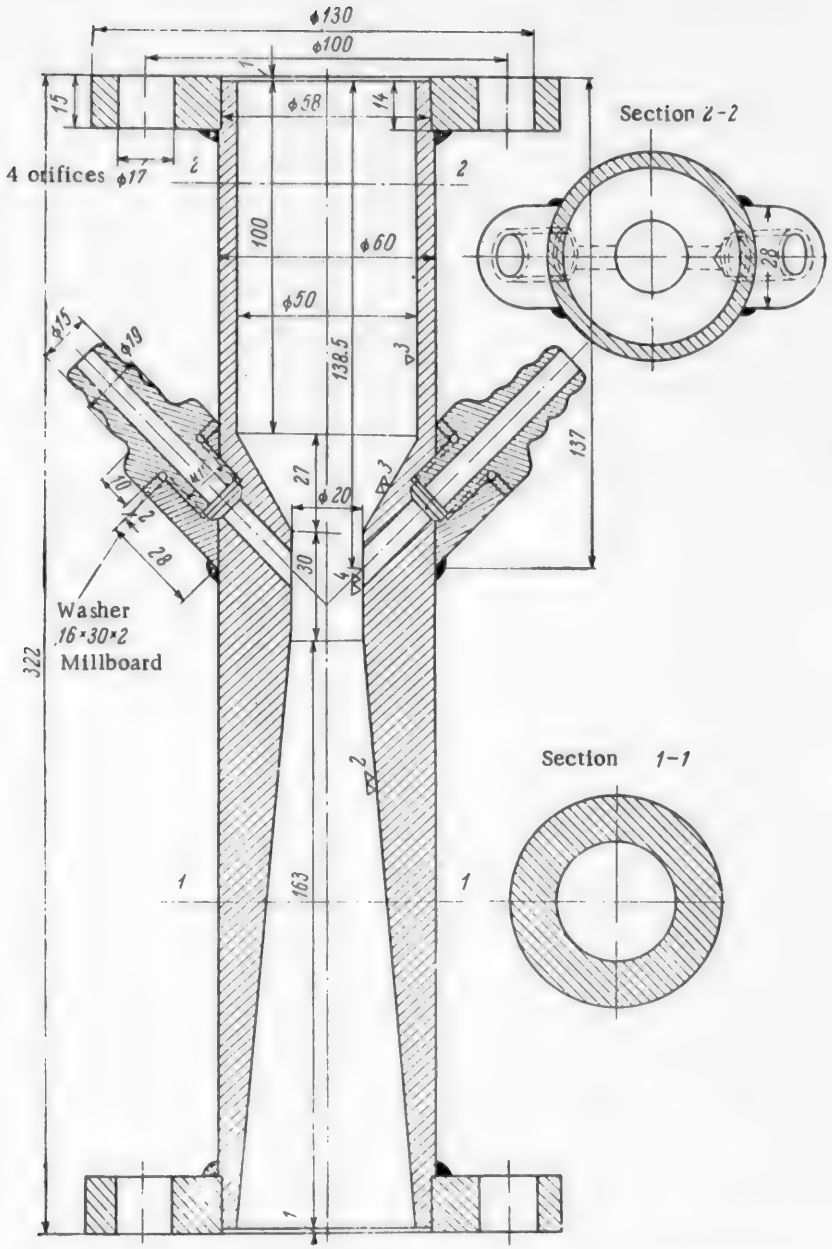

Fig. 1. Apparatus No. 1, with liquid feed oblique to the tube axis (all dimensions in mm, as in Figs. 2, 3, and 4).

The liquid used for absorption was water; this can then be fed into the reaction zone of the tower system, instead of process water, together with the absorbed nitrogen oxides and sulfuric acid. Exit gases have been cleaned in packed towers in a similar manner [9, 10].

Sodium carbonate solution containing 5-30 g of soda per liter was also used as the absorbent. Because of the difficulties involved in analysis of the gas and liquid phases, several different schemes were tested in the experimental unit (Fig. 5). The gas for the experiments was withdrawn from the gas conduit connecting the last

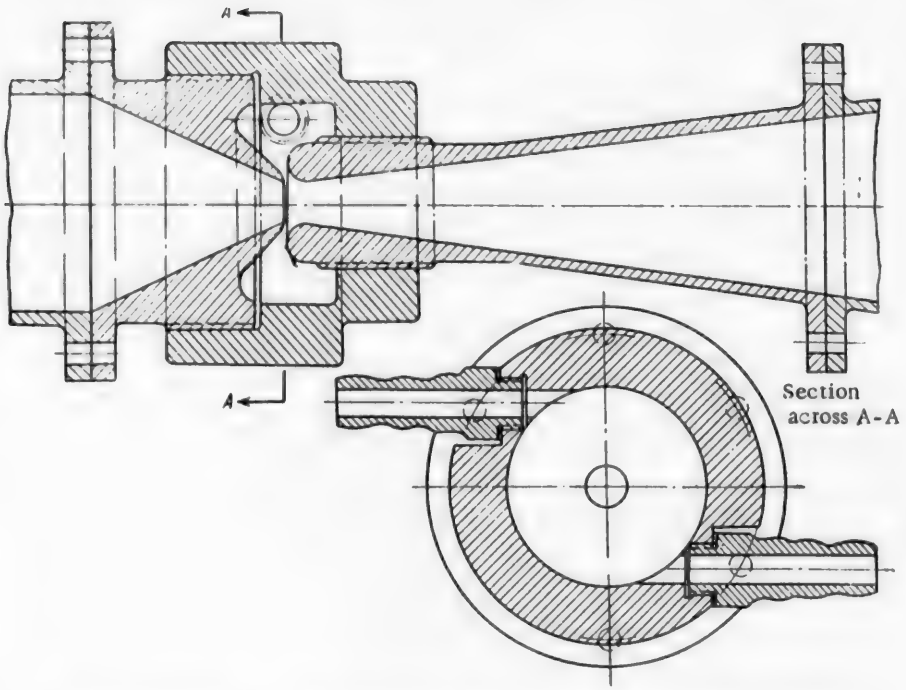

Fig. 2. Apparatus No. 2, with liquid fed tangentially into the mixing chamber.

tower of the system to the exit-gas cyclone, and drawn through the unit by suction from the last exhaust fan of the plant.*

The flow rate of the gas in Apparatus No. 4 was measured by means of a Venturi meter, and in the small unit, by means of a sharp-edged orifice.

The liquid flow rate was determined by means of calibrated flow meters. For check measurements, the liquid was collected in measuring vessels.

Analysis of the gas for H_2SO_4 spray and mist and nitrogen oxides was carried out by means of glass wool and absorbent cotton-wool plugs and evacuated bottles 20 liters in capacity; No. 4 glass filters and colorimetric tubes were also used. The analytical data were analyzed and the results calculated by the usual methods [11].

The SO_2 concentration in the exit gases was low ($\sim 0.1\%$) in the experimental conditions used. As the concentration of nitrogen oxides was also relatively low, any oxidation of SO_2 during extraction of the gas for analysis could be neglected.

The ratio of the gas and liquid volumes (G: L), a dimensionless quantity, was used as one of the principal parameters, the volume of the gas being reduced to standard conditions. This parameter determines the gravimetric gas rate and the hydrodynamic conditions in the apparatus. The specific liquid rate (in liters/m^3 gas) is the reciprocal of the G: L ratio.

Hydrodynamic studies of gas and liquid flow in these tubes showed that with oblique feed of liquid the hydraulic resistance (Δp) of the apparatus is considerably less than with radial feeding, as Fig. 6 shows. The value of Δp for Tube No. 2 increases with increase of the gap between the convergent and divergent tubes. The variation of Δp with the gas rate for Apparatus No. 4 is shown in Fig. 7. At G: L ratios ≥ 1000, Δp depends

* Laboratory assistants N. M. Kazakova, M. Iu. Viner, M. S. Gutman, V. Kosovets, and P. Varvarskaia took part in the analytical work.

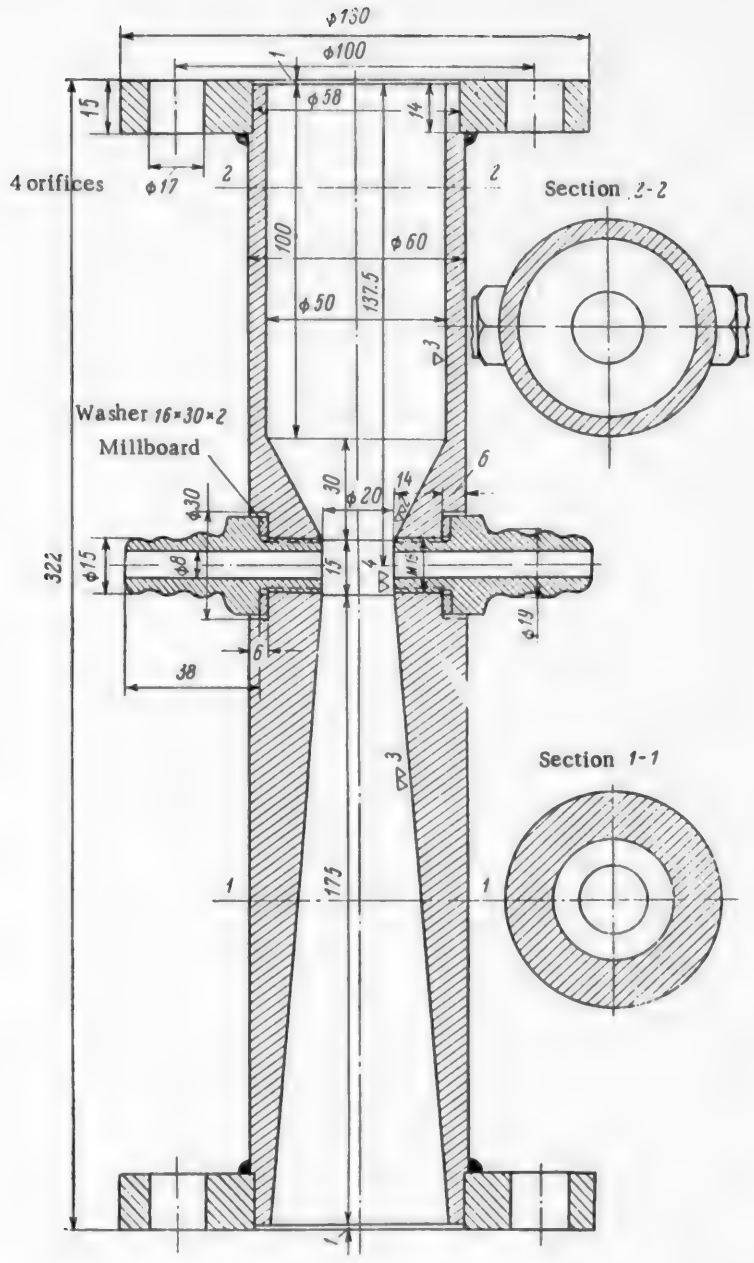

Fig. 3. Apparatus No. 3 with liquid fed radially to the tube axis.

little on the ratio, and is 40-120 mm H_2O, according to the equipment design, the gas velocity in the tube throat, the liquid rate, and the method of liquid feed.

The absorption of acid constituents from the exit gases was characterized in terms of acidities calculated as g H_2SO_4 per cubic meter of gas (Parameter A) and g H_2SO_4 per liter of solution (Parameter B), found from the results of titration of the liquid at the entry and exit of the apparatus. Parameters A and B are connected by the relationship: $\frac{B}{A} = \frac{G}{L} \cdot 1000$.

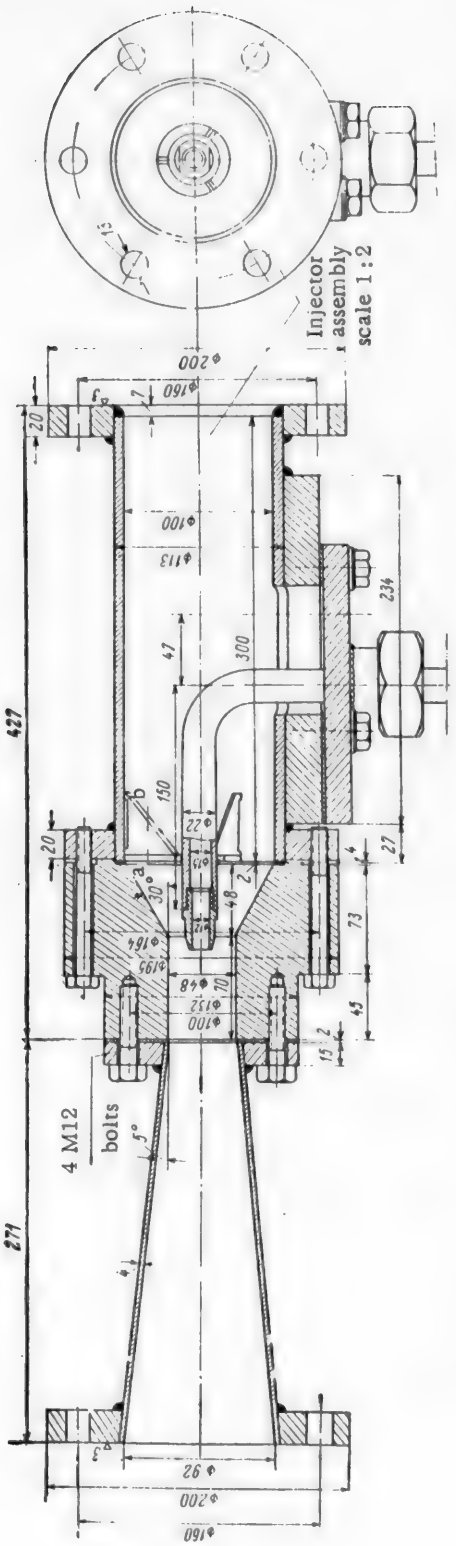

Fig. 4. Apparatus No. 4 with radial and central liquid feed (radial feed not shown).

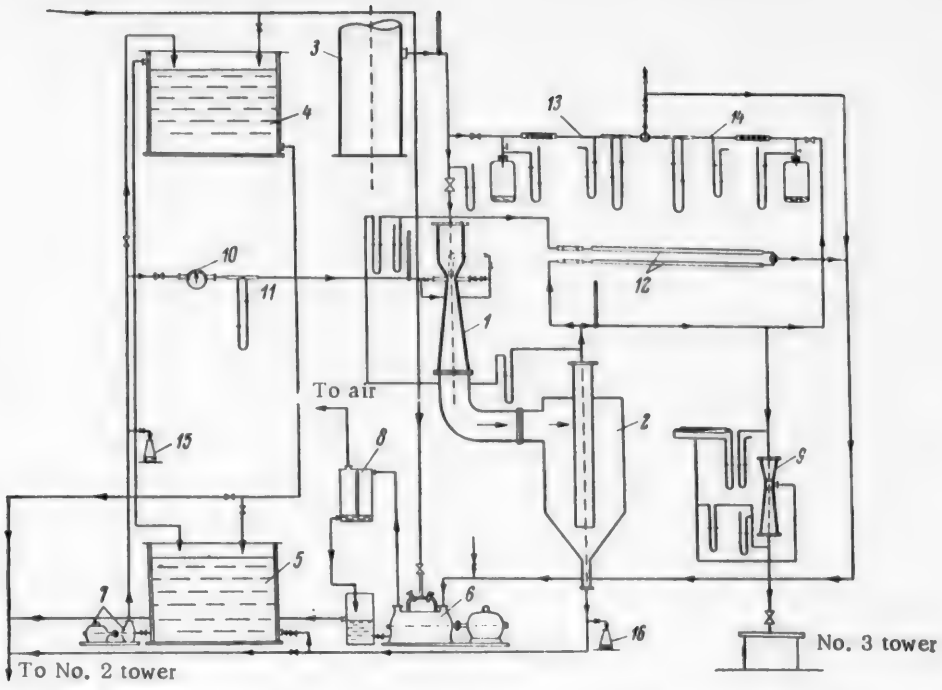

Fig. 5. Schematic diagram of the large unit. 1) Apparatus No. 4; 2) separator; 3) stand pipe connecting the last absorption tower of the system with the exit-gas cyclone of the system; 4) header tank; 5) circulation tank; 6) RMK vacuum pump; 7) centrifugal pump; 8) RMK spray trap; 9) Venturi meter; 10) water meter; 11) flow meter for liquid entering the apparatus; 12) colorimetric tubes; 13) line for gas sampling at entry to apparatus; 14) the same, at exit; 15) sampling of liquid at entry; 16) the same, at exit.

The experimental results show that A decreases with increasing G : L ratio, and depends relatively little on the gas rate. Parameter B increases slightly with increase of G : L ratio and depends little on the gas rate. Values of A for different tubes are compared below.

Parameter A as a Function of the G : L Ratio

Tube No.	Tube diameter, mm	Parameter A for G : L ratio				Liquid	Indicator
		250	500	700	1000		
1	20	1.05	0.9	0.73	0.52	Water	Methyl orange
2	11	3.3	3.05	2.7	2.5	The same	Phenolphthalein
3	20	2.8	2.5	2.1	1.80	"	The same
4	48	5.5	4.6	3.85	3.1	Soda solution	"
4	48	3.3	3.15	3.0	2.8		Mixed indicator

These results show that the highest values of A are found for Tubes Nos. 4 and 2, and the lowest, for Tube No. 1.

The degrees of absorption (η) of acid components from tower exhaust gases with the use of different tubes are compared below.

Values of η for Different Tubes

Tube no.	Throat diameter (mm)	Gas rate (in nm³/hr)		Gas velocity in throat (m/sec)		Absorbent	η for G : L ratio of			
							250	500	750	1000
1	20	33	60	29.4	52.9	Water	35.0	31.5	27.5	24
2	11	23	58	67.3	170		26.5	27.2	28.0	29
3	20	27	59	23.7	52.0		—	34.0	28.0	22
4	48	220	490	33.8	74.5	Soda solution	38.5	39.0	39.5	40

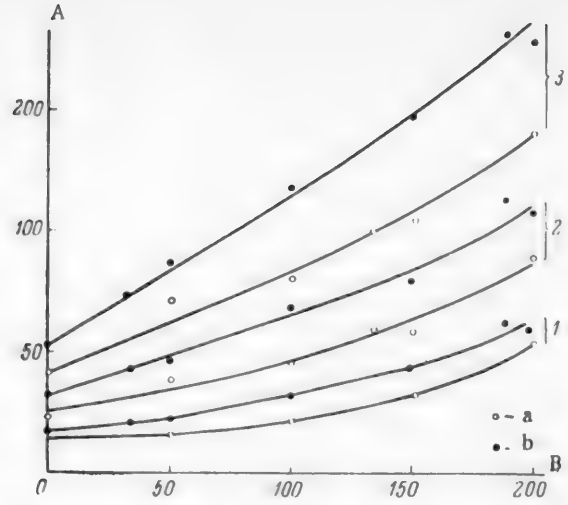

Fig. 6. Comparison of the hydraulic resistance in Tubes Nos. 1 and 3 with equal throat diameters and equal gas rates. A) Hydraulic resistance Δp (in mm H_2O), B) water rate (liters/hr). Gas rates (in m^3/hr): 1) 20, 2) 30, 3) 40. Data for tubes: a) No. 1, b) No. 3.

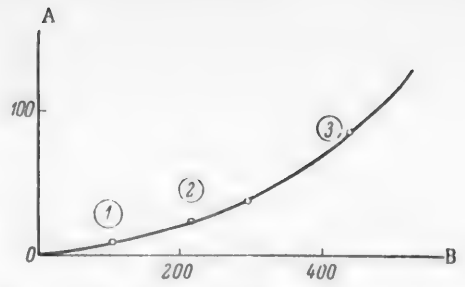

Fig. 7. Hydraulic resistance of Tube No. 4 as a function of the gas rate, with liquid rate 145-160 liters/hr. A) Hydraulic resistance Δp (in mm H_2O), B) gas rate (in m^3/hr). G: L ratio: 1) 660, 2) 1330, 3) 2700.

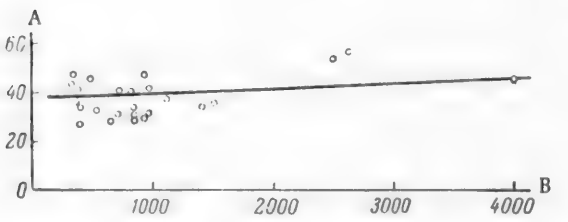

Fig. 8. Variation of the degree of purification η of exit gases with the G: L ratio in Apparatus No. 4. A) Degree of absorption η (%), B) G: L ratio.

It follows from these results that at G: L > 500, with water as absorbent, the highest values of η were obtained with Tube No. 2. At high G: L ratios the performance of Apparatus No. 1 is better than that of No. 3, and at low ratios the reverse is true.

The absorption of sulfuric acid spray and mist in the tubes was also determined separately. Average results of a large number of experiments with Tube No. 4 showed that at a gas rate of ~ 400 m^3/hr, with an average content of H_2SO_4 spray of 1.4 g/m^3 at entry, $\eta \simeq$ $\simeq$ 80%, and this value depends little on the G: L ratio.

In apparatus No. 4 with the use of sodium carbonate solution, it was possible to reach $\eta \simeq$ 40%; this value depends little on the G/L ratio, as Fig. 8 shows. The average content of acid components in the gases entering the tubes was 8-10 g per m^3, and consisted mainly of nitrogen oxides.

Such absorption is slower in packed towers [9, 10] despite the high concentration of spray and mist and the longer time during which the gas remains in the apparatus (18-25 seconds instead of 0.22 second).

Investigations have shown [12, 13] that the degree of absorption of spray and mist in tubes can be even higher.

A comparison of the degree of absorption (η) of nitrogen oxides from nitrous gases in equipment of different design shows that our values of η are of the same order as those found by others [5, 10, 14-17], but the absorption process is much more rapid in the Venturi tube, while the dimensions of the equipment are much smaller. Our relatively low values of η may be mainly attributed to the fact that the nitrogen oxides were not in a condition suitable for absorption.

Process conditions in the tower system which give slight over-oxidation of NO at the end of the system should favor an increase of the degree of absorption of nitrogen oxides from exit gases by alkalies. For evaluation of the performance of equipment of the Venturi tube type, and for comparison of efficiency of these tubes with that of packed towers, the transfer coefficients were calculated, with the aid of the critical relationship $Nu' = \varphi(Re, Pr)$, for spray equipment [18], and with the aid of the Nukiyama and Tanasawa equation [19] for calculation of the mean drop diameter.

The coefficient for the absorption rate of N_2O_3, calculated for the throat of the tube, was found to be ~ ~ 400,000 kg $N_2O_3/m^3 \cdot hr \cdot atmos$. The value calculated for the apparatus as a whole is considerably lower. The experimental value of this same coefficient is 50,000 kg $N_2O_3/m^3 \cdot hr \cdot atmos$ which is roughly 80-100 times the value for packed towers.

The total energy consumption in the unit, calculated per ton of H_2SO_4, is 5-6 kw-hr, which is 10-12% of the total energy consumption per ton of sulfuric acid produced in the tower system.

In these calculations the G: L ratio was taken as 1000-1200, and Δp = 250 mm H_2O, with a certain allowance for the resistance of the lines and separator.

SUMMARY

1. With a linear gas velocity of 30-75 m/sec in the tube throat, G: L ratio 750-1250, and with water as absorbent, the hydraulic resistance Δp of the tubes was 40-120 mm H_2O. Lower values of Δp are obtained with tubes with oblique feed of liquid.

2. In the absorption of H_2SO_4 spray and mist and nitrogen oxides, of equivalent concentration ~ 10 g H_2SO_4/m^3 gas (acidity calculated in terms of H_2SO_4), in alkali solutions in Venturi-type tubes, the degree of absorption was ~ 40%.

3. The relatively low total degree of purification of the exit gases may be attributed to the fact that the nitrogen oxides, which are the main cause of acidity in the exit gases, were not in a suitable state for absorption.

4. The energy consumption in the purification of exit gases from the tower system of the chamber process by means of equipment of the Venturi-tube type is 5-6 kw-hr per ton of H_2SO_4, which is 10-12% of the energy required for the production of chamber sulfuric acid.

LITERATURE CITED

[1] N. I. Smyslov and I. I. Bulygin, Data on Exchange of Experience, Sci. Res. Inst. Fertilizers and Insectofungicides 4 (1953).

[2] K. M. Malin and K. A. Poliakov (editors), Sulfuric Acid Handbook (Goskhimizdat, 1952).*

[3] Gas Cleaning Equipment and Its Adoption in Electrical Power Plants and Industrial Undertakings (Gosenergoizdat, 1953).*

[4] N. I. Smyslov, Data on Exchange of Experience, Sci. Res. Inst. Fertilizers and Insectofungicides 5 (1954).

[5] N. Sh. Safiulin and M. I. Olevinskii, J. Chem. Ind. 3 (1955).

[6] W. Jones, Ind. Eng. Chem. 41, 11, 242 (1949).

[7] H. Johnston and R. Feild, Ind. Eng. Chem. 8 (1954).

[8] Ekman and H. Johnston, Ind. Eng. Chem. 6 (1951).

[9] A. V. Sokol'skii, J. Chem. Ind. 2 (1954).

[10] N. Price and A. Dooley, Chem. Ind. 54, 9 (1935).

[11] K. M. Malin (editor), Control of Sulfuric Acid Production (Goskhimizdat, 1942).*

[12] B. P. Volgin and F. S. Maron, Use of New Equipment for Scrubbing Sulfur Dioxide (Ural Chemical Scientific Research Institute, 1954).*

[13] B. P. Volgin, F. S. Maron, et al., Use of New Equipment for Scrubbing Sulfur Dioxide (Ural Chemical Scientific Research Institute, 1952-1953).*

[14] I. N. Kuz'minykh, J. Chem. Ind. 3 (1953).

[15] N. M. Zhavoronkov, J. Chem. Ind. 7 (1954).

[16] V. I. Atroshchenko, Nitric Acid Technology (Goskhimizdat, 1949).*

[17] S. N. Ganz and S. B. Kravchinskaia, J. Appl. Chem. 28, 2, 145 (1955).**

[18] V. M. Ramm, Absorption Processes in Chemical Industry (Goskhimizdat, 1951).*

[19] H. Lewis and Edwards, Ind. Eng. Chem. 1 (1948).

Received June 19, 1956

* In Russian.

** Original Russian translation. See C. B. translation.

SCRUBBING ABSORPTION OF CARBON DIOXIDE IN POTASSIUM CARBONATE SOLUTION

I. G. Plit

The Dnepropetrovsk Institute of Chemical Technology

The absorption of carbon dioxide in potassium carbonate solution is a very widely used industrial process [1]. Nevertheless, it is not sufficiently well understood, and deeper studies of it are needed for the solution of a number of practical problems.

According to the accepted classification [2, 3], the absorption mechanism in the system in question corresponds to chemisorption with a reversible chemical reaction in the liquid phase. This mechanism is represented schematically in Fig. 1. The concentration of the gas being absorbed varies from P to the equilibrium value P_i within the limits of the gas film δ_G. When the gas comes into contact with the liquid, a monomolecular layer is neutralized at the interface. This is followed by displacement of the reaction zone into the liquid film δ_L (as shown in Fig. 1) until a dynamic equilibrium is established; equivalent amounts of the absorbed gas and of the chemically active part of the absorbent then reach the reaction zone. The reaction zone then divides the diffusion zone (liquid film) into a neutralized portion $\alpha \cdot \delta_L$ and a nonneutralized portion $(1 - \alpha)\delta_L$, while the concentration of the dissolved gas in the neutralized portion varies from x_i at the interface to the equilibrium value x_e in the reaction zone. Pozin's kinetic equation for scrubbing absorption in such systems contains quantities the experimental determination of which involves certain difficulties. Therefore, the following equation:

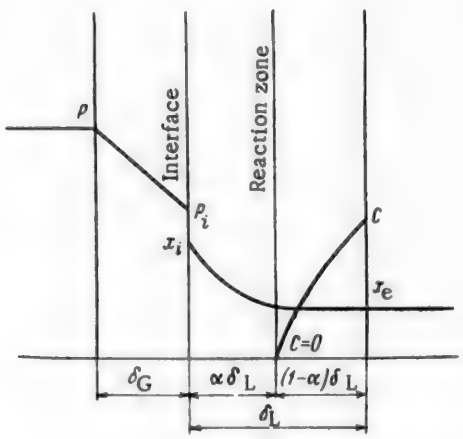

Fig. 1. Schematic representation of the mechanism of absorption.

$$\frac{G}{F \cdot \tau} = K \cdot C_m, \tag{1}$$

where the driving force is expressed in terms of the mean logarithmic difference of the solution capacity, C_m (in moles/liter), has been used for analysis of experimental data.

It should be noted that the chemical capacity of the solution across the nonneutralized film varies between C at the inner boundary of the film and C = 0 in the reaction zone. With this interpretation of the driving force, the absorption coefficient has the value $K = \frac{D_2}{(1-\alpha)\delta_L}$, and therefore depends on the position of the reaction zone. Theoretical analysis shows that the position of the reaction zone itself depends on the parameters of the two phases; we therefore express the absorption coefficient K in terms of nominal partial coefficients each of which excludes the influence of one of the phases

$$K = \frac{1}{\frac{1}{H \cdot K_G} + \frac{1}{K_L}} . \qquad (2)$$

For a countercurrent scrubber these coefficients have the following values under any operating conditions [4]:

$$K = \text{const} \frac{\left(\frac{l}{d}\right)^{1/2} \cdot \left[W\left(1 - \frac{U}{W}\right)\right]^{0.75} \cdot \gamma_G^{0.25}}{d^{0.25} \cdot \eta_G^{0.75}} , \qquad (3)$$

$$K_L = \text{const}' \frac{U^{1/2} \cdot \gamma_L^{1/6}}{\left(\frac{l}{d}\right)^{1/2} \cdot \eta_L^{5/6}} . \qquad (4)$$

where l is the height of a packing unit (in m), d is the diameter of a packing unit (in m); U is the velocity of the absorbent (in m/hr), γ is the density (in kg/m^3), η is the viscosity (in poises), H is the Henry constant (atmos · mole/liter), W is the gas velocity (in m/hr).

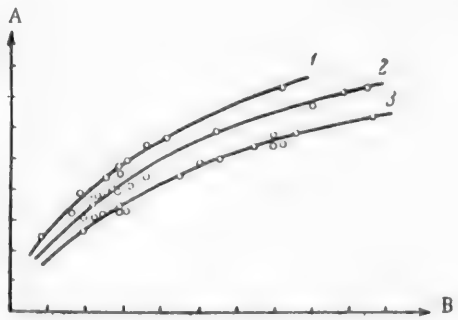

Fig. 2. Variation of the nominal absorption coefficient K_L with the velocity of the liquid phase. A) Coefficient K_L (in kg/m^2 · hr · mole/liter), B) velocity of the liquid phase U (in m/hr). Solution concentration (normality) and temperature (°C) respectively: 1) 1.8, 16; 2) 2, 30; 3) 2.85, 20.

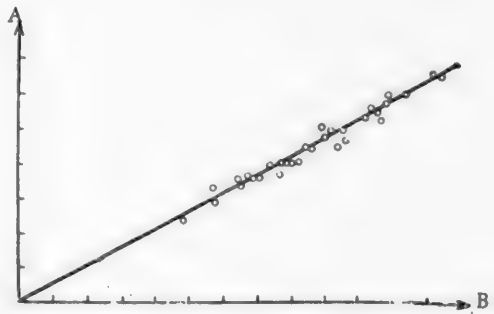

Fig. 3. Variation of the nominal partial absorption coefficient K_L with the parameters of the liquid phase. A) Coefficient K_L (in kg/m^2 · hr · mole/liter), B) value of $U^{1/2} \cdot \gamma_L^{1/6} / \left(\frac{l}{d}\right)^{1/2} \cdot \eta_L^{5/6}$.

The constant H was calculated from the equilibrium constant for the reaction $K_2CO_3 + CO_2 + H_2O \rightarrow 2KHCO_3$ as the ratio of the equilibrium partial pressure of carbon dioxide in the gas to its equilibrium concentration in solution.

The object of the present investigation was determination of the proportionality constants in Eqs. (3) and (4), and of the influence of various factors in the kinetics of the absorption process.

The experimental unit consisted of an absorption column 25.5 mm in diameter packed with 8 × 8 × 2 rings. The packing height was 465 mm.

In determinations of the nominal partial absorption coefficient K_L the influence of the gas phase was excluded by the use of 100% carbon dioxide for absorption. The experiments were performed over a considerable range of liquid velocities, from 1.83 to 18.7 m/hr, calculated for the open section of the scrubber, between 16 and 30°. The capacity of the absorbent was varied from 1.45 to 2.8 moles/liter.

Figure 2 shows a plot of the nominal partial coefficient K_L as a function of the average linear liquid velocity U. The nature of the curves confirms that $K_L \propto U^{1/2}$, as should follow from Eq. (4). The influence of the physical properties of the absorbent is represented by the expression $K_L \propto \gamma_L^{1/6} / \eta_L^{5/6}$; this is confirmed by Fig. 3, where the results of all the experiments lie on a straight line passing through the coordinate origin. This proves the validity of Eq. (4) for the nominal partial coefficient of absorption, and confirms that the proportionality

factor in this equation is constant. Its numerical value is the tangent of the slope of the curve, and is equal to $6.28 \cdot 10^{-5}$.

We thus have the final equation

$$K_L = 6.28 \cdot 10^{-5} \frac{U^{1/3} \cdot \gamma_L^{1/3}}{\left(\frac{l}{d}\right)^{1/3} \cdot \eta_L^{2/3}} \left(\frac{\text{kg}}{\text{m}^2 \cdot \text{hr} \cdot \text{mole/liter}}\right) \quad (5)$$

which relates the principal parameters of the liquid phase with the nominal absorption coefficient.

The nominal partial coefficient K_G was found by calculation. The value of K is found from an experiment with the use of a diluted gas; K_L being known, we find, from Eq. (2)

$$K_G = \frac{K_L \cdot K}{H(K_L - K)}.$$

Fig. 4. Variation of the nominal partial absorption coefficient K_G with the parameters of the liquid phase. A) Coefficient K_G (in kg/m^2 · hr · atmos), B) $\frac{\left(\frac{l}{d}\right)^{0.5}}{\left[W\left(1-\frac{U}{W}\right)\right]^{0.75} \cdot \gamma_G^{0.25}/d^{0.25} \cdot \gamma_G^{0.75}}$.

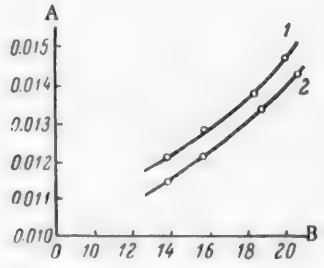

Fig. 5. Variation of the Henry constant with the gas concentration for 2 N K_2CO_3 solution at 25°. A) Constant H (in atmos/mole/liter), B) CO_2 concentration in gas (%). Relative velocity (W/U): 1) 80, 2) 62.

The system in question does not conform to Henry's law, and therefore the constant H varies with the concentrations of the reactants and therefore has different values at different heights of the column. However, since the nature of this variation along the height of the column is represented, under otherwise equal conditions, by a family of curves of the same type, this quantity can be adequately characterized by consideration of a definite cross section of the scrubber. The most convenient section is the bottom of the scrubber, where the concentrations of the incoming gas and the outgoing solution are always known. These data were used for calculation of H.

Figure 4 shows the variation of the nominal gas-film coefficient K_G with its determining parameters. It is seen that, irrespective of the gas velocity, which was varied in the experiments in the range W = 100-900 m/hr calculated on the open section of the column, of the concentration of the carbon dioxide absorbed from the air, which varied from 10 to 50% by volume, and of the absorption temperature between 20 and 30°, this relationship is linear. The slope of this curve gives the average value of the proportionality factor $2.55 \cdot 10^{-6}$, and the influence of the gas phase on the absorption coefficient can be represented by the equation

$$K_G = 2.55 \cdot 10^{-6} \frac{\left(\frac{l}{d}\right)^{0.5}\left[W\left(1-\frac{U}{W}\right)\right]^{0.75} \cdot \gamma_G^{0.25}}{d^{0.25} \cdot \gamma_G^{0.75}} \text{ (kg/m}^2 \cdot \text{hr} \cdot \text{atmos)} \quad (6)$$

For a complete characterization of the absorption coefficient K it is necessary to elucidate the variation of the constant H with its determining parameters. Theoretical analysis shows that these parameters are the concentration of the gas being absorbed, the temperature, the relative velocity of the phases, and the concentration of the absorbent solution.

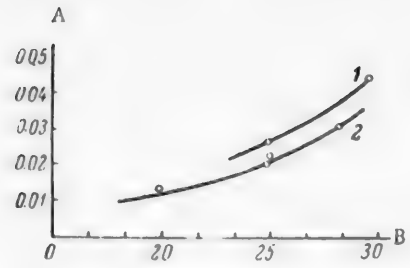

Fig. 6. Variation of the Henry constant with temperature for a gas containing 23% CO_2. A) Constant H (in atmos/mole/liter), B) temperature (°C). Velocity ratio (W/U) and concentration (normality) of K_2CO_3 solution respectively: 1) 50, 1.8; 2) 68, 2.5.

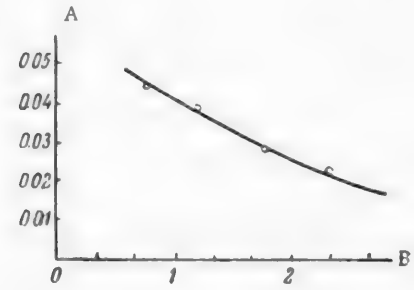

Fig. 7. Variation of the Henry constant with concentration of K_2CO_3 solution for W/U = 88.5, at 25°, with 25% CO_2 in the gas. A) Constant H (in atmos/mole per liter), B) solution concentration (normality).

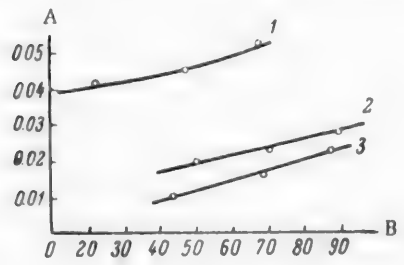

Fig. 8. Variation of the Henry constant with the velocity ratio of the phases W/U. A) Constant H (in atmos/mole/liter), B) velocity ratio W/U. Temperature (°C), solution concentration (normality), and CO_2 content of gas respectively: 1) 25, 2, 18.7; 2) 30, 0.2, 39; 3) 20, 2.5, 23.2.

The variation of H with the concentration of carbon dioxide in the gas is plotted in Fig. 5. It is seen that increase of the gas concentration results in a corresponding increase of H and, if variations of $\gamma_G^{0.25}/\eta_G^{0.75}$ in Eq. (6) (this value changes slightly with increase of concentration) are ignored, the absorption coefficient increases also. Moreover, it should be remembered that the capacity of the solution as a rule increases with increase of the gas concentration. The simultaneous increase of these parameters always leads to an ultimate intensification of the process.

The influence of temperature is somewhat peculiar. As the temperature rises, K_L increases owing to increase of $\gamma_L^{1/6}/\eta_L^{5/6}$, where the viscosity decreases more rapidly than the density. The value of K_G falls very slightly, and H increases (see Fig. 6); hence the absorption coefficient increases.

On the other hand, the equilibrium constant of the absorption reaction increases with temperature, so that the capacity of the solution decreases. Therefore, if the increase of the absorption coefficient predominates over the decrease of the solution capacity, the absorption rate increases, and vice versa. It follows that the effects of temperature on the absorption rate vary in different concentration ranges of carbon dioxide in the gas and of salts in solution. This influence can always be determined by calculation, by the use of the method described above for determination of H and of the equations for the nominal partial coefficients K_L and K_G. The solution capacity is calculated by Pozin's method [5]. In the concentration and temperature ranges in which these experiments were performed, increase of temperature is accompanied by an increase of the absorption rate. Results of calculations for higher temperatures indicate the existence of a maximum at about 50°. Above this limit the absorption rate falls with increase of temperature.

The constant H decreases with increasing concentration of the chemisorbent. This is shown by the curve in Fig. 7. At the same time, owing to the sharp increase of the solution viscosity, K_L decreases, and the absorption coefficient K also diminishes. However, a decrease of the absorption coefficient need not mean that the absorption rate falls. It is known that the solution capacity increases rapidly with increasing concentration of the absorbent. Therefore, the rate of the process as a whole must be determined by the joint influence of these factors. This is confirmed by experimental results, according to which the curve has a well-defined maximum at absorbent concentrations of the order of 150 g/liter. The absorption rate decreases appreciably above this concentration.

It follows from Fig. 8 that the velocity ratio of the phases W/U also has an appreciable influence on the value of the constant H. H increases with increase of W/U. At the same time K_G increases if the liquid velocity

remains constant. This increase continues until $1/HK_G$ becomes negligible in comparison with the resistance $1/K_L$, after which further increase of the gas velocity has no practical influence on the value of K. Nevertheless, K may be increased by increase of the liquid velocity. By suitable choice of the parameters it is eventually possible to find the optimum value for the absorption coefficient in relation to the economics of the process (i. e., the permissible specific consumption of the absorbent) and to the limit at which flooding of the absorber begins.

As W/U increases, increase of the value of K is also accompanied by increase in the capacity of the solution, since the amount of gas in contact with unit volume of the liquid phase is greater, and absorption actually takes place as if in conditions of a "highly concentrated gas." The simultaneous increase of the absorption coefficient and of the solution capacity shows that the factor W/U is highly effective in intensification of the absorption process. This is especially true for highly soluble gases; in such cases, owing to the low resistance of the liquid film, the favorable influence of increased W/U can be utilized more fully.

LITERATURE CITED

[1] Quinn and Jones, Carbon Dioxide [Russian translation] (Food Industry Press, 1940).

[2] M. E. Pozin, J. Appl. Chem. (USSR) 19, 10-11 (1946).

[3] I. G. Plit, Trans. Dnepropetrovsk Inst. Chem. Tech. 4 (1955).

[4] M. E. Pozin, J. Appl. Chem. (USSR) 20, 3 (1947).

[5] M. E. Pozin, J. Appl. Chem. (USSR) 21, 8 (1948).

Received June 30, 1956

INTENSIFIED REMOVAL OF HYDROGEN SULFIDE FROM COKE-OVEN GAS IN ROTARY HIGH-SPEED ABSORBERS*

S. N. Ganz and M. A. Lokshin

The F. E. Dzerzhinskii Institute of Chemical Technology, Dnepropetrovsk

The arsenical soda (Thylox) process for the removal of sulfur from coke-oven gas is widely used.

With a view to intensification of the absorption of hydrogen sulfide and of the regeneration of the arsenical soda liquor, we studied these processes in horizontal mechanical high-speed absorbers.**

The experiments were performed in a large laboratory unit, with the use of industrial coke-oven gas intended for ammonia synthesis.

EXPERIMENTAL

The horizontal mechanical absorber was equipped with an axial shaft fitted with disks, with 12 bent-back vanes on each disk. The absorber shaft was coupled directly to the shaft of a motor, the rotation speed of which was regulated by means of a sliding rheostat.

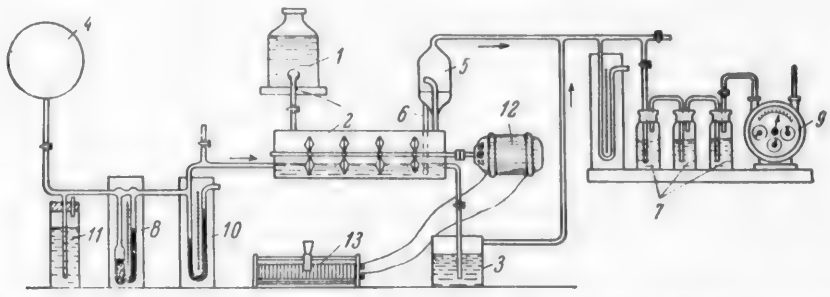

Fig. 1. Experimental unit. 1) Header, 2) mechanical absorber, 3) receiver, 4) gas holder, 5) drip trap, 6) overflow tube, 7) absorption flasks, 8) flow meter, 9) gas meter, 10) manometers, 11) manostat, 12) motor, 13) sliding rheostat.

The experimental unit is shown schematically in Fig. 1. The arsenical soda liquor was fed from the header 1 into the absorber 2, where the liquid level was maintained at 0.25 of the absorber diameter. The spent liquor passed from the absorber into the receiver 3. The gas from the works holder 4 entered the absorber 2 through the lower part of the end wall, and emerged at the opposite end through an outlet tube. The latter was connected to a drip trap 5, which was joined to the absorber by the tube 6. The gas passed through the trap into a series of absorption vessels 7, where residual hydrogen sulfide was absorbed in 3% zinc acetate solution. The number of ab-

* N. G. Chtvertka took part in the experimental work.

** Only the experimental data on absorption of H_2S are given in this paper. The results of a study of the regeneration of arsenical soda liquors in high-speed rotary equipment are presented in a separate communication.

sorption bottles was calculated to ensure complete absorption of the hydrogen sulfide. The last two bottles served as controls. The amount of gas entering the system was measured by means of the flow meter 8 and the gas meter 9; the gas pressures at the entry and exit were measured by means of the manometers 10, and the manostat 11 served to keep the gas pressure constant. The H_2S content of the gas was determined by analysis of the zinc acetate absorbent solution.

0.1 N iodine solution was added to the zinc acetate until an orange color was obtained, followed by starch to a black color; the solution was then titrated with 0.1 N thiosulfate solution.

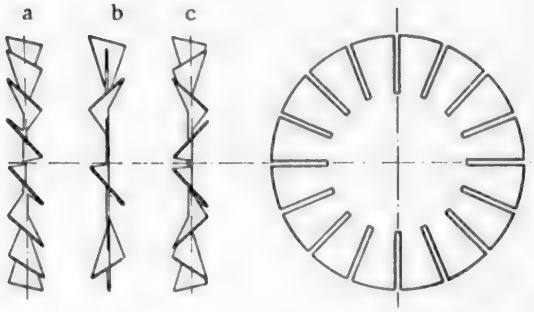

Fig. 2. Disk designs. a) All vanes set in the same direction, b) vanes facing each other alternately, c) all vanes set toward each other.

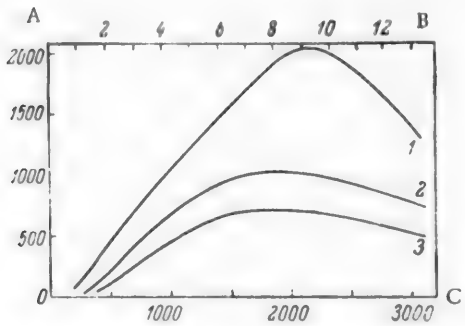

Fig. 3. Variation of the absorption coefficient K_g with the peripheral disk speed (shaft speed) and disk design. $w = 400\ m^3/m^3 \cdot hr$; $\varphi = V_L/V_a = 0.25$; $t = 24\text{-}26°$; $c_L = 8.4$ g/liter; pH = 8. A) Absorption coefficient K_g (in kg $H_2S/m^3 \cdot hr \cdot atmos$), B) peripheral disk speed v_d (in m/sec), C) shaft speed n (rpm). Disk design: 1) c, 2) b, 3) a.

The influence of hydrodynamic and physicochemical process conditions on the absorption rate was studied in the course of the investigations. The influence of the hydrodynamic factors was studied in relation to the disk design, their peripheral velocity, the gas volume rate, the amount of liquid in the absorber, and the horizontal velocity of the liquid in the apparatus.

The physicochemical factors studied were temperature, chemical capacity of the solution, and the H_2S concentration of the gas.

Most of the experiments were performed with an arsenical soda liquor containing 8.4 g As_2O_3 per liter, with pH 7.9-8.1. The influence of As_2O_3 concentration on the absorption rate was studied in a special series of experiments.

Influence of the peripheral speed and design of the disks on the absorption rate. Experiments showed that the disk design plays an important role in the development of optimum hydrodynamic conditions. We studied disks with three forms of vanes, as shown in Fig. 2, a, b, c.

The vanes in disks type a were set at ~ 15° in the same direction; in disks type b the vanes were set alternately toward each other. In disks type c all the vanes were set toward each other, and the disks were so fixed on the shaft that the openings formed by the vanes faced each other.

It was found that the last arrangement (Fig. 2,c) gives the most advantageous hydrodynamic conditions in the apparatus, with the highest absorption rate.

The peripheral disk speed plays the main role in creating turbulence of the liquid and gas. The absorption rate increases continuously with increase of the peripheral disk speed up to an optimum value. Above the optimum speeds the absorption rate decreases.

The results of investigations of the effects of peripheral speed and design of the disks on the absorption rate are plotted in Fig. 3.

These results show that the rate of H_2S absorption increases with increasing shaft speed (up to 2000 rpm, $v_d = 8.6$ m/sec) as the result of destruction of the diffusion films and of convective transfer. At n = 1700-2300 rpm the rate of the process becomes stabilized; this shows that the hydrodynamic conditions in the apparatus are then the most favorable. Further increase of the disk speed results in a decrease of the absorption rate because the liquid becomes pressed against the walls of the apparatus by centrifugal force, the liquid concentration in the gas decreases, and the phase contact area therefore diminishes.

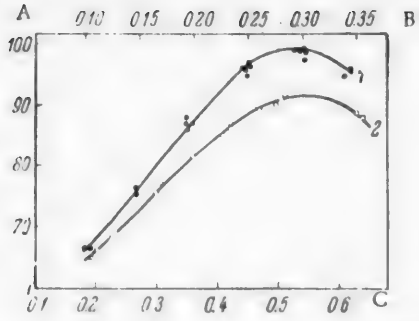

Fig. 4. Variation of the degree of absorption of H_2S (α) with the filling of the absorber ($\varphi = V_L/V_a$). w_{av} = 263 $m^3/m^3 \cdot hr$; t = 25-26°; c_L = 8.4 g/liter; pH = 8.1; x_1 = 1.51-1.58%. A) Degree of absorption of H_2S, α (%), B) filling of the absorber ($\varphi = V_L/V_a$), C) amount of absorbent in absorber V_L (in liters). Disk design and shaft speed, respectively: 1) disk c, n = 2175 rpm; 2) disk a, n = 2900 rpm.

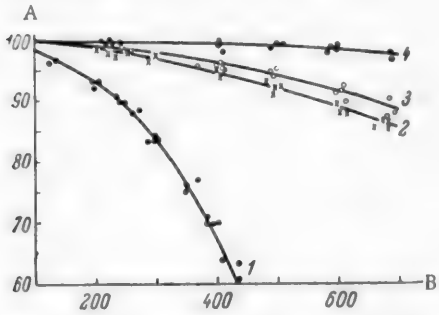

Fig. 5. Variation of the degree of absorption of H_2S (α) with the gas rate (w). n = 2175 rpm; φ = 0.25-0.30; t = 24°; c_L = 8.4 g/liter; pH = 8.1. A) Degree of absorption of H_2S, α (%); B) gas rate w (in $m^3/m^3 \cdot hr$). Temperature (°C) and disk design: 1) 24, disk a; 2) 24, disk c; 3) 30, disk c; 4) 42, disk c.

The experiments also showed that the absorption rates depends to a considerable extent on the disk design, irrespective of the disk speed. The highest absorption rate was obtained with the use of type c disks. In this case regions of liquid in foam and drop form are created between the disks, and a considerable mobile layer of foam with 1-2 mm bubbles is formed above the liquid; a gas–emulsion is formed in the apparatus at the optimum peripheral disk speed. The highest degree of absorption is obtained under these conditions.

Influence of the amount of liquid in the apparatus. A constant volume of liquid in the apparatus is an important condition for normal operation. The amount of liquid in the apparatus is one of the principal hydrodynamic factors determining the rate of the process.

The effect of the volume of liquid in the apparatus was studied under the following constant conditions: w_{av} = 263 $m^3/m^3 \cdot hr$, t = 25-26°, x_1 = 1.51-1.58% H_2S in the gas. The experiments were performed with type c and a disks at shaft speeds of 2175 and 2900 rpm, respectively.

The results of these experiments are given in Fig. 4.

It is seen that the highest degree of absorption corresponds to 25-30% of the volume of the absorber filled with liquid.

The concentration of liquid in the gas and the phase contact area decrease with decreasing amount of liquid in the absorber. If too much liquid is present, gas breaks through the apparatus in large streams, the foam becomes detached, and liquid is removed in drop form from the apparatus. In either case the absorption rate decreases.

Influence of the gas rate. The gas rate determines the productivity of the apparatus and is one of the most important factors determining the hydrodynamic conditions in the apparatus, and therefore, the absorption rate.

The effect of the gas rate was studied under the following constant conditions: $V_L = 0.28\,V_a$, pH = 7.9-8.1, c_L = 8.4 g per liter of solution, x_1 = 1.3-1.4% H_2S.

The experiments were performed with disks type a and c at n = 2175 rpm. The flow time of the liquid through the apparatus was 1 minute.

The gas rates were varied in the range 100-700 $m^3/m^3 \cdot hr$; the temperature was varied in the range 25-42°.

The results are plotted in Figs. 5 and 6.

It follows from these results that the rate of absorption of H_2S in the absorber fitted with disks type a decreases rapidly with increase of the gas rate. At w = 400 $m^3/m^3 \cdot hr$ the degree of absorption is only 66%.

With the use of disks type c the degree of absorption decreases smoothly and slowly with increase of the gas rate.

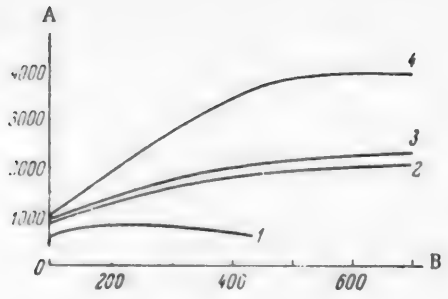

Fig. 6. Variation of the coefficient of absorption with the gas rate. n = 2175 rpm; φ = 0.25-0.30; t = 24°; c_L = 8.4 g/liter; pH = 8.1. A) Absorption coefficient K_g (in kg $H_2S/m^3 \cdot hr \cdot atmos$), B) gas rate w (in $m^3/m^3 \cdot hr$). Temperature (°C) and disk design: 1) 24, disk a; 2) 24, disk c; 3) 30, disk c; 4) 42, disk c.

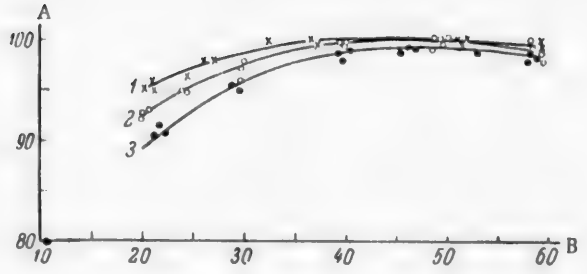

Fig. 7. Variation of the degree of absorption of $H_2S(\alpha)$ with the temperature (t). v_d = 9.4 m/sec; n = 2200 rpm; w = 400 $m^3/m^3 \cdot hr$; $\varphi = V_L/V_a$ = 0.30; c_L = 8.4 g/liter; pH = 8. Disks c. A) Degree of absorption of H_2S, α (%), B) temperature t (°C). H_2S concentration (x_1) at entry into the absorber (%): 1) 1.82-2.26; 2) 1.57; 3) 1.26-1.32.

It follows from the experimental data that at 40-42° with the use of type c disks the absorption of H_2S is virtually complete at w = 400-500 $m^3/m^3 \cdot hr$. The influence of the gas rate on the absorption coefficient is reminiscent of the influence of peripheral disk speed.

The absorption rate increases rapidly up to a definite maximum with increase of the gas rate up to the optimum. The linear velocity of the gas also increases with the gas rate, since

$$\omega_{lin} = \frac{w \cdot V_a}{3600 \cdot f_0},$$

where f_0 is the open section of the apparatus and V_a is the volume of the absorber.

The turbulence effect produced by the gas in the system diminishes with its linear velocity.

According to our data, the optimum range of linear gas velocities is 0.8-2.5 m/sec. This range corresponds to the highest degree of absorption.

Influence of physicochemical factors on the absorption rate. The principal physicochemical factors which determine the absorption rate are temperature, As_2O_3 concentration in the liquor, and H_2S concentration in the gas.

The effect of temperature on the degree and rate of absorption was studied under the following constant conditions: w = 400 $m^3/m^3 \cdot hr$, n = 2200 rpm, H_2S concentration in gas x_1 = 1.26-2.26%, and As_2O_3 concentration = 8.4 g/liter; the pH of the liquor was in the range 7.9-8.1 before absorption, and fell to 7.5-7.55 after absorption. The experimental results are plotted in Figs. 7 and 8.

Degree of Absorption of H_2S at c_L = 17.38 g As_2O_3 per liter (Disks c used)

Gas rate w ($m^3/m^3 \cdot hr$)	Shaft speed n (rpm)	Peripheral disk speed v_d (m/sec)	Filling of absorber with liquid $\varphi = V_L/V_2$	Temperature t (°C)	H_2S concentration in gas (%)		Degree of absorption (%)
					at entry x_1	at exit x_2	
421	1850	7.9	0.30	30 –32	1.2487	0.0	100
525	2000	8.6	0.30	30 –32	1.2487	0.0	100
630	2000	8.6	0.30	30 –32	1.2487	0.0025	99.8
720	2000	8.6	0.30	30 32	1.2487	0.0037	99.7

It follows from these results that the absorption rate rises with increase of temperature to 40-42°; this is to be attributed to the reaction between H_2S and sodium oxythioarsenate, according to the equation

$$Na_4As_2S_nO_2 + H_2S = Na_4As_2S_nO + H_2O.$$

Further increase of temperature above 42° lowers the absorption rate owing to the increased H_2S pressure and the consequent decrease of driving force. Moreover, the gas viscosity increases with increase of temperature. It follows from the experimental data that the optimum temperature for the process is 40-42°.

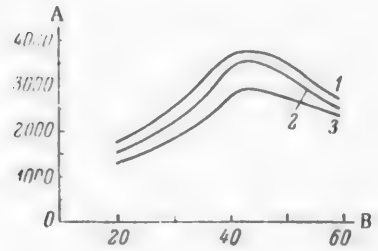

Fig. 8. Variation of the absorption coefficient (K_g) with temperature. v_d = 9.4-9.6 m/sec; n = 2200 rpm; w = 400 $m^3/m^3 \cdot hr$; $\varphi = V_L/V_a = 0.30$; $c_L = 8.4$ g/liter; pH = 7.9. Disk design c. A) Absorption coefficient K_g ($kg/m^3 \cdot hr \cdot atmos$), B) temperature t (°C). Concentration (x_1) of gas at entry into the absorber (%): 1) 1.8200-2.2600; 2) 1.5796; 3) 1.2622-1.3208.

The next important factor which influences the rate of the process is the As_2O_3 concentration in the liquor. The table contains experimental data on the absorption of H_2S by arsenical soda liquor containing 17.38 g of As_2O_3 per liter.

The tabulated data show that traces of H_2S appear only at gas rates above 600 $m^3/m^3 \cdot hr$. This means that high operating rates can be used with liquors containing 17-18 g As_2O_3 per liter, complete absorption of H_2S being ensured at gas rates of 500-550 $m^3/m^3 \cdot hr$.

The influence of H_2S concentration in the gas was studied in the relatively narrow range of 1.26-2.26% H_2S. The experiments were performed under the following conditions: w = 400 $m^3/m^3 \cdot hr$, v_d = 9.4 m/sec, amount of liquid in absorber φ = 30%, disks type c. The results are plotted in Fig. 7. It is seen that the percentage absorption increases with H_2S concentration in the gas. The difference between the absorption rates for different H_2S concentrations is especially prominent at relatively low temperatures.

Technical and economic characteristics of the proposed method. Comparison of the productivity, per reaction volume, of packed towers and rotary absorbers under equal conditions shows that rotary absorbers operate at least at 25-27 times the rate of packed towers. Therefore, for a given production rate the volume of a packed tower is 25-27 times the volume of a rotary absorber, with a 10 to 12-fold decrease in the amount of metal required for the rotary absorber.

To compare the operating costs of tower units and units with rotary absorbers, we assume that all costs with the exception of electrical power are equal for the two types of unit. Power is expended mainly for feeding the absorption liquor into the equipment and for drawing the gas through. The minimum power of the motors required for feeding the liquor to four towers (350 m^3 of liquor per power) is 360 kw. The power required to draw the gas through the absorption towers is determined by the resistance of the whole system, which is not less than 1000 mm H_2O in existing units; the corresponding power requirement is 220 kw. Thus, the total power requirement of the conventional units is 580 kw.

With the use of rotary absorbers the liquor is fed to a height not greater than 5 m. It then flows by gravity into the next absorber. In this case the power of the motor required for this purpose does not exceed 4.5 kw. The maximum resistance offered to the gas by a system with rotary absorbers is 100-200 mm H_2O. The power required to draw the gas through such a system is about 44 kw.

The power required for rotation of the working parts of the rotary absorbers is 40 kw per absorber [1]. Thus, the total power requirement for a unit with rotary absorbers is 248.5 kw, whereas the requirements of existing units are roughly 2.3 times this.

SUMMARY

1. Experimental results showed that the rate of absorption of H_2S by arsenical soda liquor in high-speed rotary absorbers is considerably higher than in packed towers.

2. The use of rotary absorbers for the absorption of H_2S should lead to a considerable decrease of the reaction volumes, lowering of metal consumption, decrease of capital investment for the equipment, and lower expenditure of energy in operation.

LITERATURE CITED

[1] S. N. Ganz and M. A. Lokshin, Trans. Dnepropetrovsk Chem. Tech. Inst. 5 (1956).

Received April 9, 1956

THERMAL DECOMPOSITION OF SILVER OXALATE

D. Trandafelov

The State University, Sofia

Our research into the thermal decomposition of silver oxalate was based on the following theoretical principles.

1. Thermal decomposition in crystal–crystal–gas systems can be classified into two large groups: equilibrium and nonequilibrium processes. For example, the decomposition of $CaCO_3$ is an equilibrium process, as it is found experimentally that the CO_2 pressure in the system $CaCO_3$–CaO–CO_2 is a function of the temperature. The system is univariant and completely reversible. In equilibrium decomposition good reproducibility is obtained only if the experiments are performed with the same sample. In equilibrium thermal decomposition, the process is determined by heating.

The thermal decomposition of the oxides of silver and mercury, and of silver oxalate, is irreversible, and the phase rule is not applicable. These substances should also decompose at normal temperatures (without heating), but at very low rates. Heating is necessary to accelerate the decomposition. Considerable variations of the experimental results are to be expected in nonequilibrium decomposition. Nonequilibrium thermal decomposition of solid systems is analogous to the boiling up of superheated water, and therefore the induction period and the rate of such a process vary within very wide limits.

2. It is known from the literature [1] that the kinetic curves for the decomposition of all substances capable of undergoing thermal decomposition pass through maxima.

The rate of thermal decomposition in an isothermal process is determined by the amount of gas liberated in unit time per unit surface. However, exact measurement of the surface is impossible, as crystals have internal and external surfaces, and the rate is therefore determined in terms of the amount of gas per unit mass.

The curves for the rates of equilibrium and nonequilibrium thermal decomposition should, in theory, differ considerably.

In equilibrium decomposition, the rate of the process should decrease continuously with time, and not pass through a maximum. If an experimental curve has a maximum, this shows that the process is not isothermal.

Consider a liquid heated to temperature t°; suppose that a definite amount of liquid (without the vapor over it) is removed by means of a suitable mechanism into an evacuated vessel heated to the same temperature. The liquid begins to evaporate at the maximum rate, which decreases with time and tends to zero, i. e., the vapor pressure will reach the equilibrium value for the given temperature. The effective rate of evaporation is then $V_{eff} = V_{abs} - V_c = 0$, where V_{abs} is the absolute rate of evaporation, calculated from the number of molecules evaporated per unit area in unit time; V_c is the absolute rate of condensation.

In equilibrium thermal decomposition we may introduce the concept of the effective rate of decomposition, equal to the difference between the absolute rate of decomposition and the absolute rate of formation of the original substance. The effective rate of decomposition becomes zero at equilibrium, so that, if enough of the original substance is present, a definite pressure which will not increase with time is reached for a given volume and given temperature.

In nonequilibrium decomposition a slight increase of the pressure in the gas phase does not decrease the effective rate of thermal decomposition and does not lead to equilibrium in the system. Equilibrium may be established at a given temperature at very high pressures, for example, in the system silver oxide–silver–oxygen.

The controversial question – do the solid reaction products act catalytically – cannot always be answered with certainty as the result of experiment [2], as the experimental data are very scattered, and the catalytic effect may be of the same order as the degree of scatter. It is highly probable that another reason why the rate of the process reaches a maximum in nonequilibrium decomposition is that the starting substance becomes coated with solid reaction products, which shield most of the internal and external surfaces.

The first question which arises in studies of thermal decomposition in a crystal–crystal–gas system is: is the decomposition an equilibrium or a nonequilibrium process? The question of the rate of nonequilibrium decomposition is highly complex. Quantitative studies of the rate of decomposition, especially nonequilibrium decomposition, are very difficult, and almost impossible without consideration of the secondary structures of the original and final substances. It will be shown later that the secondary structure of a crystalline system is highly complex, depends on a number of factors, and is little understood.

3. In investigation of thermal decomposition it must be remembered that all precipitates consist of fine crystals, smaller than 10^{-4} mm, formed into concretions at definite angles, so that large crystals always contain so-called internal surfaces. These internal surfaces adsorb ions and molecules from the mother liquor; this is known as intracrystalline adsorption [3]. Since the external visible surface area of a crystal is many times smaller than its internal surface, it is clear that subdivision, i. e., increase of the external area relative to the internal, has very little or no influence on the rate of thermal decomposition.

4. The external and internal surfaces of a crystal have heterogeneous structures. They contain vertices, edges, and sites at which fine crystals become attached to each other. The nature of the intergrowth, orientation, and contamination of the fine crystals determines the so-called secondary structure of the crystal. This secondary structure depends on the conditions in which the crystalline system is formed: temperature, solution concentration, contamination, grinding, heat treatment, precipitation rate, etc.; i. e., on the previous history of the system. The secondary structure of a particular crystalline system is decisive in relation to the structure-sensitive properties, in Smekal's terminology [4].

The thermal decomposition of a crystalline system is a typical structure-sensitive property, greatly influenced by the history of the system and, in particular, by the impurities in the system. It is found in practice [5] that nearly all the characteristics of the secondary structure depend on the conditions of thermal decomposition. That is why in studies of thermal decomposition, especially if quantitative relationships are being investigated, it is always necessary to take into consideration the secondary structure of the crystalline system – its previous history and the impurities present. It may be noted that Lewis [6], who studied the thermal decomposition of silver oxide samples prepared by different methods, found considerable differences. Pavliuchenko [7] reported that his silver oxide decomposed at 10,000 times the rate of Lewis' silver oxide.

5. Internal adsorption in a crystalline system formed from a sparingly soluble substance conforms to the Paneth-Fajans rule, but the adsorbed and double layers may contain various amounts of solvent molecules and H^+, OH^-, and other ions present in the mother liquor. Therefore, in studies of thermal decomposition it is necessary to take into consideration what ions and molecules are present in the mother liquor and then, in the investigation of the actual decomposition, the influence of various ions and molecules on this process can be taken into account.

Thermal dissociation is a surface process, and always takes place at the adsorption layers (external and internal). The structure and composition of the external and internal crystal surfaces therefore have a decisive influence on the kinetics of the process.

6. If a precipitate is left for a long time, especially at elevated temperatures, it recrystallizes and "ages." During the recrystallization process small crystals grow first, some at the expense of others, if they are present in solution or if the temperature is fairly high. Thermal decomposition should proceed at a lower rate after recrystallization.

In the light of the foregoing considerations, it was of interest to perform an experimental study of the thermal decomposition of some crystalline system. The substance chosen was silver oxalate, which is a well-defined crystalline system subjected to repeated and detailed investigations [5, 8].

EXPERIMENTAL *

We attempted to maintain photographic dark room conditions in all the experimental work on the thermal decomposition of silver oxalate. This condition was not entirely fulfilled in the weighing of silver oxalate samples.

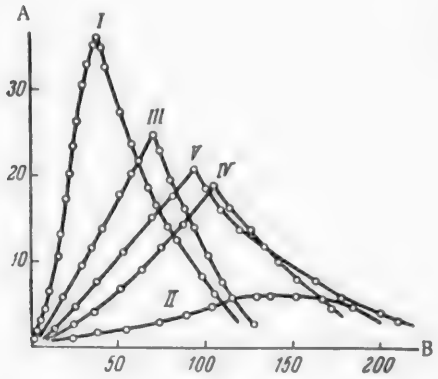

Fig. 1. Variation of the decomposition rate of silver oxalate with time at 120°. The numbers on the curves in Figs. 1, 2, 3, and 4 correspond to the sample numbers. A) $\Delta P/\Delta t$ (mm Hg/min · mg · 10^{-2}), B) time (sec).

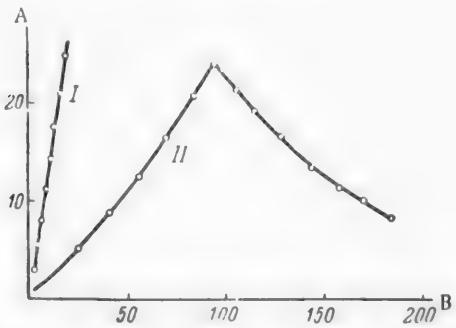

Fig. 2. Variation of the decomposition rate of silver oxalate with time at 135°. A) $\Delta P/\Delta t$ (mm Hg/min · mg · 10^{-2}), B) time (sec.).

A vacuum apparatus was used for studies of the kinetics of thermal decomposition of silver oxalate. A "Vacustat" McLoed gauge was used for convenient and rapid measurement of the CO_2 pressure; up to two measurements per minute at 10^{-3} mm Hg could be carried out. The reaction tube was heated by means of a Höppler glycerol ultrathermostat, which maintained the required temperature to within ± 0.05°. A sample of 10-20 mg of silver oxalate was weighed on an analytical balance in a small thin-walled bulb, widened at one end, and this was inserted into the reaction tube. After the required vacuum had been reached, and after prolonged desorption of the apparatus, the reaction tube was inserted into the ultrathermostat heated to the required temperature, the vacuum pump was disconnected, and the CO_2 pressure was measured at intervals of 0.5, 1, and 5 min, according to the rate of the process. A trap containing solid CO_2 was placed between the gauge and the reaction tube, in order to eliminate the catalytic influence of mercury vapor. The variations between two determinations for different samples of the same preparation were 10-20%.

The following solutions were prepared in the redistilled water: 1) 0.150 N solution of analytical silver nitrate (May and Baker, London); 2) 0.120 N solution of analytical sodium oxalate; 3) 0.095 N solution of oxalic acid, chemically-pure grade; 4) 0.095 N solution of analytical ammonium oxalate. All the reagents were additionally recrystallized.

The precipitates were prepared at room temperature. In each case 100 ml of silver nitrate solution was added from a buret to the other solution during half an hour, with mechanical stirring. The following were taken for the precipitation: I) 250 ml of sodium oxalate solution, II) 250 ml of oxalic acid solution, III) a mixture of 100 ml of sodium oxalate and 190 ml of oxalic acid solutions, IV) a mixture of 80 ml of sodium oxalate and 210 ml of oxalic acid solutions, V) 300 ml of ammonium oxalate solution.

Double the required quantity of oxalate ions was taken in all the precipitations, so that these ions, according to the Paneth-Fajans rule, formed the first adsorbed layer of the external and internal surfaces of the silver oxalate crystals. In the second precipitation, a smaller excess of oxalic acid was used, as precipitated silver oxalate is soluble in a strongly acid medium. Analysis of the precipitate formed from oxalic acid showed that it consists of normal silver oxalate, and not of acid silver oxalate as might be expected.

* A. Kr'stanov took part in the experimental work.

All the precipitates were washed 5-6 times with redistilled water by decantation, and dried on a glass filter for 12 hours under vacuum at 40°.

Several series of experiments on the thermal decomposition of silver oxalate were performed; the results of experiments at 120° are plotted in Fig. 1. It is seen that whereas Sample I decomposed at a considerable rate which had a clear maximum, Sample II decomposed at a scarcely perceptible rate, represented by a curve with a very flat maximum. The curves for the decomposition rates of Samples III, IV, and V lie between those of I and II. The curves for the thermal decomposition of Samples I and II at 135° are given in Fig. 2. At this temperature Sample II decomposes at a moderate rate, but Sample I decomposes explosively.

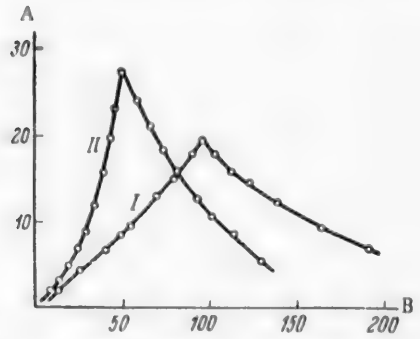

Fig. 3. Variation of the decomposition rate of silver oxalate with time at 120° after diffusion of H^+ in Sample I and of Na^+ in Sample II. A) $\Delta P/\Delta t$ (mm Hg per min · mg · 10^{-2}), B) time (sec).

The following experiments were performed to determine the influence of extraneous ions. A washed Sample I was transferred to a beaker and covered with 250 ml of oxalic acid solution (0.95 N). The precipitate was left for 4 days and stirred at intervals. A washed Sample II was covered with 250 ml of 0.120 N sodium oxalate and also left for 4 days with periodic stirring. The precipitates were then washed and dried in the usual manner. The thermal decomposition of these samples gave interesting results, shown in Fig. 3. The kinetic curves for the samples treated as described above are in the reverse sequence as compared with Fig. 1.

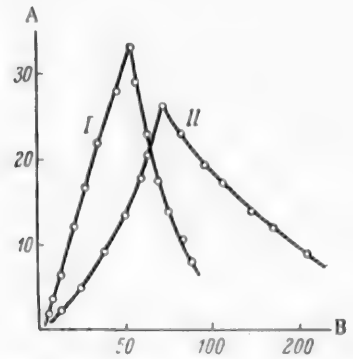

Fig. 4. Variation of the decomposition rate of silver oxalate with time at 116°. Sample II was "aged" at 50-60° for 2 hrs. A) $\Delta P/\Delta t$ (mm Hg/min · mg · 10^{-2}), B) time (sec).

In addition, the following experiment was performed. After precipitation of Sample I at 15°, the precipitate was divided into two portions. The first portion was washed, filtered off, and dried in the normal manner. The second portion was warmed together with the mother liquor and kept at 50-60° for 2 hrs. The course of the decomposition of these two samples is plotted in Fig. 4. It was found that the portion kept at a high temperature decomposed at a lower rate; these results are in agreement with Erofeev's data [8] on the thermal decomposition of silver oxalate.

Thus, our experiments on the decomposition of silver oxalate confirm the results of earlier work, according to which the kinetic curve passes through a maximum, and also show that the rate of the process greatly depends on the method used for the preparation of silver oxalate, and especially on admixtures present in the system. The experiments showed that the precipitates formed by the action of sodium oxalate or oxalic acid in 100% excess on silver nitrate solution, and then treated by the same procedure, decompose at very different rates when heated. As the experiments were repeated many times, it is certain that these results are not fortuitous. Moreover, if part of the oxalic acid was replaced by sodium oxalate, i. e., part of the H^+ was replaced by Na^+, the decomposition rate gradually increased, approximately in proportion to the amount of Na^+ introduced. Finally, on the hypothesis that H^+ and Na^+ are primarily included in the internal surfaces of the silver oxalate crystals, an experiment on the replacement of H^+ by Na^+ and of Na^+ by H^+ was carried out. This experiment qualitatively confirmed the hypothesis. Partial replacement of H^+ by Na^+ and vice versa was effected very rapidly by diffusion at the internal surfaces of the silver oxalate crystals.

It may be noted that in all the previous investigations silver oxalate was prepared by precipitation with sodium oxalate.

It may also be pointed out that the NH_4^+ ion adsorbed internally in silver oxalate crystals results in a lower decomposition rate than the Na^+ ion.

SUMMARY

1. A distinction is drawn between equilibrium and nonequilibrium thermal decomposition; arguments are advanced to show that these two types of decomposition should be represented by kinetic curves of different form.

2. The results of numerous experimental results suggest that thermal decomposition is a structure-sensitive property, in Smekal's terminology, and that the form of the kinetic curve should greatly depend on the history of the system and the impurities present in it.

3. It is shown that silver oxalate precipitated by excess of sodium oxalate decomposes at a greater rate than samples formed by precipitation with oxalic acid. It is shown that in conditions in which ion exchange by diffusion is possible these ions are adsorbed on the internal surfaces of the silver oxalate crystals.

LITERATURE CITED

[1] M. M. Pavliuchenko, J. Phys. Chem. (USSR) 29, 39 (1955); P. I. Bel'kevich, Bull. Acad. Sci. Belorussian SSR 4, 65 (1952).

[2] B. V. Erofeev, J. Phys. Chem. (USSR) 29, 1136 (1955); M. M. Pavliuchenko, J. Phys. Chem. (USSR) 30, 1169 (1956).

[3] D. Balarew, Der disperse Bau der festen Systeme (Dresden u. Leipzig, 1939); Kolloid-Beih. 50, 1-234 (1939).

[4] A. Smekal, Z. phys. Chem. 131, 6, 108 (1929); Z. angew. Chem. 42, 489 (1929).

[5] J. Y. MacDonald and C. Hinshelwood, J. Chem. Soc. (London) 127, 2764 (1925); J. Y. MacDonald, J. Chem. Soc. 832, 839 (1936).

[6] G. N. Lewis, Z. phys. Chem. 52, 310 (1905).

[7] M. M. Pavliuchenko and E. Gurevich, J. Gen. Chem. (USSR) 21, 467 (1951).*

[8] B. V. Erofeev, P. I. Bel'kevich, and A. A. Volkova, J. Phys. Chem. (USSR) 20, 1103 (1946).

Received June 1, 1957

* Original Russian pagination. See C. B. translation.

METHODS OF CHEMICAL BENEFICIATION AND CONVERSION OF NONBENEFICIATING REFUSE NICKEL ORES (TAILINGS)

D. P. Bogatskii and G. G. Urazov

It was found in a study of the chlorination of garnierite [1] that preliminary reduction of the garnierite before chlorination appreciably increases the extraction of nickel from it. As experiments on the chlorination of unreduced silicate–oxide nickel ore [2] gave considerably lower extractions of nickel than chlorination of garnierite [1], it was desired to attempt to increase the degree of chlorination of this ore by means of preliminary direct reduction; this led to the development of a new process for chemical concentration and conversion of oxidized nickel ores. The physicochemical nature of the proposed process essentially consists of a cycle of reactions for the reduction of silicate and oxide compounds of nickel [3-5], with formation of active metallic nickel or ferronickel, and subsequent chlorination of the freshly reduced metals [6]. The cobalt oxides present in the ore are reduced to the metal along with the nickel and iron [6]. Consequently, the preceding multistage direct reduction of the ore also has a beneficial effect on the degree of subsequent chlorination of cobalt, which is very often present in small amounts in nickel ores. It was therefore established [7] that multistage reduction of the ore before chlorination greatly facilitates the chlorination of all the valuable constituents of the ore. The reactivity, and therefore, the susceptibility to chlorination, of the other difficultly reduced components of the gangue decreases appreciably [8] as the result of the high temperatures to which they are subjected during the preliminary reduction. The chlorination reactivity of the gangue is decreased considerably in this process, as it has been shown [9] that the chlorination of the reduced metals can be performed at relatively low temperatures – below the temperatures of appreciable volatilization of nickel chloride. Thus, preliminary multistage direct reduction of the silicates and oxides of the valuable components of the ore, those to be extracted, ensures their selective chlorination owing to the considerable decrease of the chlorination reactivity of the unreduced, strongly heated components of the gangue.

The purpose of the present investigation was to determine experimentally whether the proposed method for chemical concentration and conversion of silicate–oxide nickel ores (by multistage direct reduction followed by chlorination roasting) can be used with tailings and lean silicate–oxide nickel ores; the material chosen for the study was a refractory unworkable ore taken from the tailings dump. The processes of direct multistage reduction of nickel ores were studied by us earlier [10]. In the present work, the optimum conditions for maximum chlorination of the reduced tailings and for the extraction of nickel from them by leaching were determined by studies of the effects of the following fundamental technological factors on these processes: 1) the conditions of leaching of the chlorinated ore, 2) the temperature of the chlorination roasting, 3) the duration of chlorination roasting.

Results of an Experimental Study of the Hydrometallurgical Stages of the Proposed Method

For determination of the optimum conditions for the leaching of the chlorinated tailings (from the point of view of maximum extraction of nickel with the least extraction of iron) a series of experiments was performed on the leaching of the products formed by chlorination roasting of the reduced tailings, under various conditions. The effects of solvent acidity and of the temperature and duration of the leaching process on the extraction of nickel and iron from the cinders were studied. The plots of the experimental data (Fig. 1) show that the extraction of nickel into solution during leaching of the cinders with water for 30 minutes increases considerably with the leaching temperature. However, not all the nickel chloride is leached out even if the pulp is boiled for 30

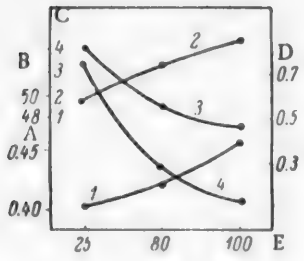

Fig. 1. Extraction of nickel and iron into solution in relation to the temperature of water leaching of the cinder formed in chlorination roasting. A) Nickel content of solutions (g/liter), curve 1; B) extraction of nickel (%), curve 2; C) extraction of iron (%), curve 3; D) iron contents of liquors (g/liter); E) temperature (°C).

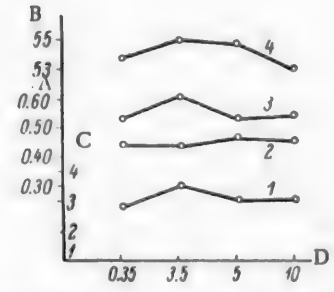

Fig. 2. Extraction of nickel and iron into solution in relation to the liquor acidity. A) Contents of nickel and iron in the liquors (in g/liter), curves 2 and 3, respectively; B) extraction of nickel (%), curve 4; C) extraction of iron (%), curve 1; D) HCl concentration (g/liter).

minutes. A whole hour of boiling with water is needed for almost complete extraction of nickel chloride. The leaching of iron by means of water decreases considerably with increase of the leaching temperature. The amount of iron in the leach liquor decreases from 0.73 g/liter in leaching at 20°, to 0.14 g/liter in leaching of the same cinders at 98-100°. This can be attributed to appreciable increase of the hydrolysis of dissolved ferric chloride with increase of the leaching temperature. The considerably lower content of iron in liquors obtained by leaching at the boil is of great practical significance for a substantial simplification of the subsequent treatment of the nickel-containing liquors, and does not give rise to any difficulties in the filtration of the pulp after leaching. The increase in the solution acidity which takes place during leaching at the boil results in highly unfavorable conditions for hydrolysis of nickel chloride; a special investigation showed that this undesirable process is reduced almost to zero. The following conclusions were drawn from the results of the investigation of the conditions for the leaching of chloride cinders in water and in aqueous solutions of hydrochloric acid of various concentrations.

Hydrochloric acid leaching is not necessary, as it has no substantial advantages over water leaching. The extraction of nickel during leaching with water depends directly on the leaching temperature. The iron content of the water leach liquors is some inverse function of the leaching temperature. Almost complete extraction of nickel chloride by water leaching is effected in one hour at the boil. The iron content of the liquors formed in conditions of almost complete extraction of nickel chloride by water leaching is about $^1/_4$ or $^1/_5$ of their nickel content; this corresponds to 0.6-0.7% extraction of iron from the ore. Aqueous leaching is fairly rapid under these conditions, and mechanical agitation is not necessary. In hydrochloric acid leaching under the conditions studied, the extraction of nickel and iron increases somewhat with the acidity from 0.01 to 0.1 N hydrochloric acid solution (Fig. 2). The extraction of nickel decreases appreciably with increase of the solution acidity to 5 g and then to 10 g per liter. The iron content of the hydrochloric acid leach liquors varies similarly to the nickel content. Almost complete extraction of nickel chloride by hydrochloric acid leaching is effected by the use of 0.01 N aqueous hydrochloric acid at 98-100° for one hour. The iron content of the liquors formed in conditions of almost complete extraction of nickel chloride by hydrochloric acid leaching is approximately equal to the nickel content; this corresponds to 2.5-3.0% extraction of iron from the ore.

Water leaching without additional heating of the pulp (as compared with hydrochloric acid leaching under the same conditions) gives a lower extraction of nickel and a higher extraction of iron. Water leaching at the boil (as compared with hydrochloric acid leaching under the same conditions) gives the same extraction of nickel, with a considerably lower extraction of iron. Water leaching at the boil (as compared with hydrochloric acid leaching under the same conditions) gives the best results, and is the most rational and economic procedure. The best results in water leaching were obtained after one hour at the boil; these may be regarded as the optimum conditions for the process.

Results of a Study of the Chlorination Roasting of Reduced Tailings with Subsequent Aqueous Leaching, and the Production of a Nickel Oxide Concentrate

The results of an experimental study of chlorination roasting of reduced silicate–oxide nickel ore tailings in the 300-600° range, and subsequent leaching with water in the optimum conditions, are given in graphical form in Figs. 3 and 4.

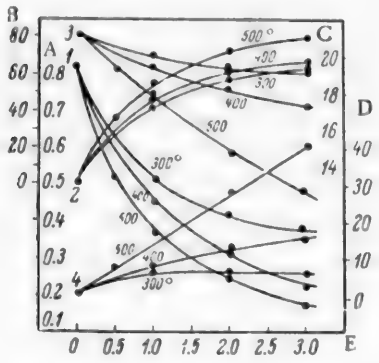

Fig. 3. Extraction of nickel and iron by water leaching of cinders from chlorination roasting in relation to the temperature and duration of the roasting of the reduced ore. A) Decrease of nickel content in the reduced ore (%), curve 1; B) extraction of nickel (%), curves 2; C) decrease of iron content in the reduced ore, curves 3; D) extraction of iron (%), curves 4; E) roasting time (hrs), without agitation.

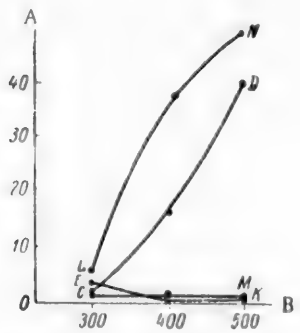

Fig. 4. Behavior of chlorinated iron in the course of chlorination roasting. A) Extraction of iron (%), B) temperature of chlorination roasting (°C). Roasting time (hrs): curves LN and CM) 5, CD and EK) 3. Explanations of the curves are given in the text.

Curves 1 (Fig. 3) represent the decrease of silicate–oxide nickel contents in the cinders with the temperature and duration of chlorination roasting. The corresponding changes of the iron contents are shown by curves 3 (Fig. 3). Curves 2 and 4 in Fig. 3 represent the variations of the degree of extraction of nickel and copper, respectively as functions of the same factors.

The behavior of iron during chlorination roasting in relation to the temperature and duration of the process is represented in Fig. 4. Curves LN and CD in Fig. 4 represent the effects of roasting time and temperature on the amount of ferric chloride volatilized, and curves EK and CM represent the effects of the same factors on the amount of chlorinated iron which passes into solution during the aqueous leach. These results show that the degree of chlorination of nickel in the reduced unworkable tailings, varies between 32.4 and 80.5%, according to the roasting conditions used. The extraction of nickel is some direct function of the temperature and time of roasting. At 600° small amounts of nickel chloride begin to volatilize together with ferric chloride; this effect is not found at 550°. To avoid loss of nickel chloride by volatilization, the temperature of chlorination roasting should not exceed 550-560°. The highest extraction of nickel without volatilization was obtained by water leaching of the product formed by chlorination roasting of the reduced ore (without agitation during the roasting) at 500° for 3 hours. Further increase of the roasting time has no significant influence on the degree of extraction of the nickel, because of its very low content in the ore. The degree of extraction can be increased further by improvement of the contact between the ore and chlorine; this is achieved by agitation during the roasting, not used in the present investigation. Large-scale laboratory and pilot plant trials on the chlorination roasting of Monche-Tundra copper–nickel ores, carried out by Urazov and Morozov [11] gave considerably higher degrees of chlorination than those attained in laboratory conditions, because of the considerably improved roasting conditions due to agitation of the ore during the roasting, easily effected under production conditions. With regard to the extraction of iron during leaching of the cinders, it is quite certain that very little passes into solution. According to the results of the present investigation, the amount of iron extracted varies from traces to 3.8% of the total iron content in the roasted ore, according to the roasting conditions. This is of great practical importance, as in the subsequent precipitation of nickel concentrate or metallic nickel from the liquors preliminary removal of iron from these liquors is unnecessary or is much easier, and the technological process is thereby simplified considerably. The slight extraction of iron during the leaching of reduced ore after chlorination roasting is probably a consequence of the lower degree of chlorination of the iron, as compared with the nickel, during the roasting. It follows from the

experimental results that the degree of chlorination of iron is some direct function of the temperature of the chlorination roasting, but its absolute value is considerably less than the degree of chlorination of nickel.

Unfortunately, it is not possible to establish any exact direct relationship between the extraction of iron during the leaching and the degree of chlorination, from the experimental data obtained. This is because the chlorination of the iron in the reduced ore is a highly complex process, involving the formation of ferric and ferrous chlorides, volatilization of ferric chloride, and hydrolysis effects during leaching, and therefore a special detailed experimental study of this question is necessary. However, it is firmly established and proved that the slight extraction of iron into solution during leaching is due not only to hydrolysis of ferric chloride, but also to some others of the factors named. Despite the very satisfactory results obtained in these experiments on the production of nickel-containing liquors with low iron contents, it is possible that the iron contents can be reduced further by the method used by Urazov and Morozov, who reduced considerably the extraction of iron in the chlorination roasting of Monche-Tundra copper–nickel ores by the introduction of water vapor into the reaction zone. It was shown in experiments on the precipitation of nickel oxide concentrate from the liquor obtained by water leaching of the cinders that the small amounts of iron present do not interfere with the production of a high-nickel oxidized concentrate from such liquors without preliminary removal of iron. For example, in two simple experiments on the precipitation of nickel oxide concentrates from the liquors by addition of milk of lime and caustic soda solution, without any purification of the liquors, hydrated precipitates were obtained which, after being dried at 105-110°, consisted of nickel oxide concentrates containing 32.51 to 37.19% nickel and 7.14 to 8.23% iron. Therefore, the nickel oxide concentrate so obtained contains 50-60 times as much nickel as the spent refractory refuse ore, and half the amount of iron present in the same ore. No significant difficulties are foreseen in the practical application of this method of chlorination after preliminary multistage reduction, as the process is considerably simpler than the highly complex process used in modern nickel plants for the extraction of nickel and cobalt from high-grade silicate–oxide nickel ores. The direct reduction of iron ores is now a practical proposition. The reduction of silicate–oxide nickel ores does not differ essentially, from the practical standpoint, from the direct reduction of iron ores effected in Russian and foreign plants. The subsequent chlorination of the reduced ore can be effected in practice by cooling of the product formed by reduction roasting, accompanied by mechanical agitation, for a definite time in a suitable insulated cooler filled with chlorine; this can be easily done under industrial conditions. Finally, the water leaching of the chlorinated ore and precipitation of the nickel concentrate from the concentrated liquors are even simpler from the practical standpoint.

Applications of the proposed process for reduction and chlorination of the ores are by no means confined to the production of concentrates, i. e., to its use as a method for chemical beneficiation of tailings and low-grade silicate–oxide nickel ores. Another promising procedure is purification and removal of cobalt from the liquors obtained by leaching of chlorinated ores, followed by electrolysis of the solution to yield pure electrolytic nickel and recovered chlorine, which is returned to the cycle. The advantages of the use of nickel chloride solutions for the production of electrolytic nickel can be now regarded as firmly established. It has been found [12, 13] that the cathodic nickel deposits formed from chloride solutions are more finely-granular, smoother, and stronger than the deposits obtained by electrolysis of nickel sulfate solutions. Chloride electrolytes are simpler than sulfate electrolytes, and much easier to regulate. The conductivity of the former is twice as high, and therefore the voltage required for a given current density is almost halved. With a correspondingly higher current efficiency, the power consumption per unit weight of nickel obtained is also about a half, which is very important from the economic aspect. The process can be carried out at higher rates by the use of high current densities, so that the productivity obtained with the use of chloride electrolytes is higher.

Nothing fundamentally new is suggested in the way of equipment for the proposed process. The ore can be reduced in multistage mechanical roasting furnaces or in rotary tubular furnaces such as are successfully used in industry for the roasting and direct reduction of various ores. Similar or other types of furnaces can be used for chlorination of the reduced ore. The most suitable equipment for the process must be chosen after pilot-plant trials of different variations of the process in the course of its industrial adoption.

The results of this experimental study of the proposed method for concentration and conversion of low-grade and refuse silicate–oxide ores by multistage direct reduction followed by chlorination roasting may be summarized as follows. Direct reduction of silicate–oxide nickel ores greatly increases the degree of chlorination during the subsequent chlorination roasting. Nickel can be extracted from lean silicate–oxide nickel ores and tailings, not smelted at present, by simple water leaching of the reduced ore after chlorination roasting at moderate temperatures. The degree of extraction achieved under the most difficult and unfavorable conditions with the

use of an unworkable silicate ore (without agitation of the ore during the reduction and chlorination roasting), by a single leach with water, is by no means the highest possible. The extraction of nickel from usual higher-grade silicate–oxide nickel ores not of the refractory type may be increased considerably under production conditions by means of ordinary agitation during the reduction and chlorination roasting; this has been demonstrated repeatedly in various chemical and metallurgical processes under industrial conditions.

In order that volatilization of nickel chloride should be avoided, the chlorination roasting of the reduced ore must be performed at temperatures below 550°. The optimum temperature for chlorination roasting under the conditions studied lies in the 400-500° range. The results show that three hours at the normal roasting temperature, even without agitation of the ore, is sufficient for the chlorination roasting. The extraction of iron during the leaching of the reduced ore with water after chlorination roasting is very slight; under the conditions studied, it varied from traces to 3.8% of the amount present in the ore. As iron is almost or entirely absent from the nickel-containing liquors formed, it is possible to precipitate a nickel-rich concentrate from them without any previous purification; this greatly simplifies the process for the production of nickel concentrates from various nickel-containing solutions. The very low extraction of iron in the leaching of ore treated by the proposed method also simplifies considerably the practical preparation of the nickel-containing solutions for electrolysis if they are to be used for the production of electrolytic nickel. Aqueous leaching of the products formed by reduction – chlorination roasting should undoubtedly be even more favorable economically in the conversion of oxidized and silicate–oxide nickel ores which are at present treated by pyrometallurgical reduction, i. e., richer than the tailings studied. After it has been developed further on the pilot scale, the proposed method should be adopted by industry as a means of chemicometallurgical enrichment of lean silicate–oxide nickel ores and tailings; this is most important for increasing the production rate of existing undertakings in the nickel industry. As has been shown above, a further improvement in the main characteristics of the proposed process is to be expected when it is used on the pilot and industrial scales; in particular, this relates to the extraction of nickel, owing to the much improved conditions for reactions of chloride formation during chlorination roasting if the ore is vigorously agitated in suitable equipment, which was not used in the present investigation. Being essentially of a multiple character, the proposed method should also allow the extraction of cobalt by a much simpler technological procedure than is now used in industry.

SUMMARY

1. Silicate–oxide nickel ores which cannot be effectively concentrated by the usual mechanical methods used in industry can be successfully concentrated and treated by the proposed method of chemical beneficiation, which has been tested experimentally.

2. The method which has been developed for the chemical concentration of silicate–oxide nickel ores is very simple with regard to the technology and equipment required, and does not require the use of costly or scarce materials and reagents.

3. The proposed method is of value not only for chemical concentration and conversion of the richest high-grade ores, but also as a means for the utilization of refractory silicate–ore tailings, which cannot be effectively enriched by existing mechanical methods used for ore concentration in industry.

4. The proposed method for chemical beneficiation of silicate–oxide nickel ores should be even more effective technically and economically if used under production conditions with agitation of the ore.

5. It is shown that the proposed method is important not only as a method of chemical concentration, but also as an original basis for new technological processes for the chemical conversion of oxidized ores, simpler and more economic than those now used in the nickel and cobalt industry.

In conclusion , the authors offer the authors offer their sincere thanks to I. P. Bardin, I. I. Cherniaev, M. A. Pavlov, I. N. Plaksin, A. A. Zadik'ian, A. Mironov, L. G. Berg, G. S. Gritsaenko, Iu. V. Baimakov, V. A. Vanlukov, and I. S. Morozov for active participation in the present investigation and review and discussion of the paper in the Scientific Councils of the Institute of General and Inorganic Chemistry and of the Institute of Metallurgy, Academy of Sciences, USSR, and in the Technical Council of the Ministry of Nonferrous Metals, USSR.

LITERATURE CITED

[1] D. P. Bogatskii, Proc. Acad. Sci. USSR 45, 2, 65 (1944).

[2] D. P. Bogatskii, Bull. Acad. Sci. USSR,OTN 9, 629 (1944).

[3] D. P. Bogatskii, Bull. Acad. Sci. USSR, OTN 6, 891 (1946).

[4] D. P. Bogatskii, J. Gen. Chem. (USSR) 21, 1, 3 (1951); 7, 9, 1937 (1937).

[5] D. P. Bogatskii, Bull. Acad. Sci. USSR, OTN 12, 1809 (1946).

[6] D. P. Bogatskii, J. Appl. Chem. 17, 6, 346 (1944).

[7] D. P. Bogatskii and G. G. Urazov, Bull. Acad. Sci. USSR, OTN 3, 108 (1955).

[8] D. P. Bogatskii, Bull. Acad. Sci. USSR, Div. Chem. Sci. 5, 272 (1944); 2, 194 (1948).

[9] D. P. Bogatskii, Coll. Sci. Trans. MITsM 3, 11, 83 (1945).

[10] G. G. Urazov and D. P. Bogatskii, Bull. Acad. Sci. USSR, Div. Chem. Sci. 9 and 10 (1956).

[11] G. G. Urazov, The Metallurgy of Nickel (1935).

[12] W. A. Wesley, Metal Industry 3, 137 (1950).

[13] N. P. Fedot'ev and Z. I. Dmitrishova, J. Appl. Chem. (USSR) 30, 2, 221 (1957).*

Received January 12, 1957

* Original Russian pagination. See C. B. translation.

CONTACT REDUCTION OF METALS FROM SOLUTION*

B. V. Drozdov

During recent decades there have been many studies both of the general theory and of the practical conditions of contact reduction. Some questions, however, remain controversial; this is because of their physicochemical complexity and by no means because of lack of interest on the part of investigators.

The mechanism of the contact reduction of a metal from solution is considered in this paper.

Different types of contact reduction of metals, and significance of films of the deposited metals. All contact-reduction reactions are electrochemical in character [1]. A distinctive feature of such reactions is the close interrelationship of the anode and cathode processes and their mutual influence. Two types of contact reduction, differing in their mechanisms, may be distinguished in relation to the degree of dispersion of the anodes and cathodes, which depends on the nature of the deposition of the metal being displaced: 1) the contact metals are solid, and the precipitated metal forms a film of variable porosity on the surface of the dissolving metal; this film offers increasing resistance to further deposition; 2) the contact metals are liquid, which mix with or dissolve in other liquid metals, and the precipitated metal is distributed relatively uniformly, according to the conditions of diffusion and mixing, throughout the alloy formed.

Examples of the second type of reaction are provided by the reduction of metals from solution by amalgams, or certain reactions in melts (such as the reduction of aluminum by magnesium). This type of reaction is characterized by absence of definite anodic and cathodic regions on the reacting surface, which is isopotential in character. The absence of a potential difference between anode and cathode makes Ohm's law and the theory of short-circuited cells inapplicable, and reactions of this type can be interpreted as spontaneous electrochemical exchange between the metal and the ions in the electrolyte.

Contact-reduction reactions of the first type are used much more widely in practice. In such cases the contact metals do not mix and are solid (as in the extraction of copper from mine waters). Because of the presence of anodes and cathodes the reacting surface is not isopotential, and Ohm's law and the theory of short-circuited cells are therefore applicable. It will be shown below that both types of reaction can also be interpreted as electrochemical exchange.

The formation of a film of the deposited metal has a significant influence on contact reduction of the first type [2]. Contradictory views on this question are advanced in the literature. According to some workers, the deposited film is so dense that even a monomolecular layer stops the process [3]. Present supporters of this theory consider that continuous contact deposition is possible only if the forming film is continuously removed. There is also the opposite view, according to which the deposited metal does not offer any resistance to further deposition [4].

The structure of a metal film formed by the contact method has well-oriented crystals and is quite analogous to the structure of electrolytic deposits, as is clear from Figs. 1-4. As in the case of metals deposited electrolytically, the structure of the metal deposited by contact may vary considerably according to the conditions of deposition, but the range in which the conditions may be varied is even more restricted, as the current strength is determined by the concentration of the discharging cations at the reacting surface, which is not the case in electrolytic deposition.

* The author thanks G. A. Nevinskii, V. Ia. Zel'des, N. I. Zedin, E. S. Kosich, and T. M. Kogan, who assisted in the experimental work.

Fig. 1. Structure of a copper film deposited by the contact method.

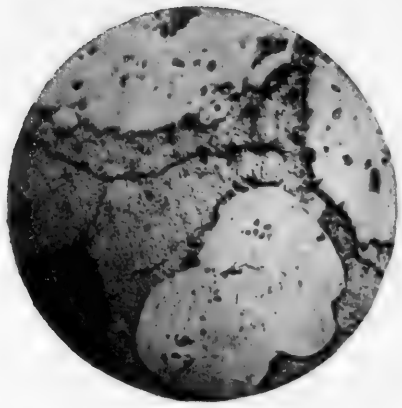

Fig. 2. Structure of a copper film on nickel powder, with degree of utilization 0.4.

Fig. 3. Structure of a copper film on nickel powder with degree of utilization 0.85.

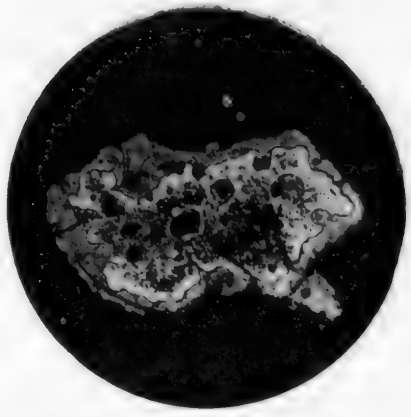

Fig. 4. Deposition of copper on internal surfaces of nickel powder.

If the process takes place at a high rate, i. e., if concentrated solutions and active metals are used, the deposits are formed in the form of dense layers of very fine needles. A film of this type is very porous and offers very little resistance to further deposition (such films are formed in the deposition of copper or silver by zinc from solutions containing 0.5-10 g/liter). Dense films, offering considerable resistance to further deposition, may be obtained by slow precipitation from dilute solutions by means of inactive metals, or in presence of inhibiting additives in the solutions.

All deposits formed either electrolytically or by contact are always more or less porous, and therefore there is no justification for the assertions that it is possible to obtain completely dense and uniform layers, especially only one molecule thick. Proof of the porosity of the films is provided by the data, given below, on the potentials of nickel powder with copper deposited on its surface. If the film was continuous, the potential would be that of copper.

We cannot agree with the opinion of Bulakh and Drachevskaia [4], according to whom the film offers no resistance to further deposition, as they performed the contact deposition under unfavorable conditions. The method of thermal circulation used did not in fact affect the part of the vessel in which the deposition took place. It was most likely that they observed the initial stage of precipitation, which is a special case and by no means a general rule.

With good stirring of a sufficiently concentrated solution with an active metal, it is always possible to obtain a film in the form of a continuous but porous layer. This was confirmed by observations of various types of deposition, with the aid of a binocular lens. Figure 2 is a micrograph of nickel powder with a copper deposit, with degree of utilization 0.4, and Fig. 3 represents a degree of utilization 0.85 (the degree of utilization is the ratio of the nickel reacted to the initial amount, i. e., the fraction of nickel replaced by copper).

The data presented below on changes of the compromise potential* with gradual growth of the film also represent increasing resistance. The reason for the retarding effect of the film is that the diffusion conditions in it are quite different from those in the main bulk of the solution.

Bulakh is also wrong in the opinion that cations are discharged only on the external surface of the metal already deposited. Figure 3 shows a considerable layer of deposited copper, adhering firmly to the nickel, which is possible only if partial penetration of copper cations into the relief takes place, while Fig. 4 shows deposition of copper in the internal pores of the relief. As in electrolytic deposition, deposition on a relief surface by the contact method takes place in accordance with the throwing power of the solution and Ohm's law.

The contacting metals are solid. In this case there are quite definite anodic and cathodic regions, to which the theory of short-circuited cells is applicable. Since the anode potential is not equal to the cathode potential, part of the energy is consumed in overcoming ohmic resistance.

TABLE 1

Calculation of Current Strength from Kinetic Data

t	C_{Cu}	K_{Ni}	K_{Cu}	I	I_c	I_a
0	970	1.94	—			
				4.6	20	2.7
5	510	1.5	0.46			
				2.9	4.85	2.14
10	224	1.22	0.74			
				0.31	0.4	0.26
30	139	1.14	0.83			
				0.18	0.2	0.16
60	1	1.08	0.94			
				0.022	0.023	0.021
120	5	1.0	0.965			

Note. t is the time (minutes); C_{Cu} is the concentration of copper in solution (in mg per liter), K_{Ni} is the nickel content of the powder (in g), K_{Cu} is the content of precipitated copper in the powder (in g), I is the current strength (in amps), I_c is the current strength per 1 g of precipitated copper, I_a is the current strength per 1 g of nickel in the powder.

Direct measurements of the cell electrode potentials and of ohmic resistances present great difficulties owing to the disturbances in the normal functioning of such cells resulting from the measurements. It is therefore of considerable interest to study a number of factors which throw indirect light on the action of these cells. One convenient method is by studies of the reaction kinetics of contact reduction.

Data on the reduction of copper from solution by means of nickel powder (Table 1) are presented as an example. The current strength in the short-circuited cells at individual stages of the process was calculated from data on variations of the copper concentration in the solution. From changes in the composition of the powder in the course of the process it is possible to calculate the current strength per 1 g of nickel and 1 g of precipitated copper present in the sample. These values give some indication of the anodic and cathodic current densities, as the specific surface of the powders used is of the order of 100 cm^2 per 1 g.

The plotting of polarization curves for such cases is extremely difficult, as not only the polarization curves but the anode and cathode surfaces alter continuously owing to the formation of a film of deposited copper and variations of the ionic concentrations at the reacting surfaces.

*In the case of solid contacting metals the anodic and cathodic regions have different potentials with respect to the solution, but the anodes and cathodes as a whole, being short circuited, have a certain common potential, known as the compromise potential, with respect to the solution.

Any attempts at separate measurements of anodic or cathodic polarization lead to results which differ substantially from the actual conditions of the process, and the data which are lacking as a consequence must be augmented by estimates or calculations.

Therefore, the polarization-curve method, while it provides a graphic explanation of the nature of the process, cannot be used for quantitative purposes, as it is based on approximate data. An attempt to plot a schematic polarization diagram based on the data in Table 1 (2.5 min after the start of the process) is given in Fig. 5. As the anode surface is 7.5 times the cathode surface, it follows that $i_c = 7.5\, i_a$. The section $E_1 - E_2$ should represent the ohmic drop of potential. Measurements of the compromise potential suggest that this quantity should in reality be smaller owing to greater polarization of the cathode and anode.

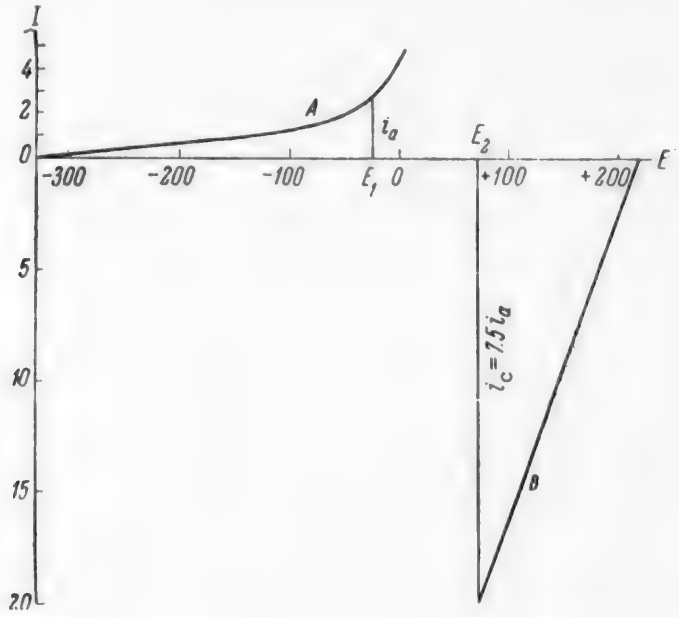

Fig. 5. Potential curves for the displacement of copper from solution by nickel powder. E) Potential (in mv), I) current strength (in amps). i_c) cathodic current strength, i_a) anodic current strength; A) anodic potential curve, B) cathodic potential curve; E_1) anode potential, E_2) cathode potential.

The tendency for the displacement of a metal from solution might be determined from diagrams of state of the Pourbaix-Shultin type [6, 7]. The reaction rate increases with increase of the reduction potential of the metal relative to the oxidation potential of the solution.

The compromise potential of a heterogeneous metallic surface is intermediate between the anode and cathode potentials [8]. It depends on the composition of the solution, and determines the reducing power of the contacting metals.

We performed experimental determinations of the compromise potentials of nickel powders in relation to the amounts of copper deposited on them.

The compromise potential of the powder was determined in a conical glass vessel with a platinum contact sealed in its base. The powder was placed in the vessel and covered with nickel electrolyte of constant composition, which was connected with a saturated calomel electrode through an agar siphon. The electromotive force of the powder–calomel electrode cell was measured by means of a potentiometer made by the "Etalon" works. The potentials were calculated on the standard hydrogen scale.

The measurements had to be performed fairly rapidly in order to avoid dissolution of the easily-oxidized copper, but it was necessary to allow enough time for the compromise potential to reach a stable value.

In illustration, values of the compromise potential (π_c) for different degrees of utilization (η) of the nickel powder are given below.

Solution contains 200 g/liter $NiSO_4 \cdot 7H_2O$, 20 g/liter H_3BO_3, 40 g/liter Na_2SO_4; pH = 5.5

η	π_c (in mv)
0.1	−300
0.25	−200
0.40	−100
0.50	−20
0.60	+40

Thus the reduction potential of the powder decreases in the course of the process as more copper is precipitated, with a simultaneous decrease of the oxidation potential r_n of the solution. The value of this potential depends on the ratio of the potentials of all the oxidizing agents to those of all the reducing agents in the solution, but for fairly pure nickel solutions of constant composition the copper content is the determining impurity. In illustration, values of r_n for the nickel electrolyte as a function of the copper content are given below (Table 2); variations of η and π_c are also given.

TABLE 2

Values of the Oxidation Potential of a Solution Containing (in g/liter): $NiSO_4 \cdot 7H_2O$, 200; Na_2SO_4, 40; H_3PO_3, 20; NaCl, 5; and Variations of the Copper Content in the Course of Reduction

Time (min)	Cu content (g/liter)	r_n (in mv)	η	π_c (in mv)
0	1.06	+626	—	—
5	1.00	+574	—	—
15	0.936	+395	0.09	−310
30	0.380	+390	0.32	−140
60	0.130	+400	0.43	− 70
90	0.040	+140	0.48	− 20
120	0.020	+ 77	0.49	− 10

Different vessels were used for determinations of r_n and π_c; the compromise potential π_c was measured with respect to a solution free from copper.

The oxidation potential of the solution was determined by measurement of the emf of a cell consisting of a platinum rod immersed in the electrolyte solution, and a calomel electrode; the potentials were calculated on the standard hydrogen scale.

The end of the contact reduction of copper is marked by a sharp decrease in its precipitation rate owing to the low potential with respect to the solution. Attempts to prolong the process further may lead to dissolution of the copper which, under the influence of atmospheric oxygen which enters the solution, begins to behave as an electrode of the second kind: $Cu \| Cu(OH)_2 \| OH^-$ or $Cu \| CuOH \| OH^-$.

The contacting metals are liquid, miscible with or soluble in another liquid metal. In this type of contact reduction a film of the precipitated metal is not formed, and the latter dissolves more or less uniformly with the formation of an alloy. The metallic surface is therefore isopotential in character. The potential difference between the metal and solution should be sufficient for kinetic exchange of ions in the double layer. The ex-

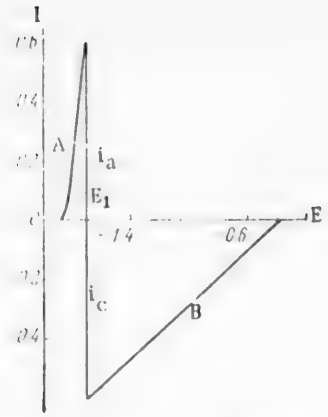

Fig. 6. Potential curves for the displacement of cadmium from solution by excess of sodium amalgam. E) Potential (in v), I) current strength (in amps); i_c) initial cathodic current strength, i_a) initial anodic current strength, A) anodic potential curve, B) cathodic potential curve, E_1) displacement potential of cadmium ions.

changeability may be represented graphically by means of diagrams of the Pourbaix-Shultin type [6, 7]. If the surface potential is uniform, the anodic and cathodic processes occur simultaneously, and their distribution is statistically random. Since the anode and cathode potentials are equal, there is no ohmic resistance, and the process takes place at the highest rate with maximum current strength in a system of this type.

Figure 6 is a schematic diagram (in the form of polarization curves) of the formation of cadmium amalgam by displacement of cadmium from a solution of its salt by an excess of sodium amalgam. If the concentration of cadmium ions in the solution is high enough, hydrogen evolution is slight because of the high overvoltage on the amalgam.

Research on the reduction of metals by amalgams is reviewed in Kozlovskii's book [5].

Simultaneous discharge of ions. As in the case of electrolytic deposition, other electrochemical reactions may, under suitable conditions, accompany the contact reduction of metals from solutions. One possible reaction is cathodic reduction of oxygen dissolved in the electrolyte. Most frequently the potential of this reaction is more positive than that of the reaction of metal precipitation, and the former reaction therefore competes with the latter. However, the amount of dissolved oxygen is not large, and if its access to the solution is limited, the possibilities of this reaction are also limited. If continuous access of atmospheric oxygen to the solution is possible, the reaction may develop extensively, and ultimately lead to wasteful losses.

An aqueous solution always contains some hydrogen ions; their concentration and the overvoltage may be such that they may be discharged at the cathode, which is also undesirable. The amount of hydrogen discharged is determined by the ordinary laws of electrolysis.

If a solution contains cations of several metals, their discharge potentials may be such that they are discharged simultaneously; in such cases there is a complete analogy with the laws of ordinary electrochemical kinetics, if the nature of the alloy formed from the discharging cations is taken into account.

SUMMARY

1. All processes of contact reduction of metals are electrochemical oxidation-reduction processes, with close interdependence of the anode and cathode processes.

2. Two types of contact reduction may be distinguished, according to the nature of the deposit formed.

3. It follows from the experimental data that the reduction potentials of metals and the oxidation potentials of solutions decrease in the course of contact reduction.

4. As in electrolysis, when a film of solid metal is formed in contact reduction the structure of the film may vary according to the deposition conditions. It is shown that the film of the deposited metal is porous in all cases, and it may gradually cover the whole surface and offer resistance to further deposition.

5. All the conditions of contact reduction conform to the laws of electrochemical kinetics.

LITERATURE CITED

[1] N. N. Beketov, Studies of the Displacement of Some Elements by Others (Khar'kov, 1865).

[2] B. V. Drozdov, Proc. Second All-Union Conference on Theoretical and Applied Electrochemistry (Acad. Sci. Ukrainian SSR Press, Kiev, 1949).*

* In Russian.

[3] Mylins u. Fromm, Ber. 27, 630 (1897).

[4] A. A. Bulakh and R. K. Drachevskaia, J. Appl. Chem. (USSR) 26, 1225 (1953).*

[5] M. T. Kozlovskii, Mercury and Amalgams in Electrochemical Methods of Analysis (Acad. Sci. Kazakh SSR Press, Alma-Ata, 1956).**

[6] M. Pourbaix, Metaux et corrosion, 13, 159, 183 (1938).

[7] A. I. Shultin, J. Phys. Chem. (USSR) 15, 359 (1941).

[8] G. V. Akimov and N. D. Tomashov, J. Phys. Chem. (USSR) 8, 623 (1936).

Received March 2, 1957

* Original Russian pagination. See C. B. translation.

** In Russian.

PASSIVATION OF ZINC ELECTRODES IN GALVANIC CELLS WITH ALKALINE ELECTROLYTES

Z. Ia. Nikitina

Scientific Research Institute for Cells and Electrocarbon

In cells with alkaline electrolytes the capacity corresponding to the amount of zinc dissolved to the point of saturation of the electrolyte with zincate (the primary period of cell operation) is generally utilized.

In order to increase the capacity of such a cell, it is of interest to find conditions for the utilization of the secondary period of its operation, when dissolution of the zinc during passage of the current is accompanied by precipitation of zinc hydroxide or oxide from the electrolyte.

At low current densities the zinc dissolves quantitatively as a function of the current, with formation of zincate. The polarization is low. When the current density increases to a certain critical value, the anode becomes passive and its dissolution ceases almost entirely. In such cases it is not necessary for the electrolyte to be saturated with zincate [1-4].

The zinc anode in a cell operates at current densities considerably below the critical value, and the electrode therefore does not become passive until a definite degree of saturation of the electrolyte with zincate has been reached. However, after such saturation the electrode may become passive at current densities below the critical value.

The question of the structure and composition of the passivating film, and of its minimum thickness in the case of a zinc anode, has not yet been finally solved. Mention must be made of the work of Fischer and Budilov [2], Huber [3], Thomson [4], and others, who attempted to solve these problems.

Passivation of Zinc in Alkali Solutions

When a freshly-cleaned zinc electrode is immersed in 0.1 N KOH solution, its potential is shifted rapidly from the equilibrium value (−1.2 v) to between −0.6 and −0.5 v, even without application of an anode current, owing to the oxygen dissolved in the alkali. Application of an anode current to such an electrolyte, even at a very low density, shifts the potential by about 1 v more.

If the experiments are performed in absence of oxygen (in an atmosphere of pure nitrogen), the equilibrium potential of zinc is retained for a long time. If the electrode is polarized by a weak anodic current ($i = 0.0001$ amp/cm^2), a result is obtained which is represented by the curve in Fig. 1. It is seen that after 16 min the anode potential reaches 1.0-1.2 v, i. e., the value at which oxygen begins to be liberated in anodic polarization. If the calculated quantity of electricity required for passivation of the zinc electrode is plotted as a function of the polarization-current density, a relationship close to linear is found; the quantity of electricity required for passivation increases with decreasing current density, because of the consumption of electricity in the simultaneous reaction of ionization zinc and passage of zinc ions into solution.

The passivation capacity may be determined from cathodic discharge (depassivation) curves. If an electrode passivated by anodic polarization in a nitrogen atmosphere is polarized by a weak cathodic current as the result of rapid current reversal, the passivating film can be reduced and data on its thickness obtained. This type of reduction is illustrated by the curve in Fig. 2; it represents the variation of electrode potential with time in the course of cathodic polarization at $i = 0.0002$ amp/cm^2 in 0.19 N KOH ($t = 18°$). It follows from Fig. 2 that

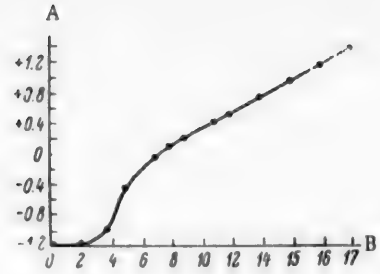

Fig. 1. Variation of the potential of active zinc with time, during cathodic polarization in 0.1 N KOH at t = 18°, i = 0.1 ma/cm². A) Potential (in v), B) time (in min).

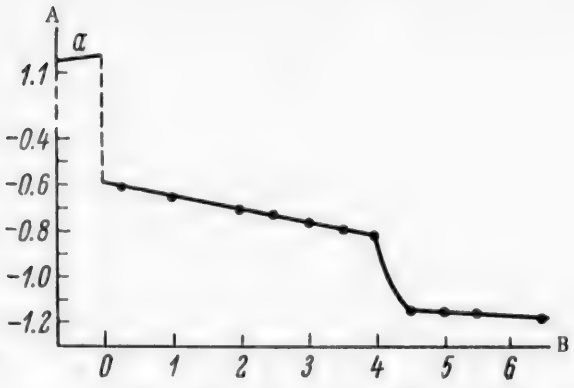

Fig. 2. Variation of the potential of passive zinc with time in the course of cathodic polarization in 0.19 N KOH, i = 0.2 ma/cm², t = 18°. A) Potential (in v), B) time (in min).

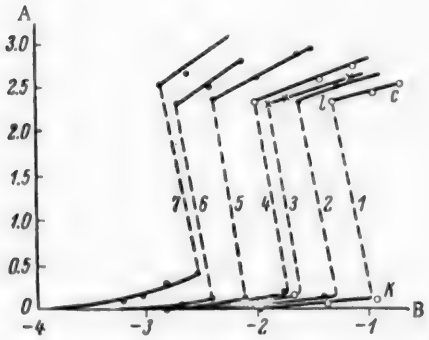

Fig. 3. Anodic polarization curves for a zinc electrode (an alloy of zinc with 1.5% Hg) in 10 N KOH. A) Potential (in v), B) log i. Temperature (in °C): 1) 20, 2) 0, 3) −10, 4) −20, 5) −30, 6)−40), 7)−50.

when the cathodic current is switched on the potential falls instantly in all the experiments from 1.0-1.1 v to −0.6 v, i. e., by 1.6-1.7 v. The passivating film is then slowly reduced by the current while the potential changes little; it is only after the potential has reached −0.8 to −0.9 v that it jumps to −1.10 to −1.15 v. During the subsequent 1-1.5 min of cathodic polarization the potential of the zinc falls further from −1.15 to −1.21 v, the value corresponding to active zinc. If the anodic current is switched off after passivation of the electrode as described above, the potential returns spontaneously to about −0.6 v, i. e., the value reached by active zinc after immersion in this alkali solution in presence of oxygen.

These factors indicate the formation of an oxide phase on zinc, with a potential of about −0.6 v.

Determinations of the capacity of the passive film in an atmosphere of pure nitrogen in terms of the quantity of electricity required for depassivation showed that its value depends on the current strength and the duration of the anodic passivation.

Values of the passivation capacity, determined from the cathodic discharge curves, for different times of passivation under an anodic current of $6 \cdot 10^{-4}$ amp/cm² are given below:

Anodic polarization time (min). . . .	1	2	5	8	12	18	30
Capacity (millicoulombs/cm²)	4.5	6.8	19	24	28.5	41	48

5 millicoulombs/cm² is a quite reliable minimum value of the quantity of electricity for a passivated anode. This corresponds to $1.65 \cdot 10^{15}$ zinc atoms per cm².

If we assume that the volume occupied by a molecule, according to Pilling and Bedworth [5], is 1.57 times the nearest distance between zinc atoms in the crystal lattice, which is 2.65 A, we can calculate the number of layers of ZnO covering the passivated anode; it is equivalent to $0.91 \cdot 10^{15}$ molecules/cm². Hence, the minimum number of molecular layers of zinc oxide in the passivating film is 18.

In his investigation of photoelectrochemical processes, Veselovskii [6] found, by removal of layers of zinc oxide by means of cathodic polarization, that the capacity of the oxide layer on anodically-passivated zinc in 0.1 N NaOH is 15-20 millicoulombs/cm². In caustic soda solutions of moderate and high concentrations, zinc anodes are passivated only at considerable current densities, and thicker films are formed.

TABLE 1

Critical Current Densities for Anodic Passivation of Zinc, at Which the Anode is Passivated in 5 Minutes

Solution composition	Critical current density (in ma/cm²) at temperature (°C)						
	18°	0°	−10°	−20°	−30°	−40°	−50°
Pure zinc (Ts-O) anode							
4.2 N NaOH . .	64	34	17	9	—	—	—
4.2 N KOH . .	76	38	32	20	—	—	—
7 N KOH . .	—	80	50	32	22	6	2.2
10 N KOH . .	114	52	26	20	8	4	2.0
Anode of Zn + 1.5% Hg alloy							
7 N KOH . .	112	70	51	34	24	12	6
10 N KOH . .	116	54	26	20	12	4	3

The potential becomes unstable at current densities close to the critical value, and therefore the potential of transition into the passive state cannot be determined exactly; it depends to a considerable extent on the rate of change of the applied potential near the critical current density. The critical current density, which is the maximum value at which the zinc anode remains active for a given polarization time, can be determined with satisfactory reproducibility.

Decrease of temperature favors passivation of the zinc anode: polarization of the active anode increases, the critical passivation-current density greatly decreases, and the potential of oxygen evolution on the passive anode also increases appreciably. This is seen from the curves in Fig. 3, plotted for 10 N KOH at 20, 0, −10, −20, −30, −40, and −50°, for an alloy of zinc with 1.5% mercury.

In determinations of these φ, $\log i$ curves the current density was doubled at each step, and each current density was held for 5 min. Because of the considerable ohmic resistance of the passivating layer, the current density at which oxygen begins to evolve (Point e, Fig. 3) is somewhat lower than the current density for the anodic dissolution of active zinc at the critical point (Point k).

The curve for the evolution of oxygen on a passive zinc electrode (region c, Fig. 3) in φ, $\log i$ coordinates approximates to a straight line the slope of which, as Fig. 3 shows, depends to a considerable extent on the temperature.

TABLE 2

Critical Current Densities i_{cr}

Solution composition	Critical current density (in ma/cm²) at temperature (°C)					
	0°	−10°	−20°	−30°	−40°	−50°
Pure Zn (Ts-O) anode						
9.3 N KOH + 2 g-equiv/liter Zn	38	21	14.2	6	1.4	0.4
5.5 N KOH + 1.68 g-equiv/liter Zn	40	33	14	10	4	1.2
Anode zinc alloy containing 1.5% Hg						
9.3 N KOH + 2 g-equiv/liter Zn	36	24.2	16.2	10	3.2	2.4
5.5 N KOH + 1.68 g-equiv/liter Zn	38	32	22	12	5	2.4
4.2 N KOH + 1 g-equiv/liter Zn	34	20	15	—	—	—
9.3 N KOH + 6 g-equiv/liter Zn	7	4	2.8	2	1.4	0.4

Table 1 gives the critical passivation-current densities in 4.2, 7.0, and 10 N KOH and 4.2 N NaOH for the above-named temperature range, for pure zinc and for zinc–mercury alloy.

The general course of the polarization curves for pure zinc (Ts-O) and alloy containing 1.5% Hg in zincate solutions is similar to that of the curves described above (Fig. 3).

Comparison of the data in Tables 1 and 2 shows that the critical passivation-current densities decrease both with decrease of alkali concentration and with increase of zincate concentration. Fall of temperature has a greater influence on the decrease of critical current density for pure zinc electrodes than for zinc–mercury alloy.

For zinc–mercury alloy, the slope factor $d\varphi/d\log i$ of the plots for the liberation of oxygen on passive zinc is also considerably less at all temperatures. The potential of passive zinc increases with time in the course of anodic polarization, the increase being greater in solutions containing zincate.

In concentrated solutions of caustic potash, passivation is a diffusion process of saturation of the layer near the electrode with zincate.

In the first approximation, this process may be represented as follows. When an anodic current is passed at density i_a through KOH solution (without stirring), the concentration c_s of the zincate at the anode surface increases, and a concentration gradient (dc/dx) becomes established near the electrode; this results in diffusion of zincate from the anode into the solution at rate i_d. At the same time the zincate anions $Zn(OH)_4^{--}$ [7] move toward the anode under the action of the electric field in the solution with the velocity

$$i_e = nFu_i c_i E, \tag{1}$$

where $c_i u_i$ is the product of the concentration and velocity of $Zn(OH)_4^{--}$ [7], and E is the field potential in the solution.

If the anodic current density is considerably below the critical value, a steady state becomes established after a certain time, represented by the equation

$$i_a = i_d - i_e, \tag{2}$$

and c_s does not reach the value at which $Zn(OH)_2$ is precipitated and passivation occurs.

In absence of stirring the diffusion is not an equilibrium process, but after a certain time, which depends on the size of the electrode, the diffusion may become steady.

In the case of nonequilibrium diffusion the concentration gradient near the electrode depends on the time

$$-\left(\frac{dc}{dx}\right)_{x=0} = \frac{c_s - c_0}{\sqrt{\pi Dt}}, \tag{3}$$

where c_0 is the zincate concentration in the bulk of the electrolyte, t is the time from the start of polarization, and D is the coefficient of diffusion. The diffusion front moves away from the electrode in the course of time, and the concentration gradient diminishes. The diffusion current therefore decreases with time t.

$$i_d = nFD\,\frac{c_s - c_0}{\sqrt{\pi Dt}}\,. \tag{4}$$

If the anodic current density is kept constant i_a = const, then for constant removal of zincate from the electrode a constant concentration gradient must be maintained, i. e., c_s must increase with time in proportion to $\sqrt{t}$, in accordance with the equation

$$c_s - c_0 = ki_d\sqrt{t}\,. \tag{5}$$

Passivation occurs when c_s reaches a value at which the KOH solution near the electrode becomes saturated with zincate and zinc hydroxide is formed. The value of c_s depends on the KOH concentration, its initial zincate concentration (c_0), and the temperature. Equation (5) may be used for calculation of the time necessary for pas-

sivation of the electrode if the coefficient of diffusion of $Zn(OH)_4^{--}$ ions under passivation conditions, and the surface concentration c_s of the zincate at which zinc hydroxide should be precipitated, are known.

We first assume the rate of electrical transfer i_e constant; we then have from Eq. (5) with c_s = const for two different values of $i_a \geq i_{cr}$

$$\frac{i_1}{i_2} = \frac{\sqrt{t_2}}{\sqrt{t_1}} \quad \text{or} \quad \frac{t_2}{t_1} = \frac{i_1^2}{i_2^2}, \tag{6}$$

assuming that $i_1 = 1$, $t_1 = A$

$$t_2 = A\frac{1}{i_2^2}, \quad \text{and} \quad \log t = A - 2\log i_a, \tag{7}$$

which is the equation for the passivation time as a function of current density.

A similar equation was derived by Müller [8] by different reasoning. Equation (7) is not accurate for the case in question; it is also necessary to take into account electrochemical transport of $Zn(OH)_4^{--}$ ions to the electrode.

If i_a, E and u are assumed constant, the concentration of $Zn(OH)_4^{--}$ near the electrode increases with time, in accordance with Eq. (5). Therefore, if we take into account the increase of electric transport with increase of $Zn(OH)_4^{--}$ concentration, which is also proportional to $\sqrt{t}$, instead of Eq. (6) we have

$$i_1 = i_2\sqrt[4]{t}; \quad t = Q\frac{1}{i^4}, \tag{8}$$

and instead of Eq. (7) we have

$$\log t = A - 4\log i_a. \tag{9}$$

Thus, the coefficient of the logarithm may be about 4.

In fact, Iofa, Mirlina, Moiseeva, and Krymakova [1] obtained the following values for this coefficient in 5.2 N KOH: 4.0 at −15°, 3.9 at 0° and 3.57 at +30°.

The constant A and the coefficient of the logarithm of the anodic current density may vary according to the conditions of ion diffusion near the electrode, and also according to the electrode shape and size.

Passivation of the Zinc Electrode in the Cell

The operating current density at the zinc electrode in the cell is always considerably below the critical passivation-current density, and hence it might be concluded that the electrodes are not passivated at all in concentrated KOH solutions. However, it is found in practice that passivation of zinc electrodes does occur, usually at the start of the secondary period of cell operation. Under normal operating conditions, the passivation process depends to a considerable extent on the nature of the zinc hydroxide precipitate formed in the layer near the electrode.

Experiments were carried out with the aim of finding a connection between the modification of the precipitate formed and passivation of the zinc electrode in the working cell. A carbon–air electrode was used as the positive pole in these experiments. The current density used was 3 ma/cm², with 3, 5, 7, and 10 N KOH solutions at 20, 0, −10, −15, and −20°.

The precipitates deposited on the electrodes and formed in solution were studied microscopically by transmitted light (magnification × 600).

These experiments showed that in 3 N KOH at room temperature only the primary process is involved in cell operation. At the start of the secondary process the zinc electrode becomes coated with a solid crust and becomes passive. The precipitate from the electrode (Fig. 4) and from the solution consists of the rhombic modi-

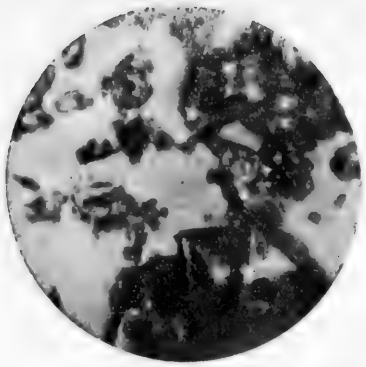

Fig. 4. Precipitate on electrode (3 N KOH) at 20°.

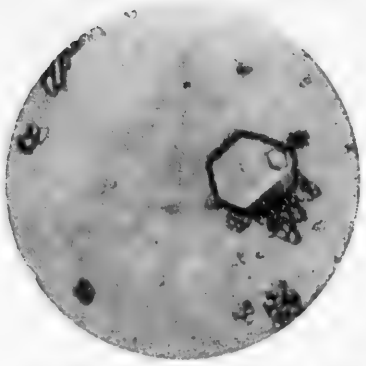

Fig. 5. Precipitate in electrolyte (3 N KOH) at 20°.

Fig. 6. Precipitate in electrolyte (3 N KOH) at 0°.

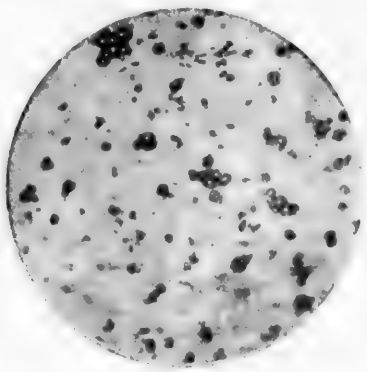

Fig. 7. Precipitate in electrolyte (7 N KOH) at 20°.

Fig. 8. Precipitate in electrolyte (7 N KOH) at 0 and 20°.

Fig. 9. Precipitate in electrolyte (10 N KOH) at 20°.

fication of zinc hydroxide ϵ-$Zn(OH)_2$. When the cell operates at 0°, the electrolyte contains, in addition to rhombic zinc hydroxide, some of the prismatic modification γ-$Zn(OH)_2$ (Fig. 6). As the precipitate accumulates, the zinc electrode becomes coated and passive at this temperature also.

At −10° the cell operation partially involves the secondary process, but the electrode is gradually coated with a crust of rhombic zinc hydroxide, and becomes passive. The precipitate formed in the solution consists mainly of prismatic zinc hydroxide, but individual rhombic crystals are also found. After passivation of the electrode, the whole precipitate gradually passes into rhombic zinc hydroxide.

Cells with 5 N KOH solution operate satisfactorily under secondary-process conditions at −15°. The electrode remains bright. The precipitate formed is fine, does not adhere to the electrode, and consists of prismatic zinc hydroxide. At room temperature, however, the electrode is coated with a hard crust of rhombic zinc hyroxide and becomes passive at the start of the secondary process.

The precipitates formed in cells with 5 N KOH solution at the stated temperatures were studied by Landsman in the x-ray laboratory of this Institute by the Debye method with the use of a BSV ion tube with a copper anode, at wavelength $\lambda = 1.934$ A.

The x-ray data showed that the precipitate formed at room temperature in a cell with 5 N KOH solution consists of rhombic zinc hydroxide crystals, whereas the precipitate formed at −15° consists of zinc oxide crystals of prismatic zinc hydroxide γ-$Zn(OH)_2$ of hexagonal structure.

In 7 N KOH solutions at room temperature only the primary process is involved in the cell operation. The zinc electrode becomes passive at the start of the secondary process. Characteristic crystals of the rhombic modification could not be detected microscopically in the precipitate. The precipitate consisted of fine crystals of zinc oxide (Fig. 7). Both the primary and the secondary processes are involved at 0 and −20°. The precipitate consists of prismatic zinc hydroxide (Fig. 8), and the precipitate formed in cells operated at 0° consists of incompletely formed short rods of prismatic γ-$Zn(OH)_2$. The electrode remains smooth and free from deposit during operation of the cell.

The precipitates formed in cells both at 0 and −20° pass on increase of temperature into well-defined crystals of rhombic zinc hydroxide, which is more stable under these conditions.

Both the primary and the secondary processes are involved in cell operation with 10 N KOH solution at room temperature. The precipitate in the solution and near the electrode consists of well-formed rods of zinc oxide, of bottle shape (Fig. 9). The precipitate is fine and does not adhere to the electrode. The zinc electrode remains smooth and free from precipitate.

At 0 and −20° only the primary process is involved. At the start of the secondary process the zinc electrode is coated with a hard crust and becomes passive. Microscopic investigation showed that the precipitate consists of rhombic zinc hydroxide with fragments of prismatic crystals which have not yet passed into the rhombic form.

The precipitate in the electrolyte consists of zinc oxide with about 20% of short fragments of rhombic zinc hydroxide.

The appearance of a particular modification of the hydroxide does not always correspond to its stability at the given temperature and alkali concentration; it also depends on the degree of supersaturation of the solution with zincate and on the rate of precipitate of the hydroxide.

At low temperatures, if the precipitation rate is rapid, concentrated solutions supersaturated with respect to zincate may deposit the least stable form γ-$Zn(OH)_2$, which cannot passivate the electrode, and which then passes very slowly into the equilibrium form ϵ-$Zn(OH)_2$ or ZnO in the bulk of the solution, without affecting the electrode process.

SUMMARY

1. It was found in a study of the behavior of zinc electrodes during anodic polarization in alkaline solutions that the critical passivation-current density decreases with decrease of temperature. This decrease is more prominent at high alkali concentrations. The critical passivation-current density also falls rapidly with increasing saturation of the caustic potash solution with zincate.

2. Investigation of charging curves in dilute KOH solutions showed that the minimum electrochemical capacity of zinc passivation is 5 millicoulombs/cm^2, which corresponds to about 18 molecular layers of zinc oxide.

3. In a working cell, passivation of the zinc anode may take place at current densities well below the critical value. In such cases passivation depends on supersaturation of the electrolyte with zincate and on the modification of the hydroxide precipitates which may be formed on the anode or in the bulk of the electrolyte.

4. Microscopical and x-ray investigations of the precipitates formed on the electrodes and precipitated within the bulk of the solution at the start of the secondary period of cell operation showed that, in agreement with the earlier findings of Iofa and associates, rhombic zinc hydroxide is in most instances responsible for passivation of zinc anodes; formation of zinc oxide or of the prismatic hydroxide under equilibrium conditions does not lead to passivation of zinc anodes.

In conclusion, I offer my deep gratitude to Prof. Z. A. Iofa, under whose guidance this work was performed.

LITERATURE CITED

[1] Z. A. Iofa, S. Ia. Mirlina, and N. B. Moiseeva, J. Appl. Chem. 22, 9, 983 (1949).

[2] H. Fischer and N. Budilov, Z.f. Metallkunde 32,100 (1940).

[3] K. Huber, Helv. Chem. Acta 26, 1037 (1943).

[4] J. J. Thomson, Proc. Phys. Soc. London 40, 79 (1928).

[5] N. P. Pilling and R. E. Badworth, J. Inst. of Metall. 29, 529 (1923).

[6] V. I. Veselovskii, J. Phys. Chem. 21, 983 (1947); 22, 1427 (1948); 24, 64 (1952).

[7] T. P. Dirkse, J. Electrochem. Soc. 102, 9, 497 (1955).

[8] E. Hedges, Protective Films on Metals [Russian translation] (1934).

Received May 16, 1956

BEHAVIOR OF CALCIUM–OXIDE CARBON ELECTRODES IN THE ELECTROLYSIS OF FUSED CHLORIDES

M. V. Smirnov, S. F. Pal'guev, and Iu. N. Krasnov

The literature contains indications of the possibility of anodic chlorination of intimate mixtures of metal oxides with carbon in fused chlorides. It was shown by Dolgov, and also in research at the Laboratory of Nonferrous Electrometallurgy of the Leningrad Polytechnic Institute [1], that in the electrolysis of fused carnallite, with an anode consisting of an intimate mixture of magnesium oxide and carbon, chlorination takes place, and the chlorine is completely utilized in the reaction; the anode gas contains CO_2 and CO only. Similar information is found in a Japanese patent [2]. Several patents [3] are concerned with the formation of the chlorides of aluminum, beryllium, and alkaline-earth metals by electrolysis in fused electrolytes with the use of anodes consisting of intimate mixtures of these metals with carbon.

According to some authors [1, 2] oxide–carbon anodes are chlorinated by the highly concentrated active chlorine liberated as the result of discharge of chloride ions. If it is assumed that only the electrochemical reaction

$$2Cl^- - 2e \rightarrow 2Cl \rightarrow Cl_2,$$

takes place at these anodes, then the potential of an oxide–carbon electrode should depend only on the pressure of the adsorbed chlorine if the activity of the chloride ions in the melt remains unchanged. The chlorine pressure evidently depends on the ratio of the rate of chlorine evolution as the result of the electrode reaction, to the rate of chlorine consumption in the chlorination of the oxide–carbon mixture.

We found that the potentials of calcium oxide–carbon electrodes in chloride melts reach values 2 v on the negative side of the potential of the chlorine electrode. This means that the pressure of the adsorbed chlorine on them is negligibly low (of the order of 10^{-19} to 10^{-20} atmos). However, the potentials of oxide–carbon electrodes remain stable under conditions in which access of chlorine is excluded, if the $CaCl_2$ concentration in the electrolyte is maintained constant. It was shown that calcium oxide–carbon electrodes are reversible with respect to calcium ions in chloride melts. In accordance with the electrode reaction

$$CaO + \frac{1}{2}C - 2e \rightleftarrows Ca^{++}(\text{melt}) + \frac{1}{2}CO_2$$

the equilibrium potentials are determined by the activity of Ca^{++} ions in the melt and the carbon dioxide pressure in the cell, in conformity to the the thermodynamic equations

$$E = E^0 + \frac{RT}{2F}\ln a_{Ca^{++}}(\text{melt}),$$

$$E = \text{const} + \frac{RT}{4F}\ln P_{CO_2}.$$

It was therefore demonstrated that the discharge of chloride ions at oxide–carbon anodes may be accompanied by a second electrochemical reaction with direct entry of metal ions into the electrolyte, as in anodic dissolution of a metal.

It was of interest to determine the extent to which these reactions are involved in the anodic chlorination of an oxide–carbon mixture. This could be done by studies of the polarization of oxide–carbon anodes over the widest possible range of current densities. Since calcium oxide readily forms the carbonate with carbon dioxide, it was also desired to determine how this reaction influences the course of anodic chlorination.

EXPERIMENTAL

The electrodes were made from pure calcium oxide which was first heated at 1000°. It was mixed with coal-tar pitch in benzene in a ball mill. The benzene was removed by evaporation in a current of warm air, and the resultant powder was molded into cylindrical electrodes. They were baked in absence of air and stored in desiccators over anhydrous $CaCl_2$ before the experiments. The electrodes contained excess carbon up to double the stoichiometric amount necessary for complete combination with the oxygen of the oxide to give carbon dioxide.

Electrolysis of Fused Chlorides with Calcium Oxide–Carbon Anodes

The apparatus used for the experiments is shown schematically in Fig. 1. The electrolyte was a fused equimolar mixture of sodium and potassium chlorides. To prevent access of the alkali metals to the anode, the cathode and anode compartments were separated by a porous corundum crucible, which served as a diaphragm.

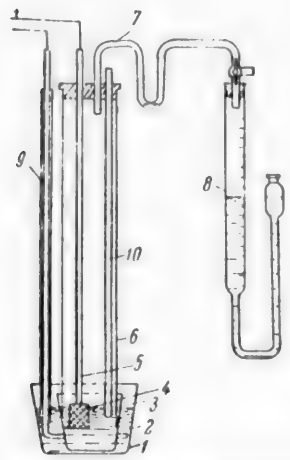

Fig. 1. Apparatus used for electrolysis experiments with oxide–carbon anodes. 1) Porcelain crucible, 2) fused electrolyte, 3) corundum crucible (diaphragm), 4) oxide–carbon anode, 5) carbon conductor, 6) quartz tube (vessel for collection of anode gases), 7) outlet tube, 8) buret, 9) molybdenum cathode, 10) thermocouple.

The anode gases were passed through a U-tube containing KI solution, which acted as an indicator for chlorine, and collected in a buret over dilute aqueous sulfuric acid. The gases were analyzed for CO_2 and CO.

The electrolyte was dissolved in water after the experiment. The remains on the anodes were washed in water, the wash waters were combined with the electrolyte solution, and the liquid was filtered to remove suspended carbon and carbonate particles. The filtrate was analyzed for chloride and calcium hydroxide.

There was little destruction of the electrodes in all the experiments performed at low current densities (about 0.1 amp/cm^2); the excess carbon remained in the form of a porous mass which persisted even when washed in water. The results of experiments in which the initial current density was 0.1 amp/cm^2 are given in the table. The temperature was 700°. The anodes contained approximately two-fold excess of carbon.

The current efficiency with respect to calcium chloride was close to the theoretical. The anode gas consisted almost entirely of carbon dioxide, containing traces of carbon monoxide (detected by the reaction with aqueous palladium chloride solution). Chlorine appeared in the anode gas at higher current densities, and only some time after the start of electrolysis (after 2 min at D_a = 2.4 amp/cm^2, and only after 20 min at D_a = 1 amp/cm^2). At current densities below 0.3 amp/cm^2 the anodes, 13 mm in diameter, were completely exhausted (the calcium oxide dissolved and a light porous mass of excess carbon remained) without liberation of chlorine.

The current efficiency with respect to carbon dioxide was influenced by the behavior of the calcium oxide–carbon anodes. If it is assumed that only the following reaction takes place at the anode:

$$CaO + \frac{1}{2}C + 2Cl^- - 2e \rightarrow CaCl_2 \text{ (melt)} + \frac{1}{2}CO_2. \qquad (I)$$

Results of Electrolysis Experiments with Calcium Oxide–Carbon Electrodes

Original anode			Quantity of electricity passed (amp-hrs)	Ca found after electrolysis (in g)		CO_2 evolved (in g)	Current efficiency (%)	
weight (in g)	including (in g)			in electrolyte	in anode residue		$CaCl_2$	CO_2 by electrode reaction (1)
	Ca	C						
3.74	2.15	0.71	0.75	0.56	1.43	0.18	100.0	52.8
3.15	1.76	0.69	1.30	0.94	0.81	—	96.6	—
3.45	1.99	0.66	1.52	1.10	0.80	0.25	101.0	40.0
4.43	2.52	0.92	2.56	1.91	0.74	0.71	100.0	67.6
4.37	2.40	0.92	2.98	2.23	0.17	0.95	100.0	77.8

then the yield of carbon dioxide is considerably below the theoretical. Figure 2 represents the results of one of the experiments; these show the variation of the rate of evolution of carbon dioxide in the course of electrolysis, with a constant current strength of 1.08 amp. It is seen that carbon dioxide appears some time after the start of electrolysis, and is formed in continuously increasing amounts. It is probable that at first the following reactions take place at the oxide–carbon anodes:

$$CaO + \frac{1}{2}C + 2Cl^- - 2e \rightarrow CaCl_2 \text{ (melt)} \quad + \frac{1}{2}CO_2 \;\&\; CaO + CO_2 \rightarrow CaCO_3.$$

and the chlorination of carbonate begins later:

$$CaCO_3 + \frac{1}{2}C + 2Cl^- - 2e \rightarrow CaCl_2 \text{ (melt)} + \frac{3}{2}CO_2. \qquad \text{(II)}$$

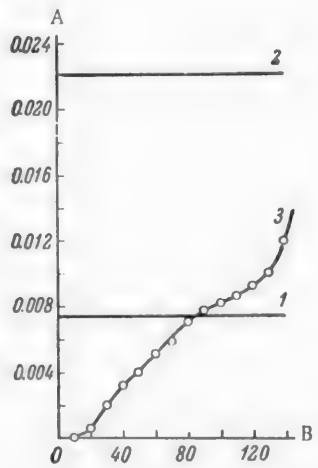

Fig. 2. Variation of the rate of evolution of carbon dioxide with exhaustion of calcium oxide–carbon electrode during electrolysis. A) Rate of CO_2 evolution (in g/min), B) electrolysis time (min). 1) Calculated for Reaction (I), 2) calculated for Reaction (II), 3) experimental curve.

Measurements showed that the equilibrium potentials of carbonate–carbon electrodes (consisting of intimate mixtures of $CaCO_3$ and carbon) are 0.1-0.2 v more positive than the potentials of calcium oxide–carbon electrodes. Therefore the oxide is chlorinated first during electrolysis, while the carbonate remains unaffected and accumulates in the surface layer of the anode. As the front of Reaction (I) penetrates deeper, polarization of the anode increases. When it has increased by 0.1-0.2 v, chlorination of the carbonate begins, accompanied by evolution of carbon dioxide. The front of Reaction (II) follows that of the first reaction at a distance which depends on the current strength, and the composition and the density of the electrode mass.

The zonal character of the electrode reactions was clearly revealed in transverse fractures of the anodes after electrolysis. Three zones were distinctly seen. The external zone consisted of an exhausted crust of carbon impregnated with the electrolyte. The intermediate layer represented the region where calcium carbonate accumulated. Unchanged oxide–carbon mass was found inside the anode.

Special experiments were performed on electrolysis with carbonate–carbon anodes. These were made from pure carbonate and coal-tar pitch in the same way as the oxide–carbon anodes. However, the baking temperature was lower (700°), to avoid decomposition of the carbonate. Carbon dioxide was liberated at these anodes

right from the start of electrolysis. The current efficiencies with respect to CO_2 and $CaCl_2$ corresponded to the theoretical values for Reaction (II).

Polarization of Calcium Oxide–Carbon Anodes in Fused Chlorides

Investigation of the electrolysis products showed that at least two other electrode reactions may take place at calcium oxide–carbon electrodes, apart from discharge of chloride ions with subsequent secondary chlorination of the oxide–carbon mixture:

$$CaO + \frac{1}{2}C - 2e \rightarrow Ca^{++}\ (melt) + \frac{1}{2}CO_2$$

$$CaCO_3 + \frac{1}{2}C - 2e \rightarrow Ca^{++}\ (melt) + \frac{3}{2}CO_2.$$

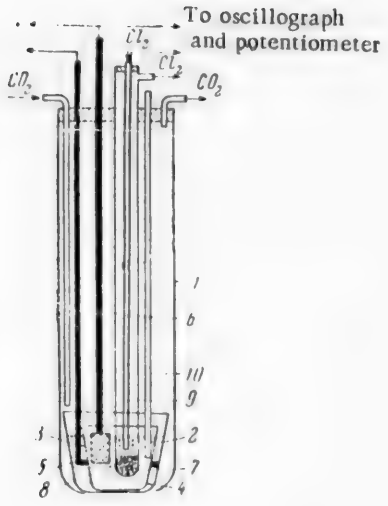

Fig. 3. Cell used for polarization measurements on calcium oxide–carbon anodes. 1) Quartz beaker, 2) porcelain crucible, 3) oxide–carbon anode, 4) corundum crucible (diaphragm), 5) molybdenum cathode, 6) quartz test tube, 7) diaphragm made from oxide–carbon crumbs, 8) quartz sand, 9) chlorine electrode, 10) thermocouple.

However, it is not possible to determine how these reactions occur in practice from the results of the experiments described above. For a more detailed elucidation of the mechanism of anodic chlorination, the polarization of calcium oxide–carbon anodes was studied over a wide range of current densities.

The experiments were performed in a closed cell the construction of which is shown schematically in Fig. 3. The electrolyte was a fused equimolar mixture of sodium and potassium chlorides with 1% of $CaCl_2$ by weight. The anode and cathode spaces were separated by a diaphragm (porous corundum crucible). Before the oxide–carbon anode was immersed in the electrolyte, its outer layer was taken off in order to remove the carbon crust which may have formed during the molding and baking. The anode potential was measured relative to a chlorine electrode, the design and operation of which were described earlier [4]. To exclude access of chlorine to the anode, the chlorine electrode was enclosed in a quartz test tube with a small hole at the end; this hole was covered with a layer of crumbled electrode mass, which very effectively absorbed the chlorine dissolved in the melt. The measurements were made with the aid of a loop oscillograph, the potential after disconnection of the polarizing current being recorded on photographic film to an accuracy of 0.01 v. The current density was varied between $2 \cdot 10^{-4}$ and 1.5 amp/cm^2. The temperature was kept at 800° to the nearest ± 2-5°. The measurements were commenced after equilibrium potential became established; this required up to 5 hours.

The results of determinations performed with 6 electrodes are given in Fig. 4 in the form of a plot of the anode potential against log current density.

In the region of low current densities (below 0.05 amp/cm^2) the anode potential of the oxide–carbon electrodes is close to the equilibrium value, and changes little with current density (a 250-fold increase of current density increases the anode potential by 0.06 v). The experimental points fit satisfactorily on a straight line represented by the empirical equation

$$\varphi_1 = -1.96 + 0.02 \log i.$$

A relatively small break is found in the course of the polarization curve when the anode potential has increased by about 0.1 v. With further increase of current density the experimental points lie on a straight line

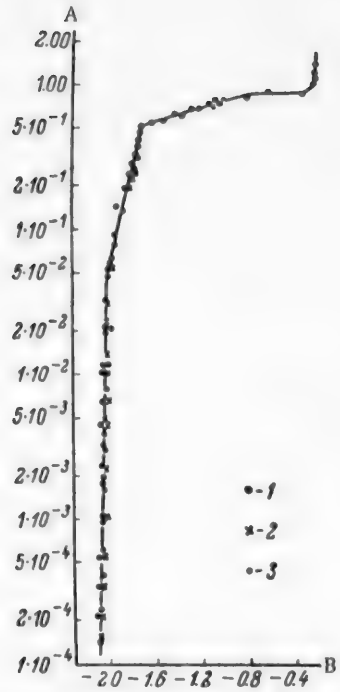

Fig. 4. Polarization curve for calcium oxide–carbon anodes. A) Current density (in amps/cm^2), B) potential relative to the chlorine electrode (in v). 1) First series; 2) second series; 3) third series of measurements.

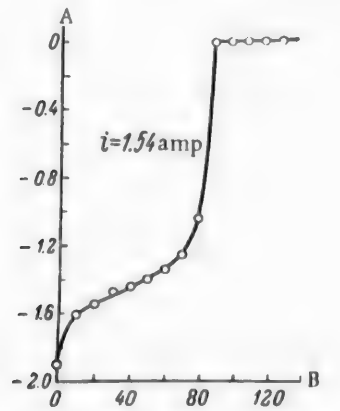

Fig. 5. Variation of the potential of a calcium oxide–carbon anode with its degree of exhaustion during electrolysis. A) Anode potential relative to the chlorine electrode (in v), B) electrolysis time (min).

(the second region of the polarization curve) represented by the empirical equation

$$\varphi_2 = -1.63 + 0.10 \log i.$$

When the potential of the oxide–carbon anode has reached a value about 1.7 v on the negative side of the potential of the chlorine electrode, the course of the polarization curve changes sharply: anode polarization rises rapidly with the current density. Finally, chlorine appears in the anode gas and the anode potential, having reached about −0.2 v relative to the chlorine electrode, becomes almost constant with further increase of current density.

This type of polarization was observed with many calcium oxide–carbon electrodes. This excludes any individual variations in the behavior of the electrodes, and makes it possible to draw certain general conclusions concerning the electrode reactions which take place at calcium oxide–carbon electrodes in chloride melts.

If we consider that only discharge of chloride ions takes place at the anode, it must be assumed that the rate of chlorine consumption in the secondary reaction of chlorination is highest during the liberation of the first portions, corresponding to pressures of the order of 10^{-19} to 10^{-20} atmos. However, this assumption does not bear close examination.

Chloride ions are discharged at the most conducting carbon particles, and the liberated chlorine is adsorbed by them. The adsorption takes place on a surface which is very heterogeneous from the energy aspect. The chlorine liberated at low current densities must naturally be adsorbed at the most active centers of the surface, and should therefore be bound more firmly with the carbon. This hinders its diffusion along the surface to points of contact of the carbon and oxide particles, i. e., the rate of the chlorination reaction is diminished.

It is likely that the following electrode reaction is the main reaction at low current densities:

$$CaO + \frac{1}{2}C - 2e \rightarrow Ca^{++} \text{ (melt)} + \frac{1}{2}CO_2.$$

Because of the low conductivity of the oxide, the front of this reaction is confined to the points of contact of the oxide and carbon particles with each other and with the electrolyte. As the current density increases, a limiting current is ultimately reached owing to the difficulties in the passage of current through the reaction zone. Further increase of the current density is possible either by discharge of chloride ions, or as the result of the entry of a second electrode reaction into the process. The latter probably occurs in calcium oxide–carbon electrodes. In all probability, the second region of the polarization curve corresponds to superposition of the electrode reaction

$$CaCO_3 + \frac{1}{2}C - 2e \rightarrow Ca^{++} \text{ (melt)} + \frac{3}{2}CO_2,$$

which has greater kinetic hindrances than the first reaction.

When the limiting current of these reactions has been reached, further increase of current density is possible only as the result of discharge of chloride ions, the chlorine being adsorbed on the surface of the carbon particles. The potential of the anode is determined by its activity (surface concentration) which is found to increase rapidly with current density. When the surface has become saturated with adsorbed chlorine, some chlorine begins to leave with the anode gas (it is carried away with carbon dioxide). As a result, the activity of the chlorine adsorbed on the anode becomes almost constant. A sharp break appears on the polarization curve; the last region of the latter is almost parallel to the log current density axis.

The partial pressure of chlorine in the anode gas is several millimeters of mercury. It gradually increases with increasing current density, and the potential of the oxide–carbon anode accordingly approaches that of the chlorine electrode. If a carbon crust is formed, the anode potential increases much more rapidly. This is seen in Fig. 5, which gives the results of an experiment on the variation of the anode potential in the course of electrolysis at constant current strength of 1.54 amps. The original anode contained 3 g of oxide and 0.7 g of carbon.

At the start of the electrolysis the potential rose fairly rapidly (from −1.9 to −1.6 v in 10 min). The rise then slowed down considerably (the increase in 60 min was 0.35 v), and then the potential rose rapidly again to a value close to the potential of the chlorine electrode.

These observations are in harmony with the electrode processes discussed above. The initial increase of the anode potential is evidently associated with deepening of the front of the first electrode reaction, and commencing development of the front of the second electrode reaction. The latter proceeds with evolution of carbon dioxide, which widens the pores of the carbon crust and assists mixing of the electrolyte. This probably accounts for the fact that a fairly large proportion of the anode becomes exhausted at relatively low polarization. As the fronts of the electrode reactions penetrate deeper, their limiting current values are ultimately reached, and the electrolysis current is then mainly due to discharge of chloride ions on the exhausted carbon crust. Access of chlorine to the inner layers of the anode becomes increasingly difficult, its pressure rises rapidly, and desorption commences, the amount of chlorine in the anode gas increasing continuously. The anode potential increases accordingly, and ultimately reaches the value of the potential of the chlorine electrode.

SUMMARY

1. It was shown in a study of the behavior of calcium oxide–carbon and calcium carbonate–carbon electrodes in the electrolysis of fused chlorides that chlorine is not liberated at relatively low current densities; the reactions taking place at the anode are chlorination of calcium oxide

$$CaO + \frac{1}{2}C + 2Cl^- - 2e \rightarrow CaCl_2 \text{ (melt)} + \frac{1}{2}CO_2$$

and of calcium carbonate which is formed by the reaction between carbon dioxide and the oxide

$$CaCO_3 + \frac{1}{2}C + 2Cl^- - 2e \rightarrow CaCl_2 \text{ (melt)} + \frac{3}{2}CO_2.$$

2. It was found in a study of the polarization of calcium oxide–carbon electrodes over a wide range of current densities ($2 \cdot 10^{-4}$ to 1.5 amp/cm^2) that below 0.05 amp/cm^2 the anode potential is close to the equilibrium value, and changes little with the current density. Above 0.5 amp/cm^2 strong polarization occurs, caused by accumulation of adsorbed chlorine.

3. On the basis of the experimental data it is suggested that below 0.5 amp/cm^2 anodic chlorination proceeds mainly by direct entry of Ca^{++} ions into the melt. At higher current densities discharge of Cl^- ions and subsequent chlorination of the oxide–carbon mixture begins to play the principal role.

LITERATURE CITED

[1] Iu. V. Baimakov, Electrolysis in Metallurgy 2 (Metallurgy Press, 1944),* p. 203.

[2] J. Egami, Japanese patent 305 (1953); Chem. Abs. 48, 1181 (1954).

[3] Gesselschaft zur Verwendung Chemisch-Technische Verfahren, French patent 830063 (1938); Chem. Abs. 33, 50 (1939); French patent 49714 (1939); Chem. Abs. 36, 2482 (1942); British patent 511076 (1939); Chem. Abs. 34, 5356 (1940); German patent 729159 (1942); Chem. Abs. 38, 306 (1944).

[4] M. V. Smirnov, S. F. Pal'guev, and L. E. Ivanovskii, J. Phys. Chem. 29, 774 (1955).

Received March 26, 1956

* In Russian.

ELECTROCHEMICAL PRODUCTION OF ALLOYS OF NICKEL WITH MOLYBDENUM OR TUNGSTEN FROM AQUEOUS AMMONIACAL ELECTROLYTES

T. F. Frantsevich-Zabludovskaia and A. I. Zaiats

Much attention has been devoted in recent years to methods of production and studies of the properties of alloys of molybdenum, tungsten, and chromium with metals of the iron group, used as corrosion-resistant or heat-resistant materials.

Such alloys can be produced by electrochemical as well as by thermal methods. Most of the electrolytes used up to the present for this purpose contain oxyacids or their salts in fairly high concentrations [1-4]; these increase the cost of the electrolyte considerably. Current efficiencies up to 70% are obtainable with such electrolytes, but we found in practice that they have an important defect – anodic decomposition of the oxyacid anions. This occurs even with the use of soluble anodes, as they always contain passive regions which serve as sites of oxygen evolution.

Accumulation of oxidation products of oxyacids in the electrolytes has an adverse effect on the quality of the deposits and ultimately lowers cathodic current efficiencies, in some instances nearly to zero.

The service life of such an electrolyte is therefore very limited; in view of its cost, this is very uneconomic. Moreover, cathodic deposits of alloys formed from such electrolytes sometimes contain up to several tenths of 1% of carbon; this increases with increasing decomposition of the oxyacid.

Searches for cheaper electrolytes, with a longer service life, are of undoubted interest.

The only noteworthy investigation in this field is that of Gol'ts and Kharlamov [5], who proposed the use of an aqueous ammoniacal electrolyte containing no other complex formers for the production of nickel–tungsten coatings. Electrolytes of this type are suitable mainly for the production of alloys of nickel with tungsten or molybdenum, since nickel is the only metal of the iron group to give readily soluble complexes with ammonia. Cobalt can only be retained in solution if a very large excess of ammonium salts is present.

Our preliminary experiments showed that ammoniacal electrolytes are suitable for the production of nickel–molybdenum as well as nickel–tungsten alloys.

EXPERIMENTAL

Certain technological relationships in the production of the above-named alloys from ammoniacal electrolytes were studied. The effects of concentrations of the principal components and ammonia in the electrolyte, cathodic current density, and temperature on the composition of the alloys and current efficiency were investigated.

The experiments were performed in small cells, 0.5 liter in volume, with circulating electrolytes and vigorous stirring; soluble anodes were used.

Nickel–Molybdenum Alloys

Effect of concentration of the principal components. In the production of nickel–molybdenum alloys, the effect of the concentrations of the main components on the composition of the alloy formed and on the current efficiency was studied in electrolytes containing 3 g of sodium chloride and 200 ml of 25% ammonia solution

(equivalent to 45 g of NH_3) per liter. Varying amounts of nickel and molybdenum were introduced in the form of nickel sulfate and ammonium molybdate. The electrolyte pH was in the range 10.6-10.8. The experiments were performed at 30 and 40°.

Figure 1 shows that the atomic percentage ratio of nickel to molybdenum in the alloy increases with increasing ratio of the molar concentrations of nickel to molybdenum in the electrolyte. The influence of molybdenum concentration in the electrolyte on the current efficiency is shown in Fig. 2. At the two temperatures studied the current efficiency increases with decreasing molar concentration of molybdenum in the electrolyte, and the percentage of molybdenum in the alloy also decreases. The latter also determines the appearance of the deposit. Deposits containing 17-20% Mo are dense and bright. With more than 20% molybdenum the deposits become increasingly dark and loose. Considerable dendrite formation takes place with less than 15% molybdenum.

TABLE 1

Effect of the Ratio of Molar Concentrations of Molybdenum and Nickel in Solution on Their Contents in the Alloy

Conc. in electrolyte				Ratio of molar concentrations	Composition of alloy*				Ni—Mo ratio (in atomic %)	Current efficiency (%)
in g/liter		molar			in wt.%		in atomic %			
nickel	molybdenum	nickel	molybdenum		nickel	molybdenum	nickel	molybdenum		
17.55	16.0	0.30	0.167	1.8	66.7	28.80	79.0	20.90	3.76	3.6
14.63	9.6	0.25	0.100	2.5	76.6	18.88	87.0	13.00	6.70	24.9
11.70	12.8	0.20	0.134	1.5	72.2	23.33	83.5	16.50	5.05	14.3
11.30	8.0	0.19	0.085	2.25	74.8	20.72	85.5	14.50	5.90	46.5
11.70	6.4	0.20	0.067	3.0	78.0	17.53	88.2	11.80	7.47	40.5
11.70	4.5	0.20	0.047	4.25	80.7	14.75	90.0	10.00	9.00	54.5
11.70	3.2	0.20	0.033	6.0	84.3	11.20	92.5	7.50	12.30	42.0
5.85	6.4	0.10	0.067	1.5	78.9	16.60	88.6	11.45	7.75	38.5
5.85	3.2	0.10	0.033	3.0	81.9	13.55	90.8	9.20	9.88	36.1

* Analysis showed that the alloys contained about 0.5% impurities, mainly nonmetals; therefore the nickel content was found by difference from 99.5%.

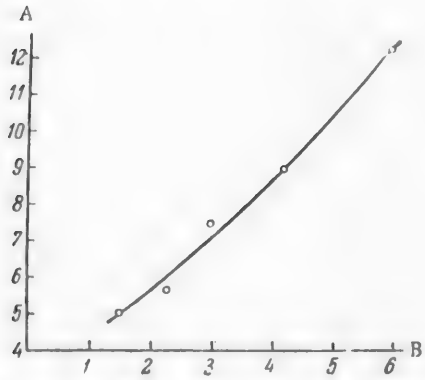

Fig. 1. Effect of the ratio of molar concentrations of molybdenum and nickel in solution on their contents in the alloy. A) Ni/Mo ratio in alloy (in atomic %), B) Ni/Mo molar ratio in the electrolyte.

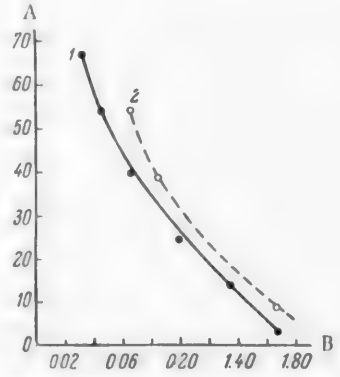

Fig. 2. Effect of molybdenum concentration in the electrolyte on current efficiency. A) Current efficient (%), B) molybdenum concentration (moles/liter). Temperature (in °C): 1) 30, 2) 40.

The effects of current density on the alloy composition and current efficiency were studied with several electrolytes, the compositions of which are given below. The results are plotted in Figs. 3 and 4. It follows from Fig. 3 that the percentage of molybdenum in the alloy always decreases with increasing current density; this is especially prominent at current densities up to 100 ma/cm^2.

Electrolyte Composition

Contents (in g/liter)		
Nickel	Molybdenum	Temperature (in °C)
14.6	9.6	2
12.0	3.4	30
12.0	6.5	30
12.0	6.5	45

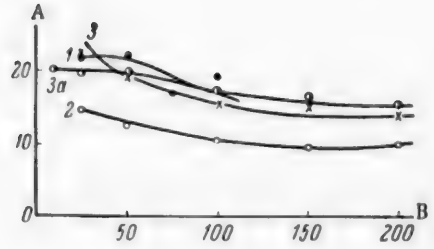

Fig. 3. Effect of current density on the molybdenum content of the alloy. A) Molybdenum content of alloy (%), B) current density D_c (ma/cm^2). Curves 1, 2, 3) 30°, 3a) 45°. Nickel concentration (g/liter): 1) 14.6; 2, 3, 3a) 12. Molybdenum concentration (g/liter): 1) 9.6; 2) 3.4; 3, 3a) 6.5.

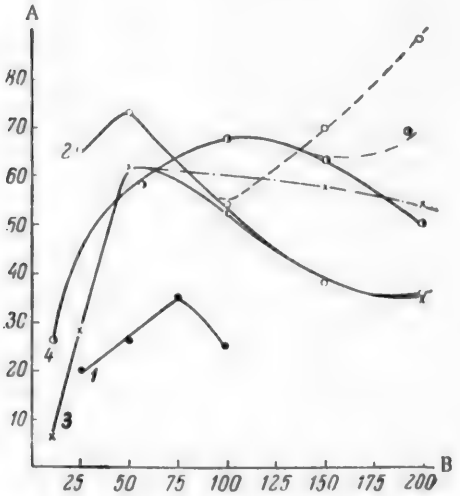

Fig. 4. Effect of current density on the current efficiency with respect to nickel–molybdenum alloy. A) Current efficiency (%), B) current density D_c (ma/cm^2). Curves 1, 2, 3) 30°; 4) 40°. Nickel concentration (g/liter): 1) 14.6; 2, 3, 4) 12. Molybdenum concentration (g/liter): 1) 9.6; 2) 3.4; 3, 4) 6.5.

It is difficult to estimate variations of current efficiency with current density, as at high current densities (150-200 ma/cm^2) vigorous formation of dendrites occurs, the composition and growth conditions of the dendrites differing from those of the rest of the metal. The amount of metal in the dendrites may be from 25 to 56% of the total metal deposited. In Fig. 4 the overall current efficiency is represented by dash lines, and the efficiency, with respect to metal without dendrites by continuous lines; the latter always pass through maxima in the region of 50-75 ma/cm^2. The maximum weight increase of the cathode per 1 amp-hr is obtained at current densities of 50-100 ma/cm^2.

Effect of ammonia concentration. The pH and ammonia content of the electrolyte were found to have an appreciable influence on the current efficiency and alloy composition. Data on the increase of the molybdenum content and decrease of current efficiency with decreasing pH of the electrolyte, for specimens of alloys obtained under similar conditions, are presented below. There is a particularly sharp drop of current efficiency when the molybdenum content of the alloy changes from 18 to over 20%, i. e., when a supersaturated solid solution is deposited.

Influence of Electrolyte pH on the Molybdenum Content of the Alloy and Current Efficiency

Electrolyte pH	Molybdenum content of alloy (%)	Current efficiency (%)
10.6	17.7	50
10.4	21.4	27.5
10.2	23.3	16

The pH of electrolytes is regulated by means of ammonia. It was therefore of interest to study the effects of ammonia concentration as well as of pH, particularly in view of the widely-held opinion [1, 2] that it is the pH that determines the current efficiency and alloy composition.

An electrolyte containing 12 g of nickel and 6 g of molybdenum per liter was used for these experiments. It may be assumed that the ammonia added to the electrolyte partially combines with the nickel forming complex hexamine cations, and the rest is present as ammonium ions or undissociated ammonium hydroxide. The amount of ammonia necessary to combine with 12 g of nickel is 21 g. The rest of the ammonia is regarded as excess.

Four electrolytes were prepared, containing 50, 100, 200, and 300% excess ammonia, respectively. The results of experiments performed at 40° and current density 100 ma/cm^2 are given below.

Effect of ammonia concentration on current efficiency

Excess ammonia (%)	Ammonia content (g/liter)	pH of electrolyte	Mo content of alloy (%)	Current efficiency (%)
50	32	10.1	17.30	68
100	42	10.6	15.74	63
200	63	11.1	15.46	47
300	84	11.2	14.76	41

These results show that both the molybdenum content of the alloy and the current efficiency decrease with increasing ammonia content in the electrolyte. Substantial changes of the ammonia concentration do not produce sharp changes of electrolyte pH, especially at high concentrations of the latter. Therefore the pH value is not a reliable criterion of the true concentration of ammonia. Consequently, the ammonia must be determined by analysis. The values of current efficiency and percentage of molybdenum in the alloy suggest that it is advantageous to have 50% excess of ammonia in the process; however, this excess of ammonia is not sufficient for dissolving the products of anodic etching, which ultimately form a dense crust of low conductivity on the anodes. It was found that the most suitable ammonia content corresponds to about 100% excess on the combined ammonia.

Nickel–Tungsten Alloys

Effect of concentrations of the principal components. In the production of nickel–tungsten alloys, the effects of the electrolyte composition on the composition of the alloy and current efficiency were studied in electrolytes containing 10 g of ammonium sulfate, 2.5 g of ammonium chloride, and 180 ml of ammonia per liter.

Different amounts of nickel were introduced in the form of nickel sulfate, and of tungsten in the form of a concentrated solution of tungstic anhydride in ammonia. The solution pH was 9.8-10.2. The experiments were performed at 27 and 42°.

TABLE 2

Effects of Nickel and Tungsten Contents in the Electrolyte on the Composition of the Alloy and Current Efficiency

	Conc. of metals in electrolyte				Tungsten content of alloy (wt.%) – I, current efficiency (%) – II			
	nickel		tungsten		I	II	I	II
	moles per liter	g/liter	moles per liter	g/liter	electrolyte temperature (°C)			
					27°		42°	
1	0.10	5.8	0.10	18.7	5.0	36.0	10.0	40.0
2	0.10	5.8	0.20	36.0	9.5	27.0	18.7	33.0
3	0.10	5.8	0.38	70.0	-	0.22	—	-
4	0.05	2.9	0.15	28.0	15.0 *	21.0	20.0	23.0
5	0.075	4.4	0.15	28.0	13.8	26.0	20.0	33.0
6	0.15	8.6	0.15	28.0	11.6	15.0	17.3	50.0
7	0.10	5.8	0.20	36.0	9.5	27.0	18.7	33.0
8	0.20	11.6	0.20	36.0	7.2	39.0	16.3	55.0
9	0.15	8.6	0.30	55.3	15.6	2.6	16.6	9.1
10	0.30	18.3	0.30	55.3	9.5	30.0	16.4	43.5
11	0.20	11.6	0.50	87.0	21.0	2.8	—	—
12	0.30	17.5	0.50	87.0	21.7	8.1	20.4	20.5
13	0.50	27.0	0.50	87.0	15.0	12.7	18.4	37.0

* The deposit was obtained in the form of black oxides, indicating that more than 40% tungsten was present. Tungsten was not determined analytically.

Two series of solutions were studied, as shown in Table 2. In the first series the nickel concentration was kept constant at 0.1 mole/liter, while the tungsten concentration was varied from 0.1 to 0.4 mole/liter. In the second series the nickel concentration was varied for each of four tungsten concentrations (0.15, 0.2, 0.3 and 0.5 mole/liter).

It is clear from the results that increase of tungsten concentration in the electrolyte with a constant nickel content as a rule leads to an increase of the tungsten content in the alloy (Nos. 1-3, 6 and 9, 8 and 11, 10, and 12 in Table 2). Conversely, increase of the nickel concentration with a constant tungsten content in the electrolyte results in a decrease of the tungsten content in the alloy (Nos. 4-6, 7-10 in Table 2). These effects are much more pronounced at the lower temperature.

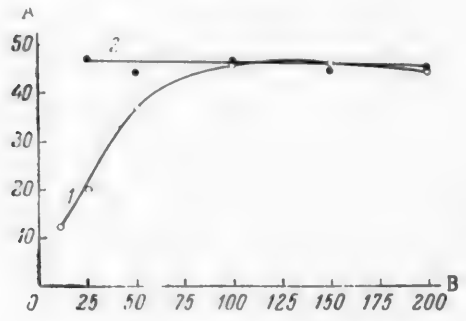

Fig. 5. Effect of current density on current efficiency with respect to nickel–tungsten alloy. A) Current efficiency (%), B) current density D_c (ma/cm^2). Temperature (°C): 1) 27, 2) 50.

Increase of the total concentration of the two metals in the electrolyte, at constant molar ratio, in most cases increases the tungsten content and lowers the current efficiency at 27°, and has almost no effect at the higher

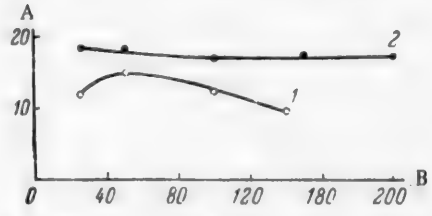

Fig. 6. Effect of current density on the tungsten content of the alloy. A) Tungsten content of alloy (%), B) current density D_c (ma/cm^2). Temperature (°C): 1) 27, 2) 50.

temperature. In the latter case the current efficiency at a given metal concentration is determined by the nickel content of the solutions (Nos. 4-6, 7-8, 12-13, Table 2).

Effect of current density. The results of a study of the effects of current density on the composition of the cathodic deposit and the current efficiency are plotted in Figs. 5 and 6.

It is clear from these results that the influence of current density differs at different temperatures. Increase of the cathode current density from 10 to 100 amp/cm^2 at 27° results in a gradual increase of current efficiency from 15 to 46%, and a decrease of the tungsten content in the alloy, whereas at 50° it has almost no effect.

Effect of ammonia concentration. The effects of ammonia concentration on the composition of the alloy and the current efficiency were also studied for tungsten electrolytes. The original solution of ammonium tungstate, used for preparation of the electrolyte and containing 200 g of tungsten per liter, had a total ammonia content of 77 g/liter, whereas the free ammonia determined analytically was only 45 g/liter. It follows that 0.11g of ammonia is combined with each gram of tungsten. It was assumed that the amount of ammonia combined with tungsten does not alter during preparation of the electrolyte. An electrolyte containing 29 g W and 6 g Ni per liter was used for the experiments. Thus, about 13 g of ammonia per liter was combined with nickel and tungsten. The rest of the ammonia was designated as excess. The results of experiments performed at 50° and current density 100 ma/cm^2 are given below.

Effects of Ammonia Concentration on Alloy Composition and Current Efficiency

Excess ammonia (%)	Ammonia content (g/liter)	pH of electrolyte	Tungsten content of alloy (%)	Current efficiency (%)
100	27	10.1	21.0	47
200	40.5	10.3	18.9	39
300	54	10.5	18.3	38
400	67.5	10.6	18.5	31
500	80	10.7	15.0	19.4

It is seen that these results are analogous to the results obtained in the study of molybdenum electrolytes; however, variations of the ammonia concentration in the range of 200-400% excess have almost no effect on the tungsten content of the alloy. In this case also sharp changes of ammonia concentration have little effect on the electrolyte pH.

Our results for the two types of alloys show that the ammonia concentration and not the pH value should be determined in ammoniacal electrolytes of high pH.

SUMMARY

1. It is shown that alloys of nickel with molybdenum or tungsten can be electrodeposited from ammoniacal electrolytes containing no oxyacids.

2. The effects of electrolyte composition and electrolysis conditions on the alloy composition and current efficiency were studied.

3. Increase of the molybdenum and tungsten concentrations at a given nickel concentration results in an increase of their percentage contents in the alloys and a decrease of current efficiency. In the production of alloys with equal contents of molybdenum and tungsten, the electrolytes differ considerably in the relative concentrations of the principal components.

4. Increase of the ammonia concentration in the electrolyte decreases both the molybdenum and tungsten contents of the alloys and the current efficiency.

5. The ammonia concentration and not electrolyte pH should be determined, as considerable variations of ammonia concentration have little effect on the pH if the latter is greater than 10.

6. Higher current efficiencies are obtained at higher temperatures. The tungsten content of the alloys increases considerably, whereas the molybdenum content is almost unchanged on increase of temperature.

7. The current efficiency passes through a maximum with increase of current density for both types of alloy. Increase of current density generally decreases the molybdenum and tungsten contents of the alloys, but has no effect on the composition of tungsten alloys at temperatures above 40°.

LITERATURE CITED

[1] M. L. Holt and L. L. Nielson, Trans. Electrochem. Soc. 82, 217 (1942); M. L. Holt and M. H. Lietzke, J. Electrochem. Soc. 94, 252 (1942); M. L. Holt and R. F. McElwee, J. Electrochem. Soc. 99, 48 (1952).

[2] A. Brenner, P. Burghead, and E. Seegmiller, J. Res. Natl. Bur. Stand. 39, 1834 (1947).

[3] H. Offermans and M. V. Strackelberg, Metalloberfläche 6, 142 (1947).

[4] I. N. Frantsevich, T. F. Frantsevich-Zabludovskaia, and E. F. Zhel'vis, J. Appl. Chem. (USSR) 25, 350 (1952);* T. F. Frantsevich-Zabludovskaia, I. N. Frantsevich, and K. D. Modylevskaia, J. Appl. Chem. (USSR) 27, 413 (1954);* T. F. Frantsevich-Zabludovskaia, A. I. Zaiats, and K. D. Modylevskaia, J. Appl. Chem. (USSR) 29, 1684 (1956).*

[5] L. N. Gol'ts and V. I. Kharlamov, J. Appl. Chem. (USSR) 9, 631, 640 (1936).

Received July 12, 1956

* Original Russian pagination. See C. B. translation.

PRECIPITATION OF COPPER AND BISMUTH BY METALLIC LEAD FROM HYDROCHLORIC ACID ELECTROLYTES

P. N. Kovalenko

The State University, Rostov-on-Don

The removal of nobler metals than Pb, such as bismuth and copper, from lead electrolytes can be effected by contact exchange between these impurities and metallic lead. The difference between the electrode potentials of Cu or Bi and of the precipitating metal – lead – is large enough to ensure complete separation of copper or bismuth under practical conditions.

The difference between electrode potentials of Bi or Cu and lead in presence of 1.0 N nitric acid and 0.1-1.0 N chloride ions indicates that the rate of the electrode reaction should be considerable (Fig. 1). The rate of this heterogeneous reaction evidently depends on the rate of diffusion of ions to the precipitating metal (Pb), while the concentration of the lead electrolyte has no appreciable influence on the electrode potentials of Bi and Cu [1].

Determination of the conditions for the maximum rate and the most complete contact exchange of these metals, for purification of lead electrolysis, is a problem of great practical interest. The development of a reliable method for determining the course of the precipitation reaction is no less important.

Determination of small quantities of copper and bismuth in presence of large quantities of lead, which is the principal component of the system under consideration, is a difficult problem. The existing methods of determination of bismuth and copper present simultaneously in lead concentrates, ores, etc. are hardly satisfactory for use in industries in which it is necessary to test the finished lead or intermediate products containing small amounts of Bi and Cu. When large amounts of bismuth are present, the phosphate or the electrochemical methods are the best for its determination. These methods can be used for determination of bismuth in presence of most metals [2].

When small amounts of Bi and Cu are present, colorimetric methods give good results [2-7]. However, for determination of small amounts of copper and bismuth in presence of large amounts of the principal component, lead, Cu and Bi must be first separated from Pb. In the present investigation bismuth and copper were separated from large amounts of lead by reduction to the metals by means of wet precipitation on lead.

The oxidation-reduction reaction of mutual displacement of metals from solution depends on a number of external factors. These factors may influence the direction of the reaction, or its rate and character. The acidity and temperature of the solution have a decisive influence on the rate and direction of oxidation-reduction reactions of bismuth and copper [8, 9].

It is known that all the metals can be arranged in a series according to their ability to displace each other from solution. However, the ability to displace other metals from solution is determined not only by the position of a given metal in the electromotive series, but also by the reaction conditions [9].

The metallic lead used in this investigation for precipitation of Bi and Cu was used in the form of plates $10 \times 4 \times 2 = 80$ cm^2 in area, and was free from copper, bismuth and antimony. The reduction of bismuth from hydrochloric acid solution by metallic lead was carried out at different concentrations of hydrochloric acid, with different reaction times and solution temperatures.

The lead plates were cleaned thoroughly with emery paper and degreased by boiling in 2.0 N caustic potash solution with the addition of 2-3 g of Rochelle salt per 100 ml of alkali [10]. The plates were then washed with alcohol and ether, and dried. The precipitation rates of metals are appreciably influenced by the concentrations of the metal ions present in solution, nature of the salts present, temperature, solution acidity, etc. Among the ions which influence the contact exchange of metals the chloride ion occupies a special position, as it tends to break down the passive film on metals which is rapidly formed in some cases after the metal is etched and immersed in the solution [11].

The precipitation of base metals is accompanied by evolution of hydrogen, which plays an important role in the process. If the hydrogen bubbles are liberated smoothly and distributed uniformly, good dense coatings of Bi and Cu metals are formed. As is known, the contact exchange of metals occurs when a metal is immersed in a solution containing a more noble metal as the result of the action of individual galvanic microcells, in which the precipitating metal acts as the negative pole and the hydrogen bubbles as the positive poles.

To bring about the contact exchange reaction, the lead plate was immersed in a beaker containing the bismuth solution, when it rapidly became coated with a gray layer of metallic bismuth. This layer was treated with 2 N nitric acid solution at 60°; small amounts of lead were dissolved, but, as was shown previously, this does not interfere either with polarographic [12] or colorimetric [13, 4] determination of bismuth.

The bismuth formed by reduction and dissolved in nitric acid was determined with the aid of a differential photocolorimeter with selenium photocells, made by the Moscow Experimental Control and Measurement Instrument Works: the galvanometer sensitivity was $1.43 \cdot 10^{-6}$ amp, R_{instr} = 211 ohms, R_{cr} = 6000 ohms.

The determination was performed by the method of internal standards. The bismuth solution was cooled to room temperature, 10 ml of 10% thiourea solution was added, and the mixture was diluted to 100 ml with distilled water; the concentration of nitric acid must not exceed 1.0 N. This solution was placed in one of the cells (B), while the other cell (A) contained a solution with all the reagents present in the unknown solution, with the exception of bismuth, and the point of balance on the photocolorimetric scale was found. Cell B was then put in the place of cell A, the same unknown solution with the addition of a definite amount of standard bismuth solution was put into cell A, and the point of balance was again found.

The amount of bismuth present in the unknown solution was found from the formula:

$$a_x = \frac{a \cdot h}{H - h},$$

where a_x is the amount of bismuth (in g), $\underline{a}$ is the amount of bismuth added (in g), $\underline{h}$ is the reading of the photocolorimeter scale for the unknown solution, and H is the reading of the photocolorimeter scale for the unknown solution with the standard solution added. The error of this method is small, being within the limits of experimental error.

In studies of the effect of hydrochloric acid concentration on the degree and rate of precipitation of bismuth from hydrochloric acid solutions, the bismuth concentration was 0.01 N. The total volume of the solution was 100 ml. The reduction reaction was performed both at room and at higher temperatures.

Each experiment was performed in triplicate. The average values are given in Table 1; the reproducibility was satisfactory.

It follows from Table 1 (Experiments 1-4) that the optimum concentration of hydrochloric acid, at which contact exchange of Bi and Pb proceeds at the highest rate, is 0.3 N. If the acidity is decreased the bismuth salt is hydrolyzed, whereas if the acidity is increased the metallic Bi begins to dissolve and the amount of metal precipitated on the lead plate decreases rapidly. On the other hand, an adequate concentration of hydrogen ions prevents the formation of oxides and basic salts of bismuth, which have a harmful effect on its quality, in the metallic deposit.

The data in Table 1 (Experiments 1-4) show that the sum of the precipitated bismuth and of the bismuth remaining in solution differs from the theoretical value by a permissible positive error.

TABLE 1

Variation of the Precipitation Rate of Bi with the Concentration of Hydrochloric Acid and the Solution Temperature (0.068 g of Bi per 100 ml of solution)

Expt. no.	HCl conc. (normality)	Bi reduced		Bi remaining in solution		Reaction time (min)	Solution temperature (°C)
		in g	in %	in g	in %		
1	0.3	0.0425	61.7	0.0278	40.2	10	18.0
2	0.5	0.0312	45.6	0.0386	56.2	10	18.0
3	0.7	0.0141	20.6	0.0565	81.9	10	18.0
4	0.9	0.0020	2.9	0.0666	98.0	10	18.0
5	0.3	0.0425	61.7	0.0278	40.2	10	18.0
6	0.3	0.0450	66.2	0.0245	36.0	15	18.0
7	0.3	0.0472	69.1	0.0221	32.0	20	18.0
8	0.3	0.0510	72.0	0.0196	28.5	30	18.0
9	0.3	0.0510	72.0	0.0196	28.5	30	20.0
10	0.3	0.0587	86.3	0.0104	15.3	30	40.0
11	0.3	0.0434	63.9	0.0260	38.5	30	60.0
12	0.3	0.0261	38.5	0.0439	64.5	30	80.0
13	0.3	0.0	0.0	0.068	100.0	30	100.0

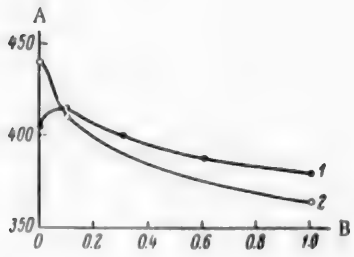

Fig. 1. Variation of the potential difference between the precipitating metal and the lead with the concentration of chloride ions in solution, for bismuth (1) and copper (2). Concentration (normality): lead 1.0, bismuth $8 \cdot 10^{-2}$, copper $5 \cdot 10^{-2}$, nitric acid 1.0. A) Potential difference $E_{Me} - E_{Pb}$ (in mv), B) chloride ion concentration (normality).

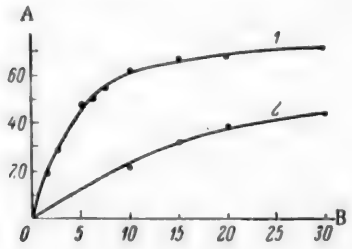

Fig. 2. Precipitation of bismuth (1) and copper (2) from 0.3 N hydrochloric acid solution at 20°. 0.068 g of bismuth and 0.032 g of copper per 100 ml of solution. A separate solution of each of the metals was used for the precipitation. A) Amount of metal precipitated (%), B) time (min).

The results of experiments on the rate and degree of reduction of bismuth at the optimum concentration of hydrochloric acid at room temperature are given in Table 1 (Experiments 5-8). These results show that the rate of contact exchange of bismuth is greatest at the start of the reaction, and decreases rapidly to a limiting value before complete reduction is attained (Fig. 2); this may be attributed to the difficulty of penetration of bismuth ions to the metallic lead surface, and to the decrease of the active surface of the metallic lead, i. e., of the surface free from bismuth.

This chemical contact-exchange reaction, like the electrode reaction in the electrodeposition of metals [14], occurs very rapidly at the interface [15], and therefore the liquid in the immediate vicinity of the lead surface is rapidly saturated with lead ions and other reaction products which hinder further chemical action. Nevertheless, bismuth ions still diffuse slowly through this layer, saturated with lead ions. As the Bi concentration in the solution falls, its diffusion rate decreases.

Theory therefore predicts that such reactions are unimolecular and depend on the diffusion rate, and the rate constant of such a unimolecular reaction, with the side reactions accompanying the precipitation of metals taken into account, can be calculated from the formula [16]:

$$K = \frac{C_0}{t} \ln \frac{C_0}{C_0 - C_x} + \beta \frac{C_x}{t},$$

where β is the coefficient of retardation, which depends on the thickness and density of the layer of precipitating

TABLE 2

Rate of Contact Exchange of Bi and Pb at 40° (Initial concentration of bismuth 0.068 g/100 ml; hydrochloric acid concentration 0.3 N)

Reaction time (min)	Bi reduced	
	in g	in %
30	0.0650	95.6
60	0.0657	96.7
90	0.0666	98.2
120	0.0666	98.2

metal, which retards the diffusion of bismuth ions to the surface of the lead plate.

In this instance $\beta = 1.3$; with the initial concentration of bismuth (C_0) and the concentration of the metal in solution at time t (C_x) expressed in g/100 ml, calculation by means of the above formula gives $K_{av} = 6.72 \cdot 10^{-4}$.

The data in Table 1 (Experiments 9-13) show that the rate of precipitation of bismuth increases with temperature only up to 40°; with further increase of temperature this rate decreases rapidly, owing to increased oxidation of bismuth by the elemental chlorine formed in the process.

Bismuth was precipitated at the optimum temperature (40°) on a lead plate with 3 times the surface area, i. e., 240 cm^2. The results are given in Table 2.

It follows from the data in Table 2 that the reduction of bismuth remains incomplete for a long time, even with a considerable area of the lead plate. Only 98.2% of the bismuth is reduced in 2 hours; the explanation is that the bismuth covers the lead plate fairly densely and greatly diminishes its active surface, thereby hindering the reaction of contact exchange between bismuth and lead.

For studies of the conditions for precipitation of copper on metallic lead, hydrochloric acid was added to a definite volume of copper chloride, the mixture was diluted to 100 ml with distilled water, and a lead plate (80 cm^2) was put into it; after a certain time the lead plate was removed, washed, treated with dilute nitric acid solution, and the solution was diluted to a definite volume. An aliquot portion of this solution was taken, 5-8 drops of potassium ferrocyanide solution was added, the mixture was made up to 100 ml, and the copper was then estimated colorimetrically as described above. The method of internal standards was used in the calculations.

The effect of hydrochloric acid concentration on the precipitation rate of copper is shown in Table 3.

It follows from the data in Table 3 (experiments 1-4) that the hydrochloric acid concentration has no appreciable effect on the precipitation rate of copper, as copper is not soluble in hydrochloric acid at these concentrations [17]; copper can be dissolved in hydrochloric acid under these conditions only in the presence of platinum catalyst.

TABLE 3

Effects of Hydrochloric Acid Concentration and Solution Temperature on the Precipitation Rate of Copper (0.032 g of Cu per 100 ml of solution)

Expt. no.	HCl conc (normality)	Cu reduced		Cu remaining in sol'n		Time (min)	Solution temperature (°C)
		in g	in %	in g	in %		
1	0.3	0.0065	20.2	0.0259	80.8	10.0	20.0
2	0.5	0.0067	20.8	0.0256	80.0	10.0	20.0
3	0.7	0.0061	19.3	0.0263	82.2	10.0	20.0
4	0.9	0.0065	20.2	0.0262	82.0	10.0	20.0
5	0.3	0.0103	32.2	0.0221	69.0	15.0	20.0
6	0.3	0.0125	39.0	0.0199	62.0	20.0	20.0
7	0.3	0.0142	44.4	0.0178	56.0	30.0	20.0
8	0.3	0.0142	44.4	0.0181	56.5	40.0	20.0
9	0.3	0.0150	46.9	0.0173	54.0	30.0	40.0
10	0.3	0.0208	65.0	0.0155	36.0	30.0	60.0
11	0.3	0.0260	81.3	0.00595	18.6	30.0	80.0
12	0.3	0.0320	100.0	0.0	0.0	30.0	100.0

TABLE 4

Simultaneous Precipitation of Copper and Bismuth by Metallic Lead from Hydrochloric Acid Solutions (Solution temperature 100°, 0.068 g of Bi and 0.032 g of copper per 100 ml; HCl concentration 3 N)

Time (min)	Bi reduced		Cu reduced	
	in g	in %	in g	in %
5	0.015	22.0	0.0096	30.0
10	0.0352	51.8	0.0202	63.6
20	0.0593	87.2	0.0312	94.4
30	0.0680	100.0	0.0320	100.0

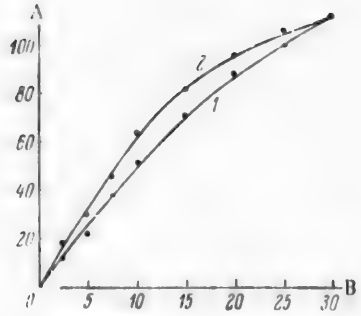

Fig. 3. Precipitation of bismuth (1) and copper (2) when present simultaneously in 0.3 N hydrochloric acid solution at 100°. 0.068 g of bismuth and 0.032 g of copper per 100 ml of solution. A) Amount of metal precipitated (%), B) time (min).

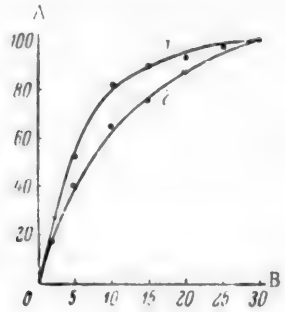

Fig. 4. Precipitation of bismuth (1) from 0.3 N nitric acid and of copper (2) from 0.1 N nitric acid at 100°. 0.068 g of bismuth and 0.032 g of copper per 100 ml of solution. Each metal was precipitated from a separate solution. A) Amount of metal precipitated (%), B) time (min).

Experiments 5-8 in Table 3 represent the course of the precipitation process with time. It is seen that the rate of contact exchange of copper and lead decreases with time, as the active surface of the metallic lead is decreased as the result of shielding by the precipitated copper (Fig. 2).

The effect of temperature on the reaction rate is illustrated by Experiments 9-12 (Table 3). It is seen that increase of temperature raises the precipitation rate of copper considerably owing to the increased diffusion rate.

The simultaneous precipitation of copper and bismuth from hydrochloric acid solution on metallic lead was studied. In 0.2 N hydrochloric acid the bismuth salt was hydrolyzed at elevated temperatures. Precipitation from a clear solution was ensured by the use of 0.3 N hydrochloric acid. The reduced copper and bismuth are precipitated on the lead plate in the form of a dark brown metallic deposit, which was dissolved in 10 ml of 10 N nitric acid, and the solution was made up to 100 ml with distilled water.

The bismuth content of this solution was determined in presence of copper by the photocolorimetric method described above, in which copper does not interfere with the determination of bismuth. Copper was determined in presence of bismuth and lead by a polarographic method in 10% sodium citrate solution at pH 4, with the M-7 manual polarograph made in 1946 in the Scientific Research Institute of the Gor'kii University. The current strength was measured by means of the mirror galvanometer of the Physical Institute, Leningrad State University; its sensitivity was $1.2 \cdot 10^{-9}$ amp/mm/m, R_{ext} = 615 ohms, R_{cr} = 1685 ohms. The distance from the scale to the center of the mirror was 0.25 m. The capillary constant was 1.44 $mg^{2/3} sec^{-1/2}$. The copper was determined by the method of internal standards.

It follows from the data in Table 4 and Fig. 3 that copper and bismuth are reduced completely in 30 min. Thus bismuth, which is not reduced completely by metallic lead in 2 hrs, is completely reduced in 30 min in presence of copper, and does not dissolve in hydrochloric acid when heated to 100°. Bismuth precipitated from a copper-free solution heated to 100° dissolved completely after precipitation.

A lead plate immersed in a hydrochloric acid solution containing bismuth and copper instantly became coated with a black deposit of these metals. This suggests that copper has a catalytic effect on the contact exchange of bismuth with lead.

It is known that heterogeneous reactions are greatly influenced by the magnitude of the surface, while in heterogeneous catalysis adsorption of the reactants by the catalyst is also of great significance. According to the Nernst theory [18], diffusion plays an important part in catalytic precipitation of metals; it determines the apparent rate of reaction if the reaction itself is more rapid than diffusion.

Investigation of the precipitation of copper and bismuth by metallic lead from nitric acid solutions showed that a 100° Cu and Bi are completely reduced in 30 min (Fig. 4).

SUMMARY

1. It is shown that metallic lead precipitates copper completely in 30 min at 100° both from nitric acid (0.3 N) and hydrochloric acid (0.1 N) solutions, whereas bismuth is not reduced at all under these conditions.

2. In presence of copper, which acts as a contact catalyst, bismuth is reduced completely in 30 min from hydrochloric acid solution at 100°, and the copper is also completely precipitated.

3. It is shown that bismuth can be determined photocolorimetrically, and copper polarographically, in their joint presence after precipitation by metallic lead.

LITERATURE CITED

[1] V. V. Ten'kovtsev, Author's Summary of Candidate's Dissertation (Rostov Press, 1953).*

[2] P. N. Kovalenko, Sci. Mem. Rostov State Univ. Trans. Chem. Faculty 2, 3, 232 (1939).

[3] G. Spacu and G. Suciu, Z. anal. Chem. 79, 196 (1930); K. Funk and J. Weinzierl, Z. anal. Chem. 81, 380 (1930).

[4] A. I. Busev and A. I. Korets, Factory Labs. 1, 30 (1949).

[5] J. H. Yoe, Colorimetry [Russian translation] (ONTI, 1933) 264, 148.

[6] E. I. Nikitina, Factory Labs. 2, 162 (1938).

[7] A. M. Dymov, Technical Analysis of Ores and Metals (State Sci.-Tech. Press, 1949), p. 418.*

[8] Iu. L. Kliachko and L. V. Timofeev, Oxidimetry and the Precipitation Method (ONTI, 1941), pp. 7-20, 35-40.*

[9] N. A. Tananaev, Proc. All-Union Conference on Analytical Chemistry II, 298, 303 (1943).

[10] P. A. Nuss, Electrolytic Coating of Metals (State Sci.-Tech. Press, 1940), p. 38.*

[11] N. A. Izgaryshev, Proc. Conference on Metal Corrosion 337 (1940).

[12] V. L. Dmitrieva and P. N. Kovalenko, Factory Labs. 4, 391 (1948); P. N. Kovalenko, Factory Labs. 2, 140 (1953).

[13] Iu. Iu. Lur'e and L. B. Ginzburg, Factory Labs. 1, 21 (1949).

[14] P. N. Kovalenko, J. Appl. Chem. (USSR) 23, 10, 1067 (1950).**

[15] E. A. Meolwyn-Hughes, Kinetics of Reactions in Solution [Russian translation] (State Sci.-Tech. Press, 1938), p. 221.

[16] B. V. Drozdov, J. Appl. Chem. (USSR) 22, 5, 483 (1949); Proc. 2nd All-Union Conference on Theoretical and Applied Electrochemistry, Acad. Sci. USSR (Kiev, 1949).

[17] Iu. V. Karlakin, Pure Chemical Reagents (ONTI, 1947), p. 322.*

[18] A. V. Rakovskii, Course of Physical Chemistry (ONTI, 1939), pp. 449, 490.*

Received June 15, 1957

* In Russian.

** Original Russian pagination. See C. B. translation.

SOME PECULIARITIES OF THE REFINING OF LEAD FROM SULFAMIC ACID ELECTROLYTES

M. A. Loshkarev, V. I. Chernenko, and I. V. Gamali

Numerous different electrolytes have been proposed for use in the electrolytic refining of lead. Their great variety itself indicates that they all have serious disadvantages; searches for new electrolytes are therefore continuing [1, 2].

In 1939 Piontelli [3] proposed the use of a sulfamic acid electrolyte. Later work on this electrolyte [4, 5] gave rise to the impression that the refining of lead from sulfamic acid electrolytes has a number of important advantages over the fluosilicate and fluoborate electrolytes used at present. However, after nearly a year of operation of a unit for the electrochemical refining of antimony-containing lead from sulfamic acid electrolytes at the "Ukrtsink" plant certain defects have been revealed. The most important of these is the rapid fall in the concentrations of lead and acid in the electrolyte during electrolysis, with consequent poor quality of the cathode deposits. The need for frequent correction of the electrolyte, resulting from its rapid impoverishment, led to considerable and at first sight inexplicable losses of acid and PbO. The decreases of the lead and acid concentrations in the course of electrolysis could not be attributed only to hydrolysis of sulfamic acid, which results in the formation of ammonium sulfate and precipitation of lead sulfate.

According to the literature [4] the rate of the reaction $HSO_3NH_2 + H_2O \longrightarrow NH_4HSO_4$ is almost zero at 25-35° (the usual electrolysis temperature). It was found in the operation of a similar unit in Italy [6] that the losses of lead as the result of hydrolysis do not exceed 20 g per ton of the final product.

Another possible cause of the decrease of lead concentration in the solutions is formation of lead sulfate, not as the result of hydrolysis, but because of oxidation of sulfamic acid at the anode. This possibility was noted by Stender [4]. Moreover, some authors believe that sulfamic acid electrolytes are very susceptible to oxidation and ". . . react not only with definite oxidizing agents, but also with glue, as shown by the formation of an insoluble precipitate (lead sulfate) and by the decrease of the sulfamate ion content in the solution, even in absence of current" [7].

The aims of the present investigation were to study peculiarities in the behavior of sulfamic acid electrolyte in electrolysis, and to determine the optimum conditions for the works refining of lead.

EXPERIMENTAL

One of the most general methods for investigation of electrolysis on the plant scale is by analysis of a potential balance for the electrolytic cell [8].

It is known that the potential drop in the cell: $Pb \mid Pb(SO_3NH_2)_2$; HSO_3NH_2; $H_2O \mid Pb$ (Sb, Bi and other impurities and additives) is the sum of the following terms; the anode potential φ_a, the cathode potential φ_c, the potential drop in the electrolyte E_e, and the potential drop in the electronic conductors and contacts E_c.

Thus we have

$$E = \varphi_a - \varphi_c + E_e + E_c \qquad (1)$$

TABLE 1

Potential Balance for Cell 1 [Service life of anodes before the measurements, 24 hours; electrolyte composition (g/liter): lead 24.19, acid 28.26, glue 1, β-naphthol 0.1; electrolyte temperature 24.5°]

Item	mv	%
Difference of irreversible electrode potentials	86.0	12.72
Including:		
a) anode potential	−127.0	
b) cathode potential	−213.0	
Potential drop in electrolyte	528.0	78.40
Potential drop at contacts:		
a) anode−anode busbar	18.0	2.66
b) cathode busbar−cathode pinchbar	28.0	4.14
c) cathode pinchbar−housing	14.0	2.08
Total	674.0	100.0

TABLE 2

Potential Balance for Cell 7 [Service life of anodes before the measurements, 5 days; electrolyte composition (g/liter): lead 28.89, acid 21.36, glue 1, β-naphthol 0.1; electrolyte temperature 27°]

Item	mv	%
Difference of irreversible electrode potentials	98.6	14.40
Including:		
a) anode potential	−86.0	
b) cathode potential	−184.6	
Potential drop in electrolyte	500.8	73.00
Potential drop at contacts:		
a) anode−anode busbar	63.5	9.25
b) cathode busbar−cathode pinchbar	19.7	2.87
c) cathode pinchbar−housing	3.1	0.48
Total	685.7	100.0

TABLE 3

Potential Balance for Cell 7 [Service life of anodes before the measurements, 10 days; electrolyte composition (g/liter): lead 28.89, acid 27.94, glue 1, β-naphthol 0.1; electrolyte temperature 25°]

Item	mv	%
Difference of irreversible electrode potentials	127.0	18.20
Including:		
a) anode potential	−74.0	
b) cathode potential	−201.0	
Potential drop in electrolyte	510.0	73.06
Potential drop at contacts:		
a) anode−anode busbar	40.7	5.83
b) cathode busbar−cathode pinchbar	13.7	1.97
c) cathode pinchbar−housing	6.3	0.94
Total	727.0	100.0

TABLE 4

Potential Drop at Contacts

Item	Average values over the unit (in mv)				Average values for all units		Maximum values	
	16	1	13	3	mv	as % of average cell volt.	mv	as % of cell voltage
Potential drop at contacts:								
anode–anode busbar	9.6	14.8	13.6	7.8	11.45	1.9	63.5	10.28
cathode busbar–cathode pinchbar	16.2	15.7	11.7	13.4	14.25	2.36	28.0	4.52
cathode pinchbar–cathode housing	9.1	18.0	16.9	11.0	13.75	2.28	14.0	2.26
Total	34.9	48.5	42.2	32.2	39.45	6.44	105.5	17.08
Potential drop in cell	695	625	660	525	619.8			

The method described by Esin and Loshkarev [8] was largely used for determination of the constituent items of the potential balance.

The individual potentials of the anode and cathode, and the potential drop in the electrolyte together with the anode potential, were determined by the compensation method by means of the P-4 potentiometer. The necessity for using two electrolytic bridges was avoided by determination of the potential drop in the electrolyte as its sum with the anode potential, and the accuracy of the measurements was thereby increased. In order to avoid accidental errors, the measurements were made at 9 points of the operating surface of each of the 18 anodes and 19 cathodes of the cell. Thus the electrode potentials and the potential drops given in Tables 1, 2, and 3 are average values of 324 measurements.

The results of measurements of individual items in the potential drop in three industrial cells are given in the same tables. The selection of the cells was based on the service life of the anodes. Variations of the anode potential with time gave an indication of the extent to which the anode remained active, and of the influence of anode activity on the electrochemical behavior of the impurities in the anode metal. The anode metal used contained (in %): Pb ≃ 90, Sb 6.4, Sn 0.86, Cu 0.31, and also small amounts of bismuth, iron, and zinc.

The potential drop at the contacts was measured by means of a multirange millivoltmeter. The average values of the potential drop at each contact are given in Tables 1,2, and 3.

The losses at the contacts in a series of units (25 cells) were determined in order to estimate the quality of work of the operatives. The average values found, which are given in Table 4, show that not enough care was taken in maintenance of the contacts.

Electrode potentials. It follows from the data in Tables 1, 2, and 3 that the divergence between the cathode and anode potentials is not too large. This indicates that both electrode processes occur without considerable chemical polarization. The maximum value of the difference $\Delta\varphi = \varphi_a - \varphi_c$, equal to the sum of the absolute values of the electrode polarizations ($\eta_a + \eta_c$), is, on the average, about 100 mv, and increases slightly only after very prolonged continuous operation of the anode. However, even in this case a positive value of φ_a corresponds to anodic polarization not exceeding 56 mv. Therefore the anode is maintained in an active state throughout the dissolution cycle.

The low value of the cathodic polarization indicates that the surface-active additive used in the plant (β-naphthol) is not effective enough. The cathode deposits of lead formed are coarsely crystalline in structure and contain considerable numbers of dendrites.

To test whether the sulfamate ion may be oxidized at the anode, additional experiments were performed on the anodic oxidation of sulfamic acid.

The oxidation of sulfamic acid was studied by the following method: an exact amount of a solution containing 20 g of sodium sulfamate and 11 g of sulfamic acid per liter was placed in a platinum basin which served as the anode. The cathode was a platinum crucible, which was immersed into the solution to the same depth in all the experiments. A definite anode potential, measured by means of a potentiometer, was applied to this electrolytic cell with the aid of a voltage divider. The fixed potential was maintained for 6 hours, and $SO_4^{''}$, $NO_2^{'}$, and H_3O^+ ions were then determined in the solution.

The determination of sulfate by the benzidine method involved certain difficulties because of the oxidation of benzidine by peroxides, probably formed in the course of electrolysis. The interfering oxidizing agents could be easily removed by the addition of a few drops of 10% stannous chloride solution.

It follows from the data in Table 5 that appreciable oxidation of sulfamate begins at potentials above +1.25 v; hence oxidation of sulfamic acid under production conditions is unlikely.

TABLE 5

Anodic Oxidation of Sulfamic Acid

Anode potential (in v)	Concentration (g-ion/liter) H_3O^+ before electrolysis	H_3O^+ after electrolysis	$SO_4^{''}$	Presence of $NO_2^{'}$
1.05	0.113	0.113	No	No
1.15		0.113	No	No
1.25		0.113	Traces	Yes
1.35		0.124	Traces	Yes
1.45		0.124	0.009	Yes
1.55		0.157	0.044	Yes
1.65		0.206	0.158	Yes

Potential drop in the electrolyte. The balance shows that the average potential drop in the electrolyte of the industrial cell is 0.506 v. The specific conductance of the electrolyte, calculated from the formula

$$\kappa = \frac{D_a \cdot l}{E_e}, \qquad (2)$$

at current density D_a = 93-95 amp/m^2 and interelectrode distance l = 5 cm, is approximately 0.093 ohm$^{-1}\cdot$cm^{-1}.

However, according to literature data [4] the conductivity of an electrolyte containing 93 g of lead sulfamate and 24 g of sulfamic acid per liter is 0.058 ohm$^{-1}\cdot$cm^{-1}. The value found by us for the conductivity of a solution containing 28 g of lead sulfamate and 27 g of sulfamic acid per liter, which approximately corresponds to the concentrations in the electrolyte studied, was only 0.0443 ohm$^{-1}\cdot$cm^{-1}.

This large discrepancy between the conductivities calculated from the potential balance data and determined experimentally cannot in any way be attributed either to the approximate nature of Eq. (2) or to the presence of a small amount of impurities in the solution. The only alternative suggestion is that the discrepancy is caused by the presence of large amounts of an extraneous, readily dissociated compound in the electrolyte. This may be ammonium sulfamate, formed as the result of hydrolysis of sulfamic acid [6].

TABLE 6

Ionic Balance of the Electrolyte

Cations (in meq/liter)		Anions (in meq/liter)	
$Pb^{++} + H^{+} + Sn^{++} + Fe^{++} + Zn^{++}$ . .	1211.2	$SO_3NH_2^-$	2165.0
NH_4^+	950.0		
Total	2161.2		2165.0

The ionic balance of the electrolyte* (Table 6) was compiled in the determination of the ammonium sulfamate concentration.

The balance data were obtained by a complete analysis of the electrolyte. Lead was determined by the chromate method, with an iodometric end point. The sulfamate was determined by titration with 0.1 N sodium nitrite solution. Starch–iodide paper was used as the indicator. Nitrogen in the electrolyte was determined by the Dumas method. The principal metallic salt impurities were determined, at our request, by the central works laboratory.

The small discrepancy between the cation and anion concentrations in the ionic balance may be largely attributed to experimental error. The difference between the nitrogen concentration determined by the Dumas method and the concentration calculated from the sulfamate content gave the content of ammonium ions.

Since analysis shows that the solution contains 950 meq of ammonium ions per liter, the ammonium sulfamate concentration is 108 g/liter.

Comparison of the conductivity of the works electrolyte with the conductivities of specially prepared solutions (Table 7) gives good agreement with the data of the ionic balance.

TABLE 7

Comparison of Conductivities

Electrolyte	Concentration (in g/liter)			κ (in $ohm^{-1} \cdot cm^{-1}$)
	$Pb(SO_3NH_2)_2$	HSO_3NH_2	$NH_4SO_3NH_2$	
Works	56	54.2	?	0.0905
Prepared solution	56	54.2	—	0.0645
The same	56	54.2	108	0.0946

As already stated, the accumulation of large amounts of ammonium sulfamate cannot be attributed to its formation as the result of hydrolysis. Another possible route by which it may accumulate is as the result of reactions between $Pb(SO_3NH_2)_2$ and the ammonium sulfate and bisulfate introduced with the technical sulfamic acid. Therefore, when sulfamic acid containing ammonium sulfate and bisulfate is used, not only is ammonium sulfamate formed, but there are unproductive losses of lead and acid.

* As by this time the electrolyte concentration had changed as the result of correction, all the subsequent reasoning applies to the works electrolyte containing 56 g of lead and 54.2 g of acid per liter.

Analysis of the works sulfamic acid showed that it contains up to 1% ammonium ions. These are formed both by hydrolysis of ammonium imidodisulfate, which is an intermediate product in the formation of sulfamic acid, and by hydrolysis of solid but moist sulfamic acid. The losses, calculated from the analytical data, are approximately 60 kg of lead and 50 kg of acid per ton of technical sulfamic acid added.

Causes of lead and acid losses in the electrolyte. The above data account fairly well for the losses of acid and lead when litharge is dissolved, but not for the decreases of acid and lead concentrations in the electrolyte. One possible way in which lead and acid may be lost from the electrolyte is mechanically in the sludge, as the lead and acid concentrations in the sludge pores may be considerable [5].

The lead and acid cannot be recovered completely from the sludge by washing, as the diffusion of lead ions through the very fine pores of the sludge is exceedingly slow. For example, analysis of washed sludge showed that it contains 7.5% of lead in the form of ions and 0.8% of free sulfamic acid, calculated on the dry weight of sludge.

It can be tentatively shown from the known contents of impurities in the anode lead and the amount of undissolved lead in the sludge that the average daily change of concentration of the works electrolyte is 1.6 g/liter; this is in fair agreement with the works data, according to which the average daily decrease of lead concentration is 1.5-2 g/liter.

However, analytical data for the sludge cannot account for the decrease of the electrolyte acidity, which is especially prominent on additions of lead sulfamate formed by the solution of litharge in sulfamic acid solution. A qualitative investigation of the dissolution process showed that when excess litharge reacts with sulfamic acid solution (pH = 4), basic lead sulfamate is formed; the latter is fairly well soluble at elevated temperatures and is precipitated after prolonged standing.

Results of Analysis of $Pb(OH)SO_3NH_2 \cdot H_2O$

	Calculated (%)	Found (%)
Pb	61.2	62.5, 60.6
N	4.15	4.38, 4.33
H	1.48	1.62, 1.5

In works practice lead sulfamate is usually made with excess litharge at temperatures above 30°; it is therefore, highly probable that the solution added to the electrolyte, containing considerable amounts of the basic salt, lowers the hydrogen-ion concentration in the electrolyte by formation of normal lead sulfamate.

SUMMARY

1. Analysis of the potential balance in industrial cells used for electrochemical lead refining showed that the anodes remain active throughout the electrolysis cycle and that anodic oxidation of sulfamic acid is improbable, as confirmed by additional experiments; the presence of a highly dissociated extraneous compound in the electrolyte was also shown.

2. Large amounts of ammonium sulfamate were detected by analysis in the works electrolyte.

3. It is shown that lead and sulfamic acid may be lost both by formation of basic lead sulfamate, and by reactions between the ammonium sulfates present in technical sulfamic acid and lead sulfamate.

4. It is shown that impoverishment of the electrolyte mainly depends on loss of lead in the sludge.

5. It is noted that β-naphthol is inadequate as a regulator of the growth of cathodic lead deposits in the electrolysis of sulfamate solutions.

LITERATURE CITED

[1] F. C. Mathers and J. F. Suttle, J. (and Trans.) Electrochem. Soc. 93, 47 (1948).

[2] F. C. Mathers and C. Gries, J. Electrochem. Soc. 94, 46 (1948).

[3] R. Piontelli and A. Giulotto, La Chimica e l'Industria 21, 478 (1939).

[4] V. V. Stender et al., Bull. Acad. Sci. Kazakh SSR, Chem. Ser. 1, 101 (1947).

[5] N. B. Pletneva, Nonferrous Metals 2, 26 (1954).

[6] R. Piontelli and L. Fagnani, La Chimica e l'Industria 34, 11, 629 (1952).

[7] P. P. Beliaev and M. G. Krasnova, Metallic Coatings in Chemical Machine Construction (Collected Papers, 15) (Mashgiz, 1954), p. 42.*

[8] O. Esin and M. Loshkarev, J. Appl. Chem. (USSR) 10-11, 1433 (1938).

Received July 8, 1956

* In Russian.

ELECTRODEPOSITION OF MANGANESE WITH INCREASED CURRENT EFFICIENCY

I. V. Ianitskii and B. B. Stul'pinas

The Kaunas Polytechnic Institute

The cathodic deposition of manganese from aqueous solutions of its salts is accompanied by evolution of hydrogen, which lowers the current efficiency. According to a number of authors [1-4], the current efficiency with the use of sulfate electrolytes without special additions does not exceed 50-60%. The current efficiency can be increased somewhat by additions of ammonium thiocyanate [5], sulfurous acid, or sulfite, but even then the current efficiency fluctuates within wide limits (50-70%) [6-12].

We showed recently [4] that very small additions of selenious acid to sulfate electrolytes increase the current efficiency to 90% and over, and the reproducibility of the experiments under equal electrolysis conditions is quite satisfactory.

This paper deals with a study of the influence of electrolyte composition, amount of selenious acid added, and cathode current density on the current efficiency and the selenium content of the manganese deposits formed, carried out in order to determine the optimum conditions of electrolysis. The experimental procedure was similar to that described in the preceding paper [4]: the anodes were used previously and then wrapped in fabric; the cathodes were square, cut from polished copper, iron, or aluminum sheet of 20 cm^2 total area on the two sides; the electrolyte volume was 250 ml and the temperature was 18-24°; the duration of electrolysis was usually 20-60 minutes, to give 2 amp-hrs/dm^2.

EXPERIMENTAL

Variation of current efficiency with the electrolyte composition at a constant concentration of selenious acid. It is known from the literature that increase of the manganese sulfate concentration increases the current efficiency [3, 4, 13]. Some authors assert that increase of the ammonium sulfate concentration lowers the current efficiency [3, 13]. According to Iankelevich [14], however, increase of ammonium sulfate concentration raises the current efficiency. Agladze [10] reports that the efficiency first decreases and then begins to increase with increasing ammonium sulfate concentration. These observations apply to electrolytes without added selenious acid. In presence of the latter we found that the current efficiency rises somewhat with increase of manganese sulfate concentration from 100 to 200 g of $MnSO_4 \cdot 5H_2O$ per liter [4].

Figure 1 shows the variations of current efficiency with cathode current density over a wider concentration range of the two principal components of the electrolyte.* The selenious acid content was 0.15 H_2SeO_3 in all cases. Each curve passes through a maximum at current densities from 2 to 4.5 amp/dm^2, according to the composition of the electrolyte. Increase of the electrolyte concentration shifts the efficiency maximum in the direction of higher current densities, and the maximum becomes flatter.

To obtain a clearer and fuller picture of the influence of the electrolyte composition on the current efficiency, we studied variations of the latter with the concentration of each of the principal electrolyte components

* The electrolyte composition in each case is denoted in g/liter, with $MnSO_4 \cdot 5H_2O$ in the numerator and $(NH_4)_2SO_4$ in the denominator.

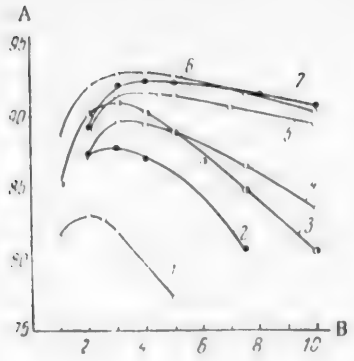

Fig. 1. Variation of current efficiency with cathode current density for different electrolytes containing 0.15 g H_2SeO_3 per liter. A) Current efficiency η (%), B) current density (in amps/dm^2). Electrolyte composition (in g/liter): 1) 50/75, 2) 75/75, 3) 100/75, 4) 100/100, 5) 200/150, 6) 200/75, 7) 300/100.

($MnSO_4$ and $(NH_4)_2SO_4$) at constant concentration of the other component, with a constant content of selenious acid (0.15 g/liter), and at a current density of 3-4 amps per dm^2. This current density corresponds to the maximum current efficiency for most of the electrolytes in Fig. 1. The results so obtained were plotted in a double diagram (Fig. 2). The curves on the left show the influence of $(NH_4)_2SO_4$ concentration on the current efficiency at constant $MnSO_4$ concentration; the curves on the right represent the influence of $MnSO_4$ concentration at constant $(NH_4)_2SO_4$ concentration. It is seen that increase of the $MnSO_4$ concentration raises the current efficiency, and that of $(NH_4)_2SO_4$ lowers it.

This diagram can be used for graphical determination of the maximum current efficiency (at a current density of 3-4 amp/dm^2) for an electrolyte of any composition between 50-200 g $MnSO_4 \cdot 5H_2O$ and $(NH_4)_2SO_4$ per liter, with 0.15 g of selenious acid per liter. For example, the dash lines passing through the points 50/50

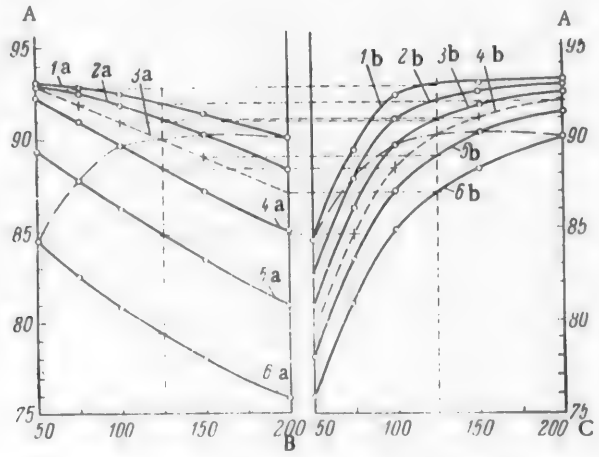

Fig. 2. Variations of current efficiency with concentrations of $MnSO_4$ and $(NH_4)_2SO_4$ with addition of 0.15 g H_2SeO_3 per liter. Current density 3-4 amp/dm^2. A) Current efficiency η (%), B) $(NH_4)_2SO_4$ content (g/liter), C) $MnSO_4 \cdot 5H_2O$ content (g/liter). Contents of $MnSO_4 \cdot 5H_2O$ (g/liter): 1a) 200, 2a) 150, 3a) 125, 4a) 100, 5a) 75, 6a) 50. Contents of $(NH_4)_2SO_4$ (g/liter): 1b) 50, 2b) 75, 3b) 100, 4b) 125, 5b) 150, 6b) 200.

75/75, 100/100, 150/150, and 200/200 represent the effect of dilution of the 200/200 electrolyte on the current efficiency. Curves 3a and 4b were found graphically for electrolytes containing 125 g $MnSO_4 \cdot 5H_2O$ and 125 g $(NH_4)_2SO_4$ per liter.

These curves were plotted as follows. Verticals corresponding to concentrations of 125 g/liter were drawn on both graphs (Fig. 2). The points of intersection of these verticals with the current-efficiency curves give: on the left-hand graph, efficiencies for 50/125, 75/125, 100/125, 150/125, and 200/125 electrolytes, and on the right-hand graphs, efficiencies for 125/200, 125/150, 125/100, 125/75, and 125/50 electrolytes. Through these points on the left-hand graph, horizontals were drawn to the verticals on the right-hand graphs for the corresponding $MnSO_4 \cdot 5H_2O$ concentrations. The points so obtained were joined to give curve 4b, representing the current efficiency as a function of the $MnSO_4$ concentration in the electrolyte for a constant $(NH_4)_2SO_4$ concentration of 125 g/liter.

Analogously, if the points of intersection of the vertical for 125 g/liter with the curves of the right-hand graph are transferred to the left-hand graph, i. e., if horizontals are drawn through them to the verticals for the corresponding concentrations of $(NH_4)_2SO_4$, curve 3a is obtained, which represents the current efficiency as a function of the $(NH_4)_2SO_4$ content in the electrolyte for a constant concentration (125 g/liter) of $MnSO_4 \cdot 5H_2O$.

It follows from the above data that for high current efficiencies the $(NH_4)_2SO_4$ concentration in the electrolyte should be decreased to 50 g/liter or less. However, an adequate concentration of ammonium ions is necessary for reliable and steady electrolysis. In absence of ammonium ions not metallic manganese but the hydroxide is deposited on the cathode. 50 g of $(NH_4)_2SO_4$ per liter is still not enough – the coatings often contain hydroxide, and the process is unstable owing to the inadequate buffer capacity of the electrolyte. Increase of ammonium-ion concentration favors smoother and more stable electrolysis, increasing the buffer capacity of the electrolyte, and makes it possible to raise the pH to 7.5-8.5, without precipitation of $Mn(OH)_2$. In general, if selenious acid is added the electrolysis should be performed at the highest possible pH. The coatings formed are then of better quality, quite level, smooth, and bright, like aluminum articles in external appearance; dendrite formation at the cathode edges is diminished. Decrease of pH below 7 makes the electrolysis less stable and selenious acid is reduced more rapidly, selenium being coagulated in the electrolyte and at the electrode; the current efficiency also falls.

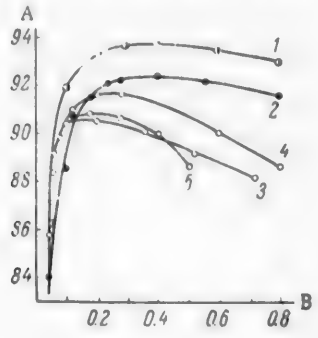

Fig. 3. Variation of current efficiency with selenious acid content. A) Current efficiency η (%), B) selenious acid content (g/liter). Electrolyte composition, current density (amp/dm^2) and pH respectively: 1) 200/75, 4, > 7; 2) 200/150, 4.5, > 7; 3) 100/75, 3.5, > 7; 4) 100/75, 3.0, > 7; 5) 100/75, 3.0, > 7.

A comparison of current efficiencies with the quality of the coatings obtained from electrolytes of different composition led to the conclusion that the electrolyte should contain not less than about 100 g of $MnSO_4 \cdot 5H_2O$ per liter. Increase of the concentration of the latter to much above 200 g/liter results in only a slight increase of current efficiency, and is limited by the solubility of manganese sulfate in solutions with high concentrations of $(NH_4)_2SO_4$, owing to the formation of the less soluble double salt. The concentration of ammonium sulfate must not be less than 75 g/liter, and with electrolytes containing much $MnSO_4$ (about 200 g $MnSO_4 \cdot 5H_2O$ per liter) it must not be less than 100 g/liter. Excessive increase of the $(NH_4)_2SO_4$ content (over 150 g/liter) is undesirable, as it leads to formation of dull deposits and lower current efficiency.

On the basis of these results the optimum recommended electrolyte is a solution containing 200-250 g $MnSO_4 \cdot 5H_2O$ and 125-150 g $(NH_4)_2SO_4$ per liter, with, of course, an addition of selenious acid. The pH of the electrolyte is regulated by addition of ammonia.

Influence of the selenious acid concentration on current efficiency and quality of the cathode deposit. Even very low concentrations of selenious acid in the electrolyte result in an appreciable increase of current efficiency. For example, electrolytes which gave efficiencies of 20-50% without this addition (under the conditions indicated in Fig. 3) gave stable yields of over 70% after addition of 0.02 g H_2SeO_3 per liter, while addition of 0.04 g H_2SeO_3 per liter raised the efficiency to 82-86%.

From the current-efficiency aspect this result is satisfactory, but the coatings obtained under such conditions are not sufficiently uniform. Increase of the selenious acid content in the electrolyte to 0.1 g/liter raised the current efficiency to 90%, and resulted in the formation of quite level, milk-white (semidull) coatings, resembling aluminum articles. With further increase of the selenious acid content the current efficiency first increases somewhat, and then begins to fall. With 0.5 g of selenious acid per liter and somewhat more, the coatings formed are almost mirror-like.

Figure 3 shows the variation of current efficiency with the selenious acid content in electrolytes of different composition at current densities close to the optimum values. The curves pass through maxima when the H_2SeO_3 content is between 0.2 and 0.4 g/liter, according to the composition of the electrolyte.

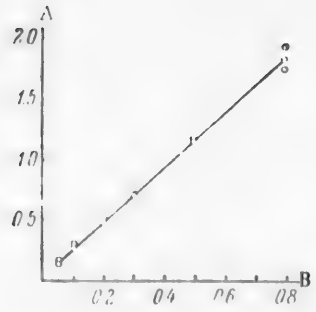

Fig. 4. Effect of H_2SeO_3 concentration on the selenium content of manganese. 200/150 electrolyte, D_C = 4.5 amp/dm^2. A) Selenium content (%), B) H_2SeO_3 concentration (g/liter).

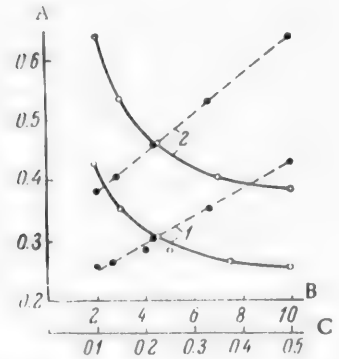

Fig. 5. Effect of cathode current density on the selenium content of manganese. 200/150 electrolyte. A) Selenium content (%), B) cathode current density D_C (amp/dm^2), C) $1/D_C$. H_2SeO_3 content (g/liter): 1) 0.1, 2) 0.2.

However, in most of the experiments, including those described above, a somewhat lower concentration of selenious acid (0.15 g/liter) was used, because increase of its concentration in the electrolyte leads to an increase of the selenium content of the deposited metal (Fig. 4). It is clear from Fig. 4 that at constant cathode current density (4.5 amp/dm^2) the selenium content of the metallic deposit is a linear function of the H_2SeO_3 concentration in the electrolyte; i. e., the two are in almost direct proportion.

The selenium content of the coatings was determined as follows. An aluminum cathode, coated with about 0.4 g of manganese, was treated with 65-70 ml of a solution consisting of 1.5 ml of concentrated hydrochloric acid, 10 ml of saturated potassium bromide solution, and bromine water. After the coating had dissolved, the electrode was rinsed in water and treated with a few drops of concentrated sodium sulfite solution to dissolve residual selenium. The solutions were combined, and 10 ml of 25% hydrochloric acid was added followed by sulfite solution until the color became pale yellow, to remove most of the excess bromine. The residual bromine was then removed by addition of a few drops of alcoholic acetanilide solution [15]. The solution was heated at about 100° for a short time, cooled, 5 ml of 10% potassium iodide solution was added, and the liberated iodine was titrated with 0.01 N thiosulfate solution [16]. When electrocoatings on copper cathodes are dissolved, the bromine water should be acidified with a large amount of hydrochloric acid (about 12 ml of 25% HCl), as otherwise some selenium remains on the copper electrode in the form of copper selenide.

The amount of selenium present in the manganese also depends on the cathode current density: it decreases with increasing current density at constant selenious acid content in the electrolyte (Fig. 5). The curves are hyperbolas, as the Se content of the deposit is a linear function of $1/D_C$ (dash lines).

It follows that to decrease the selenium content of electrolytic manganese the electrolysis should be carried out at the highest possible current density. Thus the selenious acid concentration in the electrolyte and the optimum current density should be chosen not only with the maximum current efficiency in view, but also in relation to the possibility of decreasing the selenium content in the deposited manganese.

Taking these factors into account, we recommend a current density of 4-5 amp/dm^2 with 0.1-0.2 g/liter of H_2SeO_3 in the electrolyte. If the D_C is raised above 5 amp/dm^2, dendrites begin to form at the cathode edges and the current efficiency falls appreciably.

Under the recommended conditions the amount of selenium in the manganese coatings does not exceed 0.25-0.45%, the cathodic current efficiency being about 90%. It may be noted in this connection that when, as recommended by some authors [6-12], SO_2 or sulfite is added to the electrolyte for manganese deposition, the manganese contains up to 0.3-0.5% sulfur.

For the production of protective or decorative manganese coatings, higher concentrations of selenious acid (up to about 0.5 g/liter) may be used, at current densities corresponding to maximum efficiencies as the somewhat increased selenium content has no adverse effect on the quality of the coatings and even increases their luster.

SUMMARY

1. The variation of the current efficiency in the electrodeposition of manganese with the contents of $MnSO_4$ and $(NH_4)_2SO_4$ in electrolytes containing selenious acid was studied; it was found that manganese can be deposited without the use of diaphragms, at stable current efficiencies of up to 90-94%.

2. Increase of the H_2SeO_3 concentration first increases the current efficiency to a maximum at 0.2-0.4 g per H_2SeO_3 per liter, and then lowers it.

3. The amount of selenium in the manganese coatings increases with the selenious acid concentration of the electrolyte, but decreases with increasing current density.

4. The recommended optimum electrolyte composition (in g/liter) is: $MnSO_4 \cdot 5H_2O$ 200-250, $(NH_4)_2SO_4$ 125-150, H_2SeO_3 0.1-0.2, and the optimum cathode current density is 4-5 amp/dm^2.

LITERATURE CITED

[1] K. M. Gorbunova, J. Appl. Chem. (USSR) 17, 581 (1944).

[2] S. A. Zaretskii, Proc. Acad. Sci. USSR 56, 181 (1947).

[3] P. I. Terekhov, A. K. Reikhshtadt, and A. N. Ivanova, Proc. 2nd Conference on Metal Corrosion II, 237 (1943).

[4] I. V. Ianitskii and B. B. Stul'pinas, J. Appl. Chem. (USSR) 30, 12, 1776 (1957).*

[5] W. E. Bradt and H. H. Oaks, Trans. Electrochem. Soc. 71, 279 (1937).

[6] W. C. Coaster and S. M. Shelton, Eng. and Mining J. 137, 510 (1936).

[7] S. M. Shelton, M. B. Royer, and Towne, Bur Mines Rep. Invest. 3406, 3 (1938).

[8] W. L. Hammerquist, Stahl u. Eisen 60, 307 (1940).

[9] R. S. Dean, Mining and Metallurgy 22, 5 (1941); Metal Ind., London 58, 146 (1941).

[10] R. I. Agladze, Metallurgist 9, 15 (1939).

[11] R. I. Agladze, Bull. Acad. Sci. USSR, OTN 1-2, 45 (1942).

[12] R. I. Agladze, J. Appl. Chem. (USSR) 16, 337 (1943).

[13] C. G. Fink and M. Kolodney, Trans. Electrochem. Soc. 71, 287 (1937).

[14] Z. A. Iankelevich, Mem. Inst. Chem. Acad. Sci. Ukrainian SSR 6, 1, 19 (1939).

[15] O. Foss, Acta Chem. Scand. 3, 435 (1949).

[16] R. Berg and M. Teitelbaum, Chem. Z. 52, 142 (1928).

Received June 25, 1956

* Original Russian pagination. See C. B. translation.

THE ROLE OF CATALYSTS IN THE OXIDATION OF PARAFFIN (WAX) TO FATTY ACIDS

N. K. Man'kovskaia and G. I. Moskvina

All-Union Scientific Research Institute of Fats, and the
Shebekino Combine for Synthetic Fatty Acids and Aliphatic Alcohols "SZhK and ZhS"

Studies of the liquid-phase oxidation of paraffinic hydrocarbons by molecular oxygen are becoming of increasing practical importance. The production of synthetic fatty acids on the large industrial scale requires the oxidation of technical paraffins under the optimum conditions both in regard to the reaction rate and in regard to the composition of the oxidation products. It is now beyond doubt that the liquid-phase oxidation of paraffinic hydrocarbons by molecular oxygen is a chain reaction. The role of the catalyst in directing the oxidation toward the formation of maximum amounts of carboxylic acids, and the kinetics of the process, are not yet sufficiently clear.

Knorre, Maizus, and Emanuel' [1] studied the oxidation of n-decane in presence of manganese and cobalt salts of carboxylic acids and concluded that at the initial stage the metal compounds, soluble in the oxidation mass, catalyze the oxidation process. By the time when the metal compounds are precipitated other compounds, free from metals, are formed in the system and these catalyze the oxidation further.

On the basis of these results it is postulated that there must be at least two macroscopic stages of the oxidation process, each proceeding by its own specific route. Tsyskovskii and Kiseleva [2], in a study of the liquid-phase oxidation of hydrocarbons, also showed that the presence of fatty-acid salts as catalysts is necessary only in the initial period. Tsyskovskii considers that after the chain reaction of hydrocarbon oxidation has commenced the catalyst may be removed from the reaction mixture without detriment to the course of the reaction [3].

The concepts of the existence of macroscopic stages in the oxidation process and of the mechanism of catalyst action in chain reactions, developed by Emanuel' [4], and data on the consecutive conversion of the oxidation products [5], suggest that the industrial oxidation of paraffins to fatty acids proceeds by several stages. The first stage is chain initiation and the formation of the first active intermediate products, possibly hydroperoxides; catalysts and external conditions have their specific effects on the course of this process. The second stage is a directed conversion of these intermediate products into acids; this is also influenced by catalysts and external conditions. In the present investigation an attempt was made to determine the influence of catalysts on the course of these two stages in the oxidation of paraffin wax, in the direction of maximum formation of acids. A study was made of the kinetics of acid formation in the oxidation of various technical grades of solid paraffins, both in the original state, and in mixtures with recycled paraffins of the same grade, to the same degree of conversion, i. e., to an acid number of 70 mg,* in presence of potassium permanganate catalyst, under the technological conditions used in the industrial production of synthetic fatty acids.

EXPERIMENTAL

The experiments on the oxidation of paraffin wax were performed in a semiworks-scale unit, in an oxidation vessel of stainless steel, the charge being 90 kg of paraffin. The air was blown through porous ceramic plates.

* The acid numbers are expressed in mg of caustic potash required for neutralization of the free acid contained in 1 g of the substance.

The air rate was 1.7 liters/min per 1 kg of charge. The paraffin wax and catalyst were always mixed in a special apparatus, in which 10% aqueous potassium permanganate solution was added with vigorous stirring to the paraffin wax heated to 120°. The water evaporated rapidly, while the permanganate was reduced. At the end of the mixing the mixture did not contain any potassium permanganate, the manganese being present in the form of a fine heterogeneous suspension of oxides. The mass was then rapidly transferred to the oxidation vessel, heated to 130°, and oxidized at that temperature to acid number 7-9 mg. The temperature was then gradually lowered by 2-3° per hour to 107°, and the oxidation was continued until the acid number reached 70 mg.

Preliminary tests showed that this decrease of temperature in the oxidation of paraffin wax in presence of potassium permanganate decreases the oxidation rate to only a small degree (by 20-30%) as compared with the rate at a constant temperature of 130°, but the quality of the products so obtained is much higher, with lower contents of keto acids, hydroxy acids, and polymerization products. If the entire oxidation is performed at 107°, the oxidation rate is decreased 2 to 3-fold, while the composition of the products remains almost the same.

For oxidation of mixtures of the original and recycled paraffins, an aqueous solution of potassium permanganate was added to a mixture consisting of $^1/_3$ of the original and $^2/_3$ of the recycled paraffins, heated to 120°. Otherwise the oxidation conditions were the same as for the original paraffins.

Three kinds of German tar paraffins, from the Kõpsen, Gel'tsau* and Rositz plants, and two kinds of petroleum paraffins — Drogobych and Rumanian — were used for the investigation.

These paraffins have almost the same solidification temperature but differ somewhat in fractional composition (Table 1).

TABLE 1

Characteristics of the Paraffin Waxes

Source	Solidification temperature	Hydrocarbons (%) boiling in ranges (°C)				Contents of normal hydrocarbons (%)
		up to 380	381—420	421—450	above 450	
Kõpsen	53.0	15	40	40	4	94.6
Gel'tsau	53.6	10	40	30	18	97.2
Rositz	52.8	3	70	25	Nil	97.6
Drogobych	53.6	Nil	35	37	25	92.6
Rumania	53.0	Nil	40	32	27	93.4

The paraffins from the Kõpsen and Gel'tsau works have the most diverse fractional compositions. The tar paraffins contain from 2 to 4% of unsaturated compounds. The petroleum paraffins contain no unsaturated compounds. The petroleum paraffins have the lowest contents of normal hydrocarbons as determined by the urea method. The oxidation of each type of paraffin under various conditions was performed in quadruplicate. The variations of the acid numbers did not exceed 3%.

EXPERIMENTAL RESULTS

Curves showing the course of variations of acid numbers in the oxidation of tar paraffins from Kõpsen and Gel'tsau are given in the diagram (I and II). In oxidation in presence of 0.2% potassium permanganate (curve 1), there is a distinct induction period of 2-4 hours in both cases; the rate of acid formation then increases fairly rapidly, and when acid numbers of 20-30 mg have been reached it begins to decrease somewhat, i. e., the formation of acids begins to slow down at that point. The oxidation in presence of 0.4% potassium permanganate (curve 2) takes a different course. The induction period is shorter, but it cannot be eliminated entirely despite the addition of this large amount of potassium permanganate. Evidently the formation of active centers for the development of the chain reactions is not instantaneous under these conditions. At the end of the induction period the formation of fatty acids proceeds at a high rate, which does not decrease during the process, and the whole reaction is completed in half the time.

* Transliteration of Russian — Publisher's note.

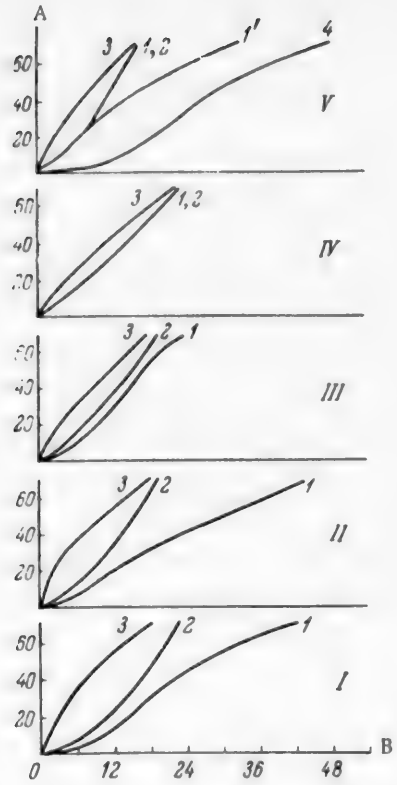

Variation of the acid numbers of different types of paraffin during oxidation. A) Acid number (in mg caustic potash), B) oxidation time (hrs). Paraffins from: I) Kõpsen, II) Gel'tsau, III) Rositz, IV) Rumania, V) Drogobych. Curves 1 and 1') paraffin with 0.2% $KMnO_4$, 2) paraffin with 0.4% $KMnO_4$, 3) mixture of original and recycled paraffins with 0.2% $KMnO_4$, 4) paraffin without catalyst.

In the oxidation of mixtures of original and recycled paraffins, the latter containing carbonyl and hydroxyl derivatives, in presence of 0.2% potassium permanganate, the oxidation begins at once (curve 3) without any induction period, and proceeds at a high rate. After an acid number of 20-30 mg the rate of acid formation begins to decrease gradually, and curves 2 and 3 converge visibly in approaching the final point. A possible explanation is that during the first period of oxidation oxygen is added, with formation of active neutral intermediate compounds, and the rate of oxidation is limited by the ability of the substances being oxidized to form free radicals, which then react with molecular oxygen. During the second period the neutral oxygen-containing intermediate compounds are converted into acids. This process cannot be accelerated by the substances which influence the first stage, and requires its own specific catalysts, which in this instance are probably heterogeneous compounds of manganese.

Paraffin from the Kõpsen works is the most difficult to oxidize, and in oxidation in presence of potassium permanganate it has a longer induction period than the other types; this is probably associated with the composition of the original paraffin. The difference between the rates of acid formation in the oxidation of the original paraffin and its mixture with the recycled paraffin is the greatest in this case, i. e., the effect produced by addition of easily oxidized carbonyl and hydroxyl derivatives is the greatest. The oxidation time is less than half (Table 2).

Similar results were obtained with Gel'tsau paraffin. These effects are less pronounced in the oxidation of Rositz paraffin (figure, III). When this paraffin is oxidized in presence of 0.2% potassium permanganate, acid formation is slow at first; the development of the process is represented by a characteristic S-shaped curve, and the oxidation is complete in 25 hrs. With double the amount of potassium permanganate the effect of the oxidation time is less significant than in the preceding cases, but the process continues at undiminishing rate to an acid number of 70 mg. The induction period is completely

TABLE 2

Times Required for Oxidation of Different Paraffins to Acid Number 70 mg KOH

Paraffin	Oxidation times (hrs) of paraffins from				
	Kõpsen	Gel'tsau	Rositz	Rumania	Drogobych
Without catalyst	—	—	—	—	48
With 0.2% $KMnO_4$	42	42	25	22	16
With 0.4% $KMnO_4$	23	20	20	22	16
$^1/_3$ original + $^2/_3$ recycled + 0.2% $KMnO_4$	18	18	18	20	16

eliminated by addition of recycled paraffin. Curves 2 and 3 almost coincide at the final point, and the oxidation is completed in 18-20 hrs.

There is no induction period in the oxidation of the more easily oxidizable Rumanian paraffin (figure, IV). No differences in the kinetics of acid formation in presence of 0.2 and 0.4% potassium permanganate were detected; the two kinetic curves coincide. Oxidation to acid number 70 mg proceeds rapidly at an undiminishing rate for 22 hrs.

Quite similar results were obtained in the oxidation of Drogobych petroleum paraffin, which is similar to it in composition and properties (figure, V, curves 1 and 3). In the oxidation of Drogobych paraffin in presence of potassium permanganate, the process of acid formation can be represented by one of two types of kinetic curve. In the first case, a very short induction period is followed by acid formation at an undiminishing rate (curve 1), and the process is completed in 16 hrs. In the second case, a similar induction period and rapid acid formation to acid number of about 20 mg are followed by a gradual retardation of the reaction (curve 1'). In all cases of oxidation represented by kinetic curves of type 1', the finely-divided, colored manganese compounds disappear from the mass, and pass partly into the sludge deposited on the walls of the vessel, and partly into soluble compounds. If the oxidation is represented by a kinetic curve of type 1, the finely-divided, colored, heterogeneous manganese oxides are present in the oxidation mass until the end of the process.

The figure, V, shows the kinetic curve for acid formation in the oxidation of Drogobych without any catalyst (curve 4). The oxidation was performed at a constant temperature at 125°, without a decrease to 107°. Comparison of curves 2 and 1' shows that in presence of potassium permanganate the induction period of oxidation is eliminated, and acid formation proceeds at a high rate from the start. After the heterogeneous manganese oxides have been removed from the reaction mass, acid formation follows the same kinetic law as in oxidation without catalysts, and the process is completed in 32-34 hrs.

These results show that the oxidation of paraffin is sharply accelerated in the initial stage by the presence of easily-oxidized carbonyl and hydroxyl derivatives introduced with recycled paraffin. At the second stage, when the neutral active intermediate products are converted into acids, oxidation in absence of catalysts proceeds at a diminishing rate, and is not accelerated in presence of carbonyl and hydroxyl derivatives. Considerable acceleration, and increased selective formation of acids, take place in presence of a heterogeneous finely-divided catalyst in the form of manganese compounds.

The presence of a heterogeneous catalyst is essential in the oxidation of paraffins for the production of fatty acids. The optimum amount of such catalyst depends somewhat on the composition of the paraffin and the reaction conditions.

SUMMARY

The oxidation of technical grades of paraffin wax under the conditions used in the production of synthetic fatty acids is sharply accelerated by additions of easily oxidized, neutral oxygen-containing compounds. Further acceleration of this process, and selective formation of acids, take place only in presence of heterogeneous finely-divided compounds of manganese.

LITERATURE CITED

[1] D. G. Knorre, Z. K. Maizus, and N. M. Emanuel', J. Phys. Chem. 29, 710 (1955).

[2] V. K. Tsyskovskii and N. A. Kiseleva, J. Appl. Chem. (USSR) 24, 672 (1951).*

[3] V. K. Tsyskovskii, in the book: Questions of Chemical Kinetics, Catalysis, and Reactivity (Izd. AN SSSR, 1955), p. 292.**

[4] N. M. Emanuel', in the book: Questions of Chemical Kinetics, Catalysis, and Reactivity (Izd. AN SSSR, 1955), p. 117.**

[5] L. S. Vartanian, Z. K. Maizus, and N. M. Emanuel', J. Phys. Chem. 30, 862 (1956).

Received June 25, 1956

* Original Russian pagination. See C. B. translation.

** In Russian.

THE CHEMICAL COMPOSITION OF DECAYED BIRCH AND ASPEN WOOD*

A. G. Rychkova

Chair of Chemistry, Voronezh Institute of Wood Technology

The forests of the USSR contain, together with healthy growths of a high quality from the commercial aspect, considerable numbers of plantations damaged by fungal growths. Fungal diseases of trees do much damage to the national economy.

Of the deciduous species, the aspen and birch are particularly susceptible to decay during growth (aspen up to 90%, birch up to 80%).

There have been few studies of the changes in the chemical composition of wood during decay. Rose and Lisse [1], Bray and Andrews [2], and Falk [3] found that the chemical composition of wood is changed by decay. For example, the fungus Trametes pini decreases the lignin content of wood by 30%, while the relative cellulose content increases by 15%. The fungus Fomes annosus decreases the lignin, cellulose, and pentosan contents of spruce wood, while the fungus Merulius lacrymans causes a large increase of the relative lignin content, with an appreciable decrease of the cellulose content.

The chemical composition of wood attacked by wood-rotting fungi was studied by Komarov [4], Komarov and Filimonova [5], and Chudakov [5]. They found that rotted wood has a much higher content of ash and of substances soluble in hot water and 1% caustic soda, and a lower pentosan content, than healthy wood. The cellulose and lignin contents of wood vary according to the type of decay.

Two main types of decay are distinguished: 1) corrosive (white rot) is caused by fungi which decrease the lignin content of wood, while the relative cellulose content increases or falls slightly; 2) destructive (brown rot) is caused by fungi which break down cellulose and pentosans; the wood becomes relatively richer in lignin.

Vanin [7] also discovered a corrosive–destructive (intermediate) type of decay, in which the cellulose–lignin ratio varies little during the process.

Nikitin, Solechnik, and Komarov [8] showed that aspen wood slightly damaged by Fomes igniarius can be used for cellulose production. According to Zherebov [9] larch wood rotted by the fungus Stereum abietinum is suitable for the production of wrapping paper and some types of technical papers. Volutskii [10] showed that rotten oak wood can be used in the production of tanning extracts.

Despite the existing possibilities for the utilization of decayed wood as a chemical raw material, it is used at present mainly as a low-grade fuel.

The purpose of the present work was to study the chemical composition of aspen and birch wood damaged by various fungi causing different types of decay, and to determine their possible uses as chemical raw materials. The main attention was concentrated on those types of birch and aspen decay about the chemical nature of which little information is available in the literature.

We did not find any data on the chemical composition of birch wood damaged by Fomes fomentarius, or of aspen damaged by Fomes pinicola, in the literature.

---

* This work was performed under the guidance of R. E. Keller, Head of the Chair of Chemistry, the Voronezh Institute of Wood Technology.

EXPERIMENTAL

We studied white (marble) rot of birch caused by the fungus Fomes fomentarius Gill., white (striped) rot of aspen caused by Fomes igniarius f. tremulae Gill., brown rot of birch caused by Polyporus betulinus Fr. and of aspen caused by Fomes pinicola Fr. Of these, white rot of birch and aspen are the most common in forests.

White rot of birch and aspen caused by the fungi Polyporus betulinus and Fomes pinicola belongs to the destructive type. White rot of birch and aspen caused by Fomes fomentarius and Fomes ignarius f. tremulae should more correctly be classified with the corrosive–destructive (mixed) type, as the rotten wood does not acquire in stage III the structure and color typical of the corrosive type.

Healthy control trees and trees damaged by rot grew under the same conditions, and were of the same age, height, and trunk diameter. The presence of sporophores on the trunk was taken as the indication of attack.

Air-dry samples were ground down to sawdust, and average samples were prepared. Sawdust passing through a sieve of 1 mm mesh and retained on a sieve of 0.5 mm mesh was taken for analysis. Some of the samples were classified by stages of decay. Stages I, II, III, and IV are distinguished, according to the degree of decay of the wood.

TABLE 1

Chemical Composition of Healthy Wood and of Wood Attacked by Wood-Rotting Fungi (in %)*

Type of wood	Cellulose	Lignin	Pentosans	Substances extracted by		Ash
				hot water	ethyl ether	
Birch						
Healthy	44.62	18.16	29.76	1.23	1.44	0.31
Damaged by *Fomes fomentarius*, white rot	50.14	19.74	24.06	5.19	0.72	0.91
Polyporus betulinus, brown rot	31.49	38.09	17.87	13.89	0.83	0.63
Healthy	48.74	20.30	27.64	2.54	0.84	0.40
Damaged by *Fomes igniarius f. tremulae*, white (striped) rot	49.39	22.34	24.49	3.18	0.80	1.62
Fomes pinicola, brown rot	40.12	27.71	21.15	6.12	0.57	0.51

* The values in this and the following tables are average for five samples in each experiment, calculated on bone-dry wood.

The moisture content of the wood was determined by drying at 100-105°; it varied from 9 to 10% for healthy wood, and from 12 to 14% for wood attacked by white and brown rot.

Duplicate samples of each specimen were taken for chemical analysis. The samples were analyzed for ash, substances extracted in hot water [11] and ethyl ether [12], for cellulose by the Kürschner and Hoffer method, for lignin by means of 72% sulfuric acid [13, 14], and for pentosans by the bromide–bromate method [15].

The results of the chemical analyses of the woods are given in Table 1.

It follows from the data in Table 1 that decayed wood has a higher content of substances extracted by hot water than healthy wood. The much higher content of substances soluble in hot water present in wood attacked by brown rot may be attributed to the fact that in this type of decay the breakdown of cellulose and pentosans leads to formation of monosaccharides and dextrin-like substances, soluble in hot water. Decayed wood has a lower content of ether-soluble substances than healthy wood.

The relative cellulose content of wood attacked by white rot is higher than of healthy wood, while more lignin is present in wood with brown rot than in healthy wood. Decayed wood has a lower pentosan content than healthy wood.

Pentosans are broken down during decay, and this breakdown is particularly extensive when wood is damaged by brown rot.

Methoxyl groups. Methoxyl groups are present mainly in lignin, and only a part of them is combined with the carbohydrates in the wood—polyuronic acids, xylan, pectins. Methoxyl groups were determined by the Zeisel method [16]. The wood was first made free from resin and dried to the bone-dry state. The results are given below.

TABLE 2

Methoxyl Group Contents in Birch and Aspen Wood*

Wood species	White rot			Brown rot			Healthy wood
	decay stage		not separated by decay stages	decay stage		not separated by decay stages	
	I – II	III – IV		I – II	III – IV		
Birch	5.17	5.13	5.20	5.91	7.15	7.98	5.71
Aspen	5.32	4.96	5.34	—	—	5.19	5.60

* In this and the following tables, on birch and aspen wood damaged, Fomes fomentarius and Fomes igniarius f. tremulae are designated as white rot, and Polyporus betulinus, Fomes pinicola as brown rot.

Table 2 shows that the methoxyl group content of wood damaged by white rot is lower than that of healthy wood, and decreases with increasing decay, while in the case of brown rot the methoxyl group content increases at later stages of decay.

The decrease of the methoxyl group content in wood damaged by white rot is probably caused by a decrease of the lignin content, while the increased content of methoxyl groups in brown rot is due to an increase of the relative content of lignin. To confirm this hypothesis, we determined the methoxyl group contents of lignin isolated from birch and aspen wood attacked by white and brown rot. Lignin was extracted by means of 72% sulfuric acid [13]. The methoxyl group contents of the lignin (in %) are given below.

Wood species	From white rot	From brown rot	From healthy wood
Birch	15.45	16.81	17.61
Aspen	13.92	15.24	18.09

It is seen that lignin isolated from wood attacked by white rot has a lower methoxyl group content than lignin isolated from wood with brown rot.

Acetyl groups. Acetyl groups were determined in wood from which water-soluble and ether substances had been previously extracted. The determination was performed by saponification of the acetyl groups by 0.5 N alcoholic caustic potash solution [17]. The analytical data are given in Table 3.

Table 3 shows that wood attacked by white rot has a lower, and wood attacked by brown rot a higher content of acetyl groups than healthy wood.

Dry distillation of wood. Our investigations showed that in decay of the destructive type (brown rot) birch wood has higher relative contents of methoxyl and acetyl groups than healthy birch wood. It was thought that wood attacked by this type of rot should give somewhat higher yields of methyl alcohol and acetic acid in dry distillation. This was verified by dry distillation of the wood under laboratory conditions. The same distillation procedure was used for all the samples. The wood was cut into pieces 3 × 1 × 1 cm. The dry distillation was

TABLE 3

Acetyl Group Contents (%) in Birch and Aspen Wood

Wood species	White rot		Brown rot		Healthy wood
	Decay stage				
	I – II	III – IV	I – II	III – IV	
Birch	8.21	8.84	10.48	10.69	9.54
Aspen	9.11	9.46	-	-	9.16

continued for 4-5 hrs, and was ended when the temperature inside the retort reached 450°. The yields of methyl alcohol, acetic acid, charcoal, gas, and tar were determined.

Air-dry wood containing 10% moisture was used for the distillation.

The charcoal was weighed after cooling. The amount of gas was found by difference between the weight of the wood taken and the sum of the weights of charcoal and distillate; it also included losses. The results of experiments on the distillation of birch wood (in %) are given below.

Type of wood	Distillate	Charcoal	Gas	Tar
Healthy	49.76	30.33	12.62	7.29
Brown rot	37.49	36.10	16.85	9.56
White rot	41.59	29.87	20.75	7.79

Since brown rot gave a higher lignin content, higher yields of charcoal and tar were obtained in the dry distillation of such wood.

The higher yield of gas in the dry distillation of wood attacked by white rot may be attributed to thermal decomposition of cellulose (which predominates in this type of decay).

The acid content of the crude acid distillate was determined by alkali titration [18].

The average acid content of the distillate, calculated as acetic acid, was 6.34% for wood with white rot, 5.17% with brown rot, and 7.80% for healthy wood. The acidity of the distillate from decayed wood is therefore higher than the acidity of the distillate from healthy wood; by 1.46% for white rot, and 2.63% for brown rot.

Methyl alcohol was determined in the crude acid distillate by the method generally used in the industry [18]. According to our results, healthy wood yielded 1.20% of methyl alcohol, while wood attacked by brown rot gave 0.66%, or half the amount. It is likely that during dry distillation a considerable part of the methyl groups is used in the formation of methane, while some remain in the charcoal and tar. This is confirmed by the higher yields of gas and tar.

Hydrolysis of wood. The hydrolysis was performed stepwise in an autoclave, in conical flasks (stoppered by corks with outlet tubes terminating in capillaries to prevent evaporation). First the easily hydrolyzed hemicelluloses and then the cellulose were hydrolyzed. The liquor ratio in the first and second stages of hydrolysis was 1:20.

Hydrolysis of easily hydrolyzed polysaccharides – hemicelluloses. A 1 to 4 g sample of bone-dry sawdust was put into a flask, covered with 0.5% sulfuric acid solution, and put in the autoclave. The hydrolysis was continued for 2 hrs at 2 atmos. The liquid was then filtered. The residue on the filter was washed with small portions of hot water to a neutral reaction. The filtrate and wash waters were combined. The solution was cooled and neutralized by dry sodium carbonate; the volume of the solution was then measured. Reducing substances in the solution were determined by Bertrand's method [19]. The results were calculated (nominally) in terms of

xylose by means of the appropriate table [20] on the assumption that hemicelluloses of deciduous trees consist mainly of pentosans, and predominantly of xylan, which yields xylose on hydrolysis. The results are given in Table 4.

TABLE 4

Yields of Xylose in the Hydrolysis of Birch and Aspen Wood (in %)

Wood species	White rot			Brown rot			Healthy wood
	decay stage			decay stage			
	I – II	III – IV	not separated by decay stages	I – II	III – IV	not separated by decay stages	
Birch	18.79	22.77	22.14	16.25	15.18	17.24	23.99
Aspen	18.85	19.03	20.61	—	—	18.45	22.24

Rotted wood gave lower yields of xylose on hydrolysis than healthy wood.

Hydrolysis of cellulose. The residue after hemicellulose hydrolysis was dried to constant weight at 100-105°, and a weighed sample was taken. The hydrolysis was performed by means of 0.5% sulfuric acid solution at 10 atmos for 2 hrs. The operating pressure was reached in 15 min. The reducing substances were determined by Bertrand's method [19]. The results were calculated in terms of glucose. The results are given as percentages on the bone-dry original wood. The glucose yields in the hydrolysis of wood are given in Table 5.

TABLE 5

Yield of Glucose in the Hydrolysis of Birch and Aspen Wood (in %)

Wood species	White rot			Brown rot			Healthy wood
	decay stage			decay stage			
	I – II	III – IV	Not separated by decay stages	I – II	III – IV	Not separated by decay stages	
Birch	22.26	20.31	22.07	15.51	15.07	15.19	22.22
Aspen	22.24	22.10	20.79		—	17.05	21.70

TABLE 6

Total Yields of Sugars from Wood (in %)

Wood species	White rot			Brown rot			Healthy wood
	decay stage			decay stage			
	I – II	III – IV	Not separated by decay stages	I – II	III – IV	Not separated by decay stages	
Birch	41.05	43.08	41.21	31.76	30.25	32.43	46.21
Aspen	41.09	41.13	41.10			35.50	43.94

It follows from Table 5 that the glucose yield decreases somewhat with increasing decay of the wood, especially in the case of brown rot, as considerable breakdown of cellulose occurs in the destructive type of decay.

Total sugars – xylose and glucose – in wood are given in Table 6 (in which average data of Tables 4 and 5 are summarized).

Table 6 shows that the total yield of xylose and glucose from birch and aspen wood attacked by white rot is close to the yield of these sugars from healthy wood.

For a better idea of the yields of various substances from decayed wood, which occupies a greater bulk for a given weight, the bulk densities of the woods were determined.

The usual method was used for the determination of bulk density [21]. The bulk densities of decayed woods (in g/cc) are given below.

Wood species	White rot	Brown rot	Healthy wood
Birch	0.268—0.340	0.263—0.322	0.629
Aspen	0.220—0.226	—	0.421

It is seen that the bulk density of decayed wood is about a half that of healthy wood. Variations in the bulk density of decayed wood depend on the degree of decay.

Xylan. It was found that birch and aspen give higher yields of xylose with white rot than with brown rot (Table 4). To confirm these data, xylan was isolated from healthy and decayed wood.

A modification of Sal'kovskii's method [13] was used for isolation of xylan. An equal volume of 96% ethyl alcohol, and not Fehling's solution, was used to precipitate xylan from the alkaline extract. The yields of crude xylan are given in Table 7.

TABLE 7

Yields and Properties of Xylan

Wood species	White rot		Healthy wood	
	Yield (%)	$[\alpha]_D^{20}$	Yield (%)	$[\alpha]_D^{20}$
Birch	9.47	—76°	12.71	—90°
Aspen	12.73	— 87	12.76	—90

Birch attacked by white rot gives a lower yield of xylan, with a lower specific rotation, than aspen attacked by white rot. Therefore, the xylan in white-rotted birch is broken down more, and less of it is present, than in white-rotted aspen. The greater breakdown of xylan in birch wood may be attributed to the specific characteristics of the fungus which attacks this wood.

Advice on the selection of healthy and decayed wood, and on phytopathological questions, was obtained from Assistant Professor of Wood Phytopathology of the Chair of Forestry Protection of the VLTI, I. Ia. Shemiakin.

SUMMARY

1. The relative cellulose contents of birch wood attacked by white (marble) rot caused by Fomes fomentarius and white (striped) rot caused by Fomes igniarius f. tremulae (destructive–corrosive or mixed decay) are higher than in healthy wood. The cellulose contents of birch wood attacked by brown rot caused by Polyporus betulinus and of aspen wood caused by Fomes pinicola (destructive decay) are lower than in healthy wood.

2. The contents of substances extracted in hot water are at least twice as high in wood attacked by white rot, and at least 3 times as high in wood attacked by brown rot (destructive decay), as in healthy wood. The contents of substances extracted by ethyl ether from wood with white and brown rot are about $^2/_3$ of the amounts extracted from healthy wood. Decayed wood is worthy of attention as a raw material for technical purposes.

3. Lignin isolated from wood attacked by white rot has a lower methoxyl group content than lignin from wood with brown rot or from healthy wood. The lignin from wood with white rot is broken down to a greater extent than lignin from wood with brown rot.

4. Ordinary dry distillation of decayed birch wood gave 1.5-2.5% less acids and half the amount of methyl alcohol obtainable from healthy wood.

5. The total yield of sugars – xylose and glucose – from birch and aspen woods with white rot is similar to the yield obtained from healthy wood. It must be remembered in practical calculations that the bulk density of decayed wood is half that of healthy wood.

6. Xylan is isolated from white-rotted birch in a lower yield and with a lower specific rotation than from white-rotted aspen. Xylan is broken down considerably during decay of the wood.

LITERATURE CITED

[1] R. Rose and M. Lisse, Ind. Eng. Chem. 9, 284 (1917).

[2] M. Bray and T. Andrews, Ind. Eng. Chem. 16, 137 (1924).

[3] R. Falk, Ber. botan. 59, 10 (1926); Ber. 60, 225 (1927).

[4] F. P. Komarov, Paper Ind. 2, 49 (1934).

[5] F. P. Komarov and G. Filimonova, J. Appl. Chem. (USSR) 10, 487 (1937).

[6] M. I. Chudakov, J. Appl. Chem. (USSR) 22, 392 (1949).

[7] S. I. Vanin, Wood Phytopathology (State Wood and Paper Press, 1955).*

[8] N. I. Nikitin, N. Ia. Solechnik, and F. P. Komarov, Trans. Experimental Forestry 2, 1 (1930).

[9] L. P. Zherebov and V. N. Komarovskii, Trans. Central Sci. Res. Inst. Wood Chemistry 2, 39 (1933).

[10] S. S. Volutskii, Trans. Central Sci. Res. Inst. Wood 1, 98 (1932).

[11] T. I. Rudneva and S. D. Antonovskii, Practical Manual of Wood and Cellulose Chemistry (Leningrad, 1951).*

[12] N. N. Ivanov, Methods of Plant Physiology and Biochemistry (Agricultural Press, 1946).*

[13] F. P. Komarov, Laboratory Manual of Cellulose and Wood Chemistry (1934).

[14] N. Ia. Dem'ianov and N. D. Prianishnikov, General Methods of Analysis of Plant Substances (1934).*

[15] N. I. Nikitin, Chemistry of Wood (Izd. AN SSSR, 1951).*

[16] L. Gattermann, Laboratory Methods of Organic Chemistry [Russian translation] (Goskhimizdat, 1932).

[17] H. Meyer, Analysis and Structure Determination of Organic Compounds [Russian translation] (Ukrainian State Sci.-Tech. Press, 1935).

[18] H. M. Bunburg, Destructive Distillation of Wood [Russian translation] (State Wood Technology Press, Moscow, 1933).

[19] A. N. Belozerskii and N. I. Proskuriakov, Practical Manual of Plant Biochemistry (Moscow, 1951).*

[20] N. Ia. Dem'ianov, General Methods of Analysis of Plant Substances (Moscow, 1923).*

[21] P. N. Khukhrianskii and I. F. Larin, Forestry Utilization (Moscow-Leningrad, 1947),* p. 22.

Received March 12, 1956

* In Russian.

STUDY OF POLYMORPHISM OF CACAO BUTTER

M. Ia. Antokol'skaia

In the light of modern physical chemistry, chocolate is a colloidal suspension in which a continuous structure (spatial network) gradually develops [1]. The disperse phase of chocolate consists of fine crystals of sugar and grains of the protein portion of the cacao bean, while the fat of the bean constitutes the dispersion medium. Structure formation in chocolate pastes, which influences the taste qualities, depends mainly on the dispersion medium, i. e., on the properties of the fat in the chocolate. In addition to its principal role as a structure former, fat increases the food value of chocolate and helps to retain the aroma. The best fat for the production of chocolate is natural cacao butter. Natural cacao butter has a number of properties which distinguish it from all other known natural fats. It has a relatively low melting point (below 36°), but has very considerable hardness and brittleness and a nonsmearing surface. Cacao butter crystallizes easily.

The principal properties of cacao butter are [2]: initial melting temperature 31-34°, final melting temperature 33-36°, solidification temperature 23-28°, titer 45-51, iodine number 34-36, thiocyanate number 32-35, Reichert-Meissl number 0.1-0.4, Polenske number 0.5-1.0, saponification number 192-200, acid number 1.0-1.5.

The glyceride composition of cacao butter (in %) is [2, 3]: dioleopalmitin 4, dipalmitostearin 2.5, oleodipalmitin 7.0, oleopalmitostearin 53.0, oleodistearin 18.5, dioleostearin 4.5, oleolinoleopalmitin 4.5, oleolinoleostearin 4.5.

The acid composition of cacao butter (in %) is [2, 3]: palmitic acid 23-24, stearic 34-35, oleic 39-40, linoleic about 2.

The individual properties of cacao butter can be partly accounted for by the above data. The content of the principal glyceride of cacao butter (oleopalmitostearin), with m. p. 34.5°, is 53%; oleodipalmitin melts at 29°, oleodistearin at 43.5°, and dipalmitostearin at 63-68°; the glycerides liquid at room temperature comprise a total of 17.5%. Therefore the melting temperature of the whole complex of triglycerides which constitute cacao butter is very close to that of the triglyceride present in the largest amount (oleopalmitostearin). The other triglycerides — the liquids and those with higher melting points — apparently either have little effect on the melting temperature of the butter as a whole, or exert a mutually-compensating effect. This accounts for the very narrow interval between the initial and final melting temperatures of the butter (when determined in a capillary tube), which is the cause of the nonsmearing surface — a very important property in chocolate manufacture.

This is also the cause of the relatively low differential Polenske number (the difference between the melting and solidifying temperature of the fat).

The low iodine number indicates that the butter is very resistant to rancidity.

In the production of chocolate and chocolate confectionery, cacao butter displays a number of peculiar and highly interesting technological properties, to which the processes of chocolate manufacture have been adapted by chocolate manufacturers without a final theoretical analysis of these properties.

This applies to the conditions of tempering of chocolate pastes, their crystallization, and storage of the finished chocolate.

These peculiar technological properties of cacao butter directly depend on its physicochemical structure.

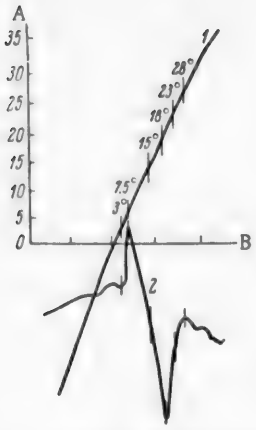

Fig. 1. Thermogram of the fusion of the γ-phase of cacao butter (1) direct and 2) differential recordings). A) Temperature (°C), B) time (min). Heating rate 4°/min.

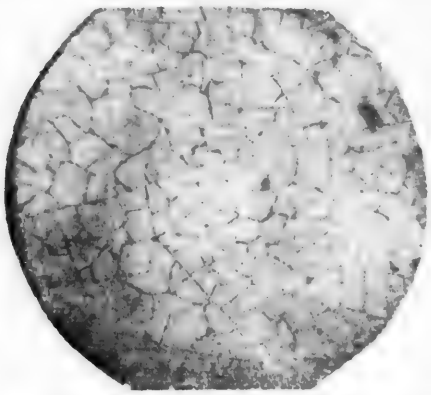

Fig. 2. Micrograph of amorphous glassy γ-phase of cacao butter.

There have been a number of special investigations of the crystallization of cacao butter in relation to the temperature conditions or, in other words, of the phase composition of cacao butter under different conditions of cooling of the melt, carried out by dilatometric, calorimetric, and other methods [4-7].

A combination of differential-thermal and microstructural analysis methods was used in our physicochemical investigations of cacao butter.

These analytical methods are not described in this paper, as they are detailed in a number of publications [8-11]. It must be pointed out, however, that a small-size cooling block of Tsurinov's design was used in the differential-thermal analysis. A special microscope cooling stage designed by Tsurinov and Vol'nova was used for the microstructure analysis. The investigations clearly disclosed the whole complexity of the phase composition of natural cacao butter.

Investigations of the phase composition of pure triglycerides have shown [12] that their multiphase structure becomes most pronounced in nonequilibrium conditions, i. e., if the melts are superheated and rapidly cooled. The cacao butter was therefore subjected to special thermal conditions before the thermograms were recorded.

A thermogram of cacao butter, recorded by the differential-thermal method by means of the Kurnakov pyrometer, is given in Fig. 1. The thermogram records the fusion of cacao butter which had previously been heated to 100° and rapidly cooled in a stream of liquid nitrogen to −80°.

The thermogram shows that the maximum endothermic effect in the fusion of the butter treated in this way is found at 18°; the whole fusion range is from 3 to 28°.

Microscopic investigation of the sample revealed a continuous amorphous field intersected by microcrevices, probably formed as the result of heat stresses during rapid cooling (Fig. 2).

This low-melting amorphous phase of cacao butter is probably its glassy, metastable γ-phase. The slight effect at 3° on the left-hand branch of the curve (Fig. 1), the exothermic effect at 7.5°, and the break in the curve at 15° may be attributed to devitrification or softening of the "glass" formed.

The effects noted on the right-hand branch of the curve at 23 and 28° are extremely interesting.

For a clearer elucidation of the character of the effects at 23 and 28°, cacao butter in the γ-phase was kept in a thermostat at 20-21° for 24 hrs; this stimulated transition of the γ-phase into the less fusible α- and β'-phases.

The thermogram in Fig. 3 represents the fusion of the phases formed in this way. A distinct two-phase structure is revealed, with phase transitions at 23.5 and 28°. The total melting range of the two phases is 20-31.6°.

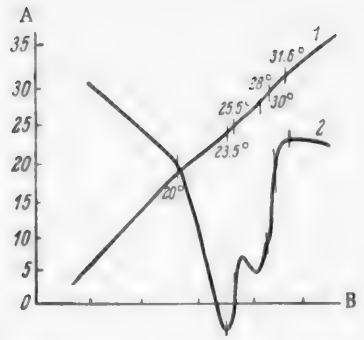

Fig. 3. Thermogram of the fusion of the α- and β'-phases of cacao butter (1 – direct and 2 – differential recordings). A) Temperature (°C), B) time (min). Heating rate 2°/min.

Thus, the hardly perceptible effects at 23 and 28° in the thermogram of Fig. 1 represent the conversion of α- and β'-phases which arise in the γ-phase. This confirms the view advanced by Ravich and Tsurinov [12] that mixtures of triglycerides in the nonequilibrium state always contain a combination of a number of phases.

The micrographs of the phases so formed (Fig. 4) clearly revealed acicular crystals of the α-phase, arranged in the form of spheroidal aggregates, and dense white formations, probably of the β'-phase, growing from the center; the next micrograph (Fig. 5) shows three phases of cacao butter at once – the α-phase aggregates are covered by small crystals, probably of the stable β-phase.

The stable phase of the cacao butter may be obtained by two routes: we may reproduce the conditions

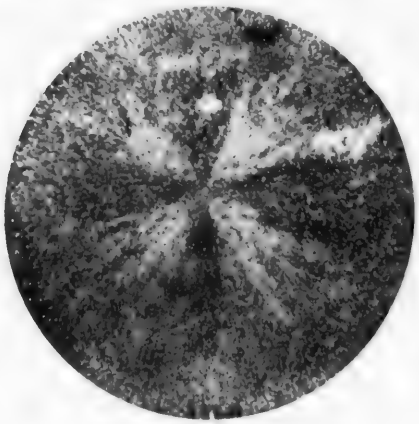

Fig. 4. Micrograph of α- and β-phases of cacao butter.

Fig. 5. Micrograph of a three-phase structure in cacao butter.

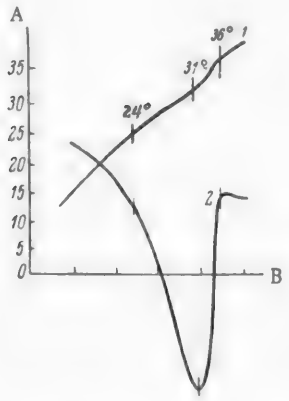

Fig. 6. Thermogram of the fusion of cacao butter in the stable β-phase. (1 – Direct and 2 – differential recordings). A) Temperature (°C), B) time (min). Heating rate 2°/min.

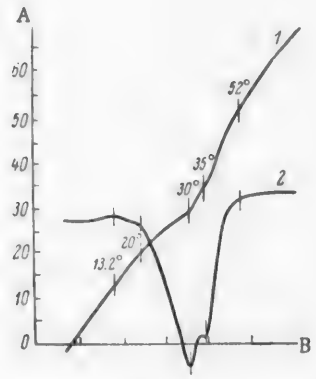

Fig. 7. Thermogram of the fusion of "aged" cacao butter in the β-phase (1 – direct and 2 – differential recordings). A) Temperature (°C), B) time (min). Heating rate 13°/min.

generally used in determinations of melting points in capillary tubes, the butter being melted and then kept for 24 hrs at room temperature, and then record the melting curve; or we may record the melting curve of the butter kept for a long time without melting.

In either case the thermogram reflects a one-phase structure. The endothermic fusion effect is found at 31° (Fig. 6). The final melting, corresponding to the final melting temperature in the capillary, occurs at the point where the discontinuity passes into the monotonic region of the curve at 36°. The total fusion range is 24-36°.

The cacao butter sample under investigation was kept for 1 year at 6-8°. In view of the numerous reports in the literature concerning the high stability of cacao butter, we were interested in variations of its phase composition during ageing. It must be emphasized that during this year the cacao butter was never melted. The melting curves of the γ-phase and of the α- and β'-phases revealed some increase of the total melting range, and reproduced completely the temperatures of the effects found for these phases in fresh cacao butter. This shows that no significant chemical changes took place in the butter during the year.

However, the fusion thermogram of "aged" cacao butter in the stable phase revealed a very interesting picture (Fig. 7). There are two distinct fusion effects in the thermogram — at 30 and 35°. The total melting range is much wider, from 13 to 52°.

As the result of this phase analysis of cacao butter, certain conclusions can be drawn concerning its physicochemical structure and the interrelationships of its constituent triglycerides.

Cacao butter, like individual triglycerides [12], exhibits polymorphism, with the following phase-transition temperatures:

Phases	Main transition effect (°C)	Total melting range* (°C)
γ	18	3–25
α	23.5 (&25.5)	22—32
β'	28	
β	30	24—35

The existence of polymorphic transitions in cacao butter suggests that the triglycerides which constitute cacao butter form a solid solution and therefore cacao butter undergoes phase transitions similar to those of an individual substance. Prolonged storage of the butter leads to separation of the solid solution into individual groups of triglycerides, with an increase of 20° in the total melting range and the appearance of a new transition effect at 35°.

In connection with the polymorphism of cacao butter, it is of interest to consider the nature of chocolate fat bloom, "this mysterious phenomenon, which is as serious a disease of chocolate as cancer is of man" [13]. According to the results of numerous workers, fat bloom is the consequence of separation of a high-melting fraction of cacao butter on the surface of the chocolate.

Let us consider how far this theory corresponds to the facts.

The chocolate mass leaves the conching machine at about 70° and enters the tempering machine where it is cooled to 30° with continuous agitation. The casting is done at the same temperature. Tempering at 30° (above the melting points of the metastable phases) stimulates the maximum formation of crystallization centers, in the form of the stable β-phase, in the melt. The cast chocolate cools and crystallizes in a cooler at 7-10°. Thus, crystallization fixes the already-formed crystallization centers of the β-phase, and the solid cast chocolate consists mainly of a solid solution of triglycerides in the stable phase, and partly in metastable phases, which pass into the stable form during storage.

Therefore tempering is a process which directs the crystallization of cacao butter toward formation of the maximum number of crystals in the stable phase, and thereby prevents further polymorphic transitions in the solid chocolate. Well-tempered chocolate therefore does not bloom for a very considerable time.

* Average values from several thermograms.

When the tempering conditions are maintained badly, a certain amount of butter remains in the melt in the form of metastable phases, and their transition into the stable phase takes place in the solid chocolate. At the same time the solid solution of triglycerides breaks down and loses its homogeneity (Fig. 7). The individual groups of triglycerides deposited in the solution themselves exhibit polymorphism, and are converted into higher-melting stable phases. The complex breakdown of the solid solution accompanied by polymorphic transitions results in the formation of visible crystals of fat on the chocolate surface.

Chocolate fat bloom is therefore the separation of the most high-melting stable polymorphic phases of the cacao butter, and of individual groups of triglycerides in it, on the chocolate surface; it is not the separation of the high-melting fractions of the cacao butter as is generally believed. Correct tempering leads to the formation of a homogeneous solution, consisting of stable triglyceride phases, which does not break down for a relatively long time.

It is known in the chocolate industry that introduction of surface-active substances or diluents into chocolate pastes (in order to save cacao butter) raises the resistance of the chocolate to fat bloom considerably.

Therefore, the addition of small amounts (0.3% by weight on the chocolate mass) of diluents (phosphatides, hydrophilic lipins with polyglycerides, etc.) has a definite physicochemical influence on the polymorphic transitions of cacao butter.

By analogy with the action of surface-active substances (modifiers) on the polymorphic transitions of certain metals, such as tin [14-16], it may be assumed that surface-active substances (diluents) likewise modify the crystallization of cacao butter, i. e., by decreasing the surface energy of the crystals, they retard or completely inhibit the polymorphic transitions.

SUMMARY

1. It was shown by phase analysis that cacao butter can exist in four polymorphic modifications.

2. The polymorphic transitions established in cacao butter indicate that the triglycerides which comprise cacao butter form a solid solution, and therefore the butter, like an individual substance, undergoes phase transitions which simulate the phase transitions in single-acid and mixed triglycerides.

3. Cacao butter breaks down on prolonged storage into separate groups of triglycerides, with an increase of the total melting range by 20°, and the appearance of a new transition effect at 35°.

4. Cacao butter stored for a year (and chocolate stored for two years) exhibited the transition temperatures of the α- and β'-phases; this shows that no significant chemical changes took place in the cacao butter during this time. This is in harmony with the frequent statements in the literature according to which cacao butter is very stable on keeping and cacao products can act as powerful antioxidants.

5. Chocolate generally retains the phase-transition temperature characteristics of pure cacao butter.

6. Fat bloom in chocolate is caused by phase transitions of cacao butter taking place in the solid chocolate; i. e., the conversion of metastable into stable phases, with simultaneous breakdown of the homogeneity of the triglyceride solution, and the consequent appearance of visible crystals of fat on the chocolate surface.

7. Proper tempering of chocolate at 30° favors the formation of the maximum number of crystallization centers in the form of the stable β-phase, and thereby decreases the possibility of polymorphic transitions and so retards blooming for some time, until considerable amounts of the breakdown products of the homogeneous triglyceride solution have accumulated.

The author offers deep gratitude to Prof. B. Ia. Golant who directed the work, and to the staff of the Laboratory of Phase Analysis of Organic Systems, Institute of General and Inorganic Chemistry, Academy of Sciences USSR, in particular the head of the Laboratory Prof. G. B. Ravich and Candidates of Technical Sciences G. G. Tsurinov and V. A. Vol'nova, who rendered much help in this investigation.

LITERATURE CITED

[1] P. A. Rebinder, Scientific Lectures, Ministry of the Food Industry USSR, 1951 (Food Industry Press, Moscow, 1952).*

* In Russian.

[2] A. A. Zinov'ev, Chemistry of Fats (Moscow, 1952).*

[3] T. P. Hilditch, Chemical Constitution of Natural Fats (1947).

[4] D. Albers, Chem. Weekblad 25, 235 (1928).

[5] I. D. Van Roon, Chem. Weekblad 27, 498 (1930).

[6] W. Reinders, C. L. Doppler, and E. L. Oberg, Rec. trav. chim. 51, 917 (1932).

[7] S. V. Vaeck, Intern. Choc. review 4 (1951); 6 (1951); 12 (1951); 11 (1952).

[8] L. G. Berg, A. V. Nikolaev, and E. Ia. Rode, Thermography (Izd. AN SSSR, Moscow, 1944).*

[9] L. G. Berg and G. G. Tsurinov, The Kurnakov Pyrometer (Izd. AN SSSR, Moscow, 1942). *

[10] G. G. Tsurinov, The Kurnakov Pyrometer (Izd. AN SSSR, Moscow, 1953).*

[11] G. B. Ravich, G. G. Tsurinov, and V. A. Vol'nova, Factory Labs. 10 (1952); 7 (1953).

[12] G. B. Ravich and G. G. Tsurinov, Phase Structure of Triglycerides (Izd. AN SSSR, Moscow, 1952).*

[13] R. Whymper, The Problem of Chocolate Fat-Bloom (Chicago, 1933).

[14] V. K. Semenchenko, J. Phys. Chem. 19, 5 (1947); Nonferrous Metals 6 (1936).

[15] V. K. Semenchenko, N. L. Pokrovskii, and V. B. Lazarev, Proc. Acad. Sci. USSR 89, 6 (1953).

[16] E. Cohen and A. van Liesehout, Z. Phys. Chem. 173, 1, 32 (1935).

Received April 12, 1956

* In Russian.

PRODUCTION OF FILM FORMERS BASED ON NONDRYING AND SEMIDRYING OILS

A. A. Ivanova

In view of the urgent necessity to find good-quality substitutes for linseed oil for the production of anti-corrosion paints, in 1937 [1, 2] we developed a method for the production of drying products from semidrying oils, and in particular from cottonseed oil, which is produced in our country in considerable amounts. The proposed method consisted essentially of the hydroxylation of semidrying oils by oxidation by means of atmospheric oxygen, followed by dehydration of the hydroxylation products. The formation of hydroxyl groups in triglycerides on oxidation, and the removal of elements of water with the formation of double bonds when the hydroxylation products are heated in presence of catalysts, was subsequently confirmed with numerous examples [3].

The theoretical basis of the dehydration of hydroxylated triglycerides [3] is in full harmony with the latest advances in the theory of high polymers [4] and the drying of oils [5, 6, 7], according to which film formation is regarded as polymerization and condensation of the oxidation products of oils, as the principle of this method is to increase the unsaturation of triglycerides in order to raise their tendency to polymerization and film formation.

In addition to confirming the above-mentioned results, according to which the film-forming capacity of semidrying oils can be increased by hydroxylation and dehydration, our investigations showed that the side reactions which take place in hydroxylation by oxidation with atmospheric oxygen increase the functionality of triglycerides by the formation of carbonyl, α-oxide, and other active oxygen-containing groups which increase the tendency of triglycerides to film formation. Studies of the mutual interaction of compounds of this type led to a number of theoretical conclusions which extended the existing theories of the oxidation and drying of oils; the general nature of the dehydration of artificially hydroxylated semidrying oils, and of nondrying castor oil containing natural hydroxyl groups, has been determined.

Further to the relationship established earlier between the properties of dehydrated castor oil [8-10], the composition of the dehydration products of methyl ricinoleate [11], and the nature of the catalysts used, it was found that sodium bisulfate is more effective than other catalysts in bringing about intramolecular dehydration with a minimum of side reactions; it is thereby possible to separate the dehydration and polymerization on processes and to obtain low-viscosity drying castor oil with a maximum content of linoleic acid isomers with conjugated double bonds.

On the basis of data [12] on the dehydration of castor oil after preliminary transesterification with pentaerythritol, we showed [13] that it is possible to obtain stronger films from semidrying oils by means of hydroxylation and subsequent dehydration, with simultaneous transesterification with pentaerythritol; this is described in the Experimental section of this paper. This section also contains data on the production of strong films from hydroxylated cottonseed oil after vinylation and dehydration.

The preparation of drying products from semidrying oils by means of hydroxylation and dehydration, with [14] and without [15] pentaerythritol was tested in trials under plant conditions. The investigations described in the Experimental section demonstrated that the dehydration of hydroxylated triglycerides is a method which can be applied with success to a large variety of raw materials, including various semidrying oils and shale oil.

Despite the increased production of alkyd varnishes which are now used as protective coatings, the demands of the national economy for oil coatings are not fully satisfied because of the deficiency of phthalic anhydride, which is required for many types of production.

The investigations described in this paper provide possibilities for a considerable extension of the range of raw materials required by varnish and paint factories, and offer a solution to the problem of substitutes for linseed oil in the production of anticorrosion paints, much needed in the national economy.

EXPERIMENTAL

Study of the properties of castor oil dehydrated in the presence of various catalysts. The composition of castor oil dehydrated in presence of various catalysts was studied by the formation and analysis of the ethyl esters.

Experiment 1. The oil was dehydrated in presence of 1.5% aluminum oxide and 3% zinc at 275° for 5.5 hrs to a viscosity of 8'53" by the NILK (Scientific Research Institute for Varnishes and Paints) viscosimeter. The ethyl esters obtained from this oil were distilled under a pressure of 0.326-0.4 mm Hg.

Experiment 2. The oil was dehydrated in presence of 5% gumbrin, activated by sulfuric acid, at 220-230° for 1 hr 40 min to a viscosity of 46". The ethyl esters were distilled at 0.14-0.24 mm Hg.

Experiment 3. The oil was dehydrated in presence of soluble zinc salts (0.2% of zinc in the oil) at 275° for 3 hrs 15 min to a viscosity of 2'30". The ethyl esters were distilled at 0.18-0.5 mm Hg.

The results of these experiments are presented below.

Constants of Dehydrated Oils and of the Ethyl Esters from Them

Product	Acid no. (mg KOH)	Diene no. (mg KOH)	Iodine no. (%I)	Acetyl no. (mg KOH)	Conjugate isomers of linoleic acid (%)
Oil dehydrated in presence of aluminum oxide and zinc	10.00	23.0	86.35	34.0	26.5
Ethyl esters obtained from it	11.40	25.5	—	—	29.4
Fractions:					
1st, 114-186° (yield 21.4%)	8.08	14.0	111.30	0	17.3
2nd, 186° (yield 24.1%)	9.35	25.5	110.20	24.5	31.5
3rd, 190° (yield 10.7%)	21.50	15.6	87.10	105.7	19.3
Residue (yield, 49.0%)	15.75	13.7	54.40	0	17.0
Oil dehydrated in presence of gumbrin	21.00	15.2	109	17.40	18.54
Ethyl esters obtained from it	3.34	17.7	—	11.60	21.59
Fractions:					
1st, 152—154° (yield, 17.93%)	0.95	12.5	125	0	15.25
2nd, 156—175° (yield, 36.85%)	2.61	19.4	123	2.90	23.67
3rd 175--190° (yield, 19.63%)	3.36	17.2	100	49.15	20.98
Residue (yield, 24.17%)	7.75	—	80.5	—	—
Oil dehydrated in presence of soluble zinc salts	31.8	—	91.0	12.00	—
Ethyl esters obtained from it	5.4	23.5	83.5	26.00	28.67
Fractions:					
1st, to 150° (yield, 3.9%)	9.4	7.1	—	10.43	2.26
2nd, 150—(175° (yield, 37.29%)	2.6	20.5	117.0	24.33	25.01
3rd, 175—185° (yield, 11.86%)	3.7	18.0	108.0	41.40	21.96
Residue (yield, 43.23%)	8.7	9.5	84.0	0.95	11.59

If it is assumed that saturated acids and oleic acid remain unchanged during the dehydration, the esters of the acids from the dehydrated oils should have the approximate composition given below (see following page).

The content of linoleic acid esters with conjugate double bonds was higher in castor oil dehydrated in presence of catalysts containing zinc than in castor oil dehydrated in presence of gumbrin. The activity of zinc and other metals in directing the isomerization of triglycerides toward formation of conjugated double bonds had been observed by us earlier [16].

TABLE 2

Composition of Esters Obtained from Oils Dehydrated in Presence of Various Catalyzates

Composition of esters (%)	Oil dehydrated in presence of		
	AlOH and Zn	gumbrin	soluble Zn salts
Esters of saturated acids (from literature data)	3.30	3.30	3.30
Esters of oleic acid (from literature data)	9.90	9.90	9.90
Esters of ricinoleic acid (from experimental acid)	8.37	5.66	10.28
Esters of linoleic acid (from experimental data)	34.63	54.35	27.53
Including:			
conjugate isomers (% of total esters)	13.44	15.04	12.20
isolated isomers (% of total esters)	21.19	39.31	15.33
Polymerized esters (from experimental data)	42.50	24.17	43.22
Losses (%)	1.30	2.62	5.77

With acid catalysts (such as gumbrin) the dehydration can be performed at lower temperatures than with zinc catalysts, with higher yields of intramolecular-dehydration products. One of the most effective acid catalysts is sodium bisulfate; according to our observations [10], this catalyst brings about intramolecular dehydration to yield a pale product of low viscosity, containing up to 60% linoleate radicals with conjugate double bonds, which yields hard water-resistant films, approaching tung-oil films in their properties.

In dehydration of castor oil in pilot units in presence of 2% sodium bisulfate at 230° for 30 min, and at 250° for 5 hrs 30 min, 15 kg of the oil gave 14.7 kg of product (98% yield).

Constants of oil	Before dehydration	After dehydration
Viscosity at 20°, by V_{3-4} instrument	225"	171"
Hydroxyl number	163.6	12.6
Acid number	1.5	12.6
Diene number	0	14.57

The analytical data show that highly dehydrated oil has a viscosity lower than that of the original oil; this is very important in relation to the segregation of the dehydration and polymerization processes in order to prepare a standard dehydrated castor oil. 1500 g of dehydrated castor oil was saponified to yield 1276 g of acids (94.6% yield). Vacuum distillation of 100 g of these acids at 14 mm Hg gave the following fractions; 1st, 174-228°, 4 g; 2nd, 228-230°, 44.7 g; 3rd, 230-234°, 4 g; residue 42 g.

The presence of over 50% of monomeric acids in dehydrated castor oil indicates that in the dehydration of castor oil in presence of sodium bisulfate most of the ricinoleic acid radicals are converted into linoleic acid radicals; this confirms that intramolecular dehydration occurs under these conditions. The conversion of ricinoleic acid radicals into linoleic acid radicals was proved by analysis of the 228-230° acid fraction, which was obtained in the highest yield. This fraction was found to have density 0.9021 at 20°, refractive index 1.4730 at 20°, acid number 201.5, iodine number 168.2, and diene number 14.45.

By these characteristics the isolated acid corresponds to linoleic acid [17].

The formation of a high-quality film former from castor oil dehydrated in presence of sodium bisulfate was confirmed under plant conditions. 600 kg of castor oil was dehydrated at 250° in presence of 2% sodium bisulfate for 5 hrs. The dehydrated oil had the following constants: viscosity by the NILK viscosimeter 9'11", diene number 41.5, acid number 12.7, acetyl number 32.7, saponification number 191.2.

This oil was used in the preparation of LM-15 varnish, which was used for the production of No. 63 enamel; these products were not inferior to the corresponding varnishes and enamels based on linseed and tung oils, with regard to drying, elasticity, hardness, water resistance, and weather resistance.

Drying oil made from castor oil dehydrated in presence of sodium bisulfate is superior in drying behavior and film hardness to drying oil made in the factory with the use of soluble lead catalyst.

Study of the composition of hydroxylated cottonseed oil, and dehydration of this oil. 300 g of cottonseed oil was taken for each experiment. In the second experiment 22.5 g (7.5%) of pentaerythritol was added to the oil. It was found that the hydroxylation of cotton seed oil by oxidation by means of atmospheric oxygen is more rapid in presence of pentaerythritol. The constants of oils hydroxylated in presence and in absence of pentaerythritol are given below.

Hydroxylation conditions	Oxidation time (hrs)	Hydroxyl number (Tserevitinov's method)		Diene number
Oxidation at 150° without pentaerythritol	8		3.23	10.4
The same	30	Acetyl number	34	9.7
Oxidation at 150° in presence of pentaerythritol	8		6.15	5.15
The same	30	Acetyl number	60.75	6.35

When oil is oxidized in presence of pentaerythritol, the product has a higher content of hydroxy acids, containing more hydroxyl groups, than the product formed in absence of pentaerythritol.

Isolation of free acids from 30 g of oil oxidized in presence of pentaerythritol yielded 17.6019 g of acids and 8.7112 g of unsaponifiables, while the same amount of oil oxidized in absence of pentaerythritol gave 18.2569 g of acids and 8.4077 g of unsaponifiables. In addition to these quantities of acids and unsaponifiables, saponification of the oil oxidized in presence of pentaerythritol yielded 0.9 g of a solid substance (47% on the pentaerythritol taken) which did not melt when heated to 280°, whereas the melting point of pentaerythritol is 253°. The substance was insoluble in ethyl alcohol and ether, and only slightly soluble in water. The average molecular weight of this substance, determined by the Rast method, was 268.4; this corresponds to dipentaerythritol. When the acids isolated from the oils were separated by treatment with 10-fold quantities of ligroine at 80° for 30 min, it was found that the acids isolated from oil oxidized in presence of pentaerythritol contained 24% of hydroxy acids, while the acids from oil oxidized in absence of pentaerythritol contained only 18% of hydroxy acids. The characteristics of the acid fractions isolated from the hydroxylated oils are given below.

The average molecular weights of the isolated acids are close to the calculated molecular weight of oleic acid and its hydroxy derivatives; this shows that the oil is hydroxylated without a side reaction of oxidation leading to scission of the molecules. This is confirmed by the saponification and acid numbers.

Constants of Acid Fractions Isolated from Oils Oxidized with and Without Pentaerythritol

	Acid fraction	Acid number	Saponification number	Acetyl number	Molecular weight
Oil oxidized w/o pentaerythritol	Insoluble in ligroine	133.25	289.85	120.25	215
The same	Soluble in ligroine	146.4	218.85	29.55	257
Oil oxidized in presence of pentaerythritol	Insoluble in ligroine	96.45	205	157	197.9
The same	Soluble in ligroine	122.35	240.55	2.65	249.3

TABLE 1

Hydroxylation of Cottonseed Oil at Various Stages of Oxidation with and Without Pentaerythritol

Characteristics	Raw oil	Samples oxidized with pentaerythritol					Oil oxidized w/o pentaerythritol
		1	2	3	4	5	
Oxidation time (hours)	-	8	30	43.5	56	68	62
Viscosity by the NILK funnel method (seconds)	3.7	9.1	35	81	85	361	360
Amount of undissolved pentaerythritol (%)	—	20	12	5	0	0	—
Acid number	1.2	3.2	5.2	10.6	10.9	6.7	6.7
Saponification no.	181.6	187.0	201.5	212.6	213.9	283.1	212.6
Acetyl number	8.1	43.8	36.1	113.1	133.0	120.7	72.3
Carbonyl number	0	20.8	12.9	12.9	7.3	2.2	0
Iodine number	108.2	74.6	67.5	64.0	66.7	63.0	66.9
Diene number	0.01	24.6	23.6	19.3	19.4	15.9	—
Molecular weight	886.0	685.1	738.4	632.9	542.2	503.0	916.5
Hydroxy-acid content (%)	0	2.6	10.45	21.8	21.8	29.2	31.5

More detailed investigations of cottonseed oil oxidized at 150° in presence of 7.5% pentaerythritol (Table 1) indicate that the hydroxyl groups are formed in the acid radicals of the oil triglycerides, as their content increases appreciably after the pentaerythritol has reacted, and not as the reaction with the latter proceeds. The decrease of the carbonyl group content during oxidation of the oil in presence of pentaerythritol indicates that the penta-

TABLE 2

Changes in the Constants of Oleic Acid During Oxidation and Heating of the Oxidation Products

Acid	Constants				
	hydroxyl number	acid number	carbonyl number	peroxide number	epoxide number
Oleic acid oxidized for:					
60 hrs . .	72.5	174	64.2	0.24	2.61
120 hrs . .	98.0	185.3	59	0.14	0
60 hrs, and heated . . .	—	168	18.75	0.061	0

erythritol or hydroxylic compounds in the oil react with carbonyl groups, or with α-oxide groups which are isomeric with the latter. The interaction of α-oxides with compounds containing alcohol groups has been reported in the literature [18, 19]. We also observed such interaction in compounds containing α-oxide groups, formed by the oxidation of oleic acid by atmospheric oxygen at 75°. It follows from the constants given in Table 2 that the hydroxyl and acid numbers of oleic acid increase during oxidation continued for more than 60 hrs. This is accompanied by decreases in the carbonyl and peroxide group contents, and complete disappearance of epoxy groups. The same is found if the oxidation products of oleic acid are heated at 144° for 50 hrs.

The changes in the constants of oleic acid during oxidation, and when the oxidation products are heated, indicate that secondary reactions take place, with interaction of the oxygen-containing groups, which leads to increases of the molecular weight of the oxidation products. Thus, the molecular weight of oleic acid is 172, after oxidation for 60 hrs it becomes 1336, and after oxidation for 120 hrs, 2518. The increase of the molecular weight of the oxidation products of oleic acid suggests that the side reactions accompanying oxidation are polymerization and condensation, the same processes as in film formation, and therefore they may increase the film-forming power of semidrying oils during chemical conversion by means of hydroxylation and dehydration. This was confirmed by the results of tests of the quality of film formers obtained from cottonseed oil by hydroxylation and dehydration in experimental plant. 7 kg of cottonseed oil, 0.176 kd each of lead and manganese resinates, 0.175 kg of ester gum, and 0.525 kg of pentaerythritol was taken for the experiment. Oxidation of the oil for 30 hrs gave 7.891 kg of product (yield 98.03%). This hydroxylated oil was dehydrated at 250° in presence of 2% sodium bisulfate for 4 hrs. The hydroxylated and dehydrated oils had the following constants.

	Hydroxylated	Dehydrated
Viscosity by the NILK funnel test	6'20"	10'15"
Acid number	7.0	7.3
Saponification number	221	227.6
Acetyl number	128.4	16.3

The drying oil made from the dehydration product dried tack-free in 7.5 hrs and completely in 24 hrs, forming a film with 55" hardness by the pendulum test, 5 days after drying. A ferric oxide paint made with this oil gave the same results as a ferric oxide paint with natural drying oil when tested in the weatherometer (rating 6 after 240 hrs). Roof tests of paints based on this oil gave the following results, expressed in arbitrary ratings.

	With cottonseed drying oil	With natural drying oil
Red iron oxide after 20 months	6	3
Green after 35 months	5	6
Ocher after 45 months	4	4

It is seen that points based on cottonseed drying oil prepared by hydroxylation and dehydration are not inferior to paints based on linseed drying oil.

Weather-resistant paints were also made from cottonseed oil treated in experimental units by dehydration of hydroxylated cottonseed oil after preliminary vinylation. 700 g of cottonseed oil, oxidized at 140° for 33 hrs 10 min, was vinylated at 160° in presence of 14 g of zinc oxide for 12 hrs, by means of a current of acetylene fed from a cylinder at 0.2-1 atmos; 200 g of the vinylated oil was heated at 150° for 4 hrs, 190 g of product (yield 95%) being obtained. The vinylated oxidized oil had the following hydroxyl numbers before and after dehydration and polymerization: oxidized, 57.3; oxidized and then vinylated, 43.0; oxidized, and then vinylated and dehydrated, 33.35.

The dehydrated drying oil dried in 24 hrs. The mechanical properties of these films before and after ageing for 120 hrs at 60° were high: bend strength 1 mm; test in press E, 7.0 mm; impact strength 50 kg/cm. Films of a red iron oxide paint based on this oil also had good mechanical properties: bend strength 1 mm, press E 6.5 mm, and impact strength 50 kg/cm. Tests of paint films in the weathering apparatus for 475 hrs gave a rating of 8.

The results obtained in the studies of hydroxylation and dehydration, and of the copolymerization of semidrying oils with tung oil and the production of drying oils from them [20], were used to develop, jointly with L. T. Sosnos, a formulation and procedure for the preparation of a cottonseed–tung drying oil. Cottonseed and tung oils were taken in 7:3 ratio. The following procedure was used: cottonseed oil was oxidized at 80-145° for 9 hrs 45 min to relative viscosity 9.5 (the viscosity of the raw oil being taken as unity); the oxidized oil was dehydrated at 255-260° in presence of lead drier, corresponding to 0.05% lead in the oil, to relative vicsocity 62.2; this was followed by copolymerization with tung oil at 200-210° to relative viscosity 120. The drying oil made from the product had the following characteristics: viscosity (in °E) 7.0, color 489 on the iodometric scale, drying time 5 hrs, cross-linked polymer content of film 46.6%, elasticity on the NILK scale 1 mm, film hardness by the pendulum test 97", no change after exposure to water for 6 hrs, abrasion resistance of film (13-15 mm) by the GIPI-4 instrument 1400.

The method for the production of this drying oil was tested under plant conditions and adopted for production.

Study of the properties of films from various semidrying oils after hydroxylation and dehydration. In view of the fact that sunflower, maize, and other oils of the poppyseed oil group have a somewhat higher tendency to film formation than oils of the olive oil group, which includes cottonseed, rapeseed, and other oils, we processed sunflower and maize oils in absence of pentaerythritol, and cottonseed and rapeseed oil in presence of pentaerythritol. The sunflower and maize oils were hydroxylated by oxidation at 145-150° in presence of 5% lead and manganese resinates, and then dehydrated at 245-250° in presence of 2% sodium bisulfate. Cottonseed and rapeseed oils were hydroxylated under the same conditions, but 7.5% of pentaerythritol and 2.5% of ester gum were added before the oxidation.

Whereas the raw semidrying oils did not dry for more than 3 days and eventually yielded tacky soft films, the processed oils dried tack-free within less than 12 hours, and completely in 24 hours. Comparative tests on films from the processed oils and from the same raw oils showed that films from raw cottonseed, maize, and rapeseed oils melted below 100°, whereas films from all the processed oils showed no signs of melting when heated above 100° to charring point, as was the case with films from linseed oil. The solubilities in white spirit of films made from the processed semidrying oils were similar to the solubility of linseed-oil films; the results of 2-hr solubility tests are given below.

Oil used as film former	Substances insoluble in white spirit in the film (%)
Raw cottonseed	53.5
Processed cottonseed	82.5
Raw rapeseed	12.4
Processed rapeseed	73.0
Raw sunflower	89.9
Processed sunflower	90.5
Raw maize	75.3
Processed maize	82.0
Polymerized linseed	100.0

The hydroxylated and dehydrated oils form films with high contents of cross-linked polymers.

The hardness, elasticity, resistance to high temperatures and ultraviolet light, and other properties of drying oils and paints based on processed semidrying oils proved to be similar to the corresponding characteristics of films and paints based on polymerized linseed oil.

Use of the hydroxylation and dehydration method for the production of film formers from shale oil. It is known that shale oil does not dry unless specially treated. We worked out a procedure for the production of drying shale oil by means of hydroxylation and dehydration.

The oil was oxidized at 140-145°, in presence of 3% of a catalyst consisting of the inorganic portion of the shale, for 5.5 hrs (yield 92%); the oil was then dehydrated at 240-250° with an additional 3% of catalyst (yield 54.5%).

	Raw	Oxidized	Dehydrated
Acid number	4.75	13.5	9.9
Saponification number	99.7	60.0	71.1
Iodine number	132.0	97.3	109.8
Acetyl number	48.0	99.3	30.4

The dehydration of hydroxylated shale oil is confirmed by the decrease of the acetyl and the increase of the iodine number.

Drying oil made from the dehydrated shale oil dried tack-free in 20 min; paints based on this oil dried completely in 24 hrs. The oil and paint films were harder than films from linseed oil and paints based on it. The elasticity of paint films containing shale oil was improved by the addition of 3% of a plasticizer (polymerized castor or other oil), which has a weather resistance of about 2 years, to the paint.

The results of laboratory work on the production of a drying oil from shale oil were confirmed by trials in GIPI-4 experimental units and under production conditions [21].

Following prolonged trials, shale drying oil and paints based on it are now being made under plant conditions.

SUMMARY

1. It is shown that the side reactions which take place in the proposed method for the production of film formers from semidrying oils improve the film-forming properties of the oils.

2. Conditions have been found for intramolecular dehydration of nondrying castor oil in presence of sodium bisulfate whereby it is possible to segregate the dehydration and polymerization processes; this is very important for regulation of the dehydration process in the production of a dehydrated oil of standard quality.

3. It is shown that addition of small amounts of pentaerythritol in the dehydration of badly-drying hydroxylated oils makes it possible to obtain hard films from such oils.

4. The strength of films from semidrying oils can also be increased by dehydration of hydroxylated triglycerides after preliminary vinylation by means of acetylene.

5. The hydroxylation and dehydration process is applicable to various types of semidrying oils (cottonseed, maize, rapeseed, etc.) and to shale oil.

6. The hydroxylation and dehydration process for the treatment of semidrying oils and shale oil has been tested under plant conditions and adopted in production.

LITERATURE CITED

[1] A. A. Ivanova, Bull. Exchange of Experience in the Varnish and Paint Ind. 11-12, 49 (1937).

[2] A. A. Ivanova, J. Appl. Chem. 11, 3, 564 (1938).

[3] A. A. Ivanova, J. Appl. Chem. 28, 7, 718 (1955).*

[4] V. V. Korshak, Chemistry of High Polymers (Izd. AN SSSR, Moscow-Leningrad, 1950), pp. 413-414, 228-229.

[5] V. S. Kiselev, Drying Oils and Varnishes (1940).**

[6] A. Ia. Drinberg, Technology of Film Formers (Goskhimizdat, 1955), pp. 157, 169.

[7] A. A. Zinov'ev, Chemistry of Fats (Food Industry Press, Moscow, 1952), p. 450.

[8] A. A. Ivanova and D. N. Bogoslovskii, Bull. Exchange of Experience in the Varnish and Paint Ind. 11-12, 38 (1937); 4, 11 and 8, 18 (1939).

[9] A. A. Ivanova and M. G. Buman, Org. Chem. Ind. 6, 320 (1940).

* In Russian.

** Original Russian pagination. See C. B. translation.

[10] A. A. Ivanova and A. I. Bespalko, J. Chem. Ind. 12, 11 (1945).

[11] V. V. Korshak and A. A. Ivanova, J. Appl. Chem. 28, 5, 523 (1955).*

[12] A. Ia. Drinberg and A. A. Ivanova, Authors' Certificate cl. 22, No. 71388 (1947).

[13] A. A. Ivanova and A. I. Bespalko, Authors' Certificiate cl. 22, No. 71623 (1947).

[14] A. A. Ivanova, Bull. Exchange of Experience in the Varnish and Paint Ind. 5, 20 and 10, 17 (1939).

[15] A. A. Ivanova, Oil and Fat Ind. 5, 22 (1954).

[16] A. A. Ivanova and A. S. Petrova, J. Chem. Ind. 8, 240 (1947).

[17] Beilst. 2, 496.

[18] A. A. Petrov, B. V. Gantseva, and O. A. Kiseleva, J. Gen. Chem. 23, 4, 737 (1953).*

[19] V. V. Korshak and A. A. Ivanova, J. Gen. Chem. 27, 3, 590 (1957).*

[20] A. A. Ivanova and T. I. Galitsinskaia, Technical Information in the Varnish and Paint Industry 1, 13 (1941).

[21] A. A. Ivanova and A. I. Bespalko, Bull. Exchange of Experience in the Varnish and Paint Ind. 4, 22 (1953).

Received October 25, 1956

* Original Russian pagination. See C. B. translation.

DETERMINATION OF ALKALOIDS IN EPHEDRA BY DISTILLATION IN SUPERHEATED STEAM

M. I. Goriaev, R. N. Sazonova, and I. M. Shabanov

Two versions of a method for the quantitative determination of total alkaloids in ephedra are described in this paper. The existing methods for the quantitative determination of alkaloids in this plant are not sufficiently accurate, require large amounts of solvents and are time-consuming; this gives rise to considerable difficulties in production control.

In illustration, we may cite the standard method for determination of total alkaloids in ephedra [1]. 40 g of ephedra (shredded to a fine powder) is weighed to the nearest 0.01 g, put into a 1 liter flask, 400 ml of 1% H_2SO_4 solution is added, and the mixture is shaken mechanically for 2-3 hrs; the mixture is allowed to settle thoroughly for 10-15 hrs, and then filtered through a fluted filter into a 500 ml flask. 150-200 ml of the filtrate is taken and NaCl is added to it to complete saturation. The filtrate is then transferred to a separating funnel, 15-20 ml of 30% NaOH solution is added, and the alkaloids are extracted stepwise in 30-40 ml portions of ether to a negative reaction for alkaloids (tested by Mayer's reagent).

The ether extracts are dried over anhydrous Na_2SO_4, filtered, the filter is washed twice with ether, and the ether is distilled off on the water bath almost to dryness (about 3 ml is left). Excess (40 ml) of 0.1 N HCl is added to the residue from the ether extract, residual ether is removed on the water bath, the solution is cooled, methyl orange indicator is added, and excess acid is titrated with 0.1 N NaOH.

The alkaloid content of the whole sample is found from the amount present in an aliquot portion, and calculated as a percentage. The analyst usually takes two days to complete the determination of alkaloids in one sample by this method. The amount of ether required for one sample is about 400 ml in winter, and over 500 ml in summer; unrecovered losses of ether per sample are 200 and 300 ml, respectively. In the summer, at temperatures above 25°, it is almost impossible to use this method.

Our two proposed versions of a method for alkaloid determination are quite independent of the degree of shredding. If the material is macerated during distillation with superheated steam, shredded and unshredded samples give identical quantitative results (Tables 1 and 2). This point is particularly stressed, as one of several causes of error in the determination of alkaloids by the standard method is insufficient shredding of the material.

We shall not discuss the various modifications of methods for the extraction of alkaloids which have been proposed [2-4], but must point out that all these methods are lengthy and involve the use of solvents. Our two proposed versions of a method based on distillation of alkaloids in steam are not new in principle. Several alkaloids, including the nicotine group and some others, distill in steam without decomposition [5-7]. Dalal and Khorana [3, 4] described a method for the quantitative determination of ephedra alkaloids by steam distillation, after preliminary solvent extraction of total bases from the plant. In brief, the procedure is as follows. 20 g of the shredded plant material is ground with 4 g of lime and wetted with benzene (200 ml); after 10 minutes 20 ml of 10% ammonia is added, the mixture is stirred for 3 hrs, left overnight, and then exhaustively extracted with benzene in a percolator. The clear benzene solution is washed with saturated NaCl solution (to remove NH_4OH). The NaCl solution is then washed with benzene, and the latter is added to the main benzene extract; 25 ml of 1% H_2SO_4 solution is added, and the benzene is distilled off. The colored substances which separate out are filtered off and washed; the acid solution is neutralized, made alkaline with 200 ml of 5% NaOH, saturated with NaCl, and the alkaloids are distilled in steam into a receiver containing 0.1 N H_2SO_4. The excess acid is titrated by 0.1 N NaOH (against methyl red). The method is very lengthy and complicated.

TABLE 1

Effect of the Amount of Distillate on the Alkaloid Content of the Ammoniacal Distillate

Source of ephedra	Moisture content (%)	Alkaloid content by standard method (%)	Alkaloid cont., distillation with superheated steam (%)			Amount of distillate (ml)			Alkaloid cont. of 1 ml of ammonical distillate (mg)	Ammonia cont. of 1 ml of ammonical distillate (mg)	Notes
			in main distillate	in ammoniacal distillate	total	basic	ammoniacal	total			
Mountain ephedra. Panfilovskii region. Taldy-Kurgan province	10.76	1.93	1.68	0.48	2.16	260	1300	1560	0.036	0.014	Sample shredded
	10.76	—	1.84	0.31	2.15	450	1100	1550	0.028	0.016	
	10.76	—	1.72	0.31	2.03	420	1200	1620	0.026	0.014	
Mountain ephedra. Aksu region, Taldy-Kurgan province	13.84	2.46	1.89	0.44	2.33	375	1200	1575	0.036	0.014	Sample not shredded
	13.84	—	2.00	0.44	2.44	440	1400	1840	0.031	0.011	
	13.84	—	2.00	0.36	2.36	550	1300	1850	0.028	0.012	
	13.84	—	1.84	0.50	2.34	500	1300	1800	0.038	0.008	
	13.84	—	1.89	0.45	2.34	500	1300	1800	0.034	0.009	
Mountain ephedra. Kugalinskii region, Taldy-Kurgan province	7.76	2.80	2.45	0.38	2.83	500	1300	1800	0.030	0.010	Sample shredded
	7.76	—	2.28	0.34	2.62	500	1000	1500	0.034	0.013	
	7.76	—	2.30	0.45	2.75	500	1300	1800	0.034	0.011	
	7.76	—	2.31	0.44	2.75	500	1000	1500	0.044	0.014	

TABLE 2

Quantitative Determination of Alkaloids in Ephedra by the Second Version of the Method (Without Solvent)

Sample no.	Source of ephedra	Moisture content (%)	Alkaloid content (%)		Amount of distillate (ml)			Notes
			by standard method	by 2nd version of method	basic	ammoniacal	total	
1	Mountain ephedra. Kugalinskii region, Taldy-Kurgan province	7.76	2.80	2.69	500	1000	1500	One determination by standard method; sample shredded
		7.76	—	2.66	500	1000	1500	
		7.76	—	2.69	500	1300	1800	
		7.76	—	2.70	500	1000	1500	
5	Mountain ephedra. Sarkandskii region, Taldy-Kurgan province	4.99	1.67	1.72	500	1000	1500	One determination by standard method; sample shredded
		4.99	—	1.70	500	1000	1500	
7	Mountain ephedra. Sarkandskii region, Taldy-Kurgan province	8.14	2.05	2.15	500	1000	1500	
		8.14	—	2.11	500	1000	1500	

TABLE 2 (continued)

Sample no.	Source of ephedra	Moisture content (%)	Alkaloid content (%) by standard method	Alkaloid content (%) by 2nd version of method	Amount of distillate (ml) basic	Amount of distillate (ml) ammoniacal	Amount of distillate (ml) total	Notes
9	Mountain ephedra. Krasnogorskii, Dzhambul province	4.99	1.30	1.79	500	1000	1500	Sample shredded
		1.99	1.86	1.78	500	1000	1500	Sample not shredded
		4.99	1.76	1.79	500	1000	1500	
12	Mountain ephedra. Sarkandskii region, Taldy-Kurgan province	7.05	1.58	1.99	500	1000	1500	Sample shredded
		7.05	1.51	1.96	500	1000	1500	
		7.05	—	2.08	500	1000	1500	
15	Mountain ephedra. Sarkandskii region, Taldy-Kurgan province	5.66	1.29	1.65	500	1000	1500	
		5.66	1.33	1.70	500	1000	1500	
17	Mountain ephedra. Kugalinskii region, Taldy-Kurgan province	7.0	2.35	2.49	500	1000	1500	One determination by standard method; sample shredded
		7.0	—	2.56	500	1000	1500	
19	Mountain ephedra. Krasnogorskii region, Dzhambul province	6.95	1.84	2.02	500	1000	1500	
		6.95	—	2.15	500	1000	1500	

We found that when ordinary steam, not superheated, is used for the distillation, a mixture of ephedrine and pseudoephedrine is not distilled over completely even after a long time (6-8 hrs). Considerable amounts of liquid accumulate in the flask during the steam distillation, so that even if the flask is heated the distillation is prolonged.

We found that if superheated steam (at 127-142°) is used, ephedra alkaloids distill over fairly rapidly and quantitatively.

Ephedrine. 0.902 g of ephedrine was taken for the distillation with superheated steam. Distillate samples were taken at 15-min intervals and ephedrine was determined in them by titration with 0.1 H_2SO_4. The amount of alkaloid found was 0.919 g (101.8%); the steam temperature in the distillation was 127-142°. The distillation rate of ephedrine is plotted in Fig. 1.

Pseudoephedrine distills over less rapidly than ephedrine under the same conditions. 1 g of pure pseudoephedrine hydrochloride, equivalent to 0.8192 g of pseudoephedrine, was put in a Kjeldahl flask, followed by 2 g of NaOH, 4 g of NaCl, and 10-15 ml of water. The pseudophedrine in the distillate was determined, as before, by titration with 0.1 N H_2SO_4; 0.7948 g (97.0%) of pseudoephedrine was found. The distillation time was 120 min. The distillation rate of pseudoephedrine is plotted in Fig. 2.

In a duplicate experiment 0.7057 g of pseudoephedrine was taken; the amount found after distillation with superheated steam (by titration with 0.1 N H_2SO_4) was 0.71445 g (101.2%). Methyl red was used as indicator in all cases. The distillation time was 90 min.

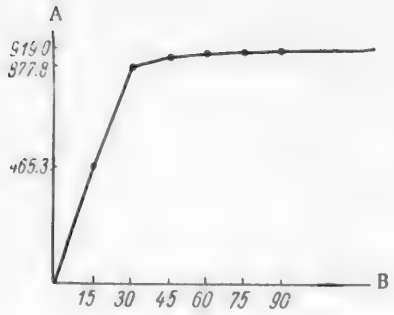

Fig. 1. Distillation rate of ephedrine. A) Amount of ephedrine distilled in steam (mg), B) distillation time (minutes).

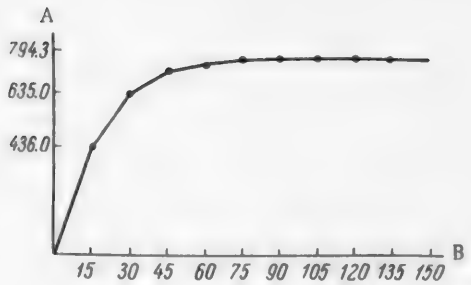

Fig. 2. Distillation rate of pseudoephedrine. A) Amount of pseudoephedrine distilled in steam (mg), B) distillation time (minutes).

Quantitative determination of total alkaloids in ephedra, with the use of a solvent (1st version). The main difficulty in the distillation of alkaloids from ephedra in superheated steam is that ammonia distills over with ephedrine and pseudoephedrine; like the alkaloids, the ammonia is titrated by any organic or mineral acid.

TABLE 3

Alkaloid Contents of Ephedra, Determined by the 1st Version of the Method

Source of ephedra	Moisture content (%)	Alkaloid contents by standard method (%)	Alkaloid contents by 1st version of method (%)	Amount of distillate (ml)	Notes
Mountain ephedra	Air dry	2.61	2.61	2100	Shredded material; without infusion in NaOH. One determination by the standard method
		—	2.65	2420	Same conditions
		—	2.61	2305	Infusion in NaOH for 24 hrs. Shredded material.
		—	2.62	2080	Shredded material; without infusion in NaOH
		—	2.72	2350	
		2.93	3.06	1700	
		1.72	1.61	2300	
		1.63	1.52	1940	
		1.29	1.40	1720	
		—	1.40	1890	
		—	1.38	1700	
Mountain ephedra. Panfilovskii region	10.76	1.93	2.05	1840	Material not shredded; without infusion in NaOH
		—	1.93	2050	Shredded material; without infusion in NaOH
		—	2.00	1550	
		—	1.82	1620	
Mountain ephedra. Aksu region	13.84	2.46	2.28	1840	Material not shredded; without infusion in NaOH
Mountain ephedra. Kugalinskii region	7.76	2.80	2.83	1800	Shredded material; without infusion in NaOH
		—	2.75	1800	
		—	2.75	1500	

Ammonia is usually present in plants in the form of salts of organic acids. The action of caustic alkalies also splits off amide nitrogen in the form of ammonia. Free ammonia is found in plant materials only after putrefaction and fermentation [8-10].

The usual methods for quantitative determination of ammonia [10-12] were of no value for our investigation, as ammonia derived from amide nitrogen is also liberated from ephedra in steam distillation in presence of caustic alkalies. The total ammonia (i. e., from organic salts and amide nitrogen) was found from the difference between total bases and total alkaloids. The determination of alkaloids was performed as follows. 10 g of finely shredded ephedra material was placed in a 1 liter Kjeldahl flask. (Our experiments showed that the same results are obtained by analysis of shredded or unshredded material. We used shredded material in order to have samples of similar weight in duplicate experiments.) 4 g of NaCl, 20 ml of 10% NaOH (or 2 g of dry NaOH) and 20 ml of water were then added. The flask was shaken slightly to ensure uniform wetting of the dry material, and a brass tube (5 mm in diameter) reaching to the bottom of the flask was then inserted. The external part of the tube was in the shape of a flat coil which was placed on an electric hot plate and covered with small sheets of asbestos. The outer end of the tube was connected to the steam generator by means of rubber tubing. A thermometer for measurement of the steam temperature, and a bent glass tube or a spray trap, for passing the steam through a Liebig condenser, were inserted into the rubber bung through which the brass tube passed. The receiver was an ordinary conical flask, 2.5-3 liters in capacity.

The distillation of alkaloids and ammonia was usually continued for 3-3.5 hrs, the steam temperature being 127° at the start and 142° at the end.

The amount of distillate collected during this time is 1500-1800 ml, which is quite sufficient even with 3.0-3.1% alkaloids in the ephedra. To the distillate, containing alkaloids and ammonia, a slight excess of 0.1 N H_2SO_4 (by methyl red) was added, and the excess water was evaporated off in a porcelain basin on a water bath to a volume of 10-20 ml, or distilled from the flask on a hot plate to a volume of 500 ml, and then evaporated from a porcelain basin on a water bath to 10-20 ml. NaCl was added to the residue, to complete saturation, followed by 15-20 ml of 30% NaOH, and all the contents of the basin were quantitatively transferred (by rinsing with water) into a separating funnel. The alkaloids were extracted in ether, and the subsequent procedure was the same as in the standard method.

The percentage total alkaloids (x) in the sample was calculated from the formula

$$x = (v_1 - v_2) \cdot 0.165$$

or, on the bone-dry weight of the sample

$$x = \frac{(v_1 - v_2) \cdot 16.5}{(100 - a)},$$

where v_1 is the volume of exactly 0.1 N H_2SO_4 solution (in ml), v_2 is the volume of exactly 0.1 N NaOH solution used for titration of the excess H_2SO_4 (in ml); a is the moisture content of the sample (%).

Several determinations can be performed simultaneously by this method, and the amount of ether required for the extraction of alkaloids is relatively small (about 150 ml). Table 3 gives the alkaloid contents of ephedra found by this method and by the standard method at present in use in chemical and pharmaceutical factories and warehouses.

In the quantitative determination of alkaloids by this version of the method, alkaloids and ammonia may be distilled into excess of standard 0.1 N H_2SO_4 solution, but this has no advantages over the ordinary distillation procedure.

Quantitative determination of total alkaloids in ephedra, without use of solvent (2nd version). It was pointed out earlier that when ephedra material is treated with alkalies and steam, the alkaloids are distilled together with ammonia. Redistillation of the distillate showed that at first ammonia and part of the alkaloids distill over, and subsequently the alkaloids only. It was found in numerous experiments that as a rule all the ammonia distills with the first 900 ml of distillate.

This may be illustrated by the data in Table 4 on the distillation of the first portions of the distillate (100 ml each) obtained by the usual method, described above, from ephedra containing 1.44% alkaloids (see also Table 1).

TABLE 4

Contents of Ammonia and Alkaloids in the First Portions of Distillate (100 ml taken from each portion)

Portion no.	ml of 0.1N H_2SO_4 taken for titration			Found (in mg)	
	total	ammonia	alkaloids	ammonia	alkaloids
1	3.1	2.996	0.104	5.09	1.72
2	2.3	2.196	0.104	3.73	1.72
3	1.5	1.396	0.104	2.37	1.72
4	1.05	0.946	0.104	1.61	1.72
5	0.6	0.496	0.104	0.84	1.72
6	0.5	0.396	0.104	0.67	1.72
7	0.3	0.196	0.104	0.33	1.72
8	0.2	0.100	0.100	0.17	1.65
	9.55	8.722	0.828	14.81	13.69

It follows from the data in Table 4 that the first 600 ml still contain ammonia, in the 7th portion (100 ml) ammonia may still be detected, while it is almost absent from the 8th portion (0.00017%).

After neutralization of all the ammoniacal distillate with 0.1 N H_2SO_4, the alkaloid content was found to be 13.69 mg. Since (according to average results) the alkaloids distill over uniformly, the amounts of alkaloids and ammonia in each 100 ml of distillate can be calculated; this is also shown by the data in Table 4.

It is clear from the foregoing that if the alkaloid content of 1 ml of ammoniacal distillate from ephedra containing from 1.5 to 3% alkaloids is determined, the total alkaloids content of the ephedra can be found from the result, without the use of a solvent. For determination of the alkaloid contents of the ammoniacal distillates, numerous experiments were performed with ephedra samples with different alkaloid contents; it was found that if the total alkaloid content of the ephedra is between 1.5 and 3% (on the bone-dry material), 1 ml of the ammoniacal distillate has the following distillate contents:

Basic distillate (ml)	Ammoniacal distillate (ml)	Alkaloid content of 1 ml of ammoniacal distillate (in mg)
800	700	0.0200
750	750	0.0225
700	800	0.0250
650	850	0.0275
600	900	0.0300
550	950	0.0325
500	1000	0.0350
500	1300	0.0350

These figures are valid if the total distillate volume is 1500-1800 ml.

It follows from the data in Table 1 that, if experimental error is taken into account, fluctuations of distillate volume (basic distillate between 260 and 550 ml, and ammoniacal distillate between 1000 and 1400 ml) do not greatly influence the total alkaloids in the ammoniacal distillate. To avoid possible error, it is best to keep to the same amounts of the total distillate and of the basic and ammoniacal distillates in the analysis.

A total distillate volume of 1500 ml, including 500 ml of basic and 1000 ml of ammoniacal distillate, may be regarded as the optimum.

Determination of alkaloids by the 2nd version. 10 g of shredded or unshredded ephedra, 4 g of NaCl, 20 ml of 10% NaOH, and 20 ml of water were put into a Kjeldahl flask 1 liter in capacity. The same conditions and apparatus were used as those described for the 1st version of the method. Superheated steam (at 127-142°)

was passed through the liquid for 3-3.5 hrs, 1500 ml of distillate being collected. 1000 ml of ammoniacal distillate was distilled out of the receiver flask, and the residual liquid (500 ml) was titrated with 0.1 N H_2SO_4 in the usual way. Alternatively, excess acid may be added and then titrated with 0.1 N NaOH.

The following conditions must be observed. Large amounts of liquid must not be allowed to accumulate in the distillation flask (not more than 200 ml). The flask must be wrapped in a towel if this should occur. The average temperature of the steam must be in the 127-142° range. The distillation should be uninterrupted as far as possible.

If all the liquid evaporates from the distillation flask, the hot plate heating the coil must be switched off for a while, and switched on again when enough condensate (50-100 ml) has collected in the flask.

The percentage alkaloid content (x), found in this case for 1500 ml of the total distillate, is calculated from the formula:

$$x = (v_1 - v_2)\,0.165 + 0.35$$

or, on the bone-dry material

$$x = \frac{(v_1 - v_2)\,16.5 + 35}{(100 - a)},$$

where v_1 is the volume of 0.1 N H_2SO_4 solution (ml), v_2 is the volume of 0.1 N NaOH solution used for titration of excess H_2SO_4 (ml); a is the moisture content of the sample (%).

Example. A 10 g sample of ephedra, containing 10% moisture, was taken, 11 ml of 0.1 N H_2SO_4 was added to the basic distillate (500 ml); 2 ml of 0.1 N NaOH solution was required for the back titration.

The first formula is used to find the alkaloid content of the sample (calculated on the air-dry material) $x = (11 - 2) \cdot 0.165 + 0.35 = 9 \cdot 0.165 = 1.485 + 0.35 = 1.835\%$, or the second formula is used to find the content on the bone-dry material

$$x = \frac{(11 - 2) \cdot 16.5 + 35}{(100 - 10)} = \frac{148.5 + 35}{90} = \frac{183.5}{90} = 2.04\%.$$

TABLE 5

Comparison of the Alkaloid Contents of Ephedra as Determined by the Standard Method and Versions 1 and 2 of Our Method

Sample no.	Source of ephedra	Moisture (%)	Alkaloid contents (%) determined by		
			standard method	1st version	2nd version
15	Mountain ephedra, Sarkandskii region, Taldy-Kurgan province	5.66	1.29	1.48	1.65
		5.66	1.33	1.49	1.70
12	The same	7.05	1.58	1.72	1.99
		7.05	1.51	—	1.96
		7.05	1.51	—	2.08
9	«	4.99	1.30	1.59	1.79
		4.99	1.36	—	1.78
		4.99	1.76	—	1.79
19	Mountain ephedra, Krasnogorskii region, Dzhambul province	6.95	1.84	1.83	2.02
		6.95	1.84	—	2.15

If 1800 ml of distillate is obtained (500 ml of basic and 1300 ml of ammoniacal), the first formula, for the air-dry sample, takes the form: $x = (v_1 - v_2) \cdot 0.165 + (1300 \cdot 0.0350) = (v_1 - v_2) \cdot 0.165 + 0.455$; for a bone-dry sample, we have $x = \frac{(v_1 - v_2) \cdot 16.5 + 45.5}{(100 - a)}$.

Results obtained by this and the standard method are compared in Table 2.

To determine the reason for the differences between the results found by the standard method and by the 2nd version of our method for Samples 9, 12, 15 and 19 (in duplicate determinations), the total alkaloids were determined by the 1st version of the method, i. e., by steam distillation of the alkaloids followed by ether extraction. It was found that these samples had considerably higher alkaloid contents than were found by the standard method (Table 5), with the exception of Sample 19, where there was no difference between the results of the standard method and the 1st version of our method.

As Table 3 shows, the standard method and the 1st version of our method give results in good agreement in quantitative determinations of ephedra alkaloids, but the results given by the 2nd version of our method apparently always differ from the results of these two methods.

These discrepancies are due to the following causes: incomplete extraction of the ephedra alkaloids by 1% sulfuric acid solution in the standard method; losses in ether extraction, which become relatively greater with decrease of the alkaloid content of the ephedra.

It is quite evident that the results given by the standard method and by the 1st version of our method can approach the results given by the 2nd version only after thorough and repeated extraction of alkaloids from ephedra. Apart from the usual small experimental errors, the 2nd version gives an almost theoretical result for the total alkaloid content of ephedra.

The advantages of the 2nd version of our method are speed and accuracy, and the fact that no solvent is needed. With suitably organized apparatus, several determinations can be performed simultaneously without overloading the analyst with work, and material of any degree of shredding can be used, whereas very fine shredding is required for determination of alkaloids by the standard method.

Another important disadvantage of the standard method is that the analyst cannot check the completeness of extraction of the alkaloids from ephedra. The Mayer reaction only indicates the degree of extraction of alkaloids from the solvent by means of ether, but not the degree of extraction by the solvent from the plant material.

SUMMARY

1. It is shown that the proposed methods of alkaloid determination are more rapid and accurate than the standard method. Shredding of the plant material is not essential; shredding does not affect the analytical results provided that a homogeneous mixture is obtained.

2. Mass analyses could be accelerated at least two-fold by the adoption of the new method for determination of ephedra alkaloids as a standard method (after approval by the laboratories concerned).

3. The new method can also be used for the analysis of preparations containing ephedrine, provided that other volatile bases (alkaloids, amines, ammonia, etc.) are absent.

4. Because of the relative simplicity of the proposed method, it can be used under field conditions for determinations of total alkaloids in ephedra stocks. The main difficulty at present is that ether must be used, with a very serous fire risk in transport.

In conclusion, the authors thank A. G. Polianskaia, head of the laboratory of the "Lekrastrest" Republican Office, who helped in the development of the new method.

LITERATURE CITED

[1] Technical Medicinal Raw Materials (State Standards Press, 1948).*

[2] O. F. Black and J. W. Kelly, Am. J. Pharmacy 99, 12, 748-51 (1927).

[3] V. D. Dalal and M. L. Khorana, Indian J. Pharmacy 15, 2, 23-24 (1953).

* In Russian.

[4] V. D. Dalal and M. L. Khorana, Referat. Zhur. Khim. 5, 14 (1954).

[5] A. P. Orekhov, Alkaloid Chemistry (Izd. AN SSSR, Moscow, 1955).*

[6] T. A. Henry, The Plant Alkaloids (1949).

[7] A. A. Shmuk, The Chemistry of Tobacco (Food Industry Press, Moscow, 1948). *

[8] A. I. Smirnov, Physiological and Biochemical Principles of Processing of Tobacco Raw Materials (Krasnodar, 1933).*

[9] A. T. March and R. V. Krzhevova, Chemical and Technical Control in the Canning Industry (Food Industry Press, Moscow, 1948).*

[10] N. Ia. Demianov and N. D. Prianishnikov, General Analytical Methods for Plant Materials (State Chem. Tech. Press, Moscow, 1934).*

[11] A. R. Kiesel, Practical Manual of Plant Biochemistry [Russian translation] (State Biological and Medical Press, Moscow, 1934).

[12] A. Longi, Landw. Versuch. Stst. 32, 1 (1885).

Received October 22, 1956

* In Russian.

POLAROGRAPHIC DETERMINATION OF BENZOYL PEROXIDE IN CERTAIN PLASTICS

V. D. Bezuglyi and V. N. Dmitrieva

The Khar'kov Factory of Dental Materials

Data on the reduction of various organic peroxides at the dropping mercury electrode are given in the literature [1-9]. Neiman and Dobrinskaia give the half-wave potentials of certain peroxides in presence of 0.1 N HCl and 0.1 N NaOH as the supporting electrolytes. According to these authors, the values all lie between − 0.4 and −1.0 v. The peroxides studied included benzoyl peroxide, which was the substance studied in the present investigation.

The authors cited determined only the half-wave potential of benzoyl peroxide, and gave no other polarographic data.

The paper by Lewis, Quackenbush, and De Vries [4] contains, in addition to the results of polarographic studies of various peroxides in nonaqueous solutions, certain data on benzoyl peroxide, which was not the main object of investigation. These authors determined the polarograms of peroxides in presence of 0.3 M LiCl, 0.2 M CH_3HSO_4, and 0.2 M $LiOCH_3$ in mixtures of 50% methanol and 50% benzene. The curves for benzoyl peroxide in 0.001% concentration show that it is reduced only in the presence of the first two electrolytes; the probable reason is that benzoyl peroxide decomposes in an alkaline medium. The half-wave potentials are not given in the paper. In the opinion of these authors, LiCl is the better of the two supporting electrolytes.

The polarographic curves obtained are distorted by the presence of maxima. The authors state that these distortions could not be eliminated completely by the addition of various maximum-suppressing agents.

Kolthoff and his associates [9] studied the kinetics of the emulsion polymerization of styrene with potassium persulfate as catalyst, and determined α-dinitrobenzene, oxygen, benzaldehyde, and peroxides by polarographic methods.

The purpose of our work was a more detailed polarographic study of benzoyl peroxide, and the use of the polarographic method for the quantitative determination of benzoyl peroxide in plastics, including polymethyl methacrylate.

The SGM-8 automatic recording polarograph (of the Geologorazvedka works) was used; the sensitivity of the galvanometer was $2.93 \cdot 10^{-9}$ amp/mm.

The solutions were always in a cell with an external anode consisting of a saturated calomel electrode, the galvanometer being adjusted to $^1/_{30}$ or $^1/_{50}$ of its maximum sensitivity. In absence of polarization, the capillary used had the following characteristics: m = 1.225 mg/sec; τ = 3.28 sec; $m^{2/3} \cdot \tau^{1/6} = 1.332$.

The concentration range of the benzoyl peroxide was from 0.1 to 1 millimole/liter.

Most of the determinations were performed in alcohol−benzene mixture containing 80% methanol and 20% benzene. This choice was determined by the conditions required for the analysis of plastics. The standard solution was 0.02 molar solution of benzoyl peroxide in benzene. The supporting electrolyte was ammonium nitrate, because of its good solubility in nonaqueous solvents. It was used at 2% concentration in the test solution.

Anode−cathode polarization was used in the polarographic determinations, as the reduction of benzoyl peroxide in presence of ammonium nitrate takes place in the positive potential region.

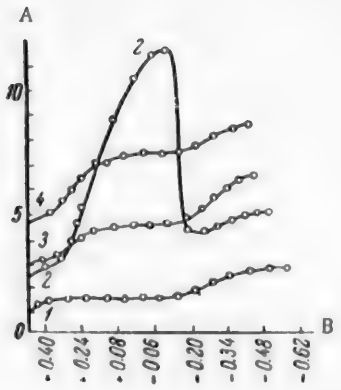

Fig. 1. Polarograms of benzoyl peroxide with 2% NH_4NO_3 as the supporting electrolyte, in a mixture of 80% CH_3OH + 20% C_6H_6. A) Diffusion current (in ma), B) potential (in v). Concentration of peroxide (in millimoles/liter): 1) supporting electrolyte, 2) 0.252, 3) 0.252 with methyl red added, 4) 0.484 with methyl red added.

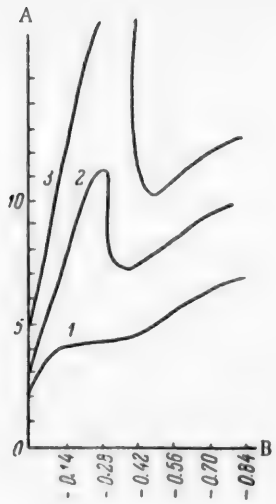

Fig. 2. Polarograms of benzoyl peroxide with 0.3 M LiCl as the supporting electrolyte, in a mixture of 80% CH_3OH and 20% benzene. A) Diffusion current (in ma), B) potential (v). Concentration of peroxide (in millimoles/liter): 1) supporting electrolyte, 2) 0.400, 3) 0.785.

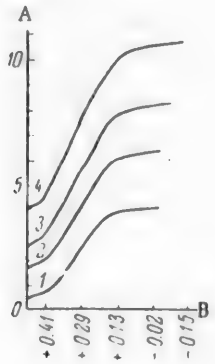

Fig. 3. Polarograms of benzoyl peroxide with 2% solution of NH_4NO_3 as the supporting electrolyte, in a mixture of 80% CH_3OH and 20% benzene, in presence of methyl red. A) Diffusion current (in ma), B) potential (v). Peroxide concentration (in millimoles/liter): 1) 0.400, 2) 0.594, 3) 0.785, 4) 0.979.

At peroxide concentrations of the order of 0.1-0.3 millimole/liter a wave with a maximum is obtained (Fig. 1, curve 3). However, in the concentration range studied this maximum is readily eliminated by addition of a small amount of methyl red, and the curve becomes regular (curves 3, 4). The polarograms of benzoyl peroxide obtained under the same conditions as the others, but in the presence of 0.3 M lithium chloride solution (as recommended by Lewis and Quackenbush [4]) in the same alcohol–benzene solution are given in Fig. 2.

The polarograms show that in the presence of this electrolyte benzoyl peroxide is reduced in the region of negative potentials, close to zero.

The maximum is not suppressed by the addition of the same amounts of methyl red as used in the determinations in presence of NH_4NO_3.

The polarogram (Fig. 3) shows that the diffusion current is a linear function of the concentration.

A calibration graph (Fig. 4) was plotted for the concentration region studied. The half-wave potential of benzoyl peroxide found from the curve at $I_d/2$ was found to be $E_{1/2} = +0.27$ v.

The half-wave potential found graphically for $\log \frac{I}{I_d - I} = 0$ is +0.26 v (Fig. 5).

The equation $E = E_{1/2} - \frac{0.058}{\alpha} \log \frac{I}{I_d - I}$ (at 18°) gives $\alpha = 0.673$. The value found for α shows that the reduction of benzoyl peroxide at the dropping mercury electrode is irreversible.

The Ilkovic equation was used to determine n, the number of electrons necessary to reduce one molecule of the substance. Tabular data for the diffusion coefficient of diphenyl (molecular weight 154) in methanol [10] were used; the diffusion coefficient of benzoyl peroxide (M = 242), by the equation $\frac{D_1}{D_2} = \frac{\sqrt{M_2}}{\sqrt{M_1}}$, is $1.24 \cdot 10^{-5}$ cm^2/sec. This gave n = 2.2.

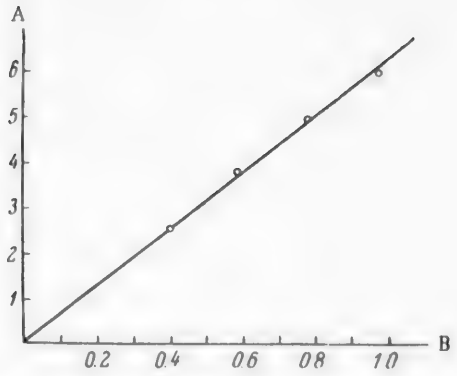

Fig. 4. Calibration graph for benzoyl peroxide with 0.25 N NH_4NO_3 as the supporting electrolyte, in 80% CH_3OH and 20% benzene. A) Diffusion current (in ma), B) peroxide concentration (millimoles/liter).

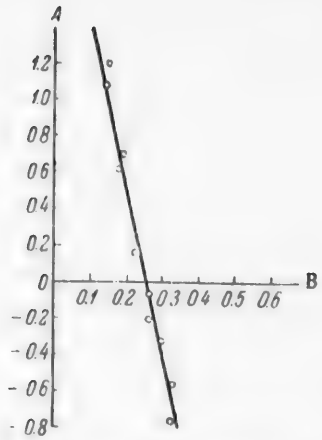

Fig. 5. Plot $\log \frac{I}{I_d - I}$ against E. A) $\log \frac{I}{I_d - I}$, B) potential (in v).

The value of n was also determined by a coulometric method [11].

A solution containing 1.033 millimole/liter of benzoyl peroxide in a mixture of 20% benzene and 80% methanol, containing methyl red to suppress the maximum, was used for this determination. 1 ml of this solution was placed in a small cell with an internal anode. A current of hydrogen was passed through the solution, and the polarographic determination was performed. A current was then passed through the solution for several hours, with a constant voltage of 0.5 v at the electrodes.

The polarographic determinations were repeated at definite intervals. A current of hydrogen was passed over the surface of the solution during the electrolysis. To prevent evaporation of the solvents, a wash bottle containing the same solvent mixture as in the cell was connected in series with the cell.

The number of electrons was calculated by means of the formula

$$n = \frac{4.403 \cdot 10^{-6} \cdot I_{d_0} \cdot \Delta T}{\Delta \log I_d \cdot v \cdot C},$$

where I_{d_0} is the initial value of the diffusion current (in ma), I_d is the diffusion current after T seconds, T is the time of electrolysis (in seconds), v is the volume of the test solution (in ml), C is the initial concentration of the test solution (in millimoles/liter).

TABLE 1

Polarographic Data on Benzoyl Peroxide

Concentration C (in mmoles/liter)	Diffusion current I_d (in μ amps)	Polarographic diffusion-current constant $K = \frac{I_d}{C \cdot m^{2/3} \cdot \tau^{1/6}}$	$E_{1/2}$ at $I_{d/2}$	$E_{1/2}$ at $\log \frac{I}{I_d - I}$
0.400	2.56	4.80		
0.594	3.83	4.83		
0.785	4.91	4.70	+0.27	+0.26
0.979	5.95	4.64		
	Mean	4.74		

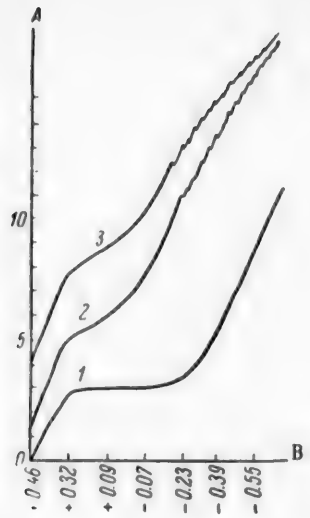

Fig. 6. Polarograms of benzoyl peroxide in presence of salicylate buffer solutions in 85% ethyl alcohol. A) Diffusion current (ma), B) potential (in v). Peroxide concentration (millimoles/liter) and pH, respectively: 1) supporting electrolyte, 3.98; 2) 0.400, 3.98; 3) 0.400, 4.48.

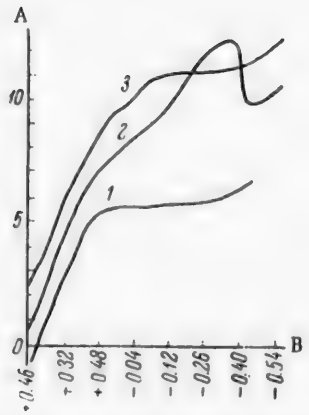

Fig. 7. Polarograms of benzoyl peroxide with benzoate buffer solutions as supporting electrolytes. A) Diffusion current (ma), B) potential (in v). Peroxide concentration (millimoles/liter) and pH respectively: 1) supporting electrolyte, 5.81; 2) 0.400, 5.81; 3) 0.400, 7.22.

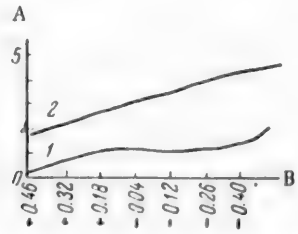

Fig. 8. Polarograms of benzoyl peroxide in presence of benzoate buffer, pH = 8.3. A) Diffusion current (in ma), B) potential (in v). Peroxide concentration (millimoles/liter): 1) supporting electrolyte, 2) 0.400.

The average value of n given by this formula was 2.11, i.e., close to 2.

Therefore, 2 electrons take part in the reduction of one molecule of benzoyl peroxide.

The reduction of benzoyl peroxide may be represented as follows:

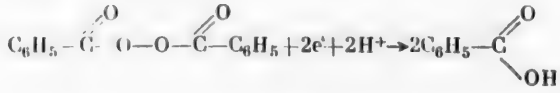

The polarographic data are presented in Table 1.

Influence of the pH of the supporting electrolyte. The polarographic behavior of benzoyl peroxide was also studied in buffer solutions of different pH values as the supporting electrolytes. The buffer solutions of different pH were salicylate and benzoate mixtures in 85% ethyl alcohol, of the compositions given by Izmailov and Frantsevich-Zabludovskaia [5].

The polarograms of benzoyl peroxide with pH of the supporting electrolyte between 3.98 and 8.3 and peroxide concentration 0.400 millimole/liter are given in Figs. 6-8.

Consideration of these polarograms shows that the peroxide wave height decreases considerably with increasing pH. At pH 3.98 and 4.48 the peroxide wave occupies almost the entire polarogram (Fig. 6).

At pH 5.81 (Fig. 7, curve 2) the peroxide wave has a maximum which cannot be suppressed by the addition of 0.2% solution of methyl red in 1 : 100 ratio (the same amounts were added in the preceding experiments). A maximum cannot be detected at lower pH values, as at this concentration of benzoyl peroxide its wave merges with the wave of the supporting electrolyte (salicylate*).

When the pH of the supporting electrolyte is 7.22 (Fig. 7, curve 3), the peroxide gives a wave with a maximum, suppressed by the addition of the same amount of methyl red; the form of the wave resembles that of benzoyl peroxide obtained in presence of ammonium nitrate.

* As in original – Publisher's note.

At pH 8.3, the height of the benzoyl peroxide wave is small, and the wave loses its usual form, becoming a line with a smooth flat slope.

The accuracy of the polarographic determination of benzoyl peroxide was tested by analysis of solutions containing known concentrations of benzoyl peroxide. Weighed samples of benzoyl peroxide were dissolved in benzene, the solution was diluted with methyl alcohol in 1:4 ratio, and 2% of ammonium nitrate was added.

The results of the determinations are given in Table 2.

TABLE 2

Analysis of Solutions Containing Benzoyl Peroxide

Amounts of peroxide (g)		Relative error (%)
taken	found	
0.0208	0.0197	−5.4
0.0060	0.0062	+3.3
0.0164	0.0156	−5.0
0.0106	0.0101	−4.8
0.0104	0.0106	+1.9
0.0122	0.01175	−3.8

TABLE 3

Determination of Benzoyl Peroxide in Polymethyl Methacrylate

Amount of peroxide (%)		Relative error (%)
added	found	
0.300	0.29	−3.3
	0.28	−6.6
	0.28	−6.6
2.00	1.97	−1.5
	1.97	−1.5
	1.98	−1.0

As already stated, the aim of our investigation was not only to carry out a polarographic study of benzoyl peroxide, but also to develop a polarographic method for the determination of benzoyl peroxide in plastics. The determination of benzoyl peroxide in plastics was a very important problem in relation to the investigations, in progress in our laboratory, on the production of the so-called "self-hardening" plastics, i. e., plastics formed by polymerization at 25-30°. These plastics contain from 0 to 2% benzoyl peroxide.

Benzoyl peroxide was determined in emulsion-polymerized polymethyl methacrylate, in the finished plastic, and in the mother liquor after polymerization.

The procedure used was as follows. A weighed sample of the powdered emulsion polymer or plastic, weighing about 1.5-1.8 g, was put in a weighed 100 ml measuring flask and 20 ml of benzene was added. After the sample had dissolved, the benzene solution was diluted with methyl alcohol until the polymer was precipitated. 2 g of ammonium nitrate and 1 ml of 0.2% methyl red solution was then added, and the liquid was made up to the mark with methyl alcohol. The liquid was thoroughly mixed and allowed to settle for 20 min; 10 ml of the solution was then put into the cell. A current of hydrogen was passed through the solution for 10 min and the polarographic determination was then performed between +0.45 and −0.2 v. The peroxide content was determined by the addition method or from the calibration graph.

To illustrate the accuracy of the polarographic method, the results of determinations of the benzoyl peroxide contents in emulsion polymethyl methacrylate polymer are compared in Table 3 with the known amounts added.

The benzoyl peroxide content of the mother liquor after polymerization was determined as follows. 100 ml of the mother liquor, containing benzoyl peroxide, was put in a separating funnel and shaken with 20 ml of benzene to extract the peroxide. After separation of the benzene extract the mother liquor was shaken with a fresh portion of benzene. The benzene extracts were combined in a 200 ml measuring flask and diluted with methyl alcohol until the polymer was precipitated. The subsequent procedure was as before.

The results of determinations of benzoyl peroxide in certain samples of the self-hardening plastic and the mother liquor are given below (see following page).

These results show that benzoyl peroxide can be determined both in polymethyl methacrylate powder and in the mother liquors.

Sample no.	Peroxide content (%)	Sample no.	Peroxide content (%)
1	0.11	7	0.09
2	0.22	8	0.86
3	1.13	9	0.50
4	1.09	10	1.87
5	0.33	Mother liquor	0.0037
6	1.98	The same	0.0039

SUMMARY

1. The polarographic behavior of benzoyl peroxide in nonaqueous solutions was studied; its principal polarographic constants were determined and the effects of pH of the supporting electrolyte on the wave height of benzoyl peroxide were investigated.

2. Ammonium is proposed as a supporting electrolyte; benzoyl peroxide gives a distinct wave in its presence.

3. It is shown that the polarographic method can be used for quantitative determination of benzoyl peroxide in plastics, and details of this method have been worked out.

LITERATURE CITED

[1] M. B. Neiman and A. A. Dobrinskaia, Factory Labs. 3, 280 (1939).

[2] A. A. Dobrinskaia and M. B. Neiman, Bull. Mendeleev All-Union Chem. Soc. 3-4, 37 (1939).

[3] W. Lewis and F. Quackenbush, J. Amer. Oil Chem. Soc. 26, 53 (1949).

[4] W. Lewis, F. Quackenbush, and F. De Vries, Anal. Chem. 21, 162 (1949).

[5] N. A. Izmailov and T. Frantsevich-Zabludovskaia, J. Gen. Chem. 15, 283 (1945).

[6] M. Bogdanezki and I. Eksner, Coll. Czech. Chem. Comm. 20, 917 (1955).

[7] M. Bernard, Compt. rend. Acad. Sci. 236, 2412 (1953).

[8] P. Mensik, Chem. Prumysl. 5, 165 (1955).

[9] J. M. Kolthoff, F. A. Bovey, W. J. Dale, and D. R. May, J. Amer. Chem. Soc. 69, 2149, 441 (1947); 70, 791 (1948).

[10] Tables of Physical Data 7 (Technical Encyclopedia Press, 1931)* p. 260.

[11] Meites, Polarographic Techniques (New York, 1955), p. 223.

Received July 2, 1956

* In Russian.

BRIEF COMMUNICATIONS

EFFECT OF SMALL ADDITIONS OF B_2O_3 ON CERTAIN PROPERTIES OF GROUND-COAT ENAMELS

G. I. Beliaev

The Dnepropetrovsk Institute of Chemical Technology

It is known that boron is present in glasses and enamels in triple and quadruple coordination [1]; it is an excellent glass former and forms part of the silicon–boron–oxygen framework in glass [2, 3]. The properties of boron ground-coat enamels, which are in direct contact with the metal and contain 10-20% of boric anhydride, have been studied by many workers [4-8]. However, the effects of small additions of B_2O_3 on enamel have not been studied sufficiently, although for economic reasons such enamels are widely used in industry.

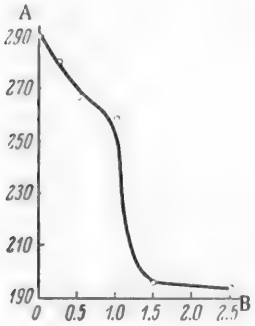

Fig. 1. Effect of B_2O_3 on the viscosity of ground-coat enamel at 530°. A) Viscosity $\eta \cdot 10^6$ (in poises), B) B_2O_3 content (%).

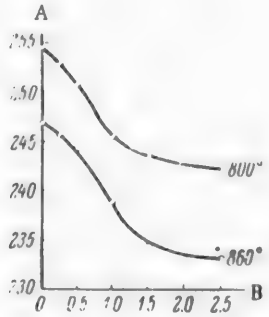

Fig. 2. Isotherms for the surface tension of ground-coat enamel as a function of added B_2O_3. A) Surface tension (dynes/cm), B) B_2O_3 content (%).

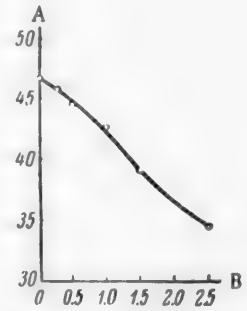

Fig. 3. Effect of B_2O_3 on the wetting of oxidized steel by enamel. A) Contact angle θ, B) B_2O_3 content (%).

The effects of small additions of B_2O_3 on the viscosity, surface tension, wetting, and other properties of boronless ground-coat enamels were studied in this investigation.* Boronless frit No. 27, widely used in production, was studied. The frit had the following composition (in %): SiO_2, 59.4; Al_2O_3, 2.5; Na_2O, 22.5; CaF_2, 13.0; Co_2O_3, 0.6 and Fe_2O_3, 2.0.

B_2O_3 was added to the original batch, to give 0.25, 0.50, 1.00, 1.50, and 2.50%, respectively, per 100 g of the glass. The boric anhydride was introduced in the form of chemically pure boric acid. The frits were melted in fireclay crucibles in an electric furnace at 1150°.

The viscosity of the enamels was determined by the stretching of a thread drawn from the melt [9], and the surface tension was measured by a simplified version of the drop-weighing method [10]. The wetting of an oxidized steel surface by the enamel was estimated from the value of the contact angle θ, determined at 850° by

* Laboratory assistant L. G. Kazankina took part in the experimental work.

the "sessile drop" method [4]. The oxidation rate of the steel during firing of the ground-coat enamel was estimated from the weight increase of the specimen [7].

The crystallizing power of the enamel glasses was determined by the forced-crystallization method [9]. Experiments showed that additions of 1% of B_2O_3 and over decrease noticeably the tendency of the enamels to crystallize.

The influence of small additions of boric anhydride on the external appearance of the ground coats was investigated by means of test coatings on steel plates 50 × 75 × 0.5 mm in size. The quality of the enamel surface with regard to blistering, swelling, and other defects is given below in terms of arbitrary points.

Influence of Additions of Boric Anhydride on the Quality of Ground-Coat Enamels

B_2O_3 added (%)	Thickness of ground coat (mm) before firing	Thickness of ground coat (mm) after firing	Average surface quality (points)
0.00	0.25	0.19	3.0
0.25	0.25	0.18	3.2
0.50	0.25	0.17	3.5
1.00	0.25	0.17	3.6
1.50	0.25	0.16	3.7
2.50	0.25	0.16	3.9

Data on the influence of small additions of boric anhydride on the viscosity, surface tension, wetting, and other properties of enamels are presented graphically in Figs. 1-4, while Fig. 5 shows the effect of additions to the slip on the oxidation rate of the steel during firing of the ground coat [7].

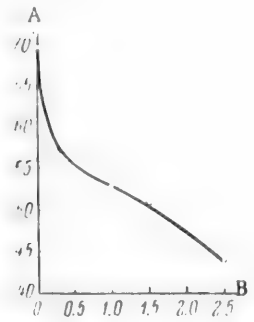

Fig. 4. Effect of additions of boric anhydride on the oxidation rate of steel during the firing of the ground coat. Firing temperature 850°, time 8 min. A) Weight increase (in mg/dm^2), B) B_2O_3 content (%).

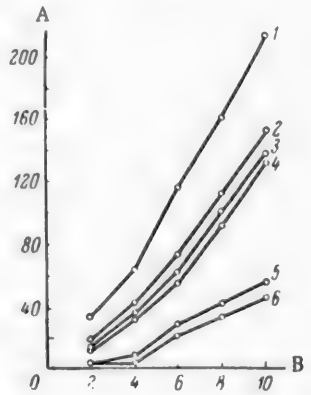

Fig. 5. Effect of additions of borax to the ground-coat slip on the oxidation rate of steel during firing of the ground coat. A) Weight increase (in mg/dm^2), B) heating time (min). Borax contents (%): 1) 0, 2) 0.5, 3) 1, 4) 1.5, 5) 2.0, 6) 2.5.

SUMMARY

1. Small additions of B_2O_3 considerably decrease the viscosity of enamel glass, lower the surface tension, improve the wetting of oxidized steel by the enamel, and reduce appreciably the oxidation rate of steel during firing of the ground coat.

2. Additions of borax to the ground-coat slip are effective in decreasing the oxidation of steel under the ground coat; the crystallization tendency of the enamel decreases with B_2O_3 additions of 1% and over. Ground coats containing B_2O_3 swell and blister much less. The results show that the thickness of the ground coat, which was always 0.25 mm before firing, varied in a regular manner after firing: increase of the B_2O_3 content of the enamel gives a thinner ground coat, and therefore decreases the blistering tendency of the enamel; small additions of boric anhydride improve considerably the spreading, luster, and quality of the fired ground coat.

LITERATURE CITED

[1] A. A. Appen, in the symposium: Structure of Glass (Izd. AN SSSR,Moscow-Leningrad, 1955).*

[2] A. A. Appen, J. Appl. Chem. 27, 2 (1954).**

[3] A. A. Appen, J. Appl. Chem. 26, 6 (1953).**

[4] K. P. Azarov, J. Appl. Chem. 27, 1 (1954).**

[5] K. P. Azarov, in the symposium: Structure of Glass (Izd. AN SSSR, Moscow-Leningrad, 1955).*

[6] A. Petzold, Email. (Berlin, 1955).

[7] G. I. Beliaev, Coll. Trans. Novocherkassk Polytech. Inst. 24 (38) (Industrial Construction Press, 1953).

[8] G. I. Beliaev, Proc. of Production and Technical Conference on Metal Enameling (Metallurgy Press, 1956).

[9] K. S. Evstrop'ev and N. A. Toropov, Chemistry of Silicon and Physical Chemistry of Silicates (Industrial Construction Press, 1950).*

[10] K. P. Azarov, Factory Labs. 3 (1954).

Received April 23, 1957

* In Russian.

** Original Russian pagination. See C. B. translation.

SOLUBILITY OF IRON OXIDES IN GROUND-COAT ENAMELS FOR STEEL

K. P. Azarov and V. V. Balandina

Many processes in silicate technology (the production of special and colored glasses, refractories, cement, etc.) are accompanied by the dissolution of iron oxides in melts. The ability of silicate melts to dissolve iron oxides is of special significance in the technology of steel and cast-iron enameling, since successful enameling depends on the interaction of the enamel (ground) melt with the oxidized metal (scale). The problem of boronless ground enamels is also associated with this question. However, the available data on the solubility of iron oxides in ground-coat enamels [1-6] are contradictory, and cannot be used as the basis for reliable conclusions concerning the role of iron oxides, and in particular, the connection between their solubility and the boric anhydride content of the melt.

Investigations were therefore carried out in order to determine the solubility of iron oxide in typical industrial ground-coat enamels: boronless Nos. 35b/b and 27b/b, borate Nos. 41b, 210b and 18b, and titanium No. 121 Ti; and to correlate the results with the technological characteristics of the corresponding ground coats.

The solubility of iron oxides was determined by the method used by Andrews and Swift [2], based on Gilard and Dubrul's data [7] on the linear variation of the refractive index of glass with the amount of iron oxide dissolved. The solubility limits were determined from the concentration of iron oxide corresponding to the maximum constant refractive index.

The enamels were first melted with iron oxide at 850° for 10 hrs and at 950° for 4 hrs until equilibrium was reached, and then cooled rapidly in water. The refractive index was determined by the Becke method under the polarization microscope at 64 and 100 magnifications. The breaks on the refractive-index curves correspond to maximum solubilities of the iron oxides.

It is clear from the diagram that the maximum solubility of iron oxides (up to 21.0-23.3%) is found for the borate ground-coat enamels Nos. 41b, 210b, and 18b. The solubility in these enamels was 2-3 times as high as in the boronless enamels Nos. 27b/b and 35b/b. The titanium ground-coat enamel No. 121 Ti dissolves more iron oxides than the boronless enamels, but is inferior to borate enamels in this respect. The discrepancies between

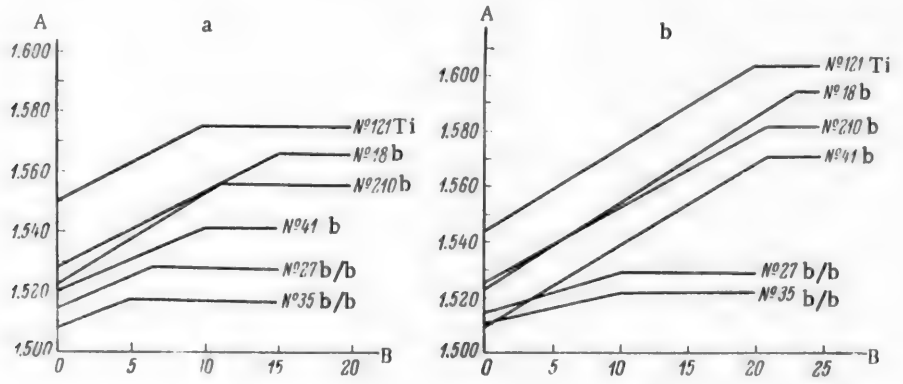

Effect of iron oxide content on the refractive index of ground-coat enamels. A) Refractive index, B) iron oxide content (in g/100 g of glass). a) Dissolved at 850°, b) dissolved at 950°.

these results and the data of other authors are due to differences in the experimental conditions. Thus, in the present investigation borate and boronless enamels were studied, whereas other workers [2, 3, and others] investigated enamels with variable contents of boric anhydride, so that their conclusions could not be applied to boronless enamels. In other investigations the time of heating of the enamels with iron oxide was so short that equilibrium was not reached between the melts and iron oxide, and the maximum solubility was therefore not attained.

The same enamels, melted with the bonding oxides, were subjected to technological tests followed by visual evaluation of the quality of the ground coats, assessed in marks (by the amount of swelling and blistering). The data below show that the highest ratings (in marks) of ground-coat quality correspond to the highest solubilities of iron oxide.

Boronless		Titanium	Borate		
No. 35 b/b	No. 27 b/b	No. 121 Ti	No. 41 b	No. 210 b	No. 18 b
3.0	2.0	3.5	4.5	4.5	5.0

Because of the lower solubility, boronless enamels are readily saturated with iron oxides. The latter then form colloidal solutions and suspensions, with a sharp increase of melt viscosity.* When a boronless ground coat is fired on steel, the inner layer of the enamel, adjacent to the oxidized metal, rapidly becomes saturated with iron oxides. Increase of the melt viscosity in this layer during the first stages of firing prevents the free escape of the gases liberated from the steel and formed in reactions between the scale and the carbon in the steel, and so favors swelling and blistering.

The lower solubility of iron oxides in boronless enamels may be attributed to: a) the high surface tension of boronless melts, which hinders the wetting and dissolution of iron oxides [8, 9]; b) the sharply increased viscosity of boronless enamels, due to structural transformations of different forms of iron, and to crystallization [10]; c) the considerable basicity of boronless melts [11], which favors the formation of FeO_4 glass-forming groups, which strengthen the glass structure.

LITERATURE CITED

[1] A. Dietzel and L. Arnold, Sprechsaal 75, 168-171 (1942).

[2] A. I. Andrews and H. R. Swift, J. Am. Cer. Soc. 27, 2, 46-50 (1944).

[3] W. Kerstan, Sprechsaal 77, 55-59, 72-76 (1944).

[4] A. Petzold, Email (Berlin, 1955).

[5] J. J. Canfield, Ceram. Industry 24, 362, 364, 366, 374 (1935).

[6] C. G. Haessler, University of Illinois (1938); cited through A. I. Andrews and H. R. Swift [2].

[7] P. Gilard and L. Dubrul, J. Soc. Glass Techn. 21, 88, 485-488 (1937).

[8] K. P. Azarov, Refractories 12, 551-555 (1950).

[9] K. P. Azarov, J. Appl. Chem. 28, 1, 33-42 (1954).**

[10] Abd.-El-Moneim Abou-El-Azm, J. Soc. Glass Techn. 38, 181, 101-145, 146-196 (1954).

[11] K. P. Azarov, Proc. Conference on the Structure of Glass (Izd. AN SSSR, 1955), pp. 276-278.

Received February 25, 1957

* The increase of viscosity in the softening region of boronless enamels, as the result of dissolution of iron oxides, was demonstrated in another investigation performed with the assistance of S. B. Grechanova.

** Original Russian pagination. See C. B. translation.

EFFECTS OF SOLUTION TEMPERATURE AND CONCENTRATION ON THE CONTENT OF ANIONS FROM THE BATH ELECTROLYTE IN AN ANODIC OXIDE FILM, DETERMINED BY THE LABELED-ATOM METHOD*

A. F. Bogoiavlenskii and A. P. Vedernikov

Our previous communication gave a description of the use of the tracer-atom method in studies of the kinetics of accumulation of electrolyte anions ($SO_4^{"}$) from the anodizing bath in the protective Al_2O_3 formed in anodizing by the sulfuric acid process. The stability and the high content (over 10% by weight) of the anion in the film raise the question of the influence of such parameters of the anodizing bath as the electrolyte temperature and concentration. This question is considered in the present communication.

The experimental procedure and the substances used were the same as before [1].

Radioactive S^{35} isotope in a ratio of 1:400 to the main carrier was added to the anodizing bath electrolyte. The $SO_4^{"}$ content of the anode film was determined by means of a Geiger-Müller end-type counter, from the radiation intensity of a comparison standard (1 ml of the original electrolyte tagged with S^{35}).

The results (mean values of 4-5 determinations) are given in Table 1.

TABLE 1

Effect of Electrolyte Concentration on the Contents of $SO_4^{"}$ Anions in the Anode Film of Al_2O_3 Anodic passivation carried out at current density D_a = 2.0 amp/dm^2. Duration of process 10 min at 37°. Cell voltage from 23 to 7.5 v. Activity of comparison standard $0.427 \cdot 10^{-6}$ g/pulse

Electrolyte (H_2SO_4) conc. (in wt%)	Thickness of anode film (in μ)	Activity of specimen (pulses/min)	Weight of film on specimen (in mg)	$SO_4^{"}$ content	
				in mg	in wt%
2.0	4.1	3242	12.7	1.29	10.2
5.0	4.06	3334	12.8	1.33	10.4
10.0	3.98	3139	12.2	1.28	10.5
15.0	3.45	3268	10.6	1.28	12.1
20.0	3.17	3060	9.7	1.22	12.6

These results show that the $SO_4^{"}$ content of the anodic oxide film increases relatively little with increasing electrolyte concentration (a 10-fold increase of the electrolyte concentration increases the anion content of the film by 2.0-2.5 wt%). The film thickness decreases with increase of electrolyte concentration, owing to increase of the corrosive action of the electrolyte on the Al_2O_3 film.

In view of the colloidal structure of the anodic oxide film [2] it may be assumed that its micelles have the composition

$$\{[nAl_2O_3 \cdot mH_2O) \cdot xSO_4]^{-2x} \cdot 2xH^+\};$$

* Communication VII in the series on the anodic passivation of aluminum.

the very high content of $SO_4^{"}$ anions (over 10%) in it is then quite explicable. The slight increase of the $SO_4^{"}$ content of the film with increase of the electrolyte concentration is probably due to increased porosity of the film as the result of the corrosive action of the electrolyte on it. The $SO_4^{"}$ anions present in the anode film can therefore be regarded as consisting of two types: structural ions (forming part of the colloidal micelle of the film), and ions sorbed in the film pores (contained in the pore channels and adsorbed on the pore walls). The latter are the cause of the slight increase of the $SO_4^{"}$ content in the anodic oxide film. The effect of the electrolyte temperature of the anodizing bath on the $SO_4^{"}$ content of the anode film is shown in Table 2.

TABLE 2

Effect of Electrolyte Temperature on the Contents of $SO_4^{"}$ Anions in the Anode Film of Al_2O_3
Anodic passivation carried out at current density D_a = 2 amp/dm^2 for 10 min in 10% H_2SO_4.
Cell voltage from 21 to 5.5 v. Activity of comparison standard $0.5 \cdot 10^{-5}$ g/pulse

Electrolyte temperature (°C)	Thickness of anode film (in μ)	Activity of specimen (pulses/min)	Weight of film (in mg)	$SO_4^{"}$ content	
				in mg	in wt%
10	4.67	3862	14.7	1.9	13.1
20	4.03	3418	13.7	1.7	12.4
30	4.17	3018	13.1	1.5	11.5
40	3.19	2412	11.0	1.2	10.9
50	1.97	1288	6.1	0.6	10.5
60	0.67	400	2.1	0.2	9.5

It follows from Table 2 that the $SO_4^{"}$ content of the anode film decreases considerably with increasing temperature of the anodizing bath. The probable reason is that the content of structural $SO_4^{"}$ ions in the film micelles decreases. This decrease of the density of the ionogenic complex of a colloidal micelle with the temperature is not at variance with the accepted views on the colloidal state.

These results in general confirm the data obtained by Mason [3] by the usual method.

SUMMARY

A study of the influence of temperature and electrolyte concentration in the anodizing bath on the $SO_4^{"}$ content of the anodic oxide film, performed by the tracer atom method, confirmed Mason's findings that the ion content of the anodic oxide film increases with increasing concentration and decreasing temperature of the electrolyte.

This result is attributed to the presence of structural $SO_4^{"}$ ions, and ions sorbed in the pore channels, in the anodic oxide film.

LITERATURE CITED

[1] A. F. Bogoiavlenskii and A. P. Vedernikov, J. Appl. Chem. 30, 12, 1868 (1957).*

[2] V. A. Kistiakovskii, Mathematics and Natural Science in the USSR (1946), p. 416. **

[3] R. Mason, J. Electrochem. Soc. 102, 12, 671 (1955); Referat. Zhur. Khim. 17, 81 (1956).

Received January 29, 1957

* Original Russian pagination. See C. B.translation.

** In Russian.

DECOMPOSITION OF GLUCOSE IN SULFITE COOKING

S. A. Sapotnitskii

In the sulfite cooking of wood, hydrolysis of hemicelluloses to simple sugars is accompanied by considerable breakdown of the latter.

Similar decomposition takes place if monosaccharides are boiled with sulfite cooking liquor.

As long ago as 1929 Hägglund [1], in a study of the influence of sugars on the stability of bisulfite solutions at elevated temperatures, concluded that bisulfite ions oxidize sugars with formation of the corresponding aldonic acid and thiosulfate ions.

$$2H_2SO_3' + 2C_6H_{12}O_6 \rightarrow S_2O_3'' + 2C_6H_{12}O_7 + H_2O.$$

Therefore, in his opinion, the reaction rate should increase with increasing concentrations of HSO_3' ions and sugar.

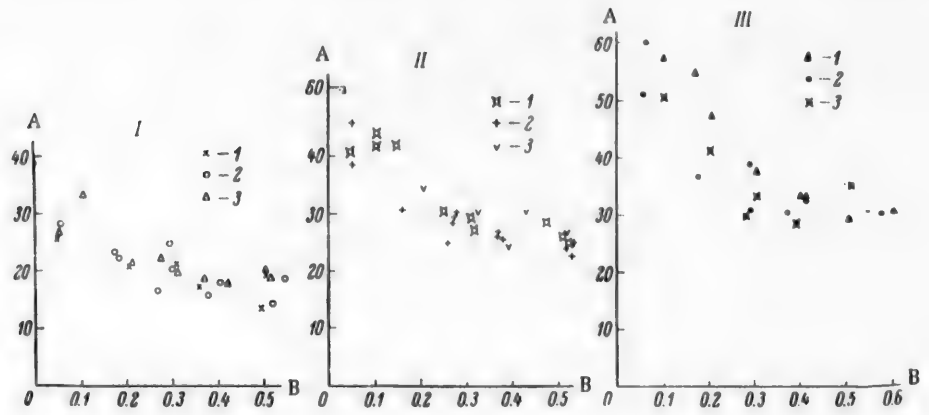

Fig. 1. Decomposition of glucose in sulfite cooking. A) Degree of decomposition of glucose (in %), B) initial concentration of glucose (mole/liter). NaOH concentration of liquor (mole/liter): I) 0.122, II) 0.240, III) 0.375. Total SO_2 content (mole/liter): 1) 0.547, 2) 0.860, 3) 1.095.

The same opinion is held by Nepenin [2], who states that the sugar content of the liquor depends to a considerable extent on the CaO content (i. e., the HSO_3' ion concentration) of the original cooking liquor; the higher the CaO concentration, the lower is the sugar yield in the sulfite cooking of wood.

However, no quantitative data are available on the effects of the sugar concentration and of the composition of the cooking liquor on the degree of decomposition of sugars.

Decomposition of Glucose in Sulfite Cooking (140°, 3 hrs)

Total SO_2 content of cooking liquor					
3.5% = 0.547 mole/liter		5.5% = 0.860 mole/liter		7.0% = 1.095 mole/liter	
initial glucose concentration (mole/liter)	% glucose decomposed	initial glucose concentration (mole/liter)	% glucose decomposed	initial glucose concentration (mole/liter)	% glucose decomposed
Series I. NaOH concentration in the cooking liquor 0.49% = 0.122 mole/liter					
0.052	25.5	0.061	28.2	0.057	26.5
0.206	20.8	0.175	23.3	0.108	33.0
0.311	21.0	0.183	22.0	0.208	20.5
0.358	17.0	0.269	16.3	0.275	22.0
0.495	13.3	0.296	24.8	0.311	19.3
0.504	19.0	0.300	20.0	0.363	18.5
—	—	0.379	15.8	0.420	17.8
—	—	0.403	17.9	0.503	20.0
—	—	0.523	15.0	0.511	18.5
—	—	0.555	18.3		
Series II. NaOH concentration in the cooking liquor 0.960% = 0.240 mole/liter					
0.050	40.6	0.055	45.5	0.106	41.8
0.110	43.8	0.057	38.3	0.211	34.3
0.150	41.8	0.167	30.8	0.328	30.3
0.255	30.7	0.264	24.3	0.391	24.7
0.318	29.5	0.273	28.8	0.433	30.0
0.322	27.0	0.277	28.2	0.520	27.0
0 487	28.6	0.278	30.0	—	—
0.513	26.0	0.372	26.9	—	—
—	—	0.372	26.4	—	—
—	—	0.380	25.5	—	—
—	—	0.520	24.1	—	—
—	—	0.528	25.2	—	—
—	—	0.533	25.4	—	—
—	—	0.533	22.6	—	—
Series III. NaOH concentration in the cooking liquor 1.50% = 0.375 mole/liter					
0.107	57.5	0.060	51.0	0.108	50.5
0.172	55.0	0.071	60.0	0.208	41.0
0.213	46.8	0.179	36.6	0 284	30.0
0.314	37.7	0.293	31.8	0.307	33.2
0.408	33.3	0.295	38.8	0.392	28.3
0.513	29.5	0.376	30.6	0.417	33.0
0.622	31.2	0.582	30.2	0.518	35.3
—	—	0.547	30.8	—	—

Experiments were therefore performed on the cooking of glucose with sulfite cooking liquor.*

The experiments were performed in sealed glass tubes in an autoclave. The cooking time was 3 hrs at 140°. The temperature was raised during 1 hr. The glucose concentration of the cooking liquor was varied from 0.05 to 0.6 mole/liter.

Three series of experiments were performed, with different contents of the base in the liquor: the NaOH concentration was 0.49 ± 0.03%, 0.96 ± 0.04%, 1.50 ± 0.02% (0.122, 0.240, 0.375 mole/liter, respectively).

In addition, the strength of the cooking liquor was also varied in each series, with a constant base content, the total SO_2 contents being 3.5 ± 0.2%, 5.5 ± 0.2%, 7.0 ± 0.3% (0.547, 0.860, 1.095 mole/liter, respectively).

* A. G. Moskaleva, B. I. Tokarev, R. M. Miasnikova, and Z. F. Osmolovskaia took part in the experimental work.

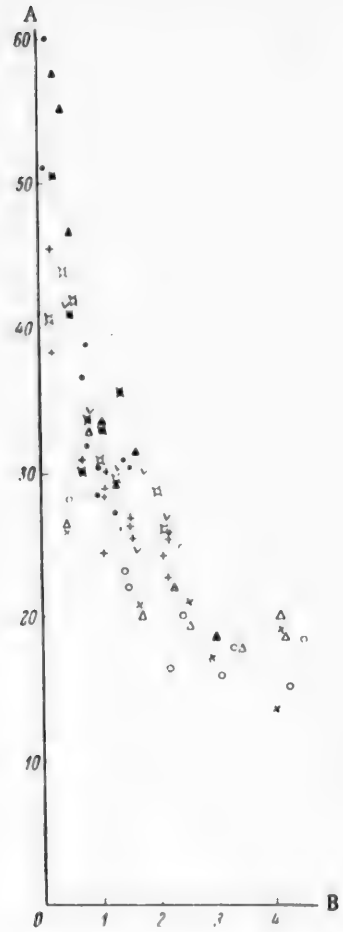

Fig. 2. Functional relationship of the degree of decomposition of glucose. A) Degree of decomposition of glucose(%), B) molar ratio of the initial glucose concentration to the concentration of bisulfite SO_2. Designations as in Fig. 1.

It follows from the results of the 75 experiments given in the table that under the conditions specified the degree of decomposition of glucose is a function of the concentration of the base in the cooking liquor and of the initial glucose concentration in the solution.

It is confirmed that the degree of decomposition of glucose increases with increasing content of base in the liquor. However, in contradiction to the results reported in the literature, it was found in a study over a wide range of glucose concentrations that the degree of decomposition of glucose decreases rather than increases with increase of its initial concentration.

This is illustrated graphically in Fig. 1. It is seen that with 0.49% NaOH (0.122 mole/liter), when the initial concentration of glucose was 0.1 mole/liter about 30% of it decomposed, while when its initial concentration was 0.5 mole/liter, about 15% decomposed. The same results are obtained with 0.96% and 1.5% NaOH. In these cases, when the initial glucose concentration was 0.1 mole/liter, about 45 and 55%, respectively, decomposed; with 0.5 mole/liter, the decomposition was about 25 and 30% respectively.

It also follows from Fig. 1 that the degree of decomposition of glucose in sulfite cooking is independent of the strength of the cooking liquor, and therefore of the concentration of the free, molecularly dissolved SO_2. Despite the considerable difference between the SO_2 contents of the liquor (from 3.5 to 7% total SO_2), the points for the decomposition of glucose at a given content of base in the liquor belong to the same group, and fit on a common curve.

The simultaneous influence of the initial glucose concentration and the concentration of base in the cooking liquor on the decomposition of sugar can be demonstrated if the degree of decomposition of glucose is represented as a function of these two variables. Fig. 2 shows that the amount of glucose decomposed during sulfite cooking (at a given temperature) is determined only by the ratio of its initial concentration to the concentration of base in the liquor or, which is the same thing, to the concentration of the bisulfite ions in the liquor, and is independent of the contents of the free, molecularly dissolved SO_2 in the liquor.

Since the same ratio of the initial glucose concentration to the concentration of base in the liquor can be obtained with different absolute values of these quantities, the degree of decomposition of sugar in sulfite cooking is in this sense independent of the absolute concentration of base in the cooking liquor.

It follows from Fig. 2 that in order to protect as much glucose as possible against decomposition in sulfite cooking the molar ratio of the initial sugar concentration to the concentration of base in the liquor should be higher than 2.5:1.

SUMMARY

1. The effects of initial glucose concentration and the composition of the cooking liquor on the degree of decomposition of sugar in sulfite cooking were studied, and it was confirmed that the degree of decomposition of glucose increases with increasing content of base in the liquor; it was also found that the degree of decomposition of glucose decreases with increasing glucose concentration over a wide range (0.05 to 0.6 mole/liter).

2. It was found that the amount of glucose decomposed during sulfite cooking is independent of the content of free, molecularly dissolved SO_2 in the liquor, and is determined (at a definite temperature) only by the ratio of the initial sugar concentration to the concentration of bisulfite ions in the liquor.

LITERATURE CITED

[1] E. Hägglund, Ber. 62, 437 (1929).

[2] N. N. Nepenin, Cellulose Technology (State Wood and Paper Press, 1956)* pp. 281-286.

Received November 5, 1956

* In Russian.

PLASTIFICATION OF STARCH PASTES

M. G. Shikher and L. A. Rybkina

The Ivanovo Scientific Research Institute of the Cotton Industry

Large amounts of thickeners, especially for printing pastes, are used in modern textile technology. Although various artificial and synthetic materials are being increasingly used, starch (and starch products) occupies the leading position as a thickener for printing pastes. Therefore, the question of improvement of the properties of starch thickeners and of the economical utilization of starch is worthy of considerable attention.

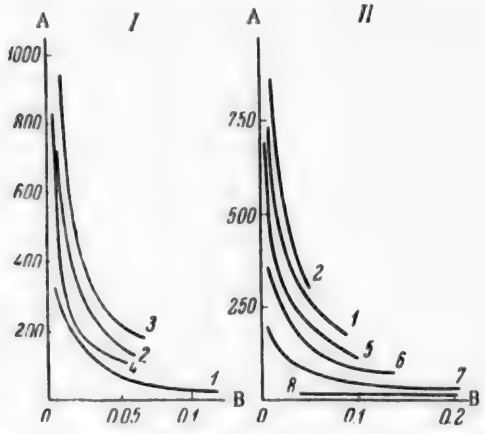

Fig. 1. Variation of thickener viscosity with the rotation velocity of the inner cylinder of the viscosimeter, for different cooking times. A) Viscosity (poises), B) angular velocity (rps). I) 5% thickener from corn starch (without additions), II) 5% solution of potato starch. Cooking times (min): 1) 5, 2) 10), 3) 15, 4) 45, 5) 30, 6) 40, 7) 60, 8) 120.

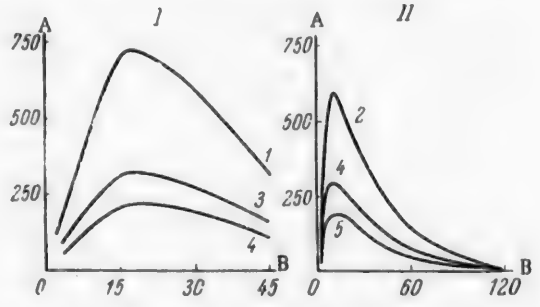

Fig. 2. Viscosity variations of 5% solutions of corn (I) and potato (II) starch during cooking. A) Viscosity (poises), B) cooking time (min). Viscosity measurements at cylinder speeds (in rps): 1) 0.01, 2) 0.02, 3) 0.03, 4) 0.05, 5) 0.09.

Among a number of problems, the most important are the thickening power and elasticity of thickeners. While the thickening power determines to a considerable extent the costs of thickeners, their quality is primarily dependent on the elasticity; the lower the elasticity, the better the quality [1, 2].

From the aspect of the economical production of thickeners, the usual methods of starch cooking require particularly critical examination. As a rule, starch is broken down very extensively during preparation of thickeners. This is illustrated by such statements as "in warm water starch grains swell and burst, and a thick sticky liquid, known as starch paste, is formed" [3]. Unfortunately, however, at this stage the paste already has a lower consistency; the bursting of the previously swollen starch grains is accompanied by a decrease in the viscosity of the starch–water system. It is pointed out in several papers [4, 5] that considerable breakdown of starch (unmodified) is necessary in size preparation in order to prevent subsequent spontaneous decrease of the viscosity of the size, and thereby to avoid disturbance of the normal warp-sizing process.

However, this risk does not generally arise in the case of thickeners, as they are generally used cold (although mechanical stresses on the printing paste in the machine have an influence). It is nevertheless found that in such cases considerable breakdown is also necessary in the usual methods for the preparation of thickeners. This fact requires explanation.

Katz [4] used mainly rather dilute (1%) starch solutions for his investigations. It is highly significant, moreover, that only the total viscosity of the solutions was studied, without consideration of the influence of the velocity gradient in the flow of the liquid through the viscosimeter capillary. For this reason no significant changes in the elasticity of starch pastes as the result of cooking were detected. Our investigations were concerned with the behavior of more highly concentrated starch pastes on cooking, especially in relation to their elasticoviscous properties.

Most of the investigations were on corn starch. The concentration of starch (bone-dry) in the pastes was 4.8% in all cases.

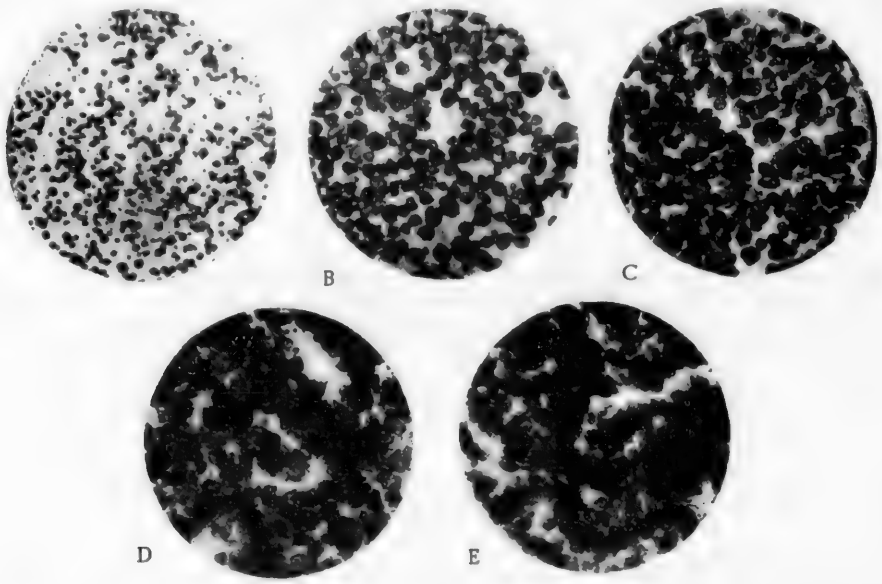

Fig. 3. Micrographs of corn starch pastes without additions, after different times of cooking. A) Before cooking; after cooking times (min): B) 5, C) 10, D) 30, E) 60.

The pastes (thickeners) were prepared as follows. A weighed sample of starch (and of all the other ingredients in the case of pastes of more complex composition) was put into distilled water heated to about 57° (not over), and the liquid (in a porcelain beaker) was warmed, with thorough stirring, on a boiling water bath; when thermal equilibrium became established, the temperature of the paste (thickener) in the beaker usually fluctuated in the range 86-89° (this was attained in 2-3 min). The level of the paste in the beaker during the cooking was kept constant by additions of warm water; at the end of the cooking the thickeners did not differ in weight from the initial weight by more than ± 2%.

The thickeners* were studied as follows. First, the viscosity was measured (at 25°) in a coaxial-cylinder viscosimeter, at different rotation velocities of the inner cylinder. Second, microphotographs of the starch grains in the paste (at × 150 magnification) were taken.

The viscosities of starch pastes after different times of cooking are plotted in Fig. 1.

These results show that both the total viscosity and the structural component of the viscosity increase with cooking time; the paste elasticity changes. Both the elasticity and the total viscosity increase at first, then they both decrease, but not symbatically. Over a certain period the structural viscosity even increases while the total viscosity decreases. Similar results are obtained in the cooking of potato starch.

The viscosity and structurization maxima of thickeners cooked for different times are seen even more clearly in Fig. 2.

* Different samples of technical starch were used for the thickeners; the elasticoviscous properties of the thickeners made from different starch samples differed numerically, but not in their nature.

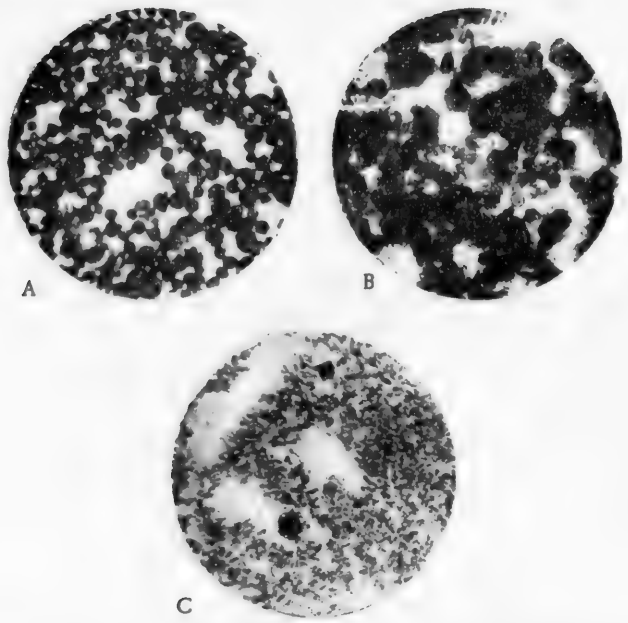

Fig. 4. Micrographs of corn starch pastes containing 0.01% HCl after cooking times (in min): A) 10, B) 20, C) 40.

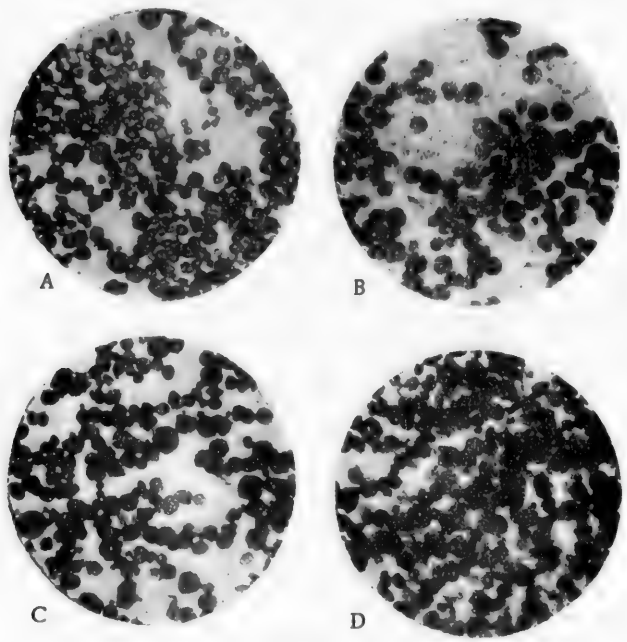

Fig. 5. Micrographs of corn starch pastes containing 6.4% NaCl after cooking times (in min): A) 10, B) 20, C) 40, D) 60.

There is no doubt that thickeners with elasticoviscous properties of the type represented by curves 3, 4 of Fig. 1 (I), or curves 2, 5 of Fig. 1 (II) must be of poor quality and unsuitable for use in production. To improve the quality of the thickeners, i. e., to lower their degree of structurization, they must be cooked further, despite the fact that the total viscosity is thereby decreased considerably, so that further cooking is disadvantageous.

Systematic investigations of changes in the state of the starch grains in the course of cooking revealed, in our opinion, some additional causes of the changes in the elasticity of starch pastes which occur during cooking.

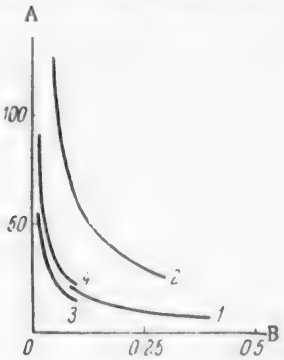

Fig. 6. Viscosity variations of 5% corn starch solution during cooking. A) Viscosity (poises), B) angular velocity (rps). Cooking time (min): 1, 4) 20; 2) 120; 3) 5. 1,2) In presence of 6.4% NaCl; 3,4) without additions.

The micrographs show that a high degree of structurization (and the consequent high viscosity) in the middle of the cooking process is the result not only of growth of the swollen starch grains, but also of mutual adhesion of the grains (Figs. 3 and 4). The pastes must therefore be cooked to complete breakdown (dispersion) of the swollen starch grains. The so-called "splitting agents," such as acids, are generally used for this purpose in the preparation of thickeners (Figs. 3 and 4).

The following question naturally arises from these results: if the cooking process cannot be stopped at any of the intermediate stages, might it not be possible to make use of the initial stage of cooking, when the viscosity of starch pastes is considerably higher than it is with the usual degree of cooking, even if not as high as it is in the middle of the cooking? We consider that the answer to this question is in the affirmative. However, the use of lightly cooked starch thickeners also involves serious difficulties. Such thickeners are not homogeneous enough (with regard to the degree of swelling of the individual starch grains) and are unstable, so that they are unsuitable for use in practice. If these defects could be eliminated, it might be possible to use lightly cooked starch thickeners.

One possible way of doing this, in our opinion, is to use the method proposed by D. I. Shul'pin for the preparation of thickeners. The principle of the method is that a considerable amount of common salt is added to the thickener. According to the available data, such thickeners have a number of favorable characteristics, in particular, with regard to their elasticoviscous properties, and to possible savings of up to 25% of starch [6]. However, the nature of these characteristics was not determined.

The behavior and properties of thickeners containing considerable amounts of common salt can be explained in the light of the above considerations and of the experimental data given below.

It has already been stated that a paste containing starch and water only has low stability at the early stages of cooking. The situation is quite different if starch is cooked in presence of electrolytes (such as sodium chloride, or magnesium chloride or sulfate).

The action of sodium chloride in 4-10% concentrations was studied in greater detail.

It follows from Fig. 5, which shows micrographs of starch pastes containing 6.4% sodium chloride cooked for different times, that the swelling (volume increase) of the starch grains proceeds slowly and, most important, the grains are dispersed little during the cooking. Such pastes are fairly stable on standing.

It must be noted that if the paste contains only 4% sodium chloride the effect of the electrolyte is somewhat weaker.

In accordance with the behavior of starch grains in presence of common salt, the viscosity variations of such starch pastes with cooking times are also different. This is illustrated in Fig. 6.

This method for the production of starch thickeners is nothing but a method of plastification without extensive cooking of the starch. The suitability and practicability of methods of this type have already been reported [2]. It is probable that the plastification of starch pastes by means of such substances as oleic acid, studied by us earlier, depends on the same principle as the use of electrolytes: our preliminary experimental data indicate that the cooking mechanism in the two processes is similar.

SUMMARY

1. The structural component of the total viscosity of starch pastes increases considerably as the result of cohesion of the swollen starch grains during cooking.

2. Electrolytes at high concentrations exert a plastifying effect in the preparations of starch pastes. This method of plastification of starch pastes (i. e., without excessive cooking of the starch, which can be avoided by the use of electrolytes) is more advantageous.

LITERATURE CITED

[1] M. G. Shikher, J. Appl. Chem. 18, 329 (1945).

[2] M. G. Shikher, J. Appl. Chem. 19, 542 (1946).

[3] P. P. Shorygin, Carbohydrate Chemistry (State Chem. Tech. Press, 1932)*, p. 157.

[4] I. R. Katz, Textile Research 9, 69 (1938).

[5] P. V. Seydel, Cotton 110, 11, 59 (1946).

[6] S. N. Iablokova and S. P. Surovtsev, Exchange of Technical Experience. Rationalization of Finishing, Coll. 105 (State Light Industry Press, 1953)*, p. 27.

Received June 29, 1956

* In Russian.

THE PROPERTIES OF SUNFLOWER PECTIN IN RELATION TO THE METHODS OF ISOLATION

T. K. Gaponenkov and Z. I. Protsenko

Laboratory of Organic Chemistry, the Voronezh Agricultural Institute

It has been shown that sunflower receptacles contain from 22 to 27% of pectic substances, according to the age of the plants [1]. After removal of the seeds, sunflower receptacles can be used as a source of food pectin. The essential property of all pectins is the power of gelation in presence of sugar and acids.

Some workers consider that the gelling power of a pectin directly depends on its methoxyl group content [2], and others believe that it depends on the molecular weight and the uronic (galacturonic) acid content [3].

It has been shown that the viscosity of pectin hydrosols is a measure of their gelling power. The viscosity and gelling power of a pectin increase with increasing molecular weight and chain length of the polygalacturonic acids present in it [4]. Therefore, the methods used for isolation of pectins may be decisive in relation to their gelling power.

Two main methods for the isolation of pectins are known: extraction in boiling water [2], and the process developed by the All-Union Confectionery Scientific Research Institute (VKNII) [5].

The main object of the present investigation was to study the chemical composition and properties of sunflower pectin prepared by different methods.

EXPERIMENTAL

The sunflower receptacles were crushed. The extraction with boiling water was continued for 2 hrs. The extract was filtered, evaporated to a small volume, and the pectin was precipitated by alcohol. The precipitate was filtered off, washed with alcohol and ether, and dried over sulfuric acid to constant weight (Sample I).

In contrast to this method, in extraction by the VKNII process the pectin was extracted in 0.4% HCl (pH = = 2.3-2.6) for 1 hr at 80°. The extract was filtered and pectin was precipitated by addition of aqueous $AlCl_3$ solution (1:4) and ammonia to pH = 3.4-3.8.

The precipitated pectin was dried, crushed, and washed first with 50% aqueous alcohol, then with 70% alcohol and 4% HCl, then again with 50% alcohol, and finally with a solution of 55% alcohol and 0.3-0.4% ammonia; the pectin was then dried and powdered (Sample II).

These two samples were studied; the results are given below.

Characteristics of Pectin Samples

Properties	Pectin samples I	II
Moisture (%)	11.1	14.7
Galacturonic acid (%)	54.26	72.75
Methoxyl groups (%)	9.0	5.4
Total ash (%)	6.58	2.46

(continued)

Properties	Pectin samples	
	I	II
Aluminum content (%)	–	0.258
Pentosans (%)	17.89	–
pH of 1% solution	4.6	3.2
Density	1.53	1.45
Refractive index	1.563	1.4920
Surface tension	71.07	75.97
Gel formation of pectin–sugar–acid (in %)	2–60–1.0	1.25–65–0.4

These results show that pectins prepared by different methods have different properties.

Pectin prepared by the VKNII process (Sample II) has a much higher galacturonic acid content, just over $^1/_2$ of the methoxyl group content, about $^1/_3$ of the ash content, and has the better gelling power, not inferior to the pectin of citrus fruits. These results also show that the methoxyl group content of pectin is not a criterion of gelling power.

Pectin prepared by the VKNII process with the use of hydrochloric acid and aluminum chloride has a lower ash content; i. e., the calcium and magnesium present in the pectin are partially replaced by aluminum.

Washing of the pectin with 50% aqueous alcohol removes pentosans (araban).

The higher acidity of the pectin hydrosol indicates that free carboxyl groups are formed in the preparation of pectin by the VKNII process. All these factors together have a significant influence on the properties of the pectin.

The evaluation of pectins by their viscosity is of great practical interest.

The relative viscosities of 0.5% pectin hydrosols at 20° are given below.

	Relative viscosity
Sunflower pectin obtained by extraction in boiling water (I)	1.37
Sunflower pectin made by the VKNII process (II)	5.81
Orange pectin	2.59
Lemon pectin	2.33
Apple pectin	1.62
Sugar-beet pectin	1.12

TABLE 1

Relative Viscosities of 0.5% Hydrosols of Pectin (II) with Different Concentrations of Sugar and Citric and Tartaric Acids

	Sugar	Acids							
		citric						tartaric	
Concentration (%)	50.0	0.00	0.5	1.0	1.5	2.0	2.5	1.5	2.0
Relative viscosity	5.51	5.81	9.23	12.26	12.87	11.88	9.76	12.95	12.59

These results clearly demonstrate the influence of the method used in the isolation of the pectin on its properties.

The viscosities of 0.5% hydrosols of Sample (II) pectin containing different concentrations of sugar and citric and tartaric acids were then studied (Table 1).

It follows from the data in Table 1 that sugar has no effect on the hydrosol viscosity. This confirms that there is no chemical action between pectin and sugar [6].

The 0.5% pectin hydrosol has maximum viscosity in presence of 1.5% of citric or tartaric acids.

To demonstrate the influence of the nature of the acid on the viscosity of pectin hydrosols, we determined the relative viscosities of 0.5% pectin hydrosols at pH = 2.9, in presence of sulfuric, hydrochloric, acetic, citric, and tartaric acids (Table 2).

TABLE 2

Effect of the Nature of the Added Acid on the Relative Viscosity of 0.5% Pectin Hydrosol at pH = 2.9

Acid	Relative viscosity
H_2SO_4	5.92
HCl	6.67
CH_3COOH	6.01
Tartaric	8.47
Citric	9.74

TABLE 3

Relative Viscosities of 0.5% Pectin Hydrosols at Different pH

pH value	Relative viscosity
3.4	5.81
2.9	8.47
2.7	9.24
2.5	12.95
2.4	12.59

For elucidation of the influence of hydrogen-ion concentration on the viscosity of pectin, 0.5% pectin hydrosols were prepared with different pH values, regulated by addition of tartaric acid (Table 3).

It is clear from Tables 2 and 3 that hydrosol viscosity is influenced both by the nature of the acid itself, and the hydrogen-ion concentration.

It must be pointed out that the specific (resinous) taste of the sunflower is a defect of confectionery articles made from sunflower pectin. This must be taken into account in the development of the technological process.

SUMMARY

1. Pectin made from sunflower receptacles by the VKNII process has better gelling power and contains considerably more galacturonic acid and less methoxyl groups and ash. The methoxyl group content is not a criterion of gelling power of pectin.

2. The viscosity of pectin hydrosols is influenced by the nature of the acid used and the hydrogen-ion concentration. It is confirmed that no chemical action occurs between pectin and sugar.

3. The gelation of sunflower pectin is most effective in presence of tartaric or citric acids.

LITERATURE CITED

[1] T. K. Gaponenkov and Z. I. Protsenko, J. Appl. Chem. 29, 1444 (1956).*

[2] F. V. Tserevitinov, The Chemistry and Commerce of Fresh Fruits and Vegetables (1930).**

[3] V. V. Arasimovich, Biochemistry of Cultivated Plants 8, 283 (1948).

[4] I. P. Zakharov, Colloids in the Food Industry 1, 138-165 (1946).

* Original Russian pagination. See C. B. translation.

** In Russian.

[5] L. B. Sosnovskii, "Production of Edible Gelling Pectin from a New Type of Raw Material – Sunflower Receptacles," Scientific Lectures, 1952 (State Light Industry and Food Industry Press, 1953)*, p. 114.

[6] S. A. Glikman, J. Appl. Chem. 4, 1041 (1931).

Received June 17, 1956

* In Russian.

PEAT FURFURAL

G. S. D'iachkov and L. K. Chukhlova

Leningrad Branch of the All-Union Scientific Research Institute for the Peat Industry

The varied uses of furfural in the organic chemical industry have stimulated searches for new raw materials for furfural production.

Chemists in the German Democratic Republic have investigated the use of peat meaterials for this purpose [1].

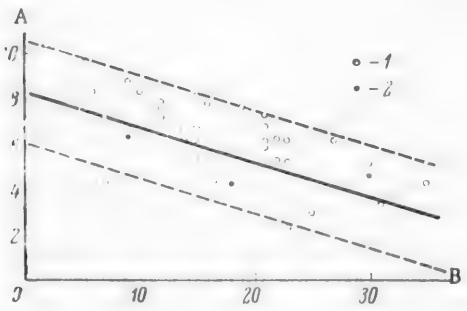

Fig. 1. Effect of the degree of decomposition of the peat on the furfural yield in hydrolysis. A) Furfural yield as % of the dry substance of the original peat, B) degree of decomposition (%). Peat: 1) upper, 2) lowland.

The use of peat for furfural production has also been considered by Soviet workers, who studied the yields of furfural from various agricultural wastes and plant materials [2]. However, these workers, not being specialists in the field of peat, did not correlate their results with the geobotanical characteristics of the raw peat, which are decisive for the yield and quality of the final product. They did not state that furfural has already been made in the Soviet Union on the industrial scale in the Boksitogorskii works for artificial dehydration of peat.

In a study of the yields of furfural from various peats, obtained under normal conditions of hydrolysis by hydrochloric acid, we found the following relationship between the yield and the degree of decomposition of the peat, as shown graphically in Fig. 1:

$$F_h = 8.3 - 0.155 \cdot r \pm 2.2\%,$$

where F_h is the % yield of furfural, calculated on the dry peat substance, obtained by acid hydrolysis; r is the degree of decomposition of the peat (in %).

It follows from Fig. 1 that lowland peats conform to the relationship found for upper peats.

If the peat is steamed in a laboratory autoclave, as in the process used in the Boksitogorskii works (steam pressure 13 atmos, pressure raised over 30 min and held at 15 min), the yield of furfural is considerably lower. In this case the relationship between the furfural yield and the degree of decomposition of upper peat, shown graphically in Fig. 2, is represented by the equation:

$$F_t = 2.18 - 0.06 \cdot r \pm 0.5\%,$$

where F_t is the % yield of furfural, calculated on the dry peat substance, obtained after heat treatment; r is the degree of decomposition of the peat (in %).

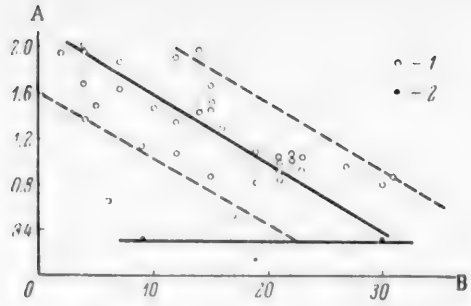

Fig. 2. Effect of the degree of decomposition of peat on the yield of furfural after heat treatment. A) Furfural yield (%) calculated on the dry peat substance, B) degree of decomposition of the peat (%). Peat: 1) upper, 2) lowland.

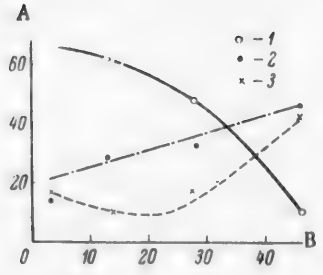

Fig. 3. Proportions of the principal components of crude furfural in relation to the degree of decomposition of the peat. A) Contents of furfural derivatives in crude furfural (%), B) degree of decomposition of the peat (%). 1) Furfural, 2) methylfurfural, 3) hydroxymethylfurfural.

For peats of the lowland type, the furfural yield is almost independent of the degree of decomposition, and is about 0.3% calculated on the dry peat substance.

The explanation is that the amount of organic acids formed in the heat treatment of lowland peats is not sufficient to catalyze the reaction of furfural formation.

The furfural yields from upper peats are somewhat higher, within the stated limits, for scheuchzeria–sphagnum peat, and somewhat lower for cottongrass- sphagnum peat. Medium and fuscum peats occupy an intermediate position.

The furfural obtained by the thermal treatment of peat (in absence of mineral acid) differs considerably in properties from the usual hydrolytic furfural. The furfural derivatives which are less stable in presence of mineral acids (methylfurfural and hydroxymethylfurfural) are decomposed much less than they are during hydrolysis, and dilute the main product. It is true that for a number of technical purposes this dilution has no detrimental effect.

The proportions of the principal components of crude furfural from medium peat of different degrees of decomposition (from analytical data of the blow-off steam condensate) are shown graphically in Fig. 3.

SUMMARY

The results show that for the industrial production of furfural it is expedient to use the weakly decomposed waste layers of hill swamps, which are of little value as fuel, and which interfere with the production of fuel from the main deposit, or the entire deposits of upper peats of a low degree of decomposition.

LITERATURE CITED

[1] E. Leibniz and G. Lange, Chemische Technik 9 (1953).

[2] A. A. Shcherbakov and Iu. K. Iur'ev, J. Appl. Chem. 29, 1, 110 (1956).*

Received June 7, 1957

* Original Russian pagination. See C. B. translation.

NARCOTOLINE IN OPIUM

A. S. Labenskii

The S. Ordzhonikidze All-Union Scientific Research Chemico-Pharmaceutical Institute

In 1936 Wrede [1] published the results of a study of a previously unknown alkaloid, narcotoline, isolated from the capsule of the poppy (Papaver somniferum L.). According to Wrede, and also to Baumgarten and Christ [2], the poppy capsule contains 0.05% of this alkaloid. Somewhat later Pfeifer and Weiss [3] showed that the narcotoline content of different samples of poppy capsules varies greatly, reaching 0.2% in some cases. According to the last-named authors, the contents of the principal alkaloid, morphine, in poppy capsules is some tenths of one percent (0.2-0.7%). Thus, the relative proportion of narcotoline in this material is fairly high. It was therefore all the more surprising that narcotoline was the only alkaloid of the poppy plant which had not as yet been found in opium. The search for narcotoline in opium was therefore of great interest, and this investigation was undertaken for that purpose. The isolation of narcotoline directly from opium, if its content in the latter is low, appeared to be a very difficult and unreliable operation. It was therefore decided to use the wastes obtained in the processing of opium, after isolation of morphine and other useful alkaloids, for the search for narcotoline. The wastes chosen for the work were those which might be expected to contain narcotoline if it had been present in the opium. The phenolic character and the weak basicity of this alkaloid were taken into consideration. A suitable waste product for the purpose was the substance known in the industry as "neutral morphine resin," formed when the mother liquors after extraction of morphine are treated by neutralization of an acidified solution of the phenol bases. This resin was treated with chloroform and a mixture $^1/_4$ of the total weight of the resin was extracted. The chloroform solution was separated chromatographically on aluminum oxide. The eluants were: first, chloroform, and then solutions of methanol in chloroform (from 2 to 50% by volume). A crystalline alkaloid which proved to be identical with narcotoline was isolated from the fraction eluted by 2 and 3% solutions. The identity was established by direct comparison with narcotoline isolated by us from poppy capsules. Approximate calculation showed that the spent opium in this case contained at least 0.03% narcotoline.

EXPERIMENTAL

100 g of "neutral" resin obtained during the production of opium alkaloids was extracted with chloroform (5 lots of 100 ml each). About 500 ml of solution was obtained. Removal of the solvent from this solution gave about 1 g of dry residue. The chloroform solution was passed through a chromatographic column containing 500 g of Al_2O_3. The first eluant was chloroform. 4 fractions of 250 ml each were collected. For the subsequent elutions, solutions of methanol in chloroform were used. 18 fractions were collected with 2% solution, 4 fractions with 3%, 3 fractions with 5%, and 5 fractions with 50%. A total of 34 fractions was collected. After removal of the solvents, all the fractions left amorphous residues; when these were warmed with a little alcohol, the solutions deposited crystalline precipitates. The same substance was isolated from fractions 8-29, in a total yield of 1.5 g; it melted at 183-184° before purification. The substance was amorphous and dissolved in excess aqueous acid or alkali. The substance was dissolved in 25 ml of water with addition of HCl. The solution was clarified by activated charcoal. Half the volume of alcohol was added to the filtrate. Ammonia was added to this solution at 65° to an alkaline reaction to bromothymol blue indicator; this precipitated 1.2 g of almost white crystals in the form of thin prisms; after recrystallization from methanol the m. p. was 188-189°. A mixture melted with narcotoline extracted from poppy capsules showed no depression; $[\alpha]_D^{20} - 186° \pm \pm 2°$ (c = 0.5, in chloroform). When a hot saturated solution of the substance (1 g) was mixed with a hot alcoholic solution of picrolonic acid (0.07 g), a yellow crystalline precipitate was obtained; after purification by warming

with alcohol, it melted at 203-204°. A mixture with narcotoline picrolonate gave no depression. Color tests (with concentrated H_2SO_4, Fröhde's reagent, formaldehyde—sulfuric acid) on the substance and on narcotoline from poppy capsules also confirmed the identity of the two substances. Because of the small amounts, the crystalline substances isolated from the other fractions could not be identified.

SUMMARY

The alkaloid narcotoline was isolated from wastes in the production of morphine from opium. Therefore this alkaloid is present in opium as well as in the poppy plant.

LITERATURE CITED

[1] F. Wrede, Arch. experim. Patologie u. Pharm. 184, 331-335 (1936).

[2] G. Baumgarten and W. Christ, Die Pharmazie 5, 80-82 (1950).

[3] S. Pfeifer and F. Weiss, Die Pharmazie 10, 658-664 (1955).

Received January 22, 1957

SIGNIFICANCE OF ABBREVIATIONS MOST FREQUENTLY ENCOUNTERED IN SOVIET PERIODICALS

FIAN	Phys. Inst. Acad. Sci. USSR.
GDI	Water Power Inst.
GITI	State Sci.-Tech. Press
GITTL	State Tech. and Theor. Lit. Press
GONTI	State United Sci.-Tech. Press
Gosenergoizdat	State Power Press
Goskhimizdat	State Chem. Press
GOST	All-Union State Standard
GTTI	State Tech. and Theor. Lit. Press
IL	Foreign Lit. Press
ISN (Izd. Sov. Nauk)	Soviet Science Press
Izd. AN SSSR	Acad. Sci. USSR Press
Izd. MGU	Moscow State Univ. Press
LEIIZhT	Leningrad Power Inst. of Railroad Engineering
LET	Leningrad Elec. Engr. School
LETI	Leningrad Electrotechnical Inst.
LETIIZhT	Leningrad Electrical Engineering Research Inst. of Railroad Engr.
Mashgiz	State Sci.-Tech. Press for Machine Construction Lit.
MEP	Ministry of Electrical Industry
MES	Ministry of Electrical Power Plants
MESEP	Ministry of Electrical Power Plants and the Electrical Industry
MGU	Moscow State Univ.
MKhTI	Moscow Inst. Chem. Tech.
MOPI	Moscow Regional Pedagogical Inst.
MSP	Ministry of Industrial Construction
NII ZVUKSZAPIOI	Scientific Research Inst. of Sound Recording
NIKFI	Sci. Inst. of Modern Motion Picture Photography
ONTI	United Sci.-Tech. Press
OTI	Division of Technical Information
OTN	Div. Tech. Sci.
Stroiizdat	Construction Press
TOE	Association of Power Engineers
TsKTI	Central Research Inst. for Boilers and Turbines
TsNIEL	Central Scientific Research Elec. Engr. Lab.
TsNIEL-MES	Central Scientific Research Elec. Engr. Lab.– Ministry of Electric Power Plants
TsVTI	Central Office of Economic Information
UF	Ural Branch
VIESKh	All-Union Inst. of Rural Elec. Power Stations
VNIIM	All-Union Scientific Research Inst. of Meteorology
VNIIZhDT	All-Union Scientific Research Inst. of Railroad Engineering
VTI	All-Union Thermotech. Inst.
VZEI	All-Union Power Correspondence Inst.

Note: Abbreviations not on this list and not explained in the translation have been transliterated, no further information about their significance being available to us. – Publisher.